Univerzita Karlova
1. lékařská fakulta

Doktorský studijní program:
Biochemie a patobiochemie

UNIVERZITA KARLOVA
1. lékařská fakulta

MUDr. František Sedlák

Fyziologická a patofyziologická role GCPII v organismu

Physiological and pathophysiological role of GCPII in the body

Disertační práce

Vedoucí závěrečné práce/Školitel: prof. RNDr. Jan Konvalinka, CSc.
Konzultant: prof. MUDr. Aleksi Šedo, DrSc.

Praha, 2022

Prohlášení:

Prohlašuji, že jsem závěrečnou práci zpracoval samostatně a že jsem řádně uvedl a citoval všechny použité prameny a literaturu. Současně prohlašuji, že práce nebyla využita k získání jiného nebo stejného titulu

Souhlasím s trvalým uložením elektronické verze mé práce v databázi systému meziuniverzitního projektu Theses.cz za účelem soustavné kontroly podobnosti kvalifikačních prací.

V Praze, 9.1.2022

František Sedlák

Podpis

Identifikační záznam:

SEDLÁK, František. *Fyziologická a patofyziologická role GCPII v organismu. [Physiological and pathophysiological role of GCPII in the body].* Praha, 2022. 96 stran, 6 příloh. Disertační práce. Univerzita Karlova, 1. lékařská fakulta, Ústav organické chemie a biochemie AV ČR, v.v.i. Vedoucí závěrečné práce: prof. RNDr. Jan Konvalinka, CSc.

Identification record:

SEDLÁK, František. *Physiological and pathophysiological role of GCPII in the body. [Fyziologická a patofyziologická role GCPII v organismu].* Praha, 2022. 96 pages, 6 appendices. PhD thesis.
Charles University, First Faculty of Medicine, Institute of organic chemistry and biochemistry of the CAS. Supervisor: prof. RNDr. Jan Konvalinka, CSc.

Poděkování

Ze všeho nejdříve bych rád poděkoval svému školiteli prof. Janu Konvalinkovi za možnost studovat a pracovat v jeho laboratoři a za seznámení se s vědeckým světem. Rád bych mu poděkoval nejen za vytvoření projektu, ale i za mnohé cenné rady, osobní přístup a podporu ve špatných chvílích. Díky svému vysokému etickému vědeckému standardu se mi tak stal vzorem, jak dělat výzkum. V neposlední řadě si vážím i velké míry důvěry a výzkumné svobody, kterou mi věnoval. Další klíčovou osobou nepostradatelnou pro vznik této práce, které bych chtěl poděkovat, byl Pavel Šácha, který mně v podstatě naučil veškerou práci v laboratoři a stal se naším „guru“ GCPII světa. Byl nevyčerpatelnou studnicí nápadů, a i když se některé zdály naprosto neproveditelné, dokázal mi, že je možné je vyzkoušet a dokázat, že je možné takřka všechno.

Dále bych chtěl poděkovat řadě svých kolegů, bez nichž by tato práce nikdy nemohla vzniknout. Báře Marešové za obrovské množství práce, co udělala na GCPII deficientní myši, ale současně také i za naprosto úžasnou duševní podporu v mých krizích ke konci studia. Tomášovi Knedlíkovi, Janu Tykvartovi, Vaškovi Navrátilovi a Michalovi Navrátilovi za to kolik to vybádali přede mnou, kolik znalosti ohledně GCPII mi předali a také kvůli skvělé lidské atmosféře v laboratoři, kterou pomáhali vytvořit. Dále studentům Martinovi Pehrovi, Anežce Kramné a Karolíně Janouškové za pomoc s experimenty a nekonečnou práci s udržováním myší kolonie. Tereze Ormsby, Monice Nedomové a Adéle Marcalíkové nejenom za čas strávený nad mými „literárními“ výplody, ale i za nekonečnou podporu v tíživých chvílích, Kristýně Blažkové, Michalu Svobodovi za skvělé diskuse a podnětné myšlenky. Robinovi Kryštůfkovi a ještě jednou Pavlovi Šáchovi za „bezva pokec“ a rady ohledně technických záležitostí. Janě Pokorné za řadu rad, pomoc a za péči o zásobování nejdůležitějšího přístroje v laboratoři. Slovy nevyjádřitelný obdiv ale patří i naším laborantkám Janě Starkové (Bimče) a Karolíně Šrámkové za obrovské množství práce a také za až téměř mateřskou péči, kterou nám všem věnovaly. Díky patří samozřejmě všem dalším z našeho „GCPII týmu“, ale i dalším kolegům z laboratoře i ústavu, kteří primárně pracovali na jiných projektech, ale vždy neváhali pomoci, když bylo potřeba. Speciální díky patří Kláře Grantz Šaškové, další úžasné osobnosti sršící nápady, za možnost se v „mezičase“, kdy nic nefungovalo, zabývat dalšími vědeckými výzvami.

Nemohu dále opomenout svého školitele konzultanta, prof. Aleksi Šeda a jeho tým, zejména Petra Buška a Marka Hilšera, kteří mi velmi pomohli, co se týče myších modelů a přípravy histologických řezů. Také bych takto chtěl poděkovat dr. Šimonu Vaculínovi za to, co mne všechno naučil v souvislosti s prací na myších modelech.

Co se týče spolupracujících skupin, bych chtěl poděkovat zejména dr. Petru Cíglerovi a jeho skupině, zejména Jitce Neburkové, za seznámení se světem nanočástic. Skupině dr. Radka Sedláčka, jmenovitě Dr. Petrovi Kašpárkovi, za přípravu GCPII-deficientního modelu a skupině doc. Forstové, hlavně Jiřině Suchanové a dr. Haně Španielové, za přípravu viru podobných nanočástic a know-how s tím spojené. Dále bych pak chtěl poděkovat skupině Dr. Etrycha, konkrétně Ing. Vladimírovi Šubrovi a dr. Liborovi Kostkovi, za přípravu modifikovaných N-(2-hydroxypropyl)methakrylamidových polymerů a doc. Friedeckému a jeho kolegům, zejména Alešovi Kvasničkovi, za uvedení do problematiky metabolomiky a lipidomiky a provedení lipidomických a metabolomických analýz.

Nemohou ani zapomenout na tým 1. interní kliniky Všeobecní fakultní nemocnice, přednostu prof. Marka Trněného, primáře Jana Kořena, prof. Ivana Špičku, ale i všechny ostatní, kteří mi umožnili kombinovat laboratorní doktorát s klinickou praxí a současně nakouknout pod pokličku klinického výzkumu.

A konečně obrovské díky mým rodičům, babičce, a ještě jednou přítelkyni za podporu, lásku a nekonečnou trpělivost se mnou v situacích, kdy to jistě se mnou bylo k nevydržení.

Abstrakt

Glutamátkarboxypeptidasa II (GCPII) je metaloproteáza zodpovědná za štěpení neurotransmiteru N-acetyl-aspartyl-glutamátu v centrálním nervovém systému na N-acetyl-aspartát a glutamát. Současně v lidském tenkém střevě napomáhá vstřebávání folátů pomocí odštěpování γ-vázaných glutamátů z folyl-poly-γ-glutamátu. GCPII je u člověka exprimována i v řadě dalších orgánů (např. ledviny a prostata) a nádorech, kde však její fyziologická funkce není známa. Při komplexním studiu role tohoto enzymu v savčím organismu jsme nejprve charakterizovali komerčně dostupné monoklonální protilátky proti GCPII. Dále jsme vyvinuli jejich plně syntetickou náhradu založenou na hydrofilním polymeru s navázanými GCPII inhibitory. Poté jsme zhodnotili vhodnost užití myšího biomodelu pro studium funkce GCPII *in vivo*, kdy jsme zachytili rozdíl v expresním profilu GCPII v myši a člověku. U myši ani v prostatě, ani v tenkém střevě jsme GCPII nepozorovali. Pro zhodnocení fyziologické a patofyziologické funkce enzymu jsme analyzovali myší GCPII-deficientní model. Kromě pozorování zvětšených semenných váčků u starších samců jsme nezjistili žádný další zjevný fenotyp. Obdobně jsme vyvrátili i schopnost GCPII štěpit amyloidní peptidy ($A\beta_{1-40}$ a $A\beta_{1-42}$). Ukazuje se tak, že chybějící aktivita GCPII v organismu nemá žádné evidentní negativní dopady. Z toho lze usuzovat, že ani farmakologická inhibice GCPII nebude vést k signifikantním nežádoucím účinkům. Lze tak předpokládat, že i klinické užití inhibitorů GCPII bude nejspíše bezpečné. V rámci cílení léčiv jsme prokázali, že interakce inhibitor-GCPII umožňuje specifické směřování rozličných nanostruktur do nádorových buněk, přičemž klíčová je optimalizace bio-nano rozhraní nanočástic k redukci nespecifické vazby.

Klíčová slova: GCPII, PSMA, FOLH1, glutamátkarboxypeptidasa II, prostaticky specifický membránový antigen, fyziologická funkce, inhibice, myší biomodel, zvětšené semenné váčky, cílení léčiv, GCPII deficientní myš, geneticky modifikovaná myš, náhrada protilátek, hydrofilní polymer, nádor, prostata, nanočástice, virům podobné částice, nanodiamanty

Abstract

Glutamate carboxypeptidase II (GCPII) is a metalloprotease responsible for cleaving the neurotransmitter N-acetyl-aspartyl-glutamate in the central nervous system to N-acetyl aspartate and glutamate. At the same time, in the human small intestine, it facilitates folate absorption by cleaving γ-linked glutamate from folyl-poly-γ-glutamate. In humans, GCPII is also expressed in a number of other organs (e.g., kidney and prostate) and tumors, where its physiological function is unknown. In an attempt to characterize the physiological function of the enzyme, we first characterized the commercially available monoclonal antibodies against GCPII. Further, we developed a fully synthetic replacement based on a hydrophilic polymer with bound GCPII inhibitors. We evaluated the suitability of using a murine biomodel to study GCPII function *in vivo*. We found the difference in GCPII expression profile in mouse and human. We did not observe GCPII in either the mouse prostate or small intestine. To assess physiological and pathophysiological functions of the enzyme we analyzed a GCPII-deficient mouse model. Apart from the observation of enlarged seminal vesicles in older males, we did not detect any other obvious phenotype. Similarly, we confirmed that GCPII cannot cleave amyloid peptides ($A\beta_{1-40}$ and $A\beta_{1-42}$). Thus, it appears that the lack of GCPII activity in the organism has no obvious negative effects. It can be therefore assumed that pharmacological inhibition of GCPII will not lead to significant adverse effects either and the clinical use of GCPII inhibitors will be likely safe. In the context of drug targeting, we have shown that the inhibitor-GCPII interaction allows specific targeting of different nanostructures to tumor cells, while the optimization of the nanoparticle bio-nano interface is important to reduce non-specific binding.

Keywords: GCPII, PSMA, FOLH1, glutamate carboxypeptidase II, prostate-specific membrane antigen, physiological function, inhibition, mouse biomodel, enlarged seminal vesicles, drug targeting, GCPII-deficient mouse, genetically modified mouse, antibody replacement, hydrophilic polymer, tumor, prostate, nanoparticles, virus-like particles, nanodiamonds

Obsah

Seznam zkratek

^{177}Lu-PSMA-617	2-[4-[2-[[4-[[(2*S*)-1-[[(5*S*)-5-carboxy-5-[[(1*S*)-1,3-dikarboxypropyl]karbamoylamino]pentyl]amino]-3-naphthalen-2-yl-1-oxopropan-2-yl]karbamoyl]cyklohexyl]methylamino]-2-oxoethyl]-7,10-bis(karboxylatomethyl)-1,4,7,10-tetrazacyclododec-1-yl]octová kyselina v komplexu s ^{177}Lu
[^{18}F]-DCFPyL	(2S)-2-[[(1S)-1-carboxy-5-[(6-(^{18}F)fluoranylpyridine-3-carbonyl)amino]pentyl]karbamoylamino]pentanediová kyselina
[^{68}Ga]Ga-PSMA11	N,N'-Bis(2-hydroxy-5-(ethylen-betakarboxy)benzyl)ethylenediamin N,N'-dioctová kyselina v komplexu s ^{68}Ga
APC	anafázi podporující komplex („anaphase promoting complex“)
AKT	proteinkináza B
BIND-014	nanočástice BIND-014 (cílené proti PSMA, obsahující docetaxel)
BiTE™	bispecifický T-buněčný aktivátor („Bi-specific T-cell engagers“)
BCG	β-citryl–L-glutamát
CAR	chimerický antigenní receptor
CAR-T	T lymfocyt s chimerickým antigenním receptorem
cAMP	cyklický adenosinmonofosfát
cGMP	cyklický guanosinmonofosfát
DM1	mertansine
ELISA	enzymový imunosorbční test („enzyme-linked immunosorbent assay“)
FAK	kináza fokálních adhezí („focal adhesion kinase“)
FDA	Úřad pro kontrolu potravin a léčiv („Food and Drug Administration“)
FOLH1	folylpoly-γ-glutamáthydrolasa I
$GABA_A$	receptor pro γ-aminomáselnou kyselinu typu A
GCPII	glutamátkarboxypeptidasa II
GCPIII	glutamátkarboxypeptidasa III
GTPasa	guanosintrifosfát fosfohydroláza
HER2	humánní epidermální receptor 2
HPLC	vysokoúčinná kapalinová chromatografie
HPMA	N-(2-hydroxypropyl)methakrylamid
HUVEC	lidské endoteliální buňky pocházející z pupečníkové žíly
IEE	izoleucyl-glutamyl-glutamát

IGF-1R	receptor pro insulinu-podobný růstový faktor 1 („insulin like growth factor 1 receptor“)
IL-6	interleukin 6
LQ	leucyl-glutamin
LQE	leucyl-glutaminyl-glutamát
LNE	leucyl-asparaginyl-glutamát
LNCaP	prostatická linie LNCaP
MAPK	mitogenem aktivovaná proteinová kináza
EGF	epidermální růstový faktor
EGFR	receptor pro epidermální růstový faktor
ERK1 / ERK2	extracelulárním signály regulovaná kináza 1 / 2
kDa	kilodalton
k_{cat}	konstanta k_{cat} (obratové číslo)
K_i	inhibiční konstanta
K_M	Michaelisova konstanta
MEF	multivalentní zesilující faktor („multivalent enhacement factor“)
mGluR3	metabotropní glutamátový receptor 3. typu
mRNA	mediátorová ribonukleová kyselina
mTOR	savčí kináza TOR („mammalian target of rapamycin“)
Myc	protein Myc
NAA	N-acetyl-L-aspartát
NAAG	N-acetyl-L-aspartyl-L-glutamát
NAAG2	N-acetyl-L-aspartyl-L-glutamyl-L-glutamát
NAALADase	„N-acetylated-alpha-linked acidic dipeptidase I“
NFκB	jaderný faktor kappa B
NMDA	N-metyl-D-aspartát
PAK-1	p21 aktivovaná kináza
PCR	polymerázová řetězová reakce
PD-1	receptor „programed cell death 1“
PEG	polyetylenglykol
PET	pozitronová emisní tomografie
PET/CT	pozitronová emisní tomografie kombinovaná s výpočetní tomografií
PI3K	fosfatidylinositol-3-kináza
PMPA	2-fosfonomethylpentandiová kyselina

PSA	prostatický specifický antigen
PSMA	prostatický specifický membránový antigen
RACK1	receptor pro aktivovanou protein kinázu 1
Ras	protein Ras
RT-PCR	polymerázová řetězová reakce v reálném čase
SDS-PAGE	polyakrylamidová gelová elektroforéza s dodecylsulfátem sodným
SPECT	jednofotonová emisní výpočetní tomografie
SPR	povrchová plasmonová rezonance („surface plasmon resonance“)
TALEN	efektorové nukleázy podobné transkripčním aktivátorům („transcription activator-like effector nucleases“)
TGFβ	transformující růstový faktor beta
TNFα	tumor nekrotizující faktor alfa („tumour necrosis factor alpha“)
TRAMP	transgenní model adenocarcinomu myší prostaty („the transgenic adenocarcinoma of the mouse prostate“)
ÚOCHB	Ústav organické chemie a biochemie Akademie věd České republiky
VEGF	vaskulární endoteliální růstový faktor
VLP	viru podobné částice („virus like particles“)

1. Úvod

Glutamátkarboxypeptidasa II (GCPII), známá též pod řadou jiných názvů jako prostatický specifický membránový antigen (PSMA), folylpoly-γ-glutamáthydrolasa I (FOLH1), či NAALADasa (N-acetylated-alpha-linked acidic dipeptidase I), je transmembránový glykoprotein II. typu. Vzhledem ke své karboxypeptidázové aktivitě, která je závislá na přítomnosti dvou atomů zinku v aktivním místě, lze ji řadit dle databáze MEROPS do skupiny M28B.

GCPII je kódována genem s názvem *FOLH1* o délce 62035 párů bází, skládajícího se z 19 exonů a 18 intronů, nacházejícím se na 11. chromozomu (11p11-p12) (O'Keefe a kol., 1998). Jako možný minimální promotor genu byl identifikován 614 páru bází dlouhý fragment, který nevykazuje striktní tkáňovou specifitu (Good a kol., 1999). Výrazně vyšší exprese v prostatické tkáni u člověka (odtud PSMA) je dána přítomností enhanceru lokalizovaného v třetím intronu (Noss a kol., 2002; Watt a kol., 2001). Aktivita tohoto enhanceru je negativně ovlivněna jak androgeny (Noss a kol., 2002), tak i zastavením vápníkové signalizace ionoforem vápníku, přes kalcium dependentní transkripční faktor NFATc1 vázající se na AP-3 část PSMA enhanceru (Lee a kol., 2003).

Z genetického hlediska byly podrobněji analyzovány dva přirozeně se vyskytující polymorfismy – rs61886492 (C1561T) a rs202676 (T484C). Obě mutace byly studovány stran ovlivnění folátového metabolismu. U polymorfismu C1561T jsou výsledky kontroverzní. Některé studie ukazují zvýšení hladiny folátu (Afman a kol., 2003; DeVos a kol., 2008; Halsted a kol., 2007; Lievers a kol., 2002; Melse-Boonstra a kol., 2004) případně i snížení hladiny homocysteinu, ale ostatní studie tento fakt nepotvrdily (Devlin a kol., 2006; Chen a kol., 2004; Morin a kol., 2003; Vargas-Martinez a kol., 2002). Polymorfismus C1561T dále vede k mutaci H475Y v proteinové sekvenci, která však neovlivňuje aktivitu rekombinantní GCPII při štěpení polyglutamylovaných folátů *in vitro* (Navrátil a kol., 2014). Druhý polymorfismus T484C, četný u skupiny matek s plody s poruchami vývoje neurální trubice v čínské oblasti Lvliang (Guo a kol., 2013), vede k mutaci Y75H. Tato mutace, na rozdíl od předchozí (H745Y), by dle molekulárního modelování (Guo a kol., 2013), mohla vést k změně sekundární i terciální struktury. Polymorfismus T484C je asociován s nižší hladinou folátu, či jeho zásobních forem (Cummings a kol., 2017; Roffman a kol., 2013), event. i se zvýšenou hladinou homocysteinu (Guo a kol., 2013). Toto zjištění je poměrně překvapivé vzhledem k poměrně vysokému výskytu tohoto polymorfismu, kdy minoritní frekvence alely dosahuje okolo 0,39 (Auton a kol., 2015). Tento polymorfismus je mimo jiné asociován se vzrůstem nitroočního tlaku (Gao a kol.,

2018). Minoritní alela je dále v nedávné práci (Zink a kol., 2020) asociována s větším množstvím transkriptu GCPII a nižším inteligenčním kvocientem. Jedním z dalších polymorfismů s fenotypickým dopadem je intronická varianta rs55728336-C (Cheng a kol., 2021), kdy u nosičů této alely dochází k snížení množství N-acetyl-aspartyl-glutamátu vylučovaného do moči.

Krom základní plnodélkové varianty mRNA PSMA, kódující protein GCPII o délce 750 aminokyselin, byla popsána řada dalších sestřihových variant - viz obrázek 1, převzato a upraveno z prací (Hlouchová a kol., 2012; Williams a Kole, 2006). PSM' varianta je zkrácena o 266 nukleotidů z 5' konce, neobsahuje tak signální sekvenci a část proteinu odpovídající intracelulární a transmembránové části. V tkáních se poměr PSMA/PSM' zvyšoval úměrně míry malignity (Su a kol., 1995). Pomoci metody „5' Rapid Amplification of cDNA Ends", tj. amplifikace pomocí jednoho primerů společného pro všechny transkripty, byly nalezeny v buněčné linii LNCaP další 2 sestřihové varianty: varianta PSM-C, jejíž potenciálně produkovaný protein by byl velmi podobným variantě PSM', a varianta PSM-D. V případě varianty PSM-D dochází k iniciaci translace v jiném místě, což vede ke vzniku alternativního exonu 1c, a tedy i k expresi nové sekvence 42 aminokyselin, následované zbytkem PSMA (O'Keefe a kol., 2001; Schmittgen a kol., 2003a). Užitím oligonukleotidů přepínajících sestřih („splice-switching oligonucleotides") na LNCaP linii byla kromě varianty PSM' identifikována i varianta postrádající exon 6 - PSMAΔ6 a varianta postrádající exon 18 – PSMAΔ18. Obě varianty vedou k výraznému zkrácení a zásahu do extracelulární části. Lze předpokládat, že výsledný protein je neaktivní (Williams a Kole, 2006). Další varianta PSM-E, jež byla objevena po sekvenaci produktu reverzní transkripce spojené s PCR z buněčné linie LNCaP, obsahuje inzerci 97 nukleotidů mezi nukleotidy 379 a 380 a neobsahuje sekvenci 93 nukleotidů mezi bázemi 2232 a 2324 PSMA sekvence. Dále jsou přítomny dva odlišné nukleotidy na pozicích 1453 a 1479. Autory je i popisována lepší korelace mezi množstvím PSM-E varianty a mírou malignity oproti variantě PSMA (Cao a kol., 2007), přičemž obdobně jako u PSMA transfekce PSM-E snižuje u PC-3 buněčné linie proliferaci, invazi a migraci (Cao a kol., 2012). PSM-F je varianta obdobná PSM-E, jen bez delece 97 nukleotidů mezi bázemi 2232 a 2324 (Hlouchová a kol., 2012).

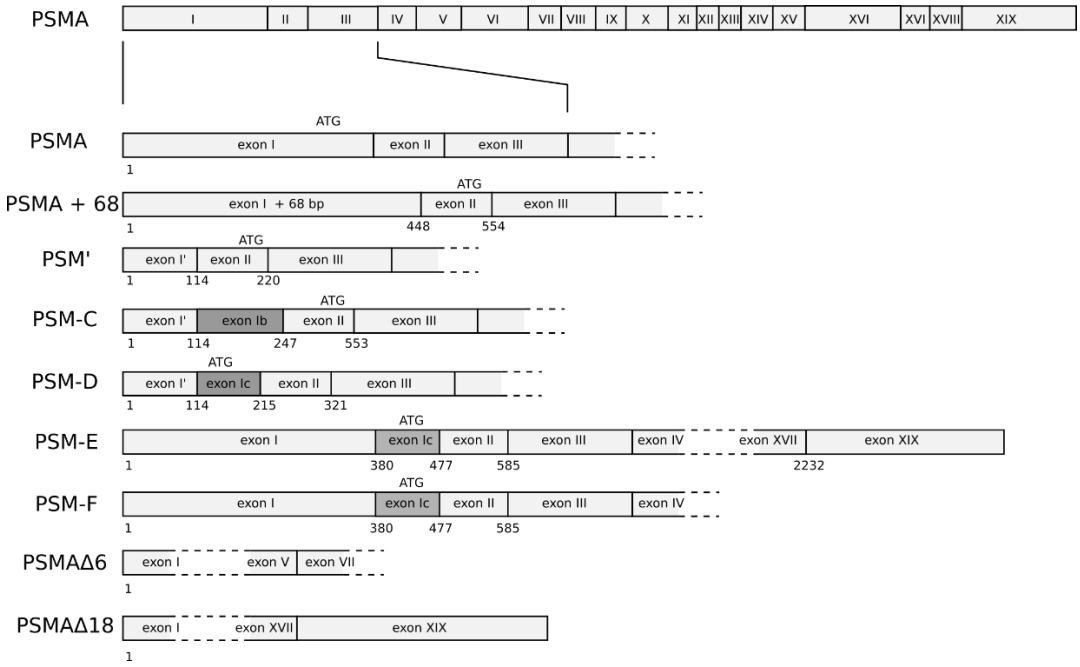

Obrázek 1 - Zobrazení exonového složení mRNA PSMA (nahoře). Zobrazení exonového složení mRNA příslušných sestřihových variant (dole), pro jednoduchost zobrazeny zejména exony se změnami oproti základní variantě PSMA. Převzato a upraveno z prací Hlouchová a kol. (2012); Williams a Kole (2006).

GCPII ve své plnodélkové formě se vyskytuje ve formě C2 symetrického homodimeru. Každý monomer se sestává z krátké intracelulární části, transmembránového úseku a velké enzymaticky aktivní extracelulární části tvořené třemi doménami – proteázovou, apikální a dimerizační (Mesters a kol., 2006). Struktura extracelulární domény je znázorněna na obrázku 2, převzatého z Mesters a kol. (2006), a je velmi podobná struktuře transferinového receptoru, se kterým sdílí 28 % sekvenční identitu. Rozdíly jsou oproti transferinovému receptoru zejména v nepřítomnosti aktivního místa a aminokyselinách zajišťujících rozpoznání substrátu.

Protein je masivně N-glykosylován. Z celkem deseti potenciálních glykosylačních míst bylo sedm pozorováno ve struktuře (Mesters a kol., 2006). Tyto glykosylace jsou nezbytné pro enzymatickou aktivitu (Barinka a kol., 2004). Glykosylace na asparaginu N638 mimo jiné díky interakci s glutamátem E276 napomáhá dimerizaci, která je taktéž kruciální pro katalytickou aktivitu (Schülke a kol., 2003). Dimerizace je dále pozitivně ovlivněna přítomností vápenatého kationtu, který stabilizuje smyčku mezi aminokyselinami 272-279 (Mesters a kol., 2006; Ptacek a kol., 2018).

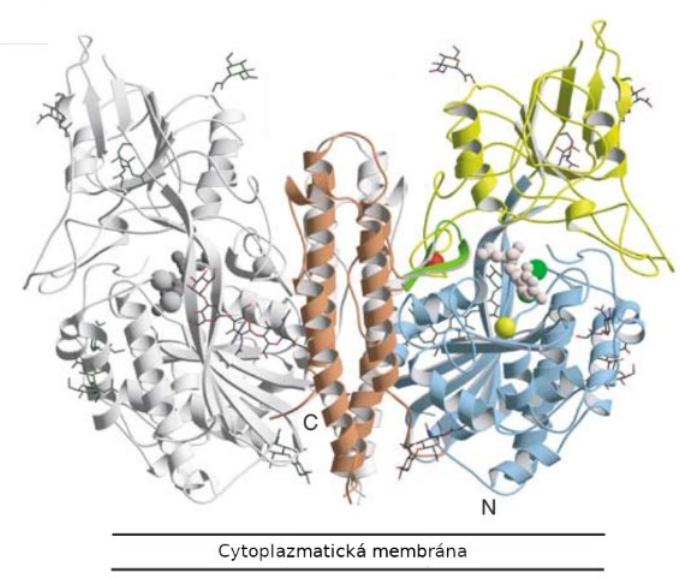

Obrázek 2 – Struktura extracelulární části GCPII, převzato a upraveno z Mesters a kol. (2006). Modře znázorněna proteázová, žlutě apikální a hnědě dimerizační doména. Zelené kuličky značí zinkové ionty, červené vápníkový kation a žluté chloridový anion.

Nejbližším homologem GCPII je glutamátkarboxypeptidasa III (GCPIII), 740 aminokyselin dlouhý protein s 67 % identickou a 81 % podobnou aminokyselinovou sekvencí (Pangalos a kol., 1999). Velmi podobná je i 3D struktura, přičemž GCPIII je schopna štěpit obdobné substráty jako GCPII – N-acetyl-aspartyl-glutamát (Hlouchova a kol., 2009; Pangalos a kol., 1999) i polyglutamylované folváty (Navrátil a kol., 2016). Oproti GCPII je schopna efektivně štěpit β-citryl-glutamát (Collard a kol., 2011; Navrátil a kol., 2016).

1.1 Enzymatická aktivita

Základní enzymatickou aktivitou GCPII, jak vyplývá z názvu enzymu, je odštěpování C-koncového glutamátu (α resp. γ vázaného) ze svých substrátů. Jako fyziologický substrát byly identifikován N-acetyl-aspartyl-glutamát (NAAG), nejrozšířenější peptidový neurotransmiter v mozkové tkáni (Robinson a kol., 1987), N-acetyl-aspartyl-glutamyl-glutamát (NAAG2) (Lodder-Gadaczek a kol., 2011), poly-γ-glutamylovaný folát (odtud název foláthydroláza) (Halsted, 1991) a v neposlední řadě také velmi neochotně štěpený substrát, který je naopak velmi dobře štěpen homologní glutamátkarboxypeptidasou III (GCPIII), β-citryl-glutamát (Navrátil a kol., 2016). Reakce se základními substráty, tj. s NAAGem a poly-γ-glutamylovanými folváty jsou zobrazeny na obrázku 3.

Jako substráty GCPII byly potvrzeny i další kyselé dipeptidy jako N-acetyl-aspartyl-methionin, N-acetyl-glutamyl-methionin, N-acetyl-alanyl-methionin a N-acetyl-glutamyl-glutamát (Barinka a kol., 2002), pro což svědčí i alternativní název NAALADase (dipeptidasa štěpící α-spojené N-acetylovené kyselé dipeptidy). Stran selektivity ke štěpení dalších kyselých dipeptidů se ukazuje, že N-terminální acetylace není nezbytná a že jsou též štěpeny, i když hůře, substráty tvořené D-stereoizomery aminokyselin a substráty obsahující v P1 pozici jinou dikarboxylovou kyselinu (např. kyselinu adipovou, glutarovou, jantarovou, malonovou) (Barinka a kol., 2008).

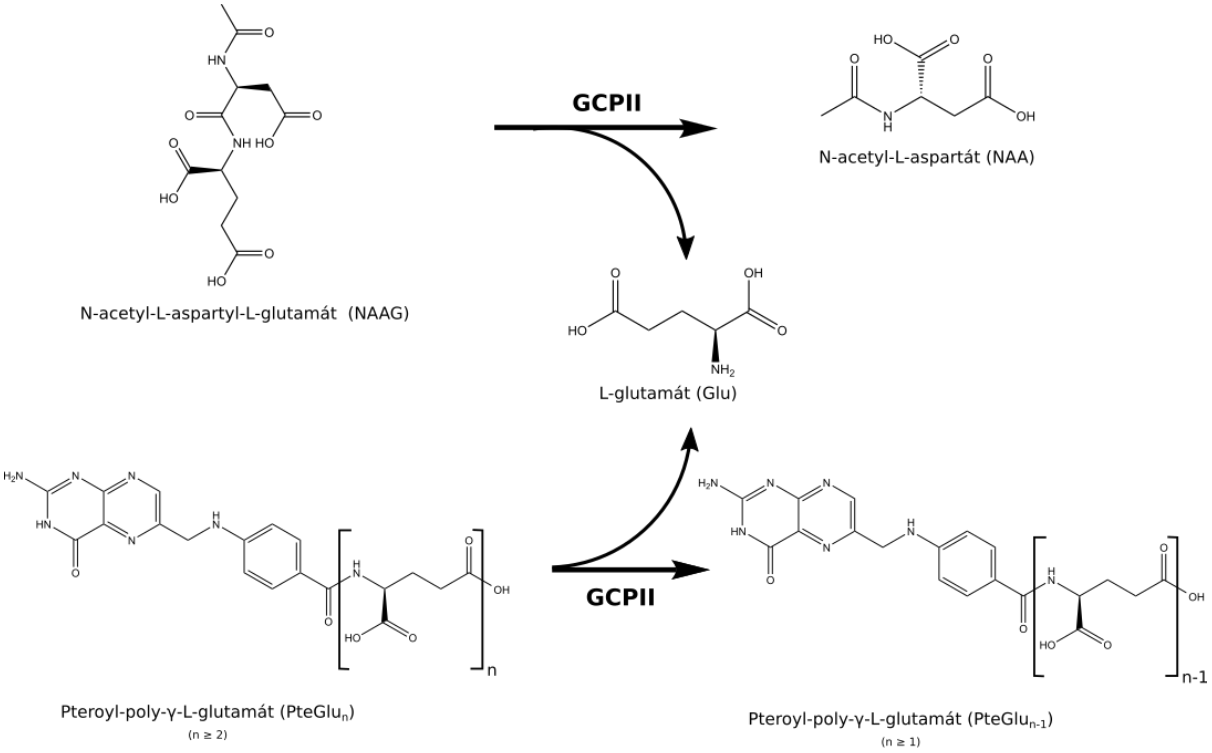

Obrázek 3 – Hydrolytické reakce katalyzované GCPII. Zobrazeny jsou základní přirozené substráty – NAAG a poly-γ-glutamylované foláty. Molekuly vody jsou pro jednoduchost vynechány.

Jako další fyziologické substráty byly identifikovány některé peptidy zakončené C-terminálním glutamátem vzniklé štěpením složky extracelulární matrix lamininu matrixovou metaloproteázou 2. Těmi jsou např. leucyl-glutaminyl-glutamát (LQE), izoleucyl-glutamyl-glutamát (IEE) a leucyl-asparaginyl-glutamát (LNE) (Conway a kol., 2016). Produkty tohoto štěpení, jmenovitě zejména leucyl-asparagin a glutamát, jsou schopny ovlivňovat buněčnou adhezi zprostředkovanou $\alpha_6\beta_1$ integrinem (Conway a kol., 2013; Conway a kol., 2016). Struktura některých další přirozených substrátů GCPII a GCPIII je zobrazena na obrázku 4.

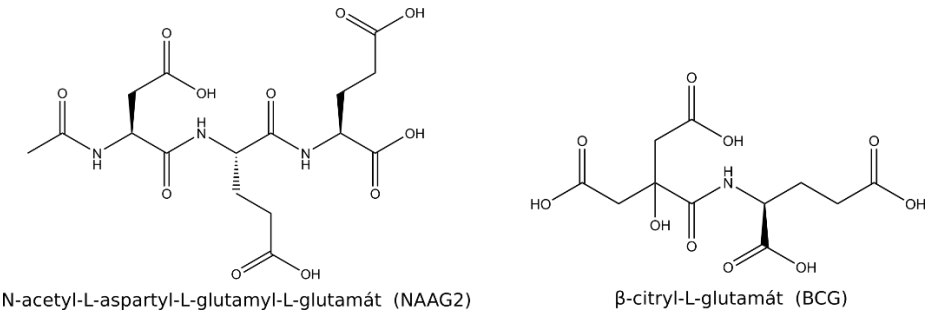

Obrázek 4 – Struktury některých dalších přirozených substrátů enzymů GCPII a GCPIII.

Poměrné kontroverzní byla identifikace GCPII jako proteázy štěpící amyloidogenní peptidy $A\beta_{1-40}$ a $A\beta_{1-42}$ v rámci Alzheimerovy choroby (Kim a kol., 2010b; Lee a kol., 2013), která však dále nebyla potvrzena (Alt a kol., 2013).

Katalytický mechanismus je znám vzhledem ke známé struktuře proteinu (Barinka a kol., 2008; Barinka a kol., 2007a; Barinka a kol., 2007b; Mesters a kol., 2006) a je obdobný jako u řady dalších metaloproteáz (Pavlícek a kol., 2012). V aktivním místě se nalézají dva zinkové kationty vázající molekulu katalyticky aktivní vody, sloužící jako centrální nukleofil. Ta je aktivována pomocí katalytické báze – glutamátu E424. Takto vzniklý hydroxylový ion nukleofilně napadá peptidovou vazbu. Po rozštěpení dochází ke zpětnému přenosu protonu z glutamátu E424 na aminoskupinu odstupujícího produktu. Reakční mechanismus při štěpení NAAGu je zobrazen na obrázku 5, převzato z publikace Pavlícek a kol. (2012) – fig.4.

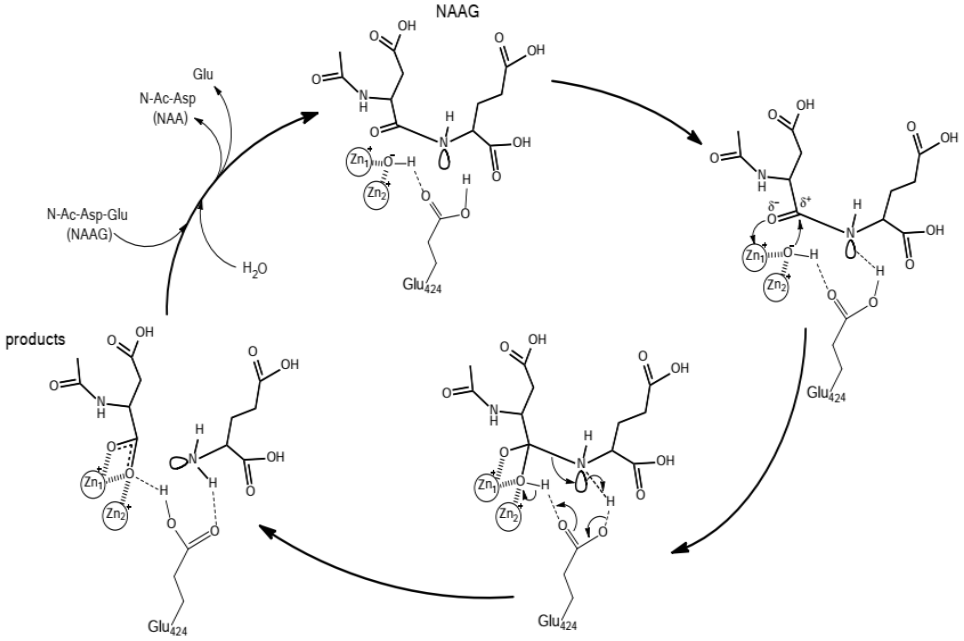

Obrázek 5 – Katalytický mechanismus štěpení NAAGu pomocí GCPII. Převzato z Pavlícek a kol. (2012).

α-karboxylová skupina C-terminální aminokyseliny (většinou glutamát) je v S1ʹ kapse vázána díky iontové vazbě s argininem R210 a dvěma vodíkovými můstky – s tyrosiny Y700 a Y552 (Mesters a kol., 2006). Postranní karboxylová skupina interaguje iontovou vazbou s lyzinem K699 a vodíkovou vazbou s asparaginem N257. Přítomnost dikarboxylové kyseliny (např. glutamát, event. ale i glutarát) v S1' místě vede ke změně struktury GCPII („induced fit" mechanismus vazby substrátu), kdy dojde k posunu a fixaci smyčky s aminokyselinami K699 a Y700, proto dle charakteru substrátu je tato část nazývána jako tzv. „glutarátový senzor".
N-terminální aminokyselina štěpeného dipeptidu (P1) je vázána do S1 kapsy, kde je vazba zprostředkována interakcí s pozitivně nabitými zbytky argininů R463, R534 a R536 a vodíkovou vazbou s asparaginem N519, což vysvětluje preferenci pro kyselé aminokyseliny. Arginin R536, díky své flexibilitě, může nabývat dvou konformací, přičemž pouze v jedné je schopen vázat substrát, k čemuž napomáhá i stabilizace pomocí vázaného chloridové aniontu a glutamátu E457 na dně S1 kapsy (Barinka a kol., 2008; Mesters a kol., 2006). Schéma vazby NAAGu do aktivního místa GCPII s příslušnými interakcemi je znázorněno na obrázku 6, který je převzat a upraven z publikace Mesters a kol. (2006).

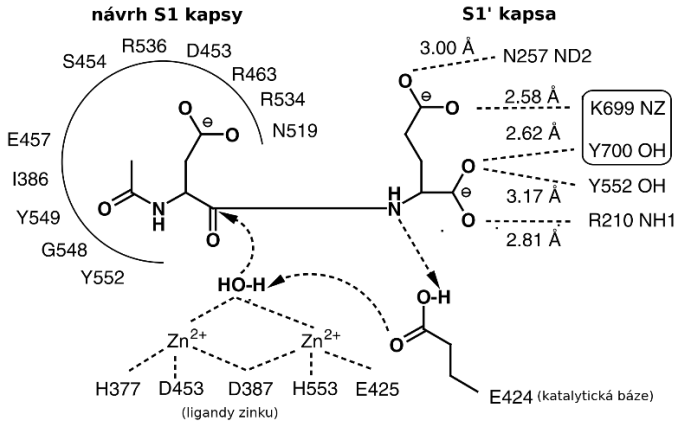

Obrázek 6 – Schématické znázornění vazby substrátu NAAG do katalytického místa GCPII. Aminokyseliny K699 a Y700 tvořící „glutarátový senzor" jsou orámovány. Převzato z publikace (Mesters a kol., 2006) a upraveno.

Vstup do aktivního místa může být uzavřen smyčkou z aminokyselin W541-G548, tzv. „entrance lid", který v případě stericky objemných inhibitorů či substrátů zůstává v otevřené konformaci, zatímco u malých substrátů dochází k změně na uzavřenou konformaci (Barinka a kol., 2008). V případě otevřené konformace dochází mimo aktivní místo ke vzniku alosterického vazebného místa (tzv. „arene binding site"), kde tryptofan W541 pomocí „π-stackingu" a arginin R511 pomocí π-kationové interakce jsou schopny vázat areny (Zhang

a kol., 2010). Zdá se, že toto alosterické vazebné místo, díky interakci s aromatickým pteroátem (Navrátil a kol., 2014) zlepšuje vazbu a následně i štěpení polyglutamylovaného folátu. Současně „arene binding site“ umožňuje konstrukci vysoce selektivních a potentních inhibitorů (Navrátil a kol., 2014).

Aktivita GCPII je dle některých prací (Anilkumar a kol., 2003; Conway a kol., 2006) překvapivě ovlivněna interakcí intracelulární části s filaminem. Tyto práce jsou však ve vzájemném nesouladu, zatímco dle Anilkumara vazba filaminu na GCPII aktivitu snižuje, tak u Conway naopak je snížena aktivita GCPII, v důsledku aktivace PAK-1 (p21 activated kinase), po poklesu vazby s filaminem. Jedním z vysvětlení může být např. fakt, že zatímco Anilkumar vztahuje aktivitu na membránovou frakci, tak Conway vztahuje aktivitu GCPII na celkovou hladinu proteinu. Neboť vazba GCPII na filamin snižuje endocytózu (Anilkumar a kol., 2003), tak lze předpokládat nabohacení GCPII v plasmatické membráně. Navýšení aktivity membránové frakce dle Anilkumara je tedy spíše v důsledku vyššího obsahu GCPII v plasmatické membráně než ovlivněním vlastní aktivity enzymu, která může být naopak nižší (Conway a kol., 2006).

1.2 Neenzymatické funkce

GCPII je exprimována i ve tkáních, kde nebyl nalezen žádný specifický substrát, případně jeho štěpení není připisována žádná fyziologická funkce (viz níže). Proto se spekuluje, že může mít i jiné funkce, které bezprostředně nesouvisejí s její proteolytickou aktivitou. Vzhledem k výše popsané aktivitě, kdy GCPII štěpí polyglutamylované foláty, byla ve studii Yao a kol. (2010) analyzována hypotéza, zda GCPII mimo jiné není schopna i transportu monoglutamylovaných folátů. Vskutku, u prostatické linie PC3 transfekované GCPII byla oproti netransfekované linii pozorována dvojnásobná akumulace folátu. Bohužel další publikace potvrzující tento výsledek se neobjevily.

GCPII vykazuje řadu podobností s transferinovým receptorem, se kterým sdílí jednak výraznou strukturní podobnost (Mesters a kol., 2006), tak i schopnost internalizace klatrinovou cestou (Liu a kol., 1998; Rajasekaran a kol., 2003). Unikátní motiv MXXXL (Rajasekaran a kol., 2003) intracelulární části GCPII interaguje pravděpodobně přes μ2 subjednotku s adaptorovým komplexem AP-2, který se přímo účastní tvorby klatrinového váčku (Pearse a kol., 2000). GCPII je následně díky své interakci s filaminem A (Anilkumar a kol., 2003), obdobně jako transferinový receptor směřována do recyklujících endosomů. Přestože internalizace GCPII je konstitutivní, vazbou specifické protilátky je výrazně urychlena (Liu a kol., 1998). Internalizace nejspíše nesouvisí s aktivitou, vzhledem k tomu, že inhibice enzymatické aktivity

GCPII fosfátem nevede k snížení endocytózy (Rajasekaran a kol., 2003). V mikrovaskulárních endoteliálních buňkách byla popsána i alternativní cesta endocytózy, kdy přibližně jedna pětina GCPII je endocytována kaveolinovou dráhou, zprostředkovanou pomocí interakce GCPII s kaveolinem-1 (Anilkumar a kol., 2006).

Směřování GCPII do recyklujících endosomů je zajímavé i v souvislosti s popsanou interakcí recyklujících endosomů a centrosomu přes Rab11 protein (Hehnly a kol., 2012) a jejich úlohou v terminální fázi cytokineze, kdy dochází k vlastnímu oddělení buněk po vytvoření dělící rýhy (Fielding a kol., 2005; Wilson a kol., 2005). Lokalizace GCPII v oblasti konců mitotického vřeténka (a tedy i v blízkosti centrosomů) byla popsána i v práci (Rajasekaran a kol., 2008), přičemž za klíčovou je považovaná cytoplazmatická část GCPII a funkce mikrotubulů. GCPII zde asociovala s APC (anaphase promoting complex) a urychlovala degradaci cyklinu B vedoucí k předčasnému ukončení mitózy. To podle Rajasekarana dále vedlo k aneuploidii a tím i zvýšení rizika nádorové progrese.

To vše nasvědčuje hypotéze, že GCPII by mohla sloužit jako receptor pro zatím neznámý ligand (Rajasekaran a kol., 2005). Receptorové funkci by mohla nasvědčovat i přítomnost polyprolinového helixu v extracelulární části, který u jiných proteinů zajišťuje interakci se Src-homology 3 doménami (Mesters a kol., 2006). Arteficiální aktivace GCPII pomocí monoklonální protilátky J591 vede u buněčné linie LNCaP k aktivaci MAPK („mitogen-activated protein kinase“) (Colombatti a kol., 2009; Perico a kol., 2016) a mTOR/AKT/BAD (Perico a kol., 2016) signální dráhy. GCPII po sesíťování vytváří makromolekulární komplex s β_1 integrinem, filaminem A, adaptorovým proteinem pp130Cas a fosforylovaným proteinem c-Src, který vede k aktivaci AKT a ERK1/2 kináz. Tento děj je inhibován potlačením exprese jakékoli složky komplexu (Perico a kol., 2016). Dochází i k aktivaci GTPas RAS, Rac1 (Colombatti a kol., 2009) a následně i kináz MAPK38 a ERK1/2 (Colombatti a kol., 2009; Perico a kol., 2016). Závěrem je i fosforylován transkripční faktor jaderný faktor kappa B (NFκB), který zvyšuje produkci cytokinu IL-6 a CCL5 (Colombatti a kol., 2009). Výše uvedený makromolekulární komplex současně asociuje s receptorem EGFR a vede k jeho fosforylacím na tyrosinech Y^{1086} a Y^{1173}, které nezávisejí na aktivaci EGF (Perico a kol., 2016). Signalizace je znázorněna na schématu převzatém a upraveném z publikace Perico a kol. (2016) uvedeném na obrázku 7.

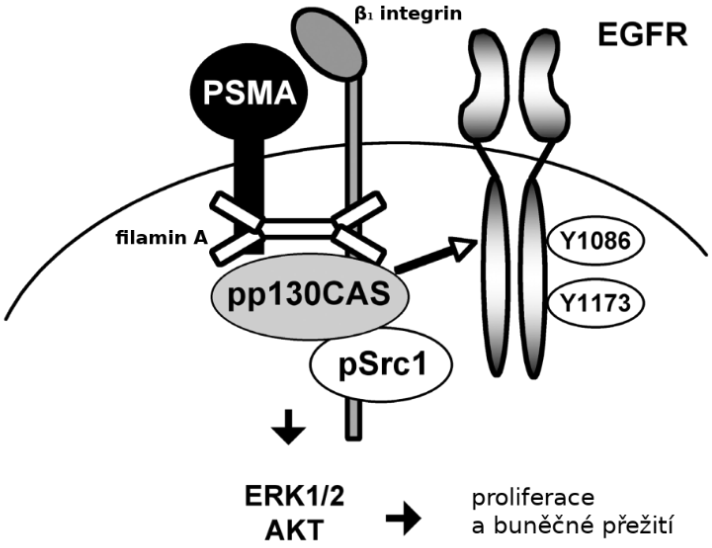

Obrázek 7 – Schématické znázornění signalizace po aktivaci GCPII/PSMA. Aktivací vzniká makromolekulární komplex GCPII s filaminem A, β_1 integrinem, proteinem pp130Cas a fosforylovaným proteinem Src1, který aktivuje AKT a ERK1/2 kinázy. Současně dochází k asociaci s EGFR receptorem a fosforylaci Y^{1086} a Y^{1173}. Převzato z publikace (Perico a kol., 2016) a upraveno.

Klíčovou se zdá souhra s integrinovými drahami, kdy signalizace GCPII v přítomnosti funkčního protoonkogenu c-Src (Perico a kol., 2016) vede k aktivaci β_1 integrinu (Conway a kol., 2006; Perico a kol., 2016) a následně cestou Rac GTPasy k aktivaci PAK-1 a tím i ovlivnění buněčné migrace. Inhibice GCPII snižuje fosforylaci FAK („focal adhesion kinase“) závislé na β_1 integrinu (Conway a kol., 2006). V experimentálních spontánních nádorech prostaty „the transgenic adenocarcinoma of the mouse prostate“ (TRAMP) byla v případě myší deficientních v genu pro GCPII pozorována nižší fosforylace FAK kinázy v hlavním autofosforylačním místě Y^{397}, oproti výrazně zvýšené fosforylaci na tyrosinu Y^{925} (Caromile a kol., 2017). Zatímco fosforylace Y^{397} je klíčová pro spojení s SH2 doménou Src kináz, tak fosforylace Y^{925} je skrze interakci s GRB2 adaptorovým proteinem zodpovědná za aktivaci MAPK signální dráhy (Hanks a Polte, 1997). Vysvětlení nabízí práce Caromile a kol. (2017), kde byla v lidské prostatické buněčné linii 22Rv1 identifikována asociace GCPII s proteinem RACK1 a receptorem IGF-1R, která snižuje interakci RACK1/IGF-1R s β_1 integrinem. To vede ke změně FAK fosforylace a aktivaci AKT signální dráhy (PI3K-AKT). To spolu s nálezem snížené signalizace v MAPK dráze (GRB2-ERK1/2) ve výše popsaných GCPII pozitivních tumorech v TRAMP myším transgenním modelu vytváří hypotézu, že za přítomnosti GCPII dochází k přesmyku signalizace z MAPK dráhy k více onkogenní dráze AKT (Caromile a kol.,

2017). Schématicky je tento děj znázorněn na obrázku 8, přejatém a upraveném od Caromile a kol. (2017).

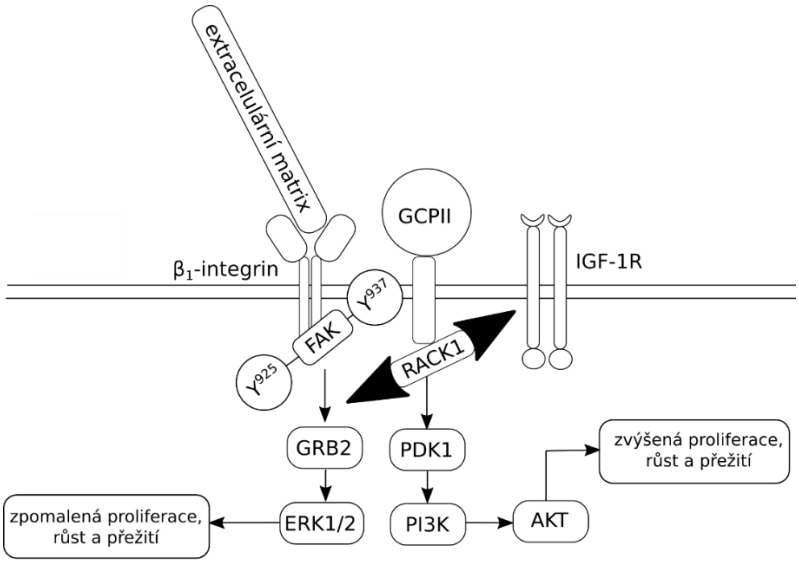

Obrázek 8 – Schématické znázornění přesmyku signalizace v důsledku přítomnosti GCPII. GCPII asociuje s proteinem RACK1 a receptorem IFG-1R, což kompetitivně snižuje interakci s RACK1/IGF-1R komplexu s β_1 integrinem. Interakce RACK1 proteinu s GCPII místo s β_1 integrinem aktivuje PI3K/AKT dráhu a vede k změně fosforylací FAK, kdy je bez další stimulace integrinovou cestou preferována fosforylace FAK na tyrosinu Y^{937} před tyrosinem Y^{925}. To vede k útlumu signalizace GRB2/ERK1/2 dráhou. Pokud jsou β_1 integrinové receptory současně přímo stimulovány kontaktem s extracelulární matrix dojde k alternativní aktivaci FAK včetně standardní fosforylace na tyrosinu Y^{925}. MAPK dráha tak zůstává aktivní. Přejato a upraveno od Caromile a kol. (2017).

Tato překvapivá domněnka není v souladu s předchozími pracemi (Colombatti a kol., 2009; Perico a kol., 2016), které naopak ukazují zvýšenou aktivitu MAPK38 a ERK1/2 po aktivaci GCPII monoklonální protilátkou; současně dochází i k rozporu v rámci exprese GCPII v rámci základního TRAMP transgenního modelu, kde oproti práci (Caromile a kol., 2017) nebyla v další studii (Simons a kol., 2019) exprese GCPII potvrzena. Jedním z možných vysvětlení může být fakt, že arteficiální aktivace GCPII pomocí monoklonální protilátky vede k rapidní internalizaci (Rajasekaran a kol., 2003), což může vést ke změně složení příslušných signalizačních komplexů.

1.3 Expresní profil

Expresní profil GCPII byl opakovaně studován jak na úrovní mRNA, tak i na proteinové úrovni. Výsledky nejsou bohužel vždy plně konzistentní, což může být dáno různorodostí analytických

metod (reverzní transkripce spojená s polymerázovou řetězovou reakcí – RT-PCR, „northern blot“, imunohistochemie, ELISA, imunoblot - „western blot“, enzymová aktivita), použitím různých detekčních protilátek s různou senzitivitou, tak i paletou a charakterem vyšetřovaných tkání.

Shodně jak na proteinové, tak i na mRNA úrovni byla u lidských tkání popsána kromě prostaty (Aggarwal a kol., 2006; Cunha a kol., 2006; Gala a kol., 2000; Horoszewicz a kol., 1987; Israeli a kol., 1994; Lopes a kol., 1990; Mhawech-Fauceglia a kol., 2007; Pangalos a kol., 1999; Renneberg a kol., 1999; Rovenská a kol., 2008; Silver a kol., 1997; Sokoloff a kol., 2000; Troyer a kol., 1995; Wolf a kol., 2010) exprese v mozku (Cunha a kol., 2006; Israeli a kol., 1994; Mhawech-Fauceglia a kol., 2007; Pangalos a kol., 1999; Renneberg a kol., 1999; Rovenská a kol., 2008; Sácha a kol., 2007; Trover a kol., 1995), ledvinách (Cunha a kol., 2006; Kinoshita a kol., 2006; Lopes a kol., 1990; Pangalos a kol., 1999; Renneberg a kol., 1999; Rovenská a kol., 2008; Sokoloff a kol., 2000), tenkém střevě (Gala a kol., 2000; Kinoshita a kol., 2006; Pangalos a kol., 1999; Rovenská a kol., 2008; Silver a kol., 1997), játrech (Cunha a kol., 2006; Kinoshita a kol., 2006; Pangalos a kol., 1999; Renneberg a kol., 1999; Rovenská a kol., 2008), v močovém měchýři (Gala a kol., 2000; Kinoshita a kol., 2006; Rovenská a kol., 2008) a v slinných žlázách (Israeli a kol., 1994; Trover a kol., 1995; Wolf a kol., 2010).

Z dalších tkání byla pozorována přítomnost GCPII proteinu v tlustém střevu (Kinoshita a kol., 2006; Rovenská a kol., 2008; Sokoloff a kol., 2000) a v některých dalších tkáních reprodukčního systému (prsní žláze, vaječnících, vejcovodu, děloze, varleti a nadvarleti) (Kinoshita a kol., 2006; Mhawech-Fauceglia a kol., 2007; Rovenská a kol., 2008; Sokoloff a kol., 2000).

Stran tělesných tekutin byla GCPII nalezena v krvi resp. plasmě (Beckett a kol., 1999; Knedlík a kol., 2014; Rochon a kol., 1994; Troyer a kol., 1995), seminální plasmě (Rochon a kol., 1994; Sokoloff a kol., 2000; Troyer a kol., 1995) a v moči (Sokoloff a kol., 2000).

Exprese jednotlivých ortologů GCPII v tkáních různých živočišných druhů je překvapivě rozdílná. Výrazná exprese GCPII v prostatě člověka je unikátní, v prostatě myši, potkana, prasete, psa, ani vysoce příbuzného makaka není pozorovatelná (Aggarwal a kol., 2006; Bacich a kol., 2001; Rovenská a kol., 2008). Exprese v děloze a varlatech je u člověka oproti praseti a potkanovi výrazně nižší. Stran reprodukčního systému je výrazněji zachována pouze exprese ve vaječníku. Obdobně v trávicím traktu je GCPII detekovatelná v tenkém střevě člověka a prasete, kdežto u potkana je záchyt minimální (Rovenská a kol., 2008; Shafizadeh a Halsted, 2007). Relativně podobná exprese mezi druhy je u ledvin a mozku, kde ji nalézáme jak u

hlodavců (myš, potkan), tak i u prasete a člověka. U myši, oproti člověku, potkanu a praseti nalézáme výrazně nižší hladinu v játrech.

Co se histologické lokalizace GCPII týče, jedná se většinou o expresi na apikální straně epiteliálních buněk, tj. acinárních buněk prostaty (Kinoshita a kol., 2006; Rovenská a kol., 2008; Silver a kol., 1997), buněk proximálním tubulu ledvin (Kinoshita a kol., 2006; Rovenská a kol., 2008; Silver a kol., 1997), acinárních buňkách slinné žlázy (Wolf a kol., 2010) a enterocytů (Kinoshita a kol., 2006; Silver a kol., 1997). Výjimkou je pozitivita stromatu u vaječníku (Kinoshita a kol., 2006). Exprese ve slinné žláze je zřejmě nejspíše spjata i s nežádoucím účinkem, xerostomií, po podání GCPII cílených radionuklidů (Kratochwil a kol., 2016).

V případě tkáně centrálního nervového systému byla lokalizace dominantně popisována v astrocytech (Berger a kol., 1999; Rovenská a kol., 2008; Sácha a kol., 2007), přičemž barvení má granulární cytoplazmatický vzor (Sácha a kol., 2007). Dále GCPII byla nalezena i v cytoplazmě ependymálních buněk (Kinoshita a kol., 2006). Stran periferního nervstva byla GCPII pozorována ve Schwanových buňkách neprodukujících myelin v oblasti neuromuskulárního spojení (Berger a kol., 1995).

Studiem exprese v nádorové tkáni se zabývalo poměrně značné množství autorů. Výrazná exprese v nádorových buňkách byla zachována u nádorů prostaty, kde byla zachycena jak v primárním nádoru, tak i v metastázách (Gala a kol., 2000; Horoszewicz a kol., 1987; Kinoshita a kol., 2006; Lopes a kol., 1990; Silver a kol., 1997; Trover a kol., 1995; Wright a kol., 1995). Některé práce se pokusily míru pozitivity (většinou zjištěnou pomocí imunohistochemie) korelovat s mírou agresivity onemocnění či s prognózou. Výsledky byly však rozporuplné. V práci Bostwick a kol. (1998), kde porovnávali prostatické intraepiteliální neoplazie s plně rozvinutým karcinomem, nezachytili signifikantního rozdílu, kdežto ve studii Perner a kol. (2007) naopak analýza doby do biochemické progrese karcinomu prostaty vykazovala signifikantní rozdíl mezi silnými a slabými expresory na úrovni $p = 0{,}003$, včetně efektu v multivariantní analýze. V práci Minner a kol. (2011) při obdobné analýze byla doba do biochemického relapsu u silně exprimujích tumorů oproti tumorům slabě exprimujícím také statisticky signifikantně kratší, avšak na hraniční úrovni ($p = 0{,}0483$). Pozitivita GCPII přitom korelovala se stadiem tumoru, preoperační hodnotou PSA a HER2 expresí.

Přítomnost GCPII byla studována i v jiných nádorech. Byla popsána v nádorových buňkách řady malignit vycházejících většinou z tkání, které primárně exprimují GCPII. Mezi nimi např. v karcinomu močového měchýře (Gala a kol., 2000; Lane a kol., 2008; Samplaski a kol., 2011), primárním karcinomu ledvin (Dumas a kol., 1999), karcinomu pankreatu (Ren a kol.,

2014), astrocytomu (Salas Fragomeni a kol., 2017). Z benigních tumorů exprimují GCPII neurofibromy u neurofibromatozy typu 1 (Gulhane a kol., 2017). Z tumorů majících původ v tkáních GCPII fyziologicky neexprimujících, byla zachycena GCPII u nemalobuněčného karcinomu plic (Schmidt a kol., 2017).

Překvapivě byla zachycena pozitivita GCPII v endoteliích cév většiny nádorů – např. u nádorů prsu, tlustého střeva, plic, štítné žlázy, ale i u glioblastomu a osteosarkomu (Baccala a kol., 2007; Bychkov a kol., 2017; Crowley a kol., 2016; Haffner a kol., 2009; Heitkötter a kol., 2018; Heitkötter a kol., 2017; Chang a kol., 1999; Kasoha a kol., 2017; Liu a kol., 1997; Matsuda a kol., 2018; Nomura a kol., 2014; Schmidt a kol., 2017; Silver a kol., 1997; Tolkach a kol., 2018; Vorlova a kol., 2019; Wernicke a kol., 2011; Wernicke a kol., 2014; Zeng a kol., 2012).

Co se exprese GCPII v modelech geneticky podmíněných nádorů prostaty u myši týče jsou dostupná rozporuplná data. Zatímco fyziologicky myší prostata GCPII neexprimuje (Bacich a kol., 2001), tak u genetického „Hi-Myc“ modelu, kdy je probasinovým promotorem řízena exprese onkogenu Myc, byla exprese pozorována již od stadia prostatické intraepiteliální neoplazie (Simons a kol., 2019). U TRAMP modelu založeného na expresi SV40 T antigenu vlivem probasinového promotoru jsou výsledky více nesourodé. V práci Simons a kol. (2019) nepopsali ani na úrovni imunohistochemie ani na pozitronové emisní tomografií kombinované s výpočetní tomografií (PET/CT) s [^{18}F]-DCFPyL sondou expresi GCPII, kdežto v případě jiných studií Schmittgen a kol.(2003b), Yang a kol. (2001) byla nalezena GCPII na úrovni mRNA, a v případě práce Caromile a kol. (2017) i na úrovni proteinu.

Pozitivita GCPII v nově tvořených cévách nebyla pozorována jen v malignitách ale i v regeneračních procesech v hojící se tkáni, v granulacích, tak i v endometriálních cévách (Gordon a kol., 2008).

Exprese je asociována i se zánětlivými onemocněními. Jak na mRNA, tak i na proteinové úrovni byla exprese GCPII zachycena v buňkách sliznice ilea při Crohnově chorobě (Zhang a kol., 2012). Kromě Crohnovy choroby byla pozorována zvýšená aktivita GCPII i u zánětem zasažené sliznice při ulcerozní kolitidě (Rais a kol., 2016). Jako vedlejší nález u vyšetření PET/CT s radioligandem značeným ^{68}Ga proti GCPII byla v řadě prací popisována pozitivita u sarkoidózy (Ardies a kol., 2017; Dias a kol., 2017; Hermann a kol., 2016; Kobe a kol., 2015), tato data však nebyla potvrzena jinou metodou a mohou souviset s nespecifickou akumulací ^{68}Ga, vzhledem k tomu že se ^{68}Ga-citrát vychytává, nejspíše cestou vazby na transferin, v zánětlivých ložiscích.

1.4 Známé fyziologické funkce

1.4.1 Nervový systém

Známá fyziologická funkce GCPII v nervové tkání je úzce spjata s jejími peptidovými substráty N-acetyl-aspartyl-glutamátem (NAAG) a N-acetyl-aspartyl-diglutamátem (NAAG2). GCPII na povrchu perisynaptických astrocytů katabolizuje tyto substáty za odštěpení C-terminálního glutamátu (Berger a kol., 1999; Robinson a kol., 1987; Sácha a kol., 2007).

NAAG je nejrozšířenější dipeptid v nervové tkáni, vyskytující se u většiny živočišných druhů – byl nalezen v řádově podobné koncentraci u králíka, potkana, morčete, slepice, holuba, ale i u želv a žab (Miyake a kol., 1981). NAAG vzniká kondenzací N-acetyl-aspartátu (NAA) a glutamátu (Arun a kol., 2006; Cangro a kol., 1987; Gehl a kol., 2004) za účasti ATP dependentní NAAG synthetázy I nebo NAAG synthetázy II (Becker a kol., 2010; Collard a kol., 2010). Koncentrace NAAGu v jednotlivých částech nervového systému králíka se pohybovala v rozmezí 0,14 – 3,09 mmol/kg a tvořila, jako u většiny druhů savců a ptáků, přibližně desetinu koncentrace jeho biosyntetického prekurzoru – N-acetyl-aspartátu (Miyake a kol., 1981). Jak vyplývá z imunohistochemických studií, naprosto převažuje neuronální lokalizace NAAGu, a to jak např. v čichové a zrakové dráze (Anderson a kol., 1986; Tieman a kol., 1987), tak i v dráze senzitivní v dorzálním gangliu (Cangro a kol., 1987). Stran sub-celulární lokalizace se NAAG nachází jak v perikaryonu, tak i axonech, přičemž nejvyšší koncentrace dle ultrastrukturních studií byla popisována v synaptických váčcích, a to jak presynapticky (Renno a kol., 1997; Williamson a Neale, 1988), v zakončení axonu, či v případě glutamatergního systému v postsynaptických váčcích v dendritech (Nordengen a kol., 2020). Na druhou stranu *in vivo* měření pomocí magnetické rezonanční spektroskopie ukazuje mírně vyšší koncentraci NAAGu v bílé hmotě 1,5 – 2,7 mM oproti hmotě šedé 0,6 – 1,5 mM (Pouwels a Frahm, 1997). NAAG se po depolarizaci uvolňuje z neuronu do synaptické štěrbiny díky fúzi synaptických váčků s cytoplazmatickou membránou, která je závislá na influxu vápníku (Tsai a kol., 1988; Walder a kol., 2013; Zollinger a kol., 1988). Transport NAAGu do synaptických váčků je zprostředkován pomocí transportéru sialinu (Lodder-Gadaczek a kol., 2013).

NAAG2 vzniká další kondenzací NAAGu s glutamátem za katalýzy NAAG synthetatasou II. Koncentrace NAAG2 koreluje s koncentrací NAAG v jednotlivých kompartmentech nervové tkáně a je cca třicet až padesátkrát nižší (Lodder-Gadaczek a kol., 2011). Zda funguje NAAG2 jako neurotransmiter není dosud zcela potvrzeno.

Za receptor NAAGu je považován metabotrobní glumátový receptor 3 (mGluR3) (Lea a kol., 2001; Neale, 2011; Wroblewska a kol., 1998; Wroblewska a kol., 1997), který po svojí aktivaci

snižuje tvorbu cAMP (Wroblewska a kol., 1998), ale i tvorbu cGMP (Wroblewska a kol., 2006). Někteří autoři (Fricker a kol., 2009; Chopra a kol., 2009) však tato data zpochybňují s poukázáním na možnou přítomnost reziduálního glutamátu v komerčně dostupném NAAGu. Receptor mGluR3 se nalézá na neuronálním synaptickém spojení jak presynapticky, tak i postsynapticky. Presynapticky negativní zpětnou vazbou snižuje uvolňování neutotransmiterů cestou redukce cyklického adenosin monofosfátu (cAMP), vedoucí ke snížení aktivity proteinkinasy A a tudíž i k poklesu množství vstupujícího vápníku při depolarizaci snížením vodivosti vápníkových kanálů L-typu (Romei a kol., 2013; Zhao a kol., 2001). Postsynapticky aktivace mGluR3 vede u GABAergních neuronů ke zvýšení exprese $GABA_A$ receptoru a tím prohloubení inhibičního signálu (Ghose a kol., 1997). U glutamatergních neuronů je naopak po aktivaci mGluR3 popisována inhibice dlouhodobé potenciace (Lea a kol., 2001; Neale a kol., 2000). Nedávno byla popsána i retrográdní inhibiční signalizace, kdy po aktivaci postsynaptického neuronu dochází působením vápníku k uvolnění NAAGu z dendritických váčků postsynaptického neuronu zpět do synaptické štěrbiny, což vede k následné aktivaci presynaptického mGluR3 receptoru a konečně i k inhibici neurotransmise (Nordengen a kol., 2020). Exprese receptoru mGluR3 byla popsána i na astrocytech, které po aktivaci NAAGem produkují neuroprotektivní faktor TGF β a zvyšují tak odolnost neuronů vůči noxám (např. NMDA, kyanid draselný) (Bruno a kol., 1998a; Bruno a kol., 1998b; Thomas a kol., 2001a). Ilustrace metabolismu NAAGu na nervové synapsi je zobrazena na obrázku 9. NAAG působí neuroprotektivně dvojím způsobem. Jednak snižuje množství uvolněných neurotransmiterů, a tím inhibuje neurotransmisi, což vede ke snížení rizika excitotoxicity (Doble, 1999). Dále působením na mGluR3 receptory astrocytů stimuluje k produkci neuroprotektivního TGF-β (Bruno a kol., 1998a; Bruno a kol., 1998b). Podání inhibitoru GCPII 2-fosfonomethylpentandiové kyseliny (PMPA) vede k prodloužení působení NAAGu a tudíž také vykazuje neuroprotektivní efekt (Slusher a kol., 1999; Thomas a kol., 2001a; Thomas a kol., 2001b; Tortella a kol., 2000).

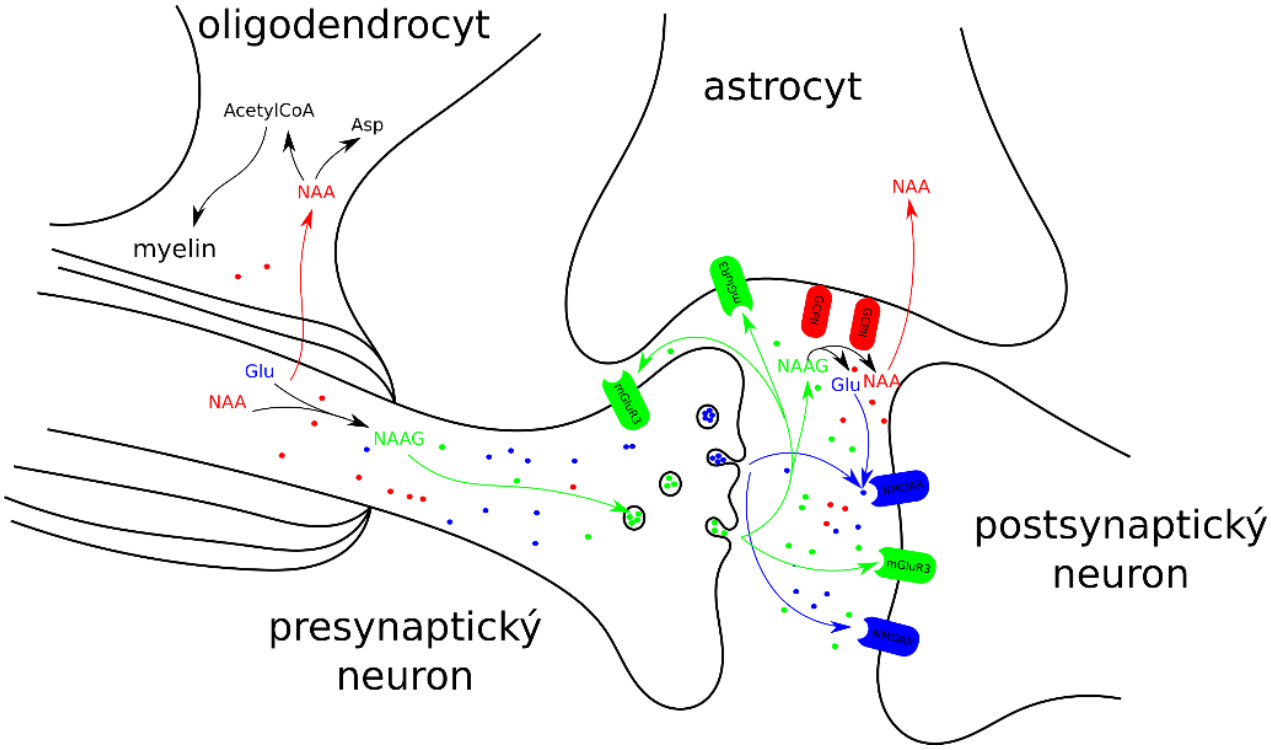

Obrázek 9 – Schématické znázornění metabolismu NAAGu na nervové synapsi. NAAG (znázorněn zeleně) je syntetizován z NAA (znázorněn červeně) a glutamátu (znázorněn modře) NAAG syntetázou I nebo II v těle neuronu. Následně je transportérem sialinem dopravován do synaptických váčků, z kterých se po depolarizaci neuronu uvolňují do synaptické štěrbiny. Nerozštěpený NAAG je schopen aktivovat mGluR3 receptory (zeleně) jak na obou neuronech, tak i na astrocytech. V synaptické štěrbině je pak aktivitou GCPII zpětně rozštěpen na NAA a glutamát. Pokud dochází k výraznějšímu štěpení NAAGu, tak může vzniklý glutamát aktivovat NMDAR receptory (modře). NAA může být též zdrojem acetylových skupin pro syntézu myelinu v oligodendrocytu.

Neuroprotektivní efekt inhibice GCPII pomocí PMPA byl pozorován i *in vivo* na modelech mozkové ischemie, kde dochází k excitotoxicitě vzhledem k přemíře intracelulárního vápníku indukovaného aktivovanými NMDA receptory. Po inhibici pomocí PMPA došlo k redukci postižené oblasti ischemickým postižením, v důsledku uzavření střední mozkové tepny, v závislosti na dávce až o 54 % (Slusher a kol., 1999). Obdobně inhibice pomocí 2-[(pentafluorophenylmethyl)hydroxyphosphinyl]methyl)-pentanediové kyseliny podané jednu hodinu po provedení přechodného uzávěru střední mozkové tepny snížila velikost infarktového ložiska o více než 50 % (Williams a kol., 2001). Obdobně došlo k redukci postižení i v modelu novorozeneckého ischemického postižení jednostrannou okluzí karotické tepny (Cai a kol., 2002). Neuroprotektivní efekt byl prokázán i v modelu traumatického poranění mozku (Zhong a kol., 2006).

Vzhledem k ovlivnění zejména glutamatergní neurotransmise pomocí mGlu3 receptoru lze předpokládat aktivitu u těch chorob, kde je tento typ signalizace klíčový. Schizofrenie

je psychiatrické onemocnění, kde je narušena řada neurotransmiterových systémů. Zatímco historicky se uvažovalo spíše o postižení dopaminergního systému, tak dle novějších poznatků, a v souvislosti s podobnými příznaky vyvolanými fencyklidinem, antagonistou NMDA receptoru, se ukazuje, že je zde i podstatná úloha glutamátergního systému (Tsai a Coyle, 2002). V případě fencyklidinového modelu vede nižší aktivita GABAergních neuronů v prefrontálním kortexu, kvůli snížené signalizaci NMDA receptoru, k desinhibici a aktivaci glutamátergních a dopaminergních neuronů vedoucím k příznakům choroby. Aktivace mGluR3 receptorů snižuje glutamátergní neurotransmisi a tudíž i snižuje příznaky v fencyklidinovém zvířecím modelu (Cartmell a kol., 1999; Moghaddam a Adams, 1998), obdobně funguje i inhibice GCPII (Olszewski a kol., 2017).

Lze předpokládat, že primárně glutamatergní signalizace bolesti je regulována ko-neurotransmiterem NAAGem, neboť primární neuron senzitivní dráhy, pseudounipolární T buňka spinálního ganglia obsahuje NAAG a exprimuje metabotropní mGluR3 receptory (Cangro a kol., 1987; Carlton a kol., 2001; Neale a kol., 2005). To umožňuje vznik negativně zpětnovazebné smyčky, kdy je cestou NAAGu snížena glutamátové neurotransmise. Tato hypotéza byla potvrzena na různých *in vivo* modelech bolesti, kdy podání látky inhibující GCPII snižovalo bolestivou odpověď (Chen a kol., 2002; Kozikowski a kol., 2004; Neale a kol., 2005; Yamamoto a kol., 2008; Yamamoto a kol., 2001a; Yamamoto a kol., 2001b; Yamamoto a kol., 2007).

U amyotrofické laterální sklerózy je považována glutamátem zprostředkovaná excitotoxicita za jeden z důležitých patogenetických faktorů (Blasco a kol., 2014; Foran a Trotti, 2009; Mennini a Bendotti, 2004; Shaw a Ince, 1997; Van Den Bosch a kol., 2006). S tím jsou spojené změny v koncentracích excitačních aminokyselin, přičemž v literatuře dochází k nesouladům. U nemocných s amyotrofickou laterální sklerózou bylo pozorováno zvýšení hladiny glutamátu, NAAGu i NAA v mozkomíšním moku. Naopak v předních míšních rozích bylo množství NAAGu i NAA u některých pacientů sníženo (Rothstein a kol., 1990). Bylo zachyceno i navýšení plasmatické koncentrace glutamátu a pokles tkáňových koncentrací aspartátu, NAA i NAAG (Plaitakis a Constantakakis, 1993). Naopak v práci Perry a kol. (1990) zvýšení koncentrace glutamátu v plasmě a mozkomíšním moku u nemocných nepozorovali. V práci Spreux-Varoquaux a kol. (2002) bylo zvýšení koncentrace glutamátu v mozkomíšním moku pozorováno u 40,8 % pacientů, převážně u pacientů se spinálním začátkem choroby, dominujícím postižením končetin a výraznějším poškozením svalstva. Co se týče aktivity GCPII, tak u amyotrofické laterální sklerózy bylo pozorováno zvýšení aktivity GCPII s korespondujícími lokálními redukcemi tkáňových koncentrací endogenního aspartátu,

glutamátu, NAA i NAAG (Tsai a kol., 1991). V myším modelu amyotrofické laterální sklerózy pozorován signifikantní účinek inhibitorů GCPII. U kohorty léčené inhibitorem 2-fosfonomethylpentandiovou kyselinou docházelo k pozdějšímu nástupu neurologických příznaků a signifikantně se prodloužila doba přežití, až o 15 % průměrné doby (Ghadge a kol., 2003).

Ovlivněním kognitivních schopností NAAG neurotransmiterovým systémem se zevrubně zabývá práce (Neale a Olszewski, 2019), zkráceně, inhibice GCPII event. vyřazení genu pro GCPII zlepšuje u myší dlouhodobou paměť v testu rozpoznávání objektu (Janczura a kol., 2013), přičemž mechanismem je patrně prodloužené působení nerozštěpeného NAAGu na metabotropní mGluR3 receptor (Olszewski a kol., 2017). Bylo pozorováno i zlepšení v testech krátkodobé paměti v rámci trojitého transgenního modelu Alzheimerovy choroby a v modelu akutní intoxikace ethanolem (Olszewski a kol., 2017). V případě ethanolové intoxikace byla současně po podání inhibitoru zlepšena motorická koordinace, přičemž obdobný efekt byl pozorován i po podání agonisty 2. třídy metabotropních glutamátových receptorů, což dále podporuje hypotézu o účasti NAAGu. Obdobně v rámci modelu experimentální imunitní encefalitidy byl prokázán dávkově závislý prokognitivní efekt inhibitoru GCPII – PMPA v Barnesově bludišťovém testu (Hollinger a kol., 2016). Studie Neale a Olszewski (2019) přisuzuje prokognitivní efekt inhibice GCPII a NAAGu jednak zvětšením dynamického rozsahu synaptické transmise, cestou presynaptických mGluR3 receptorů, tak i cestou postsynaptických receptorů, snížením hladiny cAMP a tím i z buněčného hlediska ovlivněním dlouhodobé potenciace resp. deprese.

Za choroby spjaté s výrazným narušením NAA-NAAG systému patří Canavanova choroba a Pelizaeus-Merzbacherova choroba, případně „Pelizaeus-Mezbaracher-like“ choroba. Zatímco Cavanova choroba je porucha odbourávání N-acetylaspartátu při defektním genu pro aspartylacylasu (lokalizované v oligodendrocytech) vedoucí k akumulaci NAA i NAAG a defektní myelinizaci cestou nedostatku acetátu odvozeného z NAA (Namboodiri a kol., 2006), tak Pelizaeus-Merzbacherova choroba je dána mutací genu pro proteolipidový protein, který je složkou myelinu nervových buněk (Burlina a kol., 2006). Elevace NAAGu byla pozorována i u „Pelizaeus-Merzbacher-like“ choroby (Sartori a kol., 2008) způsobené mutací genu GJC2, která vede k produkci defektního connexinu-47 zodpovědného za tvorbu „gap junctions“ v oligodendrocytech. Ztráta vede k dysfunkci „polokanálu“ (Diekmann a kol., 2010) a hypomyelinizaci.

I v další případech (Wolf a kol., 2004) byla popsána asociace mezi vyšší hladinou NAAGu a hypomyelinizací. Jednou z možných hypotéz je degradace NAA pomocí aspartoacylázy

oligodendrocytu a využití takto vzniklých acetylů jako substrátů pro tvorbu myelinu (Francis a kol., 2016), což je v souladu s prací Singhal a kol. (2017), kde u myší s defektní syntézou NAA dochází ke snížení množství sfingomyelinu a sulfatidů. Bylo popsáno i ovlivnění metylace H3 histonů na základě zvýšení koncentrace α-ketoglutarátu v oligodenrocytech po přidání NAA (Singhal a kol., 2017).

1.4.2 Tenké střevo

Deriváty kyseliny listové, vitaminu B9, tvoří klíčové kofaktory pro metabolismus jedno-uhlíkatých zbytků v organismu (Ducker a Rabinowitz, 2017; Scaglione a Panzavolta, 2014). Jedno-uhlíkaté zbytky se používají při syntéze složek nukleových kyselin – jmenovitě při tvorbě purinů a thymidinu a dále při metylačních reakcích organismu, jako např. při metylacích DNA či při biosyntéze methioninu a cholinu. Katalyticky aktivní folát je v naprosté většině reakcí v redukované formě tetrahydrofolátu, přičemž pro zajištění retence je v buňkách, a tedy i v tkáních, polyglutamylován (Boarman a Allegra, 1992; Butterworth a kol., 1969; Darcy-Vrillon a kol., 1988; Zhao a kol., 2009). V důsledku toho je i naprostá většina přirozeně dostupného folátu v dietě ve formě různě N5 resp. N10 substituovaného polyglutamylovaného tetahydrofolátu, většinou ve formě 5-methyltetrahydrofolátu (Zhao a kol., 2009).

Polyglutamylovaná forma tetrahydrofolátu není přímo vstřebávána (Butterworth a kol., 1969; Darcy-Vrillon a kol., 1988; Rosenberg a kol., 1969), ale je sliznicí tenkého střeva, duodena a proximálního jejuna metabolizována na monoglutamylovanou formou 5-methyltetrahydrofolátu, která se tak stává dominantní transportní formou v organismu (Damaraju a kol., 2008; Wright a kol., 2007). Toto potvrzuje i neschopnost dominantního transportéru folátu ve střevě („proton-coupled folate transporter“) vázat polyglutamylované foláty (Qiu a kol., 2007). Oproti tomu kyselina listová, oxidovaná forma folátu, se vstřebává nezměněna a je metabolizována na 5-methyltetrahydrofolát v játrech (Wright a kol., 2007).

Byly identifikovány dva enzymy zodpovědné za odštěpení glutamátů lokalizované ve sliznici jejuna (Reisenauer a kol., 1977). Zatímco první je vázán na membránu, tvoří dimer s exopeptidázovou aktivitou, závislou na koncentraci zinku (Halsted, 1991; Chandler a kol., 1986), s pH optimem dle původní práce v rozmezí 5,5-7,5, a byl identifikován jako GCPII (McNulty a Pentieva, 2004), druhý je lokalizován intracelulárně v lysozomech, má endopeptidázovou aktivitu a pH optimum je posunuto výrazněji do kyselé oblasti – pH 4,5 (Wang a kol., 1986) a dále je označovan jako γ-glutamyl hydroláza. Zatímco u člověka a prasete jsou ortology GCPII v tenkém střevě přítomny, a lze tedy předpokládat, že jsou zodpovědné za konjugázovou aktivitu (McNulty a Pentieva, 2004), tak u hlodavců (myš, potkan) nalezeny

nebyly a lze předpokládat, že odštěpování glutamátů zprostředkovává γ-glutamyl hydroláza (Shafizadeh a Halsted, 2007).

1.4.3 Urogenitální trakt

GCPII je velmi silně v exprimována urogenitálním traktu (viz kapitola 1.3). Prostata, resp. ledviny jsou orgány s největší expresí GCPII u člověka, resp. u myši. Přesto o fyziologické funkci GCPII zde je známo velmi málo. Vzhledem k histologické lokalizaci enzymu na luminální straně epiteliálních buněk na cytoplazmatické membráně byla navržena hypotéza o funkci GCPII jako folátovém transportéru (Yao a kol., 2010). Tato práce též spekuluje o reabsorpci folátu z moče v ledvinách. Obdobně i v prostatě bylo pomýšleno o blíže nespecifikované transportní funkci GCPII, což bylo dále podpořeno nálezem folát vázajícího proteinu o velikosti 100 kDa v prostatickém lyzátu (Holm a kol., 1993). Tyto hypotézy však nicméně nebyly zatím experimentálně potvrzeny.

1.4.4 Angiogeneze

Výrazná exprese GCPII v endoteliích novotvořených cév (viz kapitola 1.3), ať již při procesu obnovy tkání, nebo při maligní transformaci, nasvědčuje úloze v angiogenezi. Myš s vyřazeným genem pro GCPII vykazuje sníženou angiogenezi pro nižší schopnost invaze skrz extracelulární matrix (Conway a kol., 2006). Nepřítomnost GCPII, v důsledku nižší aktivace β_1 integrinů, obzvláště narušuje motilitu na lamininovém povrchu. Alterace integrinové signalizace vede ke snížení aktivace PAK-1 kinázy, která tvoří jeden z proteinů klíčových pro architekturu cytoskeletu a cílenou migraci (Conway a kol., 2006). Tato činnost je dána nejspíše aktivací peptidů vznikajících proteolytickým štěpením lamininu, např. LQE, IEE, LNE (Conway a kol., 2013; Conway a kol., 2016). Tyto peptidy jsou aktivovány odštěpením glutamátu, a zejména kombinace dipeptidu leucyl-glutaminu (LQ) a glutamátu vede k zvýšení buněčné adheze cestou aktivace β_1 integrinu a FAK kinázy (Conway a kol., 2016).

Alternativní hypotézou funkce GCPII v angiogenezi je zajišťování dostatečného množství kofaktoru tetrahydrobiopterinu doposud neznámým způsobem pro funkci endotelové NO synthasy (Gordon a kol., 2008). Vzniklý oxid dusnatý stimuluje angiogenezi (Duda a kol., 2004).

GCPII není na lidských endoteliálních buňkách pocházejících z pupečníkové žíly (HUVEC) standardně přítomna, ale lze ji *in vitro* indukovat působením kondiciovaného media některých nádorových linií (např. MDA-MB-231, SK-RC-13, HCT-15) (Liu a kol., 2011; Nguyen a kol.,

2016). Na otázku, která složka je zodpovědná za indukci, se pokusili autoři rozdělit medium do frakcí podle molekulové hmotnosti. Zatímco první studie (Nguyen a kol., 2016) ukazuje efekt ve frakci 10-50 kDa, přičemž nižší hmotnosti nestuduje, tak druhá studie (Liu a kol., 2011) popisuje efekt ve frakci menší než 3 kDa a ve frakci větší než 30 kDa, která však také není podrobněji rozdělena. Porovnáním tak lze usoudit na efekt složek v oblastech menších 3 kDa, ale i složek o velikosti 30-50 kDa. Efekt indukce GCPII na buňky HUVEC byl pozorování i *in vivo* v modelu xenotransplantátu, kdy byla injektována směs buněk HUVEC s nádorovou linií (Nguyen a kol., 2016).

Úlohu GCPII v angiogenezi na sítnici a patogenezi retinopatií byla studovaná na modelu kyslíkem indukované retinopatie (Grant a kol., 2012). Na novotvořených endoteliích na sítnici („cévních trsech“) byla pozorována exprese GCPII. Zatímco za fyziologického stavu nebyla u myší s vyřazeným genem pro GCPII pozorována změna v architektuře cév a jejich vývoji, tak při relativní hypoxii po odejmutí kyslíku v rámci modelu kyslíkem indukované retinopatie byla vzniklá patologická angiogeneze u myší s vyřazeným genem pro GCPII výrazně redukována. Architektura i struktura cév se jevila normálnější – byla méně chaotická a organizovanější, množství „cévních trsů“ bylo sníženo, rozsah avaskulární zóny byl snížen, perfuse zlepšena. Obdobných výsledků bylo dosaženo po podání inhibitorů GCPII systémově i intravitreálně. Lze předpokládat, že efekt nepřítomnosti GCPII aktivity na angiogenezi nebyl zprostředkován růstovým faktory VEGF ani angiopoetinem 2, vzhledem k tomu, že množství transkriptů příslušných k daným růstovým faktorům zůstalo nezměněno.

1.5 Patologické funkce

1.5.1 Nádorová tkáň

Vzhledem k výrazné expresi GCPII v nádorové tkáni, a to jak na úrovni nádorových buněk, tak i buněk nádorových endotelií (viz kapitola 1.3), nabízí se myšlenka úlohy GCPII při vzniku nádoru a nádorové progresi. Klinicky byl nejvíce studován efekt exprese GCPII v případě nádoru prostaty, většinou však s poměrně rozporuplnými výsledky, kdy intenzita exprese GCPII neodpovídala agresivitě onemocnění (Bostwick a kol., 1998), korelace nebyla výrazná (Minner a kol., 2011), či naopak se signifikantními rozdíly (Perner a kol., 2007). Obtížnost studia karcinogeneze zhoršuje i rozdílný expresní profil a fyziologie běžně dostupných *in vivo* modelů, kdy hlodavci mají výrazně nižší četnost prostatických nádorů oproti lidem a je nutno používat transgenních modelů.

Co se týče mechanismu, byla pro svoji enzymatickou funkci odštěpování glutamátu z polyglutamylovaných folátů zvažována funkce v rámci vstřebávání derivátů kyseliny listové. Přítomnost GCPII zlepšuje proliferaci v případě fyziologické koncentrace folátu a současné přítomnosti penta-γ-glutamylovaného folátu (Yao a Bacich, 2006). Byla pozorována vyšší proliferace a přibližně 2× vyšší akumulace folátu v případě prostatické buněčné linie PC3 exprimující GCPII oproti linii PC3 bez exprese za podmínek nízké koncentrace folátu v mediu (pod 50 nM) (Yao a kol., 2010). To by mohlo svědčit pro transportní funkci GCPII.

Zajímavou hypotézou týkající se eventuální prokarcinogenní funkce metabolitu NAAGu je možnost, že by v případě agresivnějších malignit NAAG sloužil jako zdroj glutamátu (Nguyen a kol., 2019). Autoři ukazují, že agresívnější nádory, zastoupené buněčnými liniemi B-buněčného lymfomu či ovariálního karcinomu, přeměňují více dodaného glutaminu na peptid NAAG. Byla zvažována role GCPII i v rámci nádorové glutámátové signalizace (Foss a kol., 2012).

Obdobně vyšší koncentrace NAAGu pozorovali i v klinických vzorcích glioblastomu oproti gliomu stupně II-III. Obdobné změny koncentrace NAAGu, korelující s velikostí tumoru, byly detekovány i v plasmě pacientů a v případě myšího modelu xenograftu s Myc-inducibilní lidskou linii P493-6. V případě exogenní aplikace NAAGu přímo do nádorů docházelo k zvětšení tumorů. Inhibice GCPII pomocí PMPA, event. použití buněčných linií bez exprese GCPII vedlo naopak k signifikantnímu poklesu velikosti. V nádorech docházelo k přeměně NAAGu na NAA, aspartát a glutamát. Změny v koncentraci NAAGu a NAA se nachází i v případě nádorů ovaria (Fong a kol., 2011).

Řada prací se zabývá případnou úlohou GCPII v nádorové a buněčné signalizaci, která je detailněji popsána v kapitole 1.2. Ve stručnosti – aktivace molekul GCPII pomocí monoklonální protilátky J591 spouští proliferativní MAPK signální dráhu včetně kináz MAPK38, ERK1/2 (Colombatti a kol., 2009; Perico a kol., 2016) a anti-apoptotickou mTOR/AKT/BAD signální dráhu (Perico a kol., 2016). Tato aktivace GCPII zvyšuje schopnost buněčné linie LNCaP tvořit kolonie v matrigelu, a to jak v přítomnosti séra, tak i bez jeho přítomnosti. *In vitro* identifikovaná signalizace GCPII, např. aktivace β_1 integrinu, fosforylace EGFR Y^{1086}, byla prokázána i na vzorcích nádorové prostatické tkáně vyššího stupně malignity (Perico a kol., 2016).

V experimentálním transgenním myším modelu karcinomu prostaty TRAMP byl růst nádorů v případě vyřazení genu GCPII signifikantně pomalejší (Caromile a kol., 2017), přičemž byla pozorována změna signalizace z Ras/MAPK dráhy na signální dráhu PI3K/AKT. Tento přesmyk v signalizaci byl vysvětlen rozdílem v signalizaci IGF-1R receptoru, kdy GCPII kompetuje s β_1 integrinem o interakci s IGF-1R a RACK1 (Caromile a kol., 2017) – blíže obrázek 8 na straně 23. Přes jiný typ signalizace a zpočátku pomalejší růst tumorů v TRAMP modelu se však postupem času vyvinou karcinomy i v případě vyřazení genu GCPII, což nasvědčuje tomu, že i aktivace méně potentní signální dráhy Ras/MAPK k onkogenezi postačuje (Caromile a kol., 2017).

V neposlední řadě, jak již bylo uvedeno v kapitole 1.2, rychlejší degradace cyklinu B vlivem GCPII v rámci APC komplexu vede k urychlení konečné fáze mitózy (Rajasekaran a kol., 2008). Snížení efektivity tohoto kontrolního bodu vede ke snížení chromozomální stability, může vést k aneuploidii a tím i k riziku vzniku nádoru.

Velmi rozsáhlá skupina prací analyzuje užití GCPII jako cíle pro zobrazení nádorů např. pomoci pozitronové emisní tomografie, event. uvažuje GCPII jako molekulárního cíle ke směřování léčiv (např. radioligandů) – podrobněji rozepsáno v kapitole 1.6 na straně 38.

1.5.2 Imunopatologické stavy

Exprese GCPII byla zaznamenána, jak již bylo také uvedeno v kapitole 1.3, ve sliznici střeva v rámci idiopatických střevních zánětů – a to jak u Crohnovy choroby (Rais a kol., 2016; Zhang a kol., 2012), tak i v případě ulcerózní kolitidy (Rais a kol., 2016). Obdobných výsledků bylo dosaženo i v myších experimentálních modelech idiopatického střevního zánětu – jako jsou dextran sulfátový model, model myši deficientní v genu pro IL10, či model po podání trinitrobenzensulfonové kyseliny (Date a kol., 2017; Rais a kol., 2016). Inhibice GCPII pomocí inhibitoru PMPA, podaného systémově nebo lokálně, vedla u těchto modelů k poklesu aktivity

onemocnění i histologické závažnosti (Date a kol., 2017; Peters a kol., 2019; Rais a kol., 2016). Pro roli GCPII v etiopatogenezi svědčí i fakt, že podání dextran sulfátu sodného vedlo u myši s deficiencí v genu pro GCPII k výrazně nižším projevům střevního zánětu (Rais a kol., 2016). Na základě role GCPII ve střevních zánětech a úloze NAAGu v transmisi zánětlivé bolesti skrze mGluR3 receptor je zvažována komplexnější úloha NAAGu v zánětlivé odpovědi (Neale a Yamamoto, 2020). V souvislosti s tím byly v řadě převážně francouzských studií zkoušeny protizánětlivé účinky NAAGu. NAAG byl s rozdílným efektem zkoušen jako stabilizátor žírných buněk a protizánětlivý peptid v rámci řady očních imunitně podmíněných onemocnění jako jsou alergie, jarní keratokonjuktivitida, oční aktivní anafylaxe, syndrom suchého oka (Brignole-Baudouin a kol., 2009; Denis a kol., 1998; Goldschmidt a Luyckx, 1996; Leonardi a kol., 2007). Obdobně byl s částečným efektem zkoušen v terapii alergické rinitidy (Althaus a Pichler, 1994; Datz a kol., 1988). Vzhledem ke klinickému účinku byly oční kapky s 4,9 % roztokem sodné soli NAAGu schváleny ve Francii pod názvem „Naabak“ k léčbě očních alergií.

Mechanismus účinku byl přisuzován inhibici aktivace komplementu (Feuillard a kol., 1991), inhibici syntézy leukotrienů (Jambou a Lapalus, 1990), ale i snížení adheze leukocytů k aktivovaným endoteliálním buňkám. NAAG v koncentraci 1-10 mM v závislosti na dávce inhiboval, jak klasickou, tak i alternativní cestu aktivace komplementu (Feuillard a kol., 1991). NAAG od koncentrace 10^{-9} M, inhiboval syntézu leukotrienů v makrofágové buněčné linii po aktivaci vápníkovým ionoforem (Jambou a Lapalus, 1990). NAAG dále ve výsledné koncetraci 2,45 % inhiboval adhezi leukocytů na endoteliální linii HUVEC stimulovanou pomocí TNFAα cestou redukce exprese adhezivních molekul na TNFα aktivovaných endoteliích (Bouhlal a kol., 2002).

Vzhledem k známým fyziologickým koncentracím NAAGu lze očekávat, že inhibiční efekt na aktivaci komplementu bude limitován striktně na oblast nervového systému, zatímco ovlivnění leukotrienového metabolismu může být rozsáhlejší. O fyziologickém efektu na adhezi leukocytů vzhledem k použité extrémně vysoké koncentraci NAAGu lze jen spekulovat.

1.6. GCPII jako terapeutický a diagnostický cíl v onkologii

Jak již bylo uvedeno v dřívější kapitole (1.3), GCPII se exprimuje v řadě nádorů jak na samotných nádorových buňkách, tak i na nádorových endoteliích. Člověk exprimuje nejvíce v prostatě a jejích nádorech, kde množství GCPII přibližně 10–80× převyšuje ostatní tkáně (Sokoloff a kol., 2000). Odtud mimo jiné také vznikl alternativní název PSMA. Tato relativně specifická lokalizace GCPII se přímo nabízí k užití GCPII jako tkáňově specifického nádorového markeru pro diagnostiku a terapii, či jejich kombinaci, tzv. teranostiku.

Naprostá většina výzkumu užití GCPII jako tumorového markeru pro teranostiku se zabývala radioligandy GCPII. V počátcích bylo pro diagnostické účely zvažováno použití protilátek. První takto použitou protilátkou, přes epitop v intracelulární oblasti, se stala překvapivě 7E11-C5.3 v podobě konjugátu s chelatovaným ^{111}In, známá jako (^{111}In) capromab pendetid. Byla použita, schválena americkou lékovou agenturou US Food and Drug administration (FDA) a registrována pod komerčním názvem Prostascint^{TM} pro diagnostiku karcinomu prostaty (Kahn a kol., 1994) pomocí jednofotonové výpočetní tomografie (SPECT). Spolehlivost sice nebyla vysoká, ale přesto lepší než užití positronové emisní tomografie s ^{18}F fluordeoxyglukosou (Haseman a kol., 1996). Senzitivita v poslední studii dosahovala 62 % a specifita 72 % (Manyak a kol., 1999). Obdobně varianty capromabu pendatidu s chelatovaným ^{90}Y a ^{177} Lu byly rovněž neúspěšně zkoušeny v terapii. Podání (^{90}Y) capromab pendetidu nevedlo k biochemickým remisím v podobě poklesu hladiny PSA, a navíc vykazovalo výraznou hematologickou toxicitu (Deb a kol., 1996; Kahn a kol., 1999). Malou efektivitu lze objasnit cílením protilátky 7E11-C5.3 na intracelulární úsek a proto i neschopností vázat se na živé buňky (Rahbar a kol., 2018).

Lepších výsledků bylo dosaženo při použití humanizované protilátky J591 proti extracelulární části GCPII. Zkoušenými konjugáty J591 s ^{111}In a ^{177}Lu bylo u hormonálně nezávislých nádorů prostaty dosaženo souhrnné senzitivity 94 % (32/34) pro kostní a 72 % (13/18) pro měkkotkáňové léze (Bander a kol., 2003). Vzhledem k vhodnějším charakteristikám positronové emisní tomografie (PET) byl hodnocen i humanizovaný konjugát ^{89}Zr-huJ591, kde z 12 biopticky ověřených lézí bylo 11 PET avidních (Pandit-Taskar a kol., 2014). ^{111}In-J591 konjugát byl, pro expresi GCPII na nádorových endoteliích, zkoušen i na jiných nádorech než karcinom prostaty. Použitím scintigrafie bylo správně zobrazeno 74 % (20/27) skeletálních lézí, 53 % (18/34) lymfatických uzlin a 64 % (70/109) měkkotkáňových či ostatních lézí (Pandit-Taskar a kol., 2015). Terapeuticky u hormonálně nezávislého karcinomu prostaty byl použit humanizovaný konjugát ^{177}Lu-J591, který v klinické studii fáze I vykázal u 11 % (4/35)

pacientů ≥ 50 % pokles PSA a u 46 % (16/35) vedl k stabilizaci PSA (Bander a kol., 2005). Obdobných výsledků bylo dosaženo i v klinické fázi II, kde ≥ 50 % pokles PSA byl u 10 % (3/30) pacientů a ke stabilizaci/poklesu PSA došlo u 57 % (17/30) pacientů (Tagawa a kol., 2008). Po dalším rozšíření kohorty došlo u 10,6 % (5/47) k poklesu ≥ 50 % PSA, u 36,2 %, (17/47) byl pokles ≥ 30 % PSA a celkem byl zaznamenán pokles PSA u 59,6 % (28/47) pacientů (Tagawa a kol., 2013). Maximální tolerovaná dávka byla limitována zejména hematologickou toxicitou, obzvláště trombocytopenií 4.stupně, která se vyskytovala až ve 47 % (22/47) případů. V jiných studiích, jak preklinických tak klinických, byly zkoušeny v kombinaci s protilátkou J591 i jiné radionuklidy. Např. ^{90}Y, který vedl k poklesu PSA > 50 % u 7 % (2/29) pacientů resp. ke stabilizaci PSA u 21 % (6/21) (Milowsky a kol., 2004). Dále byly testovány také radioizotopy ^{213}Bi (McDevitt a kol., 2000), ^{131}I (Tagawa a kol., 2010).

Použití protilátek s radioligandy v diagnostice však má výrazné limity, neboť vzhledem ke své poměrně veliké molekulové hmotnosti mají limitovanou schopnost se dostávat do nádorů, což si vynucuje poměrně dlouhé časy mezi podáním radiofarmaka a vlastním zobrazováním a s tím i spojenou větší radiační zátěž (Rahbar a kol., 2018). Snaha byla proto použít látky s menší molekulovou hmotností, např. fragmenty protilátek „single chain“ (Frigerio a kol., 2017; Frigerio a kol., 2019; Nawaz a kol., 2017; Viola-Villegas a kol., 2014), „nanobodies“ (Evazalipour a kol., 2014; Chatalic a kol., 2015), aptamery (Jiao a kol., 2021), ale zejména inhibitory GCPII (Neels a kol., 2021).

Radioaktivně značené inhibitory GCPII se většinou skládají ze struktury lysin-močovina-glutamát spojené linkerem s přímo navázaným fluorem ^{18}F, resp. chelatační skupinou vázající vhodný radionuklid. Zkoušeny jsou radioizotopy vhodné jak pro PET (^{18}F, ^{68}Ga, ^{64}Cu, ^{44}Sc, ^{152}Tb), SPECT (^{111}In, ^{99m}Tc), tak i léčbu (^{177}Lu, ^{225}Ac) (Neels a kol., 2021). V množství různých inhibitorů stojí za zmínku zejména [^{18}F]-DCFPyL (piflufolastat) (Keam, 2021), pod komerčním názvem PYLARIFY®, a [^{68}Ga]Ga-PSMA11 (gozetotid) (Bois a kol., 2020), známý jako isoPROtrace-11. Tyto látky totiž byly schváleny FDA k medicínskému využití jako PET sondy pro zobrazování relapsů nádoru prostaty. V klinické multicentrické studii 2/3 fáze „OSPREY“ hodnotící užití [^{18}F]-DCFPyL bylo dosaženo na skupině 93 pacientů se suspektním relapsem karcinomu prostaty, resp. metastatickým karcinomem prostaty, uspokojivé senzitivity pro léze mimo prostatu 95,8 %. Oproti tomu záchyt u nově diagnostikovaných 252 pacientů byl výrazně nižší, senzitivita byla pouze 40,3 % (Pienta a kol., 2021). I když specifita byla 97,9 % (Pienta a kol., 2021), tak to vedlo FDA ke schválení indikace pouze pro užití u relapsů. Obdobně fungovalo i zobrazování pomocí PET sondy [^{68}Ga]Ga-PSMA11 u rekurentního karcinomu prostaty. Na skupině 2533 pacientů PET pozitivita korelovala s hodnotou PSA, přičemž

pozitivita na PET/CT byla zachycena ve 43 % pro PSA ≤ 0,2 ng/ml; 58 % pro PSA > 0,2 a ≤ 0,5 ng/ml; 72 % pro PSA > 0,5 a ≤ 1 ng/ml a 93 % pro PSA > 10 ng/ml (Afshar-Oromieh a kol., 2021). Porovnání [^{68}Ga]Ga-PSMA11 s PET sondou ^{18}F-fluormethylcholinem ukázalo, že obě metody jsou podobně citlivé k detekci relapsu karcinomu prostaty po radikální prostatektomii (Emmett a kol., 2019).

Co se týče vnitřní radioterapie karcinomu prostaty, vykázal naprosto výjimečné výsledky inhibitor ^{177}Lu-PSMA-617, který tak tvoří jeden z úspěšných příběhů nukleární medicíny (Czernin a Calais, 2021). ^{177}Lu-PSMA-617 byl taktéž schválen FDA pro klinické použití. Již v rámci klinické studie 2. fáze „LuPSMA“ dosáhlo 57 % (17/30) nemocných > 50 % poklesu PSA. Obdobně objektivní odpovědi v uzlinách či orgánech dle zobrazovacích metod dosáhlo 82 % (14/17) pacientů. Z nejčastějších nežádoucích účinků byla pozorována suchost v ústech (26 pacientů - 87 %, stupeň 1), přechodná nevolnost (15 pacientů - 50 %, stupeň 1-2) a únava (15 pacientů – 50 %, stupeň 1-2). Naproti tomu trombocytopenie stupně 3-4 se oproti konjugátům protilátek vyskytovala výrazně méně často – u 4 pacientů (13 %) (Hofman a kol., 2018). V rámci klinické studie 3. fáze „VISION“ bylo hodnoceno použití ^{177}Lu-PSMA-617 se standardní léčbou oproti standardní léčbě u metastatického hormonálně rezistentního karcinomu prostaty. Na základě 831 zařazených pacientů s dobou sledování 20,9 měsíců byl u ^{177}Lu-PSMA-617 léčené skupiny pozorován výrazně delší čas do progrese – medián 8,7 měsíce vs. 3,4 měsíce. Obdobně se léčbou prodloužila i doba celkového přežití z 11,3 měsíců na 15,3 měsíce (Sartor a kol., 2021). Jeden z hlavních nových nežádoucích účinků – xerostomie v důsledku postižení slinných žláz – je v souladu se zvýšenou akumulací radionuklidu v této oblasti, kdy akumulace 1,4 Gy/GBq přesahuje dávku jak v ledvinách (0,75 Gy/GBq), tak i v kostní dřeni (0,03 Gy/GBq) (Kratochwil a kol., 2016). Tato akumulace není překvapivá, vzhledem k již popisované expresi GCPII ve slinných žlázách (Wolf a kol., 2010). Pro ilustraci struktury těchto nových FDA schválených léčiv a diagnostik jsou zobrazeny na obrázku 10.

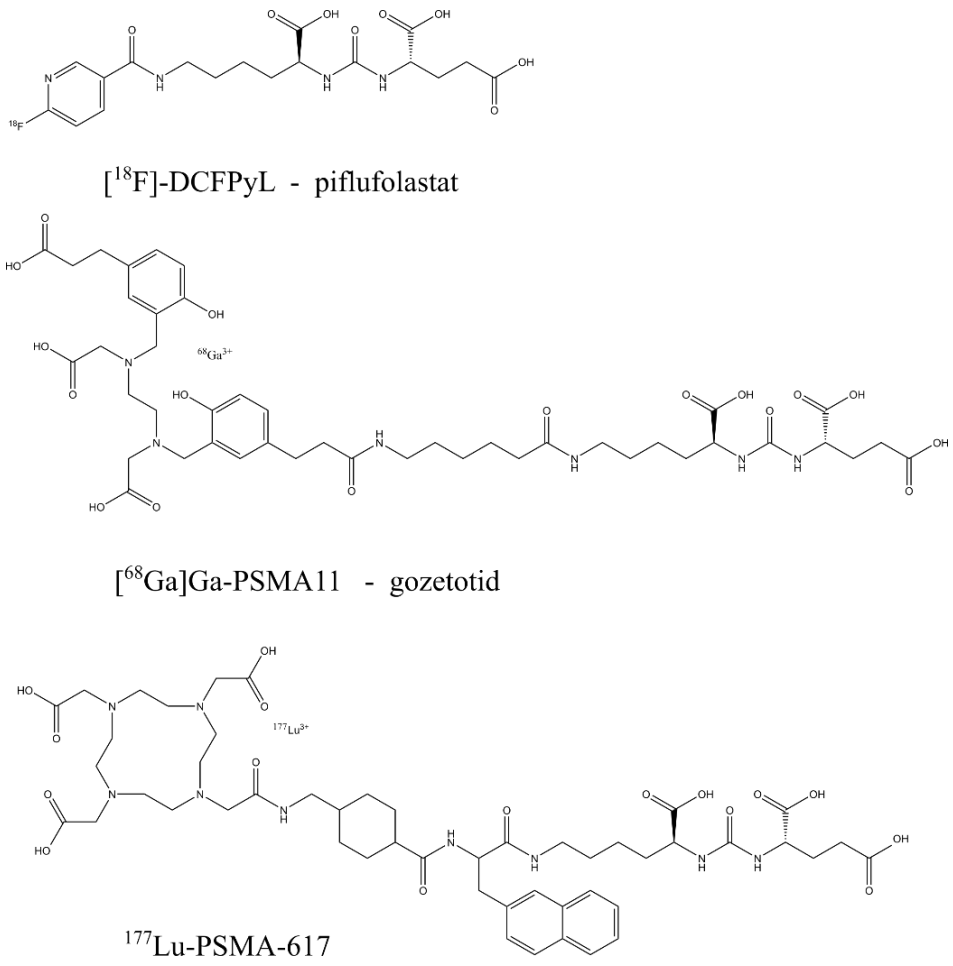

Obrázek 10 – Chemické struktury vybraných radioaktivně značených inhibitorů používaných v klinické praxi

Mimo velmi úspěšných teranostik - radioligandů byly připraveny i konjugáty s toxiny, a to jak s protilátkami (DiPippo a kol., 2015; Huang a kol., 2020; Kuroda a kol., 2010; Meng a kol., 2017; Milowsky a kol., 2016; Petrylak a kol., 2019; Petrylak a kol., 2020; Wang a kol., 2011), jejich fragmenty (Huang a kol., 2004; Michalska a kol., 2016; Wolf a kol., 2008; Xing a kol., 2021; Zhang a kol., 2013), tak s inhibitory (Leamon a kol., 2019; Machulkin a kol., 2022; Morris a kol., 2017; Rogers a kol., 2021). Jako toxiny byly užity malé molekuly, povětšinou mikrotubulární jedy, jako např. monometylauristatin, tubulysin, docetaxel či mertansin (DM1), nebo různorodé toxické proteiny, jako např. různé bakteriální toxiny, derivát ricinu, či saporin (Wolf, 2021). Konjugát s monomethylauristatinem vedl v klinické studii 2. fáze u 14 % (16/113) pacientů k ≥ 50 % poklesu PSA (Petrylak a kol., 2020), což je výsledek velmi podobný efektivitě protilátek s radioligandy (Tagawa a kol., 2013). Mezi nežádoucí účinky patřila hematologická toxicita, neuropatie, zácpa. Zatímco v hematologické toxicitě se podobal profil nežádoucích účinků konjugátům protilátek s radioligandy (Tagawa a kol., 2013), tak novou

toxicitou byla neuropatie, zácpa, což jsou zase příznaky typické pro léčbu konjugáty protilátek s mikrotubulárním jedy (Bendell a kol., 2014; Younes a kol., 2010). Méně efektivní byl konjugát protilátky MLN591 spojený disulfidickým linkerem s toxinem DM1. V klinické studii 1/2 fáze pouze 8% (5/62) pacientů dosáhlo poklesu PSA >50 %, a to většinou jen přechodně a za cenu výrazné neurotoxicity, kterou vykazovalo 71 % pacientů (44/62), z toho 10 % (6/62) stupně 3-4.

Specifickým přístupem je použití přímého konjugátu inhibitoru s toxinem a to, jako nízkomolekulárního jako je tubolysin (Leamon a kol., 2019; Morris a kol., 2017) či docetaxel (Machulkin a kol., 2022), tak i proteinového (Rogers a kol., 2021). Užití inhibitoru GCPII konjugovaného hydrazidovou vazbou s tubolysinem B (látka s kódem EC1169) bylo zkoušeno i v klinické studii 1. fáze, kdy toxicita odpovídala užití toxinu (mikrotubulárního jedu) tj. trombocytopenie, únava, zácpa (Morris a kol., 2017). Stran aktivity je hodnocení limitované malým počtem zahrnutých pacientů. Slibnou preklinickou aktivitu vykazoval i konjugát docetaxelu s GCPII inhibitorem (Machulkin a kol., 2022).

Mezi další objekty cílené pomocí GCPII patří plejáda různých nanostruktur. Opět bylo použito řady přístupů –protilátek, aptamerů, peptidů či inhibitorů. Mezi částice patří např. struktury s anorganickým jádrem (Kim a kol., 2010a; Mukherjee a kol., 2014; Nagesh a kol., 2016), polymerními strukturami (Banerjee a kol., 2017; Kolishetti a kol., 2010; Sanna a kol., 2017; Xu a kol., 2017), liposomy (Tian a kol., 2021; Yari a kol., 2019) či exosomy (Severic a kol., 2021). Jediné nanočástice cílené proti GCPII, které byly klinicky zkoušeny, byly označeny pod kódem BIND-014 a obsahovaly docetaxel. V klinické studii fáze 1, kde byly zkoušeny u pacientů s pokročilými solidními nádory, byly dle autorů poměrně dobře tolerovány (hematologická toxicita, průjem, únava u více jak 20 % pacientů) a vedly u 2 % (1/ 52) pacientů ke kompletní remisi a u 10 % (5/52) k parciální remisi (Von Hoff a kol., 2016). V klinické studii 2. fáze podání BIND-014 vedlo u hormonálně necitlivých karcinomů prostaty k poklesu PSA u 30 % (12/40) pacientů a měřitelné odpovědi u 32 % (6/19). Toxicita byla opět mírná, 1-2 stupně, únava 69 % (29/42), nausea 55 % (23/42), neuropatie 33 % (14/42) a jeden pacient měl febrilní neutropenii.

Inovativním přístupem pro terapii nádorů jsou i metody, kterou vedou k posílení imunitní odpovědi proti tumoru. Jedním z přístupů je užití bispecifických protilátek, tzv. BiTE^{TM} (bispecifický T-buněčný aktivátor) které aktivují T lymfocyty proti nádorovým buňkám. Mezi BiTE^{TM} tak patří např. diabody anti GCPII×CD3 (Baum a kol., 2013), bispecifická protilátka „biJ591“ sestávající ze „single chain“ J591 a „single chain“ anti-CD3 v polymerní depotní formulaci (Leconet a kol., 2018) nebo konstrukt AMG160 s prodlouženým poločasem (Deegen

a kol., 2021). Unikátním, na půl syntetickým přístupem je užití kombinace inhibitoru s Fab fragmentem anti CD3 protilátky (Patterson a kol., 2017). Cestou je i přímé vytvoření efektorových buněk z T či NK lymfocytů genetickou manipulací, kdy je vytvořen tzv. chimerický antigenní receptor (CAR), který aktivuje buňku proti buňkám nesoucím nádorový antigen. Modifikované CAR-T-buňky byly zprvu zkoušeny samostatně, a to jak CAR-T 1. generace (Santoro a kol., 2015), tak i s lepšími výsledky v CAR-T 2. generace (Ma a kol., 2014). Vzhledem k imunosupresivnímu účinku nádorového mikroprostředí není u solidních malignit léčba CAR-T natolik účinná jako v případě hematologických malignit (Ma a kol., 2019). Proto byly zkoušeny léčebné kombinace nebo vylepšené CAR-T, jako např. kombinace CAR-T s protilátkou proti PD-1 receptoru (Serganova a kol., 2017), CAR-T rezistentní proti imunosupresivnímu prostředí způsobeném TGF-β (Kloss a kol., 2018), či v klinické studii fáze 1 použití kontinuální konkomitantní infuze interleukinu 2 (Junghans a kol., 2016). Překvapivě u karcinomu prostaty mohou být některá vylepšení, jako užití CAR-T 3. generace, vlivem „superstimulace“ a smrti způsobené z aktivace, kontraproduktivní a vykazovat horší výsledky než CAR-T 2. generace (Zuccolotto a kol., 2021). Nakonec je možné užití nádorové vakcíny za použití modifikovaných dendritických buněk, které jsou schopné stimulovat cytotoxické lymfocyty proti buňkám exprimujícím GCPII (Meng a kol., 2016). V klinické studii vedlo podání GCPII ošetřených dendritických buněk spolu s peptidem survivinem u pacientů k imunitní odpovědi. Vakcinace v porovnání s docetaxelem a prednisonem vedla k 9,1 % (1/11) vs. 0 % (0/11) parciálním remisím; 54,5 % (6/11) vs. 45,4 % (5/11) stabilní chorobě a v 27,2 % (3/11) vs. 54,5 % (6/11) k progredující chorobě.

2 Cíle disertační práce

- Zhodnotit dostupné nástroje, tj. protilátky pro stanovení obsahu GCPII, porovnat možnosti užití daných protilátek pro použití v jednotlivých imunochemických metodách a posoudit možnosti stanovení homologů GCPII (GCPIII, myší, lidské proteiny). Pokusit se nahradit ne vždy spolehlivé protilátky proti GCPII polymerními konjugáty.
- Zhodnotit možnosti využití myšího *in vivo* modelu pro studium GCPII porovnáním biochemických charakteristik myší a lidské GCPII a srovnáním expresního profilu tohoto proteinu u myši a člověka.
- Posoudit roli GCPII v Alzheimerově chorobě vzhledem k možnému štěpení amyloidu β, a tím i zhodnotit možný dlouhodobý nežádoucí efekt inhibice GCPII.
- Charakterizovat model a fenotyp GCPII deficientní myši a pomocí něj prozkoumat další možné fyziologické funkce GCPII, případně fyziologické důsledky inhibice GCPII.
- Porovnat možnosti cílení GCPII jako známého nádorového antigenu pomocí různých typů nanostruktur (polymerní nanostruktury, částice podobné virům).

3. Metody

Metody použité v této disertační práci jsou podrobně rozepsány v jednotlivých publikacích, přičemž můj podíl ke každé práci je uveden na konci jednotlivých souhrnů k publikacím v kapitole 4 (Výsledky). Naprostá většina práce byla vykonána na Ústavu organické chemie a biochemie Akademie věd České republiky (ÚOCHB AV ČR). V rámci spoluprací mimo ÚOCHB AV ČR byly připraveny hydrofilní polymery na bázi N-(2-hydroxypropyl)methakrylamidu (HPMA) ve skupině dr. Etrycha (Ústav makromolekulární chemie Akademie věd české republiky). Myší model deficientní v genu pro GCPII byl vyvinut ve skupině funkční genomiky Dr. Sedláčka (BIOCEV). Virům podobné nanočástice odvozené z myšího polyomaviru byly vytvořeny ve skupině doc. Jitky Forstové (Katedra genetiky a mikrobiologie Přírodovědecké fakulty Univerzity Karlovy).

Zde pouze uvádím stručný seznam metod, které byly mnou přímo využity v souvislosti s přípravou této disertační práce.

Preparativní metody: purifikace malých molekul i proteinů užitím chromatografických technik, purifikace nanočástic užitím ultracentrifugace, kovalentní modifikace nanočástic i s použitím bioortogonálních technik

Analytické metody: vysokoúčinná kapalinová chromatografie (HPLC), měření fluorescenčních spekter, polyakrylamidová gelová elektroforéza s dodecylsulfátem sodným (SDS-PAGE), imunoblot („western blot“) s chemiluminiscentní i fluorescenční detekcí, měření koncentrace proteinů Bradfordovou metodou, měření inhibičních konstant inhibitorů (K_i) pomocí stanovení enzymové aktivity metodou konečného bodu (tj. měření koncentrace produktu po zastavení enzymové reakce), imunohistochemické metody, charakterizace interakcí látek s živými savčími buňkami (včetně kultivace tkáňových kultur) metodami konfokální mikroskopie a průtokové cytometrie, analýza obrazu

***In-vivo* metody:** práce s experimentálními zvířaty (myši), disekce jednotlivých orgánů

4. Výsledky

Mé výsledky studia proteinu GCPII vyústily ve vznik šesti publikací, z nichž všechny prošly recenzním řízením, přičemž na dvou publikacích jsem prvním autorem (jedno prvoautorství je sdílené). Mimo to, studium metod analýzy proteinu GCPII pomocí HPMA polymeru nakonec vyústilo v obecnější analytický přístup, na který byla získána mezinárodní patentová ochrana. Dále mám v souvislosti s tématem disertace rozpracovány dvě prvoautorské práce, které jsou ve fázi těsně před odesláním k publikaci. Vzhledem k tomu, že ještě nejsou publikovány, rozhodl jsem se je nakonec do této disertace nezařadit. Každá takto vzniklá publikace byla dílem řady autorů, přičemž můj přínos je vždy shrnut na konci příslušného popisu.

4.1 Porovnání jednotlivých protilátek proti GCPII

Tykvart J, Navrátil V, **Sedlák F**, Corey E, Colombatti M, Fracasso G, Koukolík F, Bařinka C, Šácha P, Konvalinka J. **Comparative analysis of monoclonal antibodies against prostate-specific membrane antigen (PSMA).** *Prostate.* 2014 Dec;74(16):1674-90.

Monoklonální protilátky tvoří vzhledem ke své specifické vazbě s antigenem jeden ze základních analytických nástrojů v biochemii. Konkrétně pro analýzu GCPII je v současnosti k dispozici řada různě charakterizovaných protilátek pocházejících jak z akademické sféry, tak od komerčních institucí. Vzhledem k tomu, že řada těchto protilátek doposud nebyla důkladně popsána, mohlo by jejich užití vést k rozdílným výsledkům, a i k případným chybám v interpretaci. Cílem této práce bylo charakterizovat 13 nejběžnějších monoklonálních protilátek za použití standardních biochemických analytických metod.

Pomocí metody ELISA („enzyme-linked immunosorbent assay“) a pomocí povrchové plasmonové rezonance (SPR – „surface plasmon resonance“) byla kvantifikována vazba protilátek na nativní event. i denaturovaný antigen. S nativní GCPII interagovaly protilátky D2B, J415, J591, 2G7, 107-1A4, 24.4E6 a GCP-05 (tabulka 1), kdežto na denaturovanou GCPII se vázaly protilátky GCP-04, J591, GCP-02, 3E6, 7E11-C5.3, YPSMA-1, YPSMA-2 (tabulka 2). Byly pozorovány výrazné rozdíly jak v koncentracích, při kterých k vazbě docházelo, tak i v maximálním signálu (až 7 × pro nativní, respektive až 54 × pro denaturovaný antigen). Protilátky GCP-02, 3E6 a GCPII-04 byly navíc schopny vázat i denaturovaný myší homolog GCPII a protilátka GCPII-04 dokonce i lidský a myší homolog GCPIII. K lepšímu pochopení vazby protilátek na homology GCPII bylo u protilátek vázajících denaturovaný antigen provedeno mapování epitopu.

Tabulka 1 – Vazba protilátek na nativní GCPII. Výsledek proložení saturačních křivek vazby protilátek na antigen pomocí metody ELISA. Maximální signál udává relativní maximální dosaženou hodnotu lumininiscence v metodě ELISA pro danou protilátku. 50 % saturace vyjadřuje koncentraci protilátky, při které bylo dosaženo 50 % maximálního signálu. Maximální signál u protilátek 24.4E6 a GCP-05 nebyl určen pro použití jiného množství imobilizované GCPII („NC“).

Protilátka	50% saturace	Maximální signál
D2B	0,072 ± 0,013 nM	4.8
J415	0,163 ± 0,022 nM	3.9
J591	1,4 ± 0,27 nM	6.9
2G7	2,89 ± 0,25 nM	1.0
107-1A4	3,81 ± 0,43 nM	2.6
24.4E6	365 ± 77 nM	NC
GCP-05	550 ± 130 nM	NC

Tabulka 2 – Vazba protilátek na denaturovanou GCPII. Výsledek proložení saturačních křivek vazby protilátek na antigen pomocí metody ELISA. Maximální signál udává relativní maximální dosaženou hodnotu lumininiscence v metodě ELISA pro danou protilátku. 50 % saturace vyjadřuje koncentraci protilátky, při které bylo dosaženo 50 % maximálního signálu. Maximální signál u protilátek 7E11-C5.3 nebyl určen pro použití jiného antigenu (intracelulární peptid). Epitop značí sekvenci peptidu, který je schopen interagovat s danou protilátkou, přičemž čísla udávají jeho lokalizaci na primární sekvenci lidské GCPII.

Protilátka	50% saturace	Maximální signál	Epitop
GCP-04	0,628 ± 0,066 nM	54	91–108
J591	3,06 ± 0,89 nM	1	ND
GCP-02	5,2 ± 1,2 nM	40	271–288
3E6	9,8 ± 1,7 nM	9	118–135
7E11-C5.3	9,9 ± 3 nM	NC	1–21
YPSMA-1	61 ± 17 nM	7	469–486
YPSMA-2	216 ± 55 nM	42	469–486
24.4E6	267 ± 49 nM	5	640–657

S výsledky kvantitativní analýzy úzce souvisí kvalitativní výsledky použitých protilátek v běžných biochemických metodách. Zatímco protilátky interagující s denaturovaným antigenem vykazovaly na „western blotu“ silný (GCP-02, GCP-04 a YPSMA-1) respektive střední signál (3E6, YPSMA-2 a 7E11-C5.3), protilátky reagující i s nativním antigenem vykazovaly slabý signál (24.4E6, D2B a J591). Obdobně u imunohistochemie na parafinových řezech bylo barvení na GCPII pozitivní v případě protilátek proti denaturovanému antigenu (GCP-02, GCP-04, YPSMA-1, YPSMA-2, 24.4E6, 3E6). Naproti tomu použití nativní průtokové cytometrie nepřekvapivě vyžadovalo použití protilátek vázajících nativní antigen (J591, J415, D2B, 107-1A4, 2G7 nebo GCP-05). Výsledky praktického užití protilátek v jednotlivých biochemických metodách jsou semikvantitavně zhodnoceny v tabulce 3.

Tabulka 3 – Semikvantitavní hodnocení protilátek pro jednotlivé bioanalytické metody („FC“ značí průtokovou cytometrii, „WB“ – imunoblot - „western blot“ a IHC-P – imunohistochemii na parafinových řezech). Vhodnost je znázorně na škále, kde „– “ znamená nevhodné a naopak „+++“ nejvhodnější. Protilátka 7E11-C5.3 je označena hvězdičkou (*) vzhledem k použití syntetického intracelulárního peptidu v metodě ELISA.

	nativní GCPII		denaturovaná GCPII		
Protilátka	ELISA	FC	ELISA	WB	IHC-P
J591	+++	+++	+	+	–
J415	+++	+++	–	–	–
D2B	+++	+++	+	+	–
107-1A4	+++	+++	–	–	–
2G7	++	++	–	–	–
GCP-05	+	+++	–	–	–
7E11-C5.3*	++	–	++	++	–
GCP-02	–	–	+++	+++	+++
GCP-04	–	–	+++	+++	+++
YPSMA-1	–	–	++	+++	+++
YPSMA-2	–	–	++	++	+++
3E6	–	–	++	++	++
24.4E6	+	–	+	+	++

Můj příspěvěk

Mým podílem na této práci bylo provedení všech imunohistochemií a jejich interpretace. U vybraných protilátek (GCP-02 a GCP-04) jsem provedl i předběžné zhodnocení vazby homologů GCPII pomocí „western blotu“ a též předběžné mapování epitopu. Podílel jsem se i na vyhodnocení dalších experimentů a diskusi výsledků.

4.2 Syntetická náhrada protilátek (iBodies) na bázi hydrofilního polymeru

Šácha P, Knedlík T, Schimer J, Tykvart J, Parolek J, Navrátil V, Dvořáková P, **Sedlák F**, Ulbrich K, Strohalm J, Majer P, Šubr V, Konvalinka J. **iBodies: Modular Synthetic Antibody Mimetics Based on Hydrophilic Polymers Decorated with Functional Moieties.** *Angew Chem Int Ed Engl.* 2016 Feb 12;55(7):2356-60.

Selektivní vazba protilátek k antigenu je klíčová vlastnost umožňující jejich využití jako nástroje v biochemii. Vzhledem k tomu, že naše předchozí studie (kapitola 4.1) ukázala, že vlastnosti běžně dostupných protilátek proti GCPII se značně liší, a vzhledem k našemu pozorování, že modifikace protilátek může být obtížná, pokusili jsme se navrhnout čistě syntetický systém, který by umožnil protilátky v bioanalytických metodách nahradit, nebo event. i překonat.

Základní součástí náhrady protilátek, kterou v této práci představujeme, byl polymer na bázi N-(2-hydroxypropyl)methacrylamidu (HPMA), na který byl kovalentně navázán cílící ligand,

např. inhibitor, a dále pak afinitní kotva (biotin) a vhodný fluorofor (obrázek 11). Tento postup byl otestován na modelovém případě proteázy GCPII, proteázy z viru HIV, pepsinu a proteinu s polyhistidinovou sekvencí. Vzhledem k tomu, že na jednu molekulu polymeru (iBody) bylo navázáno větší množství cílícího ligandu – u polymeru proti GCPII průměrně 19 molekul inhibitoru, byl navíc pozorován výrazný aviditní efekt, kdy hodnota K_i poklesla cca 465 × ve srovnání s hodnotou volného inhibitoru (K_i polymeru 4,3 pM vs. K_i inhibitoru 2 nM). Toto výrazné zvýšení afinity přibližuje disociační konstantu daného iBody (< 20 pM) k nejlepším dostupným protilátkám proti GCPII (viz. kapitola 4.1.).

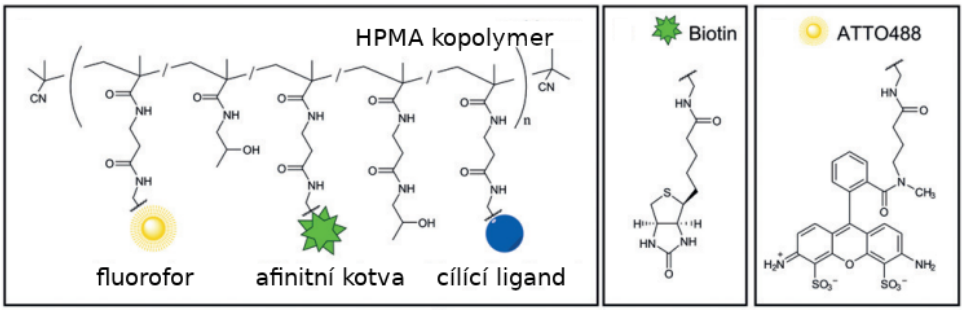

Obrázek 11 – Schematické zobrazení struktury HPMA polymeru s kovalentně navázaným fluoroforem (ATTO488), afinitní kotvou (biotin) a cílícím ligandem (např. inhibitor GCPII).

Kromě užití iBody k inhibici byla na různých modelových případech potvrzena vazba pomocí SPR, a možnost využití v metodě ELISA, průtokové cytometrie, zobrazovaní živých buněk (imunocytochemie pomocí konfokální mikroskopie), imunoprecipitace a metody imunoblotu - „western blot“. Připravené iBody proti GCPII je současně univerzálním nástrojem pro další analýzu funkce GCPII (obrázek 12).

Můj příspěvěk

Mou prací byla optimalizace využití iBodies pro použití v zobrazovaní živých buněk (imunocytochemie) pomocí konfokální mikroskopie.

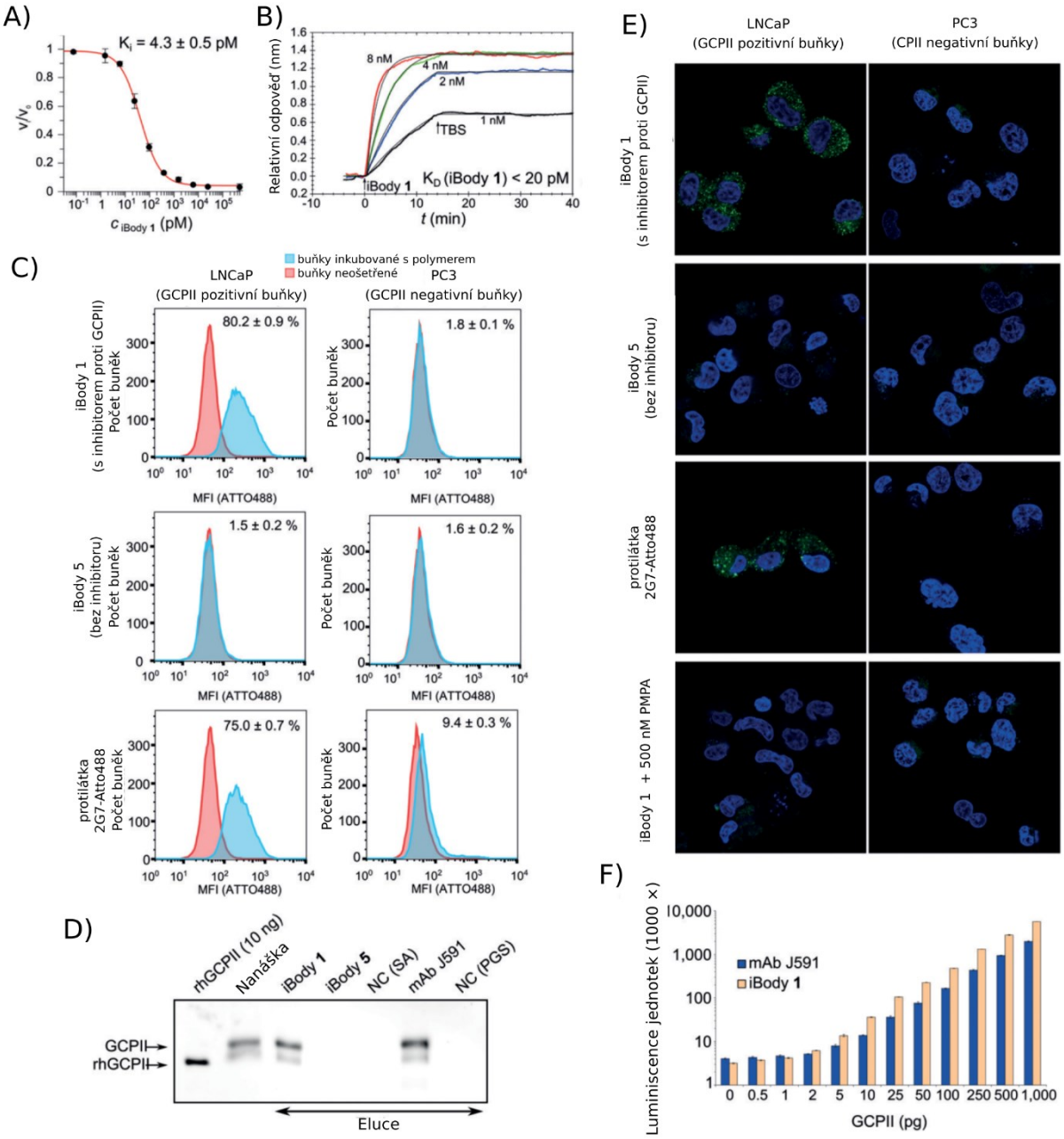

Obrázek 12 – Přehled možných použití iBody proti GCPII. A) Schopnost inhibovat aktivitu GCPII s vysokou efektivitou. B) SPR vazba polymeru na GCPII potvrzující pikomolární interakci. C) Průtoková cytometrie s využitím cíleného (iBody 1) a necíleného (iBody 5) polymeru v porovnání s přímo značenou protilátkou 2G7 (viz. 4.1) na buněčné linii s expresí GCPII (LNCaP) a bez exprese GCPII (PC3). D) Imunoblot – „western blot" prokazující možnost izolace GCPII pomocí iBody v porovnání s imunoprecopitací užitím protilátky J591 (viz. 4.1). NC značí negativní kontrolu – přičemž SA je samotná Streptavidin Agarosa a PGS je Protein G Sepharosa. rhGCPII je zkratkou pro rekombinantní lidskou extracelulární doménu GCPII. E) Vizualizace buněk s expresí GCPII (LNCaP) a bez exprese GCPII (PC3) pomocí cíleného (iBody 1), necíleného (iBody 5) polymeru a přímo značenou protilátkou 2G7. Jako poslední je i znázorněna kompetice cíleného polymeru s inhibitorem GCPII PMPA. F) Porovnání iBody 1 s J591 protilátkou (viz. 4.1.) v roli detekující protilátky v sendvičové modifikaci ELISA pro detekci GCPII.

4.3 Porovnání lidské a myší GCPII

Knedlík T, Vorlová B, Navrátil V, Tykvart J, **Sedlák F**, Vaculín Š, Franěk M, Šácha P, Konvalinka J. **Mouse glutamate carboxypeptidase II (GCPII) has a similar enzyme activity and inhibition profile but a different tissue distribution to human GCPII.** *FEBS Open Bio*. 2017 Aug 29;7(9):1362-1378.

Pro výzkum fyziologických a patofyziologických funkcí na úrovni organismu je nezbytný *in vivo* model. Vzhledem k tomu, že myší modely jsou obecně nejběžněji používané a dostupné, pokusili jsme se v předkládané práci zhodnotit jejich využitelnost pro studium GCPII. Optimální zvířecí model totiž musí pro přenositelnost poznatků do humánní medicíny, kromě dostupnosti, splňovat podmínku dostatečné podobnosti s člověkem.

Porovnání myší a lidské GCPII proběhlo nejprve na proteinové úrovni. Nepřekvapivě vzhledem k vysoké podobnosti v aminokyselinové sekvenci – 86 % identita, 91 % podobnost (Bacich a kol., 2001) byla zachována enzymová aktivita i substrátová specifita. Myší homolog GCPII byl schopen štěpit NAAG na NAA a glutamát, stejně tak jako odštěpovat γ-koncové glutamáty s pteroylpoly-γ-glutamátu. Enzymatická aktivita myšího homologu byla však nižší, zejména pro vyšší hodnotu K_M (viz tabulka 4). Substrátová specifita studovaná na N-terminálně acetylované dipeptidové knihovně vykazovala u myší GCPII obdobný vzor jako u lidského homologu, pouze byla zvýrazněna specifita pro štěpení dipeptidů s C-terminálním glutamátem. Naprostá většina inhibitorů byla schopná identicky inhibovat myší i lidskou variantu GCPII.

Tabulka 4 – Kinetické parametry rekombinantní myší a lidské GCPII stanovené pro NAAG radioenzymatickou metodou (Tykvart a kol., 2012) nebo pro pteroyl-di-L-γ-glutamát HPLC metodou (Navrátil a kol., 2014), zobrazeny průměrné hodnoty ± směrodatná odchylka.

Enzym	NAAG			Pteroyl-di-L-glutamát		
	K_M [nM]	k_{cat} [s^{-1}]	k_{cat}/K_M [× 10^7 s^{-1} M^{-1}]	K_M [nM]	k_{cat} [s^{-1}]	k_{cat}/K_M [× 10^7 s^{-1} M^{-1}]
Avi-mGCPII	1900 ± 100	1,44 ± 0,02	0,077 ± 0,001	290 ± 20	3,63 ± 0,09	1,26 ± 0,08
Avi-hGCPII	550 ± 60	1,45 ± 0,04	0,265 ± 0,007	39 ± 2	5,09 ± 0,09	13,20 ± 0,80

Dále byl porovnán expresní profil (obrázek 13), a to jak na úrovni aktivity (hydrolýza NAAG na NAA a glutamát), tak i exprese samotného proteinu. Vzhledem k velmi podobným vlastnostem myší GCPII a GCPIII, byla pro jejich odlišení aplikována i analýza v tkáních přítomné mRNA. V myši, obdobně jako u člověka byla zachycena vysoká exprese v mozku a v ledvinách, naopak u myši oproti člověku nebyla zachycena exprese v prostatě a ve větší míře ani v tenkém střevě (jejunu ani ileu). Vedlejším nálezem byla variabilní exprese GCPII v myších slinných žlázách, která byla dále potvrzena imunohistochemicky a to zejména v podjazykové slinné žláze. Vzhledem k výrazné podobnosti mezi GCPII a jejím homologem GCPIII, jak v enzymatické aktivitě, tak i schopnosti být rozpoznán použitou protilátkou

GCP-04 (kapitola 4.1) bylo doplněno i hodnocení na úrovni transkriptů, které korelovalo s nálezem na proteinové úrovni.

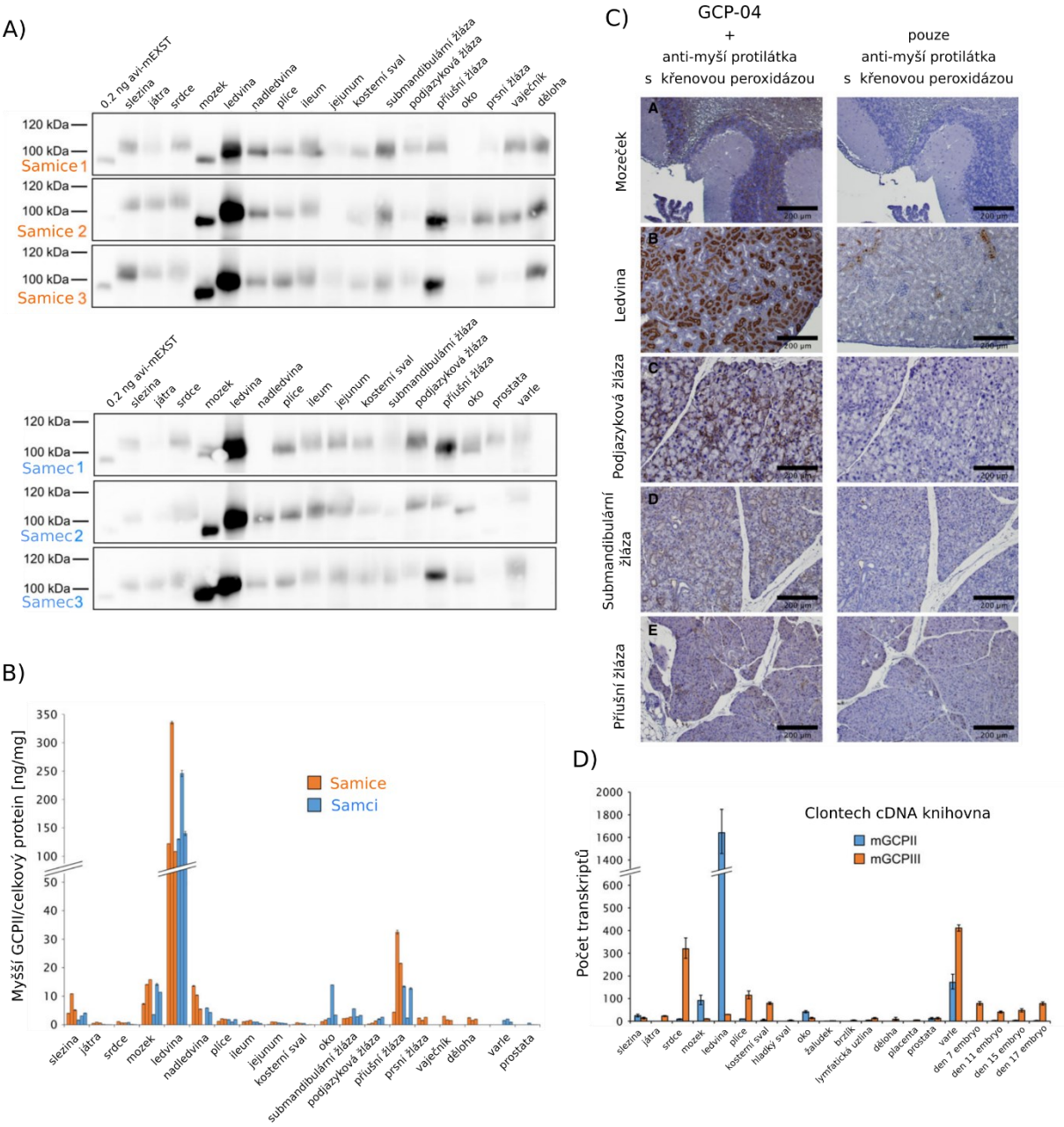

Obrázek 13 – Přehled analýzy expresního profilu u myši. A) Analýza expresí v orgánech pomocí imunoblotu – „western blotu“. Byli analyzovány tkáně ze třech samců a samiček, popisky jednotlivých orgánů jsou uvedeny v záhlaví. Avi-mEXST je standard (rekombinantní extracelulární doména myší GCPII). B) Stanovení obsahu GCPII pomocí enzymatické aktivitní metody (štěpení NAAG), analyzovány samci a samičky v biologickém triplikátu. C) Imunohistochemické detekce GCPII ve vybraných tkáních s vyšší expresí GCPII. Pozitivní barvení choroidní pleteně, stratum granullare a bílé hmoty v mozečku, pozitivita luminální strany proximálních tubul a Bowmanovy kapsuly. Pozitivita abluminálních buněk ve slinných žlázách. D) Srovnání expresního profilu myší GCPII (mGCPII) a myší GCPIII (mGCPIII) na úrovni mRNA.

Souhrnně, biochemická charakterizace na proteinové úrovní neukázala výraznější rozdíly. Oproti tomu exprese GCPII v myši se lišila chybějící expresí v prostatě a do značné míry i v tenkém střevě. Zatímco u prostaty to může být dáno výrazně odlišnou anatomicko-histologickou strukturou (Oliveira a kol., 2016), tak u střeva může být obdobně jako u potkana (Shafizadeh a Halsted, 2007) funkce štěpení pteroyl-poly-glutamátu zprostředkována aktivitou gamma-glutamyl hydrolázy. Vzhledem k této tkáňové distribuci lze předpokládat, že myší modely funkce GCPII v nervovém systému jsou přenositelné i na člověka, kdežto stran studia karcinogeneze v prostatě není volba myši, jako experimentálního zvířete, ideální.

Můj příspěvěk

Mým podílem v této práci byl odběr vybraných myších tkání a provedení imunohistochemické analýzy. Podílel jsem se i na analýze a diskusi experimentálních výsledků.

4.4 Myš s vyřazeným genem GCPII má ve stáří zvětšené semenné váčky

Vorlová B, **Sedlák F**, Kašpárek P, Šrámková K, Malý M, Zámečník J, Šácha P, Konvalinka J. **A novel PSMA/GCPII-deficient mouse model shows enlarged seminal vesicles upon aging.** *Prostate.* 2019 Feb;79(2):126-139.

Jeden ze základních prostředků pro výzkum fyziologické a patofyziologické aktivity jednotlivých genů tvoří zvířata deficientní v daném genu. Přestože byla již publikována řada myších modelů s vyřazeným genem pro GCPII, výsledky byly ve vzájemném nesouladu. Zatímco některé práce (Han a kol., 2009; Tsai a kol., 2003b) uvádějí embryonální letalitu, tak další studie (Bacich a kol., 2002; Gao a kol., 2015) neprokazují žádný zjevný patologický fenotyp. Proto jsme vytvořili další nezávislý model GCPII deficientní myši pomoci TALEN (efektorové nukleázy podobné transkripčním aktivátorům). Zatímco v předchozích pracích (Bacich a kol., 2005; Gao a kol., 2015) byl ponejvíce analyzován efekt GCPII na funkci nervového systému, ostatní možné fenotypy, mimo jiné např. v urogenitálním systému, byly studovány do výrazně menší hloubky, navíc v přechozích studiích nebyly studovány stárnoucí myši.

U stárnoucích myší jsme obdobně jako v práci (Finch a Girgis, 1974) pozorovali zvětšení semenných váčků, přičemž ke zvětšení u myší deficientní v genu pro GCPII ($Folh1^{-/-}$) docházelo dříve. Reprezentativní fotografie semenných váčků a porovnání velikostí semenných váčků je zobrazeno na obrázku 14.

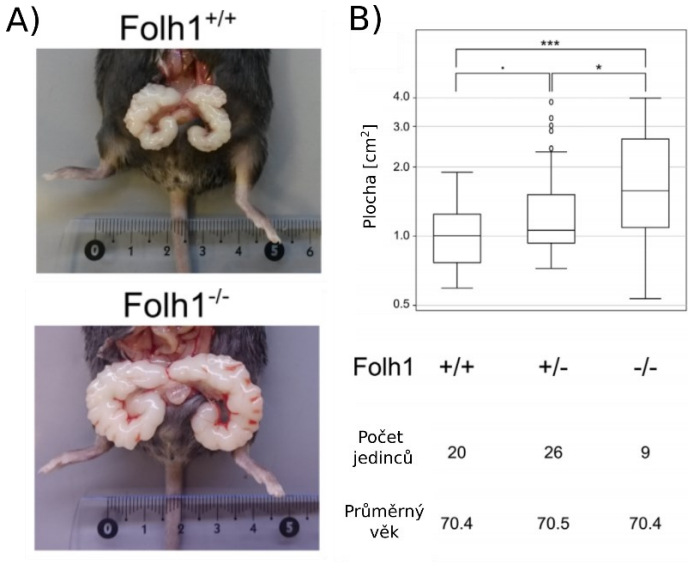

Obrázek 14 – A) Obrázek semenných váčků reprezentativních myší divokého kmene (Folh1$^{+/+}$) a myší deficientních v genu pro GCPII (Folh1$^{-/-}$). B) Statistická analýza zvětšených semenných váčků v závislosti na genotypu pro GCPII - Folh1$^{+/+}$ značí myši divokého kmene, Folh1$^{+/-}$ myši s heterozygotní konstitucí v genu pro GCPII a Folh1$^{-/-}$ myši plně deficientní v genu pro GCPII

Následně provedená histologická analýza zvětšených semenných váčků prokázala pouhou dilataci, bez dalších přídavných patologií. Vzhledem k tomuto pozorování jsme provedli zevrubné měření aktivity GCPII ve většině tkání urogenitálního systému, přičemž pouze v ledvině, nadvarleti a chámovodu jsme zachytili významnou expresi GCPII (182 ± 12 ng GCPII/mg tkáně v nadvarleti a 2.3 ± 1 ng/mg tkáně v chámovodu). Takto výrazný záchyt GCPII v nadvarleti, představující cca desetinásobek obsahu v mozku, byl nadále potvrzen pomocí imunohistochemie, jak na vzorcích myšího, tak i lidského nadvarlete (obrázek 15). Celkově tak zvětšení semenných váčků u starších myší tvoří první fenotyp v urogenitálním systému související s expresí GCPII.

Můj příspěvek

Mým přínosem byl podíl na pitvách jednotlivých tkání, obzvláště v oblasti urogenitálního traktu, měření plochy semenných váčků a předběžná statistická analýza. Dále jsem provedl imunohistochemii lidských i myších nadvarlat. Podílel jsem se i na analýze a diskusi experimentálních výsledků.

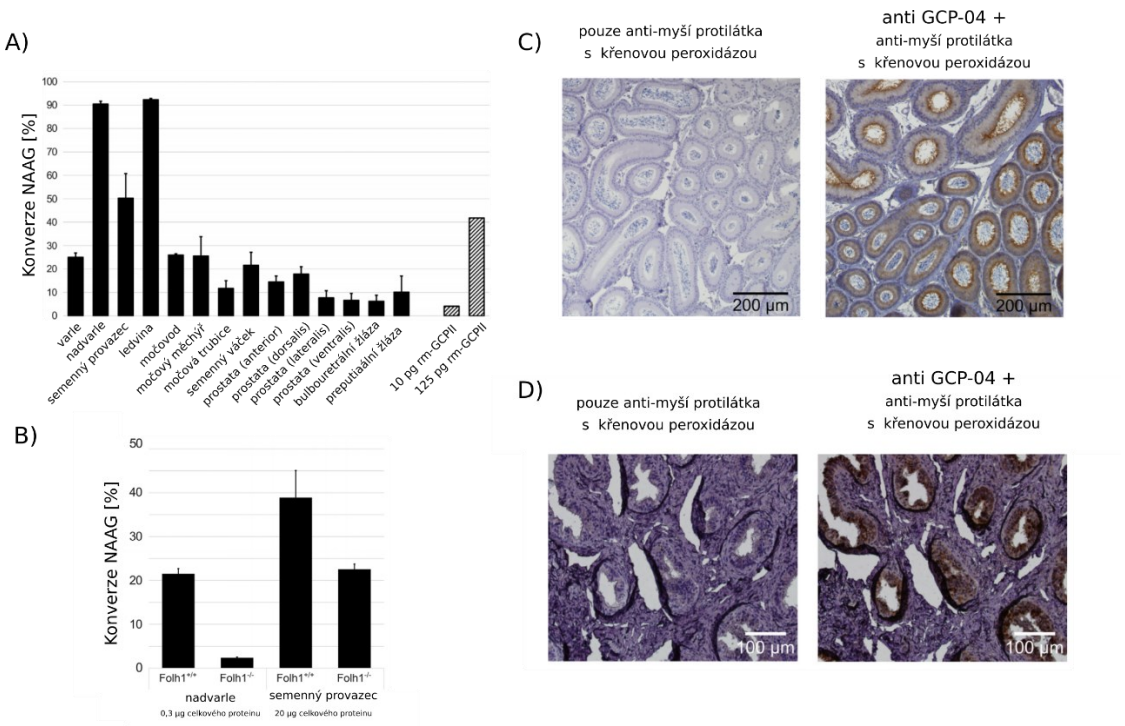

Obrázek 15. Měření exprese GCPII v urogenitálním traktu. A) Zhodnocení přítomnosti GCPII pomoci měření aktivity štěpení NAAGu, rm-GCPII (rekombinantní myší GCPII) slouží jako aktivitní standard B) Porovnání štěpení NAAGu u tkání pocházejících z myší divokého kmene (Folh1$^{+/+}$) a myší deficientních v genu pro GCPII (Folh1$^{-/-}$) potvrzuje přítomnost GCPII v nadvarleti a semenném provazci. C) Imunohistochemie myšího nadvarlete nasvědčuje přítomnosti GCPII na luminální straně tubulů. D) Imunistochemie lidského nadvarlete svědčí pro přítomnost GCPII taktéž na luminální straně tubulů.

4.5 GCPII neštěpí peptidy amyloidu β

Sedlák F, Šácha P, Blechová M, Březinová A, Šafařík M, Šebestík J, Konvalinka J. **Glutamate carboxypeptidase II does not process amyloid-β peptide.** *FASEB J.* 2013 Jul;27(7):2626-32.

Fyziologická funkce GCPII v nervovém systému je štěpit neurotransmiter NAAG na NAA a glutamát (Robinson a kol., 1987), což vzhledem k neuroprotektivnímu chování NAAGu (Lu a kol., 2000), nasvědčuje možnosti užití inhibitorů GCPII jako neuroprotektiva (Cai a kol., 2002; Vornov a kol., 1999; Williams a kol., 2001; Zhong a kol., 2006). Nicméně, v r. 2010 byla v prestižním FASEB J. publikována velmi překvapivá práce korejských autorů, která reportovala schopnost GCPII degradovat amyloid β a amyloidní fibrily (Kim a kol., 2010b). To vedlo ke znepokojivé hypotéze, zda by aplikace GCPII inhibitorů by mohla mít jako vedlejší nežádoucí účinek případný vznik plaků amyloidu β a tím podněcovat vznik Alzheimerovy choroby. Kdyby se tato hypotéza potvrdila, znamenalo by to zastavení velmi slibných

klinických experimentů s inhibitory GCPII v řadě dalších terapeutických nebo diagnostických indikací, které popisuji v teoretickém úvodu této práce (kapitola 1.6, str. 38).

K prošetření tohoto problému jsme rekombinantní protein GCPII inkubovali se synteticky připravený peptidem amyloid-$\beta_{1\text{-}42}$. Případné degradační produkty a vlastní úbytek amyloidu-β jsme pozorovali pomocí kapalinové chromatografie spojené s hmotnostním spektrometrem. Zatímco kontrolní proteázy (neprilysin, chymotrypsin) amyloid-β štěpily, štěpení pomocí GCPII se nám, kromě velmi pomalého odštěpení jedné N-terminální aminokyseliny – aspartátu, nepodařilo potvrdit. Výsledky jsou shrnutě zobrazeny na obrázku 16. Aktivita vlastního rekombinantního proteinu byla následně ověřena štěpením NAAGu. Obdobných výsledků dosáhli i v paralelně publikované práci (Alt a kol., 2013) u peptidu amyloid-$\beta_{1\text{-}40}$. Souhrně lze usoudit, že GCPII amyloidní peptidy neštěpí, a tudíž riziko nežádoucích účinků ve smyslu iniciace Alzheimerovy choroby u inhibitorů GCPII je nepravděpodobné.

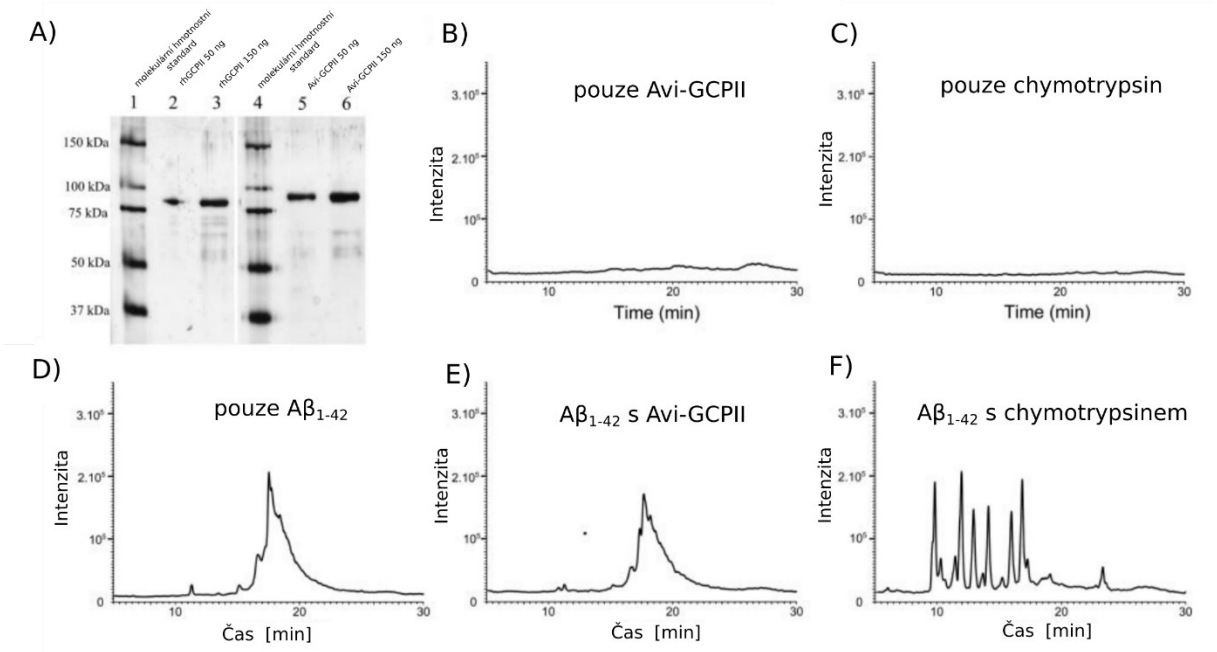

Obrázek 16. HPLC-MS analýza reakčních směsí a kontroly hydrolýzy $A\beta_{1\text{-}42}$ A) SDS-PAGE elektroforetogram prokazující čistotu rekombinantních proteinů GCPII. Popisky nad elektroforetogramem uvádějí nanášky v jednotlivých jamkách gelu. V částech B-F jsou zobrazeny chromatogramy zobrazující celkový iontový proud pro jednotlivé enzymové reakce a kontroly, přičemž v B) je samotný enzym Avi-GCPII, v C) samotný chymotrypsin, v D) samotný amyloid $A\beta_{1\text{-}42}$, v E) reakce amyloidu $A\beta_{1\text{-}42}$ s GCPII a v F) reakce amyloidu $A\beta_{1\text{-}42}$ s chymotrypsinem.

Můj příspěvek

Mým příspěvkem byla purifikace peptidu amyloidu $A\beta_{1-42}$, návrh i provedení vlastních štěpení amyloidu β pomocí GCPII a kontrolními proteázami, optimalizace separace vzniklých peptidů použitím kapalinové chromatografie a charakterizace čistoty enzymu pomocí gelové elektroforézy. Všechny experimenty jsem analyzoval, jejich výsledky diskutoval a podílel se na sepsání publikace.

4.6 Využití interakce inhibitor-GCPII k cílení nádorových buněk

Neburková J, **Sedlák F**, Žáčková Suchanová J, Kostka L, Šácha P, Šubr V, Etrych T, Šimon P, Bařinková J, Kryštufek R, Španielová H, Forstová J, Konvalinka J, Cígler P. **Inhibitor-GCPII Interaction: Selective and Robust System for Targeting Cancer Cells with Structurally Diverse Nanoparticles.** *Mol Pharm.* 2018 Aug 6;15(8):2932-2945.

Cílení GCPII jako nádorového antigenu pomocí řady přístupů (inhibitor, protilátka, aptamer, atp.) bylo již popsáno v řadě publikací (Banerjee a kol., 2017; Behnam Azad a kol., 2015; Fan a kol., 2016; Hrkach a kol., 2012; Huang a kol., 2014; Chandran a kol., 2008; Chen a kol., 2016; Kasten a kol., 2013; Kim a kol., 2010a; Mukherjee a kol., 2014; Nagesh a kol., 2016; Sanna a kol., 2017; Von Hoff a kol., 2016; Xu a kol., 2017; Zhu a kol., 2016). V naší přecházející práci (viz. výše 3.2.) jsme taktéž prokázali velmi silnou interakci polymeru na bázi HPMA dekorovaného inhibitory GCPII s vlastní proteázou GCPII, umožňující vizualizaci buněk. Na základě tohoto úspěšného cílení jsme se pokusili vytvořit řadu různých dalších nanostruktur, které by byly cíleny pomocí GCPII inhibitoru, a tak ověřit, jak je systém GCPII – inhibitor robustní pro případnou diagnostiku a event. terapii cílenými léčivy.

Jako příklady nanočástic byly zvoleny nanodiamanty, virům podobné částice (VLP) z bakteriofágu Qβ a myšího polyomaviru a polymerní nanostruktury založená na HPMA. VLP byly pro porovnání kromě přímé modifikace pomocí inhibitoru i dekorovány pomocí HPMA polymeru. Tyto částice se výrazně lišily jak ve své velikosti, rigiditě, tak i bio-nano rozhraní. Přesto všechny vytvořené částice interagovaly s rekombinantním GCPII, jak bylo prokázáno inhibicí enzymatické aktivity, tak i pomocí SPR (tabulka 5 a obrázek 17). Stran inhibiční aktivity byl pozorován aviditní efekt, který koreloval s množstvím navázané inhibiční substance na částici, zatímco základní inhibitory měly inhibiční konstantu K_i v nízkém nanomolárním rozmezí (2-14 nM), tak v případě polymerních částic došlo ke snížení K_i na subnanomolární koncentrace (323 pM) a v případě ostatních částic až na hodnoty v pikomolární oblasti (0,6-3,92 pM). Předpokládáme, že dosažení takto nízkých inhibiční konstant bylo

umožněno výrazně pomalejší disociací nanočástic pro velmi nízkou hodnotou k_{off} způsobenou aviditním efektem.

Tabulka 5. Charakterizace inhibičních konstant nanočástic i zdrojových inhibitorů. Označení nanočástic je následující: „ND-inh“ – částice nanodiamantu s inhibitory, „pol-inh“ – HPMA polymer s inhibitory, „Qβ-pol-inh“ – VLP částice Qβ s navázanými HPMA polymery s inhibitory, „Qβ-inh“ – VLP částice Qβ s navázanými inhibitory, „MPγV-pol-inh“ – VLP částice myšího polyomaviru s navázanými HPMA polymery s inhibitory, „MPγV-inh“ – VLP částice myšího polyomaviru s navázanými inhibitory. Měření provedeno HPLC metodou (Navrátil a kol., 2014). MEF („multivalent enhacement factor“) značí podíl K_i (základní inhibitor)/ K_i (nanočástice).

nanočástice	typ inhibitoru	počet inhibitorů na částici	inhibice: K_i ± 1 SD [pM]	MEF
ND-inh	4	250	3,7 ± 0,67	3780
pol-inh	1	6	323 ± 50	6,63
Qβ-pol-inh	1	12	3,92 ± 0,83	546
Qβ-inh	5	180	30,3 ± 4,5	373
MPγV-pol-inh	1	180	2,87 ± 0,6	746
MPγV-inh	5	540	0,60 ± 0,11	18800

inhibitor	inhibice: K_i ± 1 SD [pM]
1	2140 ± 290
4	14000 ± 1700
5	11300 ± 1200

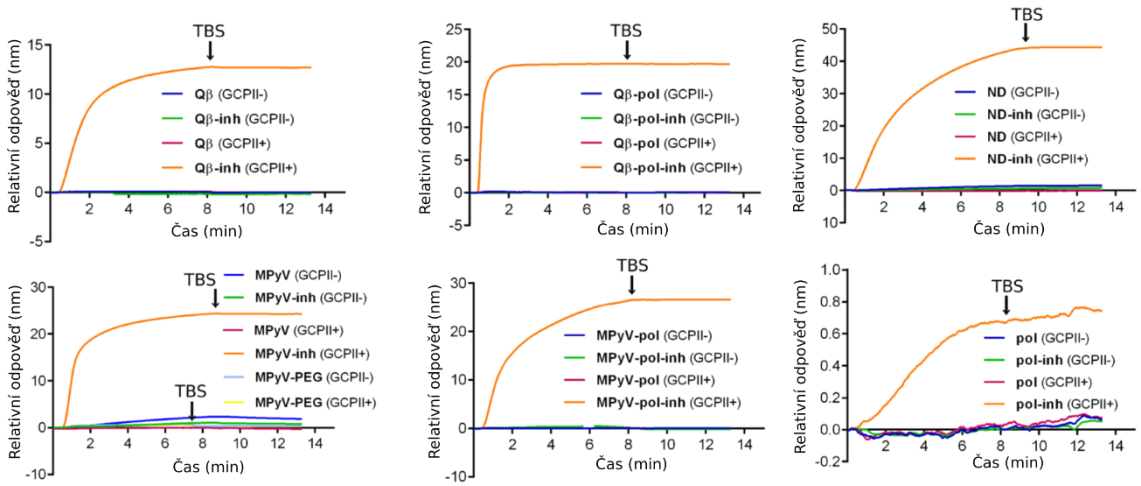

Obrázek 18. Charakterizace interakce částic s GCPII pomocí SPR. Označení nanočástic je identické jako v tabulce 5, krom toho značí „Qβ"– inhibitorem nemodifikované VLP částice Qβ, „Qβ-pol" – VLP částice Qβ modifikované HMPA polymerem, ND – inhibitorem nemodifikované částice nanodiamanty, „MPγV-pol"– VLP částice myšího polyomaviru s navázaným HPMA polymerem, „MPγV" – inhibitorem nemodifikované VLP částice myšího polyomaviru, „MPγV-PEG" - VLP částice myšího polyomaviru s navázaným PEG-karboxylátem. Proteáza GCPII byla imobilizována (na GCPII +) pomocí interakce biotin-neutravidin, negativní kontrolou byl samotný neutravidin (GCPII-).

Pro aktivitu na buněčných liniích mělo kromě klíčové interakce GCPII – inhibitor charakterizované inhibiční konstantou, výrazný vliv i nano-bio rozhraní. U všech částic s výjimkou nemodifikovaných VLP myšího polyomaviru bylo dosaženo rozdílu ve vazbě na GCPII exprimující a neexprimující buňky. Zatímco u naprosté většiny částic (polymery, nanodiamanty, VLP charakteru bakteriofágu Qβ) byla interakce s buňkami neexprimujícími GCPII zanedbatelná, tak VLP částice nemodifikovaného nebo polymery modifikovaného myšího polyomaviru vykazovala stále schopnost vázat i buňky bez exprese GCPII. Předpokládáme, že tento jev může být vysvělen tím, že základní vlastností VLP myšího polyomaviru, jako původních virových částic, je schopnost vázat se na savčí buňky. Toto chování souhlasí i s pozorováním jednotlivých buněk metodou konfokální mikroskopie, kde po inkubaci s nemodifikovanými VLP částicemi myšího polyomaviru dochází zejména k vazbě na buněčnou membránu, oproti cílené internalizaci u částic modifikovaných inhibitorem (obrázek 18). Tato nespecifická interakce je odstranitelná modifikací nano-bio rozhraní částic pomocí PEG_{13} karboxylové kyseliny, který je jako malá molekula schopen se navázat v daleko větší kvantitě než HPMA polymer, a tedy i lépe maskovat původní bio-nano rozhraní z myšího polyomaviru.

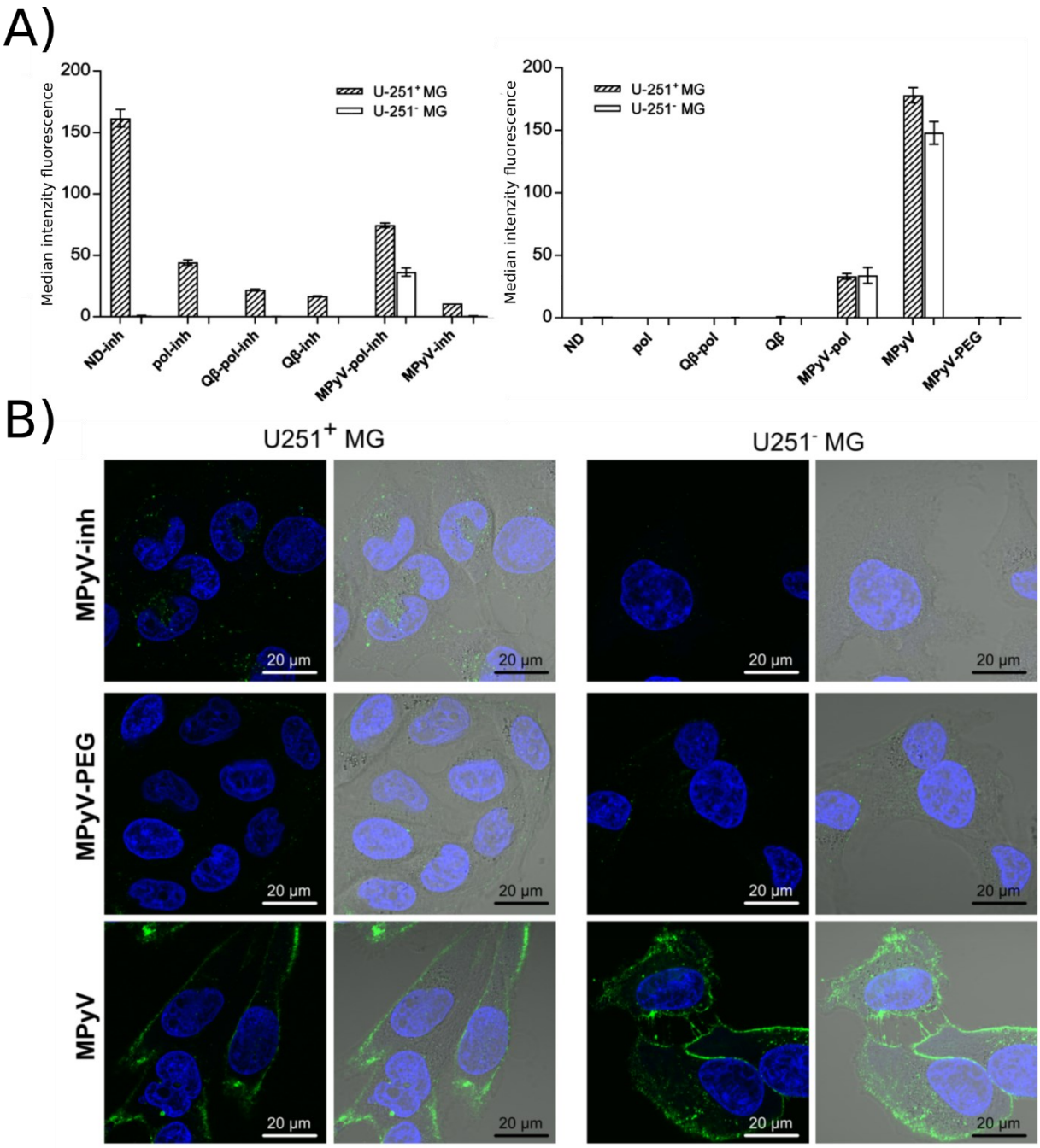

Obrázek 18. Charakterizace interakce částic s GCPII na buněčných liniích. Označení nanočástic je identické jako u tabulky 4 obrázku 8. A) Interakce nanočástic s buňkami buněčné linie U251-MG exprimujících GCPII ($U251^+$ MG) respektive neexprimujících GCPII ($U251^-$ MG). Data jsou prezentovány jako medián intensity fluorescence normalizovaný na autofluorescenci negativních buněk ($U251^-$ MG) a korigovaný dle relativní fluorescence částic. Standardní odchylka je vypočtena z triplikátu měření. V levé části jsou zobrazeny výsledky s nanočásticemi modifikovaných inhibitorem GCPII, kdežto v pravé části jsou výsledky s nanočásticemi bez navázaného inhibitoru B) Reprezentativní obrázky z konfokální mikroskopie zobrazující vazbu nanočástic odvozených s VLP myšího polyomaviru na buňky U251 MG buněčné linie s expresí GCPII ($U251^+$ MG), resp. bez exprese GCPII ($U251^-$ MG). Zeleně je zobrazena fluorescence nanočástic, modře jsou znázorněny jádra (barvení pomocí Hoechst barviva).

Lze shrnout, že silná interakce GCPII-inhibitor umožňuje specifické cílení velmi různorodými typy nanočástic, přičemž pro další zvýšení specifity je kritické omezení nespecifických interakcí optimalizací bio-nano rozhraní vlastních částic.

Můj příspěvek

Mým přínosem na této práci byla optimalizace modifikace bio-nano rozhraní VLP částic myšího polyomaviru k redukci nespecifické vazby a pomoc s přípravou nanočástic modifikovaných polymery. Dále jsem provedl charakterizaci částic stran fluorescenčních vlastností, měření inhibičních konstant částic a přípravu obrázku z konfokální mikroskopie. Podílel jsem se i na měření vstřebávání částic buňkami pomocí průtokové cytometrie a zobrazování navázaných nanočástic pomocí konfokální mikroskopie. Podílel jsem se na návrhu jednotlivých experimentů, analýze vzniklých experimentálních dat, jejich diskusi a konečně i na sepsání rukopisu.

5. Diskuze

V první části disertace jsem se zaměřil na zhodnocení dostupných možností a vývoj nových metod a bioanalytických nástrojů pro analýzu obsahu GCPII. Tyto metody umožňují měřit zastoupení a sledovat GCPII, jak na úrovni organismu, tkání, buněk, tak i subcelulárně, a tím i pomáhají pochopit jeho biologickou funkci. Protilátky obzvláště monoklonální, díky své specifické interakci s antigenem, tvoří klíčový analytický nástroj (Packer, 2021) a vskutku právě protilátka 7E11-C5.3., vzniklá imunizací lyzátem prostatické buněčné linie LNCaP, vedla v minulosti k objevu PSMA (alias GCPII) (Horoszewicz a kol., 1987). Naším prvním krokem proto bylo důkladné zhodnocení vlastností protilátek. Špatná charakterizace protilátek totiž může pro případné nespecifické interakce vést k zavádějícím výsledkům, obzvláště v případě komplexnějších biologických vzorků. Užití nevhodných protilátek současně může vést k rozdílným výsledkům různých autorů.

Protilátky pro studium GCPII byly užity v řadě metod jako imunohistochemie (Baccala a kol., 2007; Haffner a kol., 2009; Chang a kol., 1999; Kinoshita a kol., 2006; Liu a kol., 1997; Silver a kol., 1997), ELISA (Navrátil a kol., 2017; Sokoloff a kol., 2000) a imunoblot – „western blotu“ (Rovenská a kol., 2008; Troyer a kol., 1995), přesto doposud nebylo v literatuře provedeno komparativní srovnání dostupných monoklonálních protilátek. Srovnání není dostupné i proto, že řada publikací neuvádí experimentální podmínky do dostatečných detailů. Naše výsledky, měření interakce jednotlivých protilátek s denaturovanou a nativní formou GCPII pomocí metody ELISA, umožnily určit kromě odhadované síly interakce i preferenční formu antigenu, kterou daná protilátka rozpoznává (nativní vs. denaturovaný). To nám umožnilo roztřídit protilátky do skupiny vhodné pro metody s denaturovaným antigenem (např. imunohistochemie na parafinových řezech, imunoblot – „western blot“) a pro metody spíše s antigenem nativním (průtoková cytometrie, ELISA, imunoprecipitace) a odhadnout dle síly interakce i nutnou koncentraci protilátky pro danou metodu. Oproti dostupné literatuře (Horoszewicz a kol., 1987; Chang a kol., 1999; Kinoshita a kol., 2006) jsme nebyli schopni úspěšně využít protilátku 7E11-C5.3, jak na imunohistochemii, tak ani na průtokové cytometrii, což může být způsobeno tím, že jako jediná dostupná protilátka interaguje s intracelulárním epitopem, který může vyžadovat odlišné metody provedení analýzy. Některé další protilátky (zejména např. protilátka J591), které interagují převážně s nativním antigenem, jsou překvapivě úspěšně využívány v literatuře (Wang a kol., 2011) pro metody s denaturovaným antigenem jako je imunoblot – „western blot“. Možné vysvětlení může být např. nedostatečná denaturace antigenu vedoucí k přítomnosti nativního antigenu.

Protilátky kromě pozitivních vlastností mají i řadu nevýhod jako např. často velmi zdlouhavou přípravu, omezenou stabilitu, v některých případech i obtížnou modifikovatelnost danou vlastní proteinovou strukturou. To nás vedlo, zejména v případě protilátek proti nativní GCPII, k tomu pokusit se najít jejich adekvátní náhradu. V literatuře byla popsána řada různých náhrad protilátek, založených na biopolymerech, jako např. protein, RNA, či syntetických polymerech nebo dokonce malých molekulách (McEnaney a kol., 2014). Co se týče proteinových náhrad, jedná se např. o „affibodies" na základě modifikovaného bakteriálního receptoru (Nord a kol., 1997), či o navrhované proteiny s opakujícími se ankyrinovými doménami (Binz a kol., 2003). U RNA se používají krátké, cca 100 párů basí dlouhé, sekvence zvané aptamery (Ellington a Szostak, 1990). Zástupcem skupiny syntetických polymerů můžou být např. „molecular imprinted polymers" získané polymerizací za přítomnosti antigenu, který je vzniklým polymerem obklopen (Haupt a Mosbach, 1998; Wulff, 1995). Využití HPMA polymeru jako nosiče pro diagnostiku a terapii bylo již ověřeno dříve (Kopecek a Kopecková, 2010; Lu, 2010). Náš inovativní přístup, kdy jsme na HPMA polymer kovalentně navázali malou cílící molekulu (inhibitor) - iBodies, se ukázal jako mimořádně univerzální. Podařilo se nám takto úspěšně nahradit protilátky v průtokové cytometrii, ve vizualizaci na buněčných liniích, v metodě ELISA i v afinitní purifikaci, přičemž v některých případech tato námi vytvořená náhrada vykazovala lepší vlastnosti než dostupné protilátky, mimo jiné např. ve stabilitě.

Po ověření vlastností analytických nástrojů jsme pro další studium fyziologických a patofyzioloických efektů GCPII přistoupili k charakterizaci jednoho z nejdostupnějších biomodelů, tj. myši. Jedině *in vivo* studie totiž může poskytnout dostatečné množství relevantních informací na úrovni celého organismu. Výrazná podobnost užitého biomodelu s člověkem je podmínkou, aby vzniklé poznatky mohly být užitečné i pro humánní medicínu. Myš tvoří pro svoji dostupnost jeden ze základních biomodelů pro studium fyziologických a patofyziologický jevů. Co se týče GCPII však myší biomodel nebyl doposud plně charakterizován, přestože v literatuře je dostupná řada prací, která analyzuje efekt GCPII na myším modelu, zejména v oblasti nervového systému – např. (Bacich a kol., 2005; Gao a kol., 2015; Vornov a kol., 1999). Z toho důvodu jsme nejprve zevrubně prozkoumali enzymologické a biochemické vlastnosti myšího homologu GCPII. Až na mírně nižší aktivitu z důvodů vyššího K_M a striktnější substrátovou specifitu, nevykazovala myší GCPII výraznější biochemické odchylky oproti lidské GCPII. Dále jsme provedli analýzu expresního profilu GCPII v myši, který oproti jiným biomodelům, jako potkan, prase (Rovenská a kol., 2008), nebyl dosud zevrubně studován a byly dostupné pouze limitované informace týkající se vybraných tkání

(Aggarwal a kol., 2006; Bacich a kol., 2001; Bacich a kol., 2002). Obdobně jako v předchozích pracích (Bacich a kol., 2001; Bacich a kol., 2002) jsme identifikovali výraznou expresi v mozku a ledvinách, zatímco expresi v prostatě jsme nepozorovali (Aggarwal a kol., 2006). Mimo to jsme zachytili expresi ve slinných žlázách, zejména u žlázy podjazykové. Tento nález je v souladu i se známou expresí GCPII ve slinných žlázách člověka (Israeli a kol., 1994; Troyer a kol., 1995; Wolf a kol., 2010). Přestože v myši i člověku je GCPII přítomna ve slinných žlázách, histologická lokalizace je odlišná, u člověka převažuje lokalizace v acinárních buňkách (Wolf a kol., 2010), zatímco v myši jsme pozorovali pozitivitu zejména v nesekrečních abluminálních buňkách. Obdobně jako u potkana (Rovenská a kol., 2008) jsme u myši nepozorovali výraznou expresi GCPII v tenkém střevě. Expresní profil v orgánech urogenitálního traktu jsme dále upřesnili v další publikaci, kde jsme opět nebyli schopni nalézt expresi GCPII v žádné části myší prostaty. Nově jsme ale zachytili výraznou expresi v nadvarleti, a to jak u myši, tak u člověka.

Celkově lze shrnout, že myš pro biochemické podobnosti myšího homologu GCPII a podobný expresní profil tvoří adekvátního biomodel pro *in vivo* studie nervového systému a patrně i ledvin. Naproti tomu vzhledem k nepřítomnosti GCPII v myším tenkém střevě (ileum a jejunum) lze předpokládat, že GCPII není pro vstřebávání folátů u myši zásadní. Může to souviset i s nižší aktivitou myšího homologu GCPII vůči pteroyl-di-glutamátu oproti lidskému homologu. Lze předpokládat, že u myši i u potkana, je místo GCPII odštěpování γ-vázaných glutamátů z folylpolyglutamátů zprostředkováno γ-glutamyl hydrolázou (Shafizadeh a Halsted, 2007). Myš tak pro folátový metabolismus nejspíše není vhodným biomodelem. V urogenitálním traktu jsme souhrnně zachytili výraznější expresi GCPII pouze v nadvarleti, v prostatě oproti člověku v souladu s literaturou (Aggarwal a kol., 2006; Bacich a kol., 2001) jsme přítomnost GCPII nepozorovali. Lze tedy předpokládat, že poznatky získané na myším modelu spojené s aktivitou GCPII v urogenitálním systému budou mít limitovanou přenositelnost do humánní medicíny. Vzhledem k tomu, že v myší prostatě nebyla GCPII detekována, můžeme uvažovat ve vztahu ke GCPII nad správností ortotopických myších modelů karcinogeneze prostaty. Ostatně i u myších transgenních modelů karcinomu prostaty nejsou data v plném souladu – viz kapitola 1.3. Stručně, v „Hi-Myc“ modelu, kde exprese onkogenu Myc je řízená probasinovým promotorem specifickým pro prostatu, byla pozitivita popsána (Simons a kol., 2019). V TRAMP modelu, vytvořených expresí SV40 T antigenu opět pod probasinovým promotorem, byla exprese GCPII v některých pracích nalezena (Caromile a kol., 2017; Schmittgen a kol., 2003b; Yang a kol., 2001), kdežto v jiných nikoli (Simons a kol.,

2019). Na druhou stranu není zjištění absence GCPII v myší prostatě natolik překvapivé vzhledem k výrazným anatomickým a histologickým rozdílům mezi myší a lidskou prostatou (Oliveira a kol., 2016).

Prokázaná částečná podobnost mezi biochemickými vlastnostmi a expresními profily u člověka a myši, nám umožnila použít model myši deficientní v genu pro GCPII k dalšímu studiu fyziologické a patofyziologické funkce GCPII. Dosavadní výsledky fenotypů myší deficientních v GCPII byly ve značném rozporu. Zatímco někteří autoři pozorovali embryonální letalitu (Han a kol., 2009; Tsai a kol., 2003b), jiní nepozorovali žádný výrazně nepříznivý fenotyp (Bacich a kol., 2002; Gao a kol., 2015). Všechny tyto kmeny myší deficientní v genu pro GCPII byly vytvořeny standardní technikou pomocí manipulace embryonálních kmenových buněk, jednotlivé cíle zásahu však byly odlišné. V jedné z prvních prací byl zásah v intron-exonovém rozhraní prvního a druhého exonů s vložením několika stop-kodonů (Bacich a kol., 2002). Dalšími přístupy byla delece exonů 9 a 10 (Tsai a kol., 2003b), exonů 3-5 (Gao a kol., 2015), nebo prvního a druhého exonu (Han a kol., 2009). Zda tyto vlastní konkrétní postupy přímo vedly k embryonální úmrtnosti není dosud zcela objasněno (Vorlova a kol., 2019).

V naší práci jsme vytvořili nový myší model v genu pro GCPII odlišnou metodou – pomocí specifických TALEN (endonukléz). Vzniklé myši deficientní v GCPII nevykazovaly žádný zjevný fenotyp kromě tendence k dřívější dilataci semenných váčku ve stáří. Jedná se tak o první nalezený fenotyp delece GCPII genu v urogenitální oblasti. Patofyziologický proces, který vedl k této dilataci, se nám zatím nepodařilo rozklíčovat. Mezi možné hypotézy může patřit např. defekt vnitřní signalizace mezi jednotlivými orgány urogenitálního systému při chybějící fyziologické expresi GCPII v nadvarleti. Alternativně, absence GCPII v centrálním nervovém systémů může ovlivnit míru fyzické aktivity, a tak druhotně ovlivnit velikost semenných váčku (Chigurupati a kol., 2008).

V rámci výzkumu fyziologické funkce GCPII jsme se zaměřili i na publikovanou velmi překvapivou schopnost štěpit amyloidogenní peptidy $A\beta_{1-40}$ a $A\beta_{1-42}$ (Kim a kol., 2010b; Lee a kol., 2013). Tato aktivita by totiž měla dalekosáhlé důsledky v případném klinickém užití inhibitorů GCPII, neboť snížením degradace amyloidogeních peptidů inhibicí GCPII by mohlo dojít k zvýšení rizika tvorby amyloidogenních plaků, a tedy i dojít ke zvýšení rizika vzniku Alzheimerovy choroby. Neobvyklost amyloidogenních peptidů jako substrátů GCPII vyplývá již ze základní katalytické a enzymové specifity GCPII, kde GCPII má primárně karboxypeptidasovou aktivitu pro C-terminální acidické aminokyseliny. Schopnost degradace

amyloidogenních peptidů se nám stejně jako v práci (Alt a kol., 2013) nepodařilo potvrdit (viz kapitola 4.5).

GCPII alias PSMA, díky své expresi na nádorových buňkách se stává jednou z často užívaných cílových molekul pro směřování léčiv i pro diagnostiku. Řada publikací užila pro cílení různých přístupů, např. protilátek (Mukherjee a kol., 2014; Nagesh a kol., 2016; Tian a kol., 2021), aptamerů (Kim a kol., 2010a; Kolishetti a kol., 2010), peptidů (Severic a kol., 2021) či inhibitorů (Banerjee a kol., 2017; Chen a kol., 2016; Sanna a kol., 2017; Xu a kol., 2017; Yari a kol., 2019), přičemž vlastní částice byly tvořeny nanočásticemi s anorganickým jádrem (Kim a kol., 2010a; Mukherjee a kol., 2014; Nagesh a kol., 2016), polymerními strukturami (Banerjee a kol., 2017; Kolishetti a kol., 2010; Sanna a kol., 2017; Xu a kol., 2017), liposomy (Tian a kol., 2021; Yari a kol., 2019) či exosomy (Severic a kol., 2021).

Velmi slibné výsledky s HPMA polymery vázající GCPII nás vedly k hypotéze, zda interakce GCPII-inhibitor nemůže sloužit jako univerzální metoda pro směřování nanostuktur. Dalším vodítkem byla i hodnota inhibiční konstanty námi použitých inhibitorů, která se pohybovala v nanomolárním rozmezí, a tak se blížila k interakčním konstantám běžně užívaným k směřování léčiv – jako je interakce transferin-transferinový receptor (Ward a kol., 1982) či interakce „RGD“ peptidů s $\alpha_v\beta_3$ integriny (Sancey a kol., 2009). Modifikovali jsme částice jak rigidní (nanodiamanty), tak flexibilnější (polymerní nanočástice), tak i dva typy původně biologických částic – VLP částice bakteriofágu Qβ a VLP částice myšího poliomaviru. Kovalentní navázání proběhlo jak cestou konjugace s malou molekulou, tak i navázáním celého HPMA polymeru s již navázanými inhibitory. Všechny přístupy vedly k částicím, které jak *in vitro,* tak i na buněčných liniích byly schopny efektivně vázat GCPII, přičemž byl pozorován signifikantní aviditní efekt, vedoucí k výraznému poklesu inhibiční konstanty, daný tím, že na nanočástice bylo navázano více molekul inhibitoru.

Klíčovým parametrem pro specifitu vazby nanočástic na buňky buněčných linii bylo vlastní bio-nano rozhraní nanočástic. Zatímco HPMA polymerní částice, HPMA pokryté nanodiamanty a částice bakteriofágu Qβ vykazovaly samy o sobě nízkou interakci s testovanými buněčnými liniemi, tak VLP částice myšího polyomaviru vykazovaly bez dalších modifikací poměrně výraznou nespecifickou interakci. Tato nespecifická vazba, je nejspíše způsobena faktem, že myší polyomavirus je schopen se díky VP1 kapsidovému proteinu vázat na gangliosidy na buňkách (Tsai a kol., 2003a; You a kol., 2015). Tato nespecifita je však odstranitelná modifikací přirozeného bio-nano rozhraní VLP částic navázáním velkého proteinu (Zackova Suchanova a kol., 2017). V našem případě byla velmi účinná modifikace

pomocí PEG-karboxylové kyseliny, kdežto navázání HPMA polymerů bylo účinné výrazněji méně, nejspíše vzhledem k nízkému množství navázaných molekul polymeru a tím i malou chráněnou plochou nanočástice. Prokázali jsme tím značnou míru univerzálnosti cílícího systému s využitím GCPII inhibitoru pro další potenciální biomedicínské použití.

6. Souhrn

Ve své disertační práci jsem se v první řadě zaměřil na analýzu vhodných analytických nástrojů pro studium GCPII. Zevrubně jsme charakterizovali komerčně dostupné používané monoklonální protilátky a současně jsme vyvinuli plně syntetickou náhradu protilátek založenou na HPMA polymeru s navázanými inhibitory GCPII, která v některý parametrech vykazovala, např. ve stabilitě, lepší vlastnosti. Pro *in vivo* studii fyziologické a patofyziologické role GCPII jsme zvolili myš jako experimentální biomodel, tento model jsme charakterizovali jak na biochemické, tak i expresní úrovni a porovnali s dostupnými poznatky u člověka. Naše výsledky prokázaly dobrou přenositelnost získaných poznatků v oblasti nervového systému. Data získaná v urogenitální oblasti a trávicím traktu budou vzhledem k rozdílnému expresnímu profilu aplikovatelná do humánní biomedicíny jen částečně. Jako vedlejší výsledek jsme nově pozorovali expresi v nadvarleti a slinných žlázách. Následně jsme vzhledem k dosavadním nesouladům v literatuře (Bacich a kol., 2005; Gao a kol., 2015; Han a kol., 2009; Tsai a kol., 2003b) vytvořili ve spolupráci se skupinou funkční genomiky Dr. Sedláčka (BIOCEV) vlastní myší GCPII-deficientní model pomocí TALEN (endonukleáz). Tento model jsme charakterizovali, a kromě pozorování zvětšených semenných váčků u starších samců jsme nezaznamenali žádný další zjevný fenotyp. Zvětšení semenných váčků může souviset s chybějící expresí GCPII v nadvarleti, ale nelze ani vyloučit např. ovlivnění vzorců fyzické aktivity zpětně ovlivňující urogenitální systém (Han a kol., 2009; Chigurupati a kol., 2008). Pro důkladnější pochopení patofyziologie však bude jistě nutný další výzkum. Nepřítomnost žádného výrazného fenotypu, a v souladu s prací (Alt a kol., 2013) vyvrácená schopnost štěpit amyloidní peptidy ($A\beta_{1-40}$ a $A\beta_{1-42}$) ukazuje, že chybějící aktivita GCPII v organismu nemá žádné evidentní negativní dopady. Toto pozorování je obzvláště důležité pro užití inhibice a cílení GCPII jako důležitého přístupu v terapii a diagnostice neurologických a onkologických onemocnění. Když nepřítomnost enzymu nevyvolává žádné výrazné nežádoucí účinky, lze předpokládat, že ani farmakologická inhibice GCPII nebude vést k signifikantním nežádoucím účinkům. Závěrem jsme, díky výborné schopnosti našich polymerních HPMA částic vázat GCPII, provedli rozsáhlou analýzu, zda interakce GCPII-inhibitor může sloužit jako univerzální přístup k specifickému cílení léčiv do nádorových buněk. Vazba inhibitor-GCPII umožnila specifické směřování jak anorganických a rigidních (nanodiamanty), flexibilních (polymerní částice) tak i VLP částic, přičemž klíčová byla optimalizace bio-nano rozhraní k redukci nespecifické vazby. Nanočástice s navázaným GCPII inhibitorem tak mohou tvořit novou cestu, jak specificky dopravovat léčivo např. do nádorových buněk.

7. Seznam publikací

Publikace, které jsou podkladem dizertační práce

1. Tykvart J, Navrátil V, **Sedlák F**, Corey E, Colombatti M, Fracasso G, Koukolík F, Bařinka C, Šácha P, Konvalinka J. **Comparative analysis of monoclonal antibodies against prostate-specific membrane antigen (PSMA).** *Prostate.* 2014 Dec;74(16):1674-90. **IF (2014) = 4,051**
2. Šácha P, Knedlík T, Schimer J, Tykvart J, Parolek J, Navrátil V, Dvořáková P, **Sedlák F**, Ulbrich K, Strohalm J, Majer P, Šubr V, Konvalinka J. iBodies: **Modular Synthetic Antibody Mimetics Based on Hydrophilic Polymers Decorated with Functional Moieties.** *Angew Chem Int Ed Engl.* 2016 Feb 12;55(7):2356-60. **IF (2016) = 11,994**
3. Knedlík T, Vorlová B, Navrátil V, Tykvart J, **Sedlák F**, Vaculín Š, Franěk M, Šácha P, Konvalinka J.: **Mouse glutamate carboxypeptidase II (GCPII) has a similar enzyme activity and inhibition profile but a different tissue distribution to human GCPII.** *FEBS Open Bio*. 2017 Aug 29;7(9):1362-1378. **IF (2017) = 1,81**
4. Vorlová B, **Sedlák F**, Kašpárek P, Šrámková K, Malý M, Zámečník J, Šácha P, Konvalinka J.: **A novel PSMA/GCPII-deficient mouse model shows enlarged seminal vesicles upon aging.** *Prostate.* 2019 Feb;79(2):126-139. **IF (2013) = 3,279**
5. **Sedlák F**, Šácha P, Blechová M, Březinová A, Šafařík M, Šebestík J, Konvalinka J.: **Glutamate carboxypeptidase II does not process amyloid-β peptide.** *FASEB J.* 2013 Jul;27(7):2626-32. **IF (2013) = 3,188**
6. Neburková J, **Sedlák F**, Žáčková Suchanová J, Kostka L, Šácha P, Šubr V, Etrych T, Šimon P, Bařinková J, Kryštufek R, Španielová H, Forstová J, Konvalinka J, Cígler P: **Inhibitor-GCPII Interaction: Selective and Robust System for Targeting Cancer Cells with Structurally Diverse Nanoparticles.** *Mol Pharm.* 2018 Aug 6;15(8):2932-2945. **IF (2013) = 4,65**
7. UOHCB AV ČR, UMCH AVCR, PřF UK. **Macromolecular conjugates for visualization and separation of proteins and cells,** Původci: Šácha P, Konvalinka J, Schimer J, Knedlík T, Navrátil V, Tykvart J, **Sedlák F**, Majer P, Cígler P, Šubr V, Ulbrich K. Strohalm J. Evropský patent EP3245514B1. Publikováno 10.července 2019, přihlášeno 14.1.2015. – **Bez IF.**

Ostatní publikace

1. Šlegerová J, Hájek M, Řehoř I, **Sedlák F**, Stursa J, Hrubý M, Cígler P.: **Designing the nanobiointerface of fluorescent nanodiamonds: highly selective targeting of glioma cancer cells.** Nanoscale. 2015 Jan 14;7(2):415-20 **IF (2015) = 7.76**
2. Sivá M, Svoboda M, Veverka V, Trempe JF, Hofmann K, Kožíšek M, Hexnerová R, **Sedlák F**, Belza J, Brynda J, Šácha P, Hubálek M, Starková J, Flaisigová I, Konvalinka J, Šašková KG: **Human DNA-Damage-Inducible 2 Protein Is Structurally and Functionally Distinct from Its Yeast Ortholog.** *Sci Rep.* 2016 Jul 27;6:30443. **IF (2016) = 4,59**
3. Fassmannová D, **Sedlák F**, Sedláček J, Špička I, Grantz Šašková K: **Nelfinavir Inhibits the TCF11/Nrf1-Mediated Proteasome Recovery Pathway in Multiple Myeloma.** *Cancers (Basel).* 2020 Apr 25;12(5):1065. **IF (2020) = 6,639**
4. Radocha J, Jelinek T, Pour L, Spicka I, Minarik J, Popkova T, Jungova A, Pavlicek P, Brozova L, Stork M, **Sedlák F**, Krhovska P, Maisnar V, Heindorfer A, Sykora M, Wrobel M, Mikula P, Kessler P, Ullrychova J, Hajek R: **Urine immunofixation negativity is not necessary for complete response in intact immunoglobulin multiple myeloma: Retrospective real-world confirmation.** *Int J Lab Hematol.* 2021 Oct;43(5):e244-e247. **IF (2021) = 2,877**
5. Hejdanková Z, Vaněk V, **Sedlák F**, Procházka J, Diederichs A, Kereïche S, Novotná B, Budešínsky M, Birkuš G, Šašková KG, Cígler P: **Lipid Nanoparticles for Broad-Spectrum Nucleic Acid Delivery.** *Adv. Funct. Mater.* 2021, 31, 2101391. **IF (2020/2021) = 18,808**
6. **Sedlák F.**: **Léčba epizody bolesti u pacienta s pokročilým B-buněčným lymfomem.** *Acta Medicinae*, 2016, vol. 5, s. 34-35. **Bez IF.**
7. Špička I, **Sedlák F**: **Mnohočetný myelom - jsme schopni pacienta v roce 2020 vyléčit?.** *Postgraduální medicína*, 2020, vol. 22, s. 53-58. **Bez IF.**
8. ÚOCHB AV ČR. **Odběrová sada k nasálnímu steru s integrovaným imuno-chromatografickým testem.** Původci: Pokorný V, Šácha P, Kryštůfek R, **Sedlák F**, Bakeš R. Užitný vzor. CZ35263U1, přihlášeno 10.3.2021. **Bez IF.**
9. **Sedlák, F., Jednoduché měření geomagnetického pole**, Jemná mechanika a optika, 2005, 50 (5), 155-156. **Bez IF.**

8. Seznam referencí

Afman, L.A., Trijbels, F.J., and Blom, H.J. (2003). The H475Y polymorphism in the glutamate carboxypeptidase II gene increases plasma folate without affecting the risk for neural tube defects in humans. The Journal of nutrition *133*, 75-77.

Afshar-Oromieh, A., da Cunha, M.L., Wagner, J., Haberkorn, U., Debus, N., Weber, W., Eiber, M., Holland-Letz, T., and Rauscher, I. (2021). Performance of [(68)Ga]Ga-PSMA-11 PET/CT in patients with recurrent prostate cancer after prostatectomy-a multi-centre evaluation of 2533 patients. Eur J Nucl Med Mol Imaging *48*, 2925-2934.

Aggarwal, S., Ricklis, R.M., Williams, S.A., and Denmeade, S.R. (2006). Comparative study of PSMA expression in the prostate of mouse, dog, monkey, and human. The Prostate *66*, 903-910.

Alt, J., Stathis, M., Rojas, C., and Slusher, B. (2013). Glutamate carboxypeptidase II is not an amyloid peptide-degrading enzyme. FASEB journal : official publication of the Federation of American Societies for Experimental Biology *27*, 2620-2625.

Althaus, M.A., and Pichler, W.J. (1994). Nasal application of a gel formulation of N-acetyl-aspartyl glutamic acid (NAAGA) compared with placebo and disodium cromoglycate in the symptomatic treatment of pollinosis. Allergy *49*, 184-188.

Anderson, K.J., Monaghan, D.T., Cangro, C.B., Namboodiri, M.A., Neale, J.H., and Cotman, C.W. (1986). Localization of N-acetylaspartylglutamate-like immunoreactivity in selected areas of the rat brain. Neuroscience letters *72*, 14-20.

Anilkumar, G., Barwe, S.P., Christiansen, J.J., Rajasekaran, S.A., Kohn, D.B., and Rajasekaran, A.K. (2006). Association of prostate-specific membrane antigen with caveolin-1 and its caveolae-dependent internalization in microvascular endothelial cells: implications for targeting to tumor vasculature. Microvascular research *72*, 54-61.

Anilkumar, G., Rajasekaran, S.A., Wang, S., Hankinson, O., Bander, N.H., and Rajasekaran, A.K. (2003). Prostate-specific membrane antigen association with filamin A modulates its internalization and NAALADase activity. Cancer research *63*, 2645-2648.

Ardies, P.J., Gykiere, P., Goethals, L., De Mey, J., De Geeter, F., and Everaert, H. (2017). PSMA Uptake in Mediastinal Sarcoidosis. Clinical nuclear medicine *42*, 303-305.

Arun, P., Madhavarao, C.N., Moffett, J.R., and Namboodiri, M.A. (2006). Regulation of N-acetylaspartate and N-acetylaspartylglutamate biosynthesis by protein kinase activators. J Neurochem *98*, 2034-2042.

Auton, A., Abecasis, G.R., Altshuler, D.M., Durbin, R.M., Abecasis, G.R., Bentley, D.R., Chakravarti, A., Clark, A.G., Donnelly, P., Eichler, E.E.*, a kol.* (2015). A global reference for human genetic variation. Nature *526*, 68-74.

Baccala, A., Sercia, L., Li, J., Heston, W., and Zhou, M. (2007). Expression of prostate-specific membrane antigen in tumor-associated neovasculature of renal neoplasms. Urology *70*, 385-390.

Bacich, D.J., Pinto, J.T., Tong, W.P., and Heston, W.D. (2001). Cloning, expression, genomic localization, and enzymatic activities of the mouse homolog of prostate-specific membrane antigen/NAALADase/folate hydrolase. Mammalian genome : official journal of the International Mammalian Genome Society *12*, 117-123.

Bacich, D.J., Ramadan, E., O'Keefe, D.S., Bukhari, N., Wegorzewska, I., Ojeifo, O., Olszewski, R., Wrenn, C.C., Bzdega, T., Wroblewska, B.*, a kol.* (2002). Deletion of the glutamate carboxypeptidase II gene in mice reveals a second enzyme activity that hydrolyzes N-acetylaspartylglutamate. J Neurochem *83*, 20-29.

Bacich, D.J., Wozniak, K.M., Lu, X.C., O'Keefe, D.S., Callizot, N., Heston, W.D., and Slusher, B.S. (2005). Mice lacking glutamate carboxypeptidase II are protected from peripheral neuropathy and ischemic brain injury. J Neurochem *95*, 314-323.

Bander, N.H., Milowsky, M.I., Nanus, D.M., Kostakoglu, L., Vallabhajosula, S., and Goldsmith, S.J. (2005). Phase I trial of 177lutetium-labeled J591, a monoclonal antibody to prostate-specific membrane antigen, in patients with androgen-independent prostate cancer. J Clin Oncol *23*, 4591-4601.

Bander, N.H., Trabulsi, E.J., Kostakoglu, L., Yao, D., Vallabhajosula, S., Smith-Jones, P., Joyce, M.A., Milowsky, M., Nanus, D.M., and Goldsmith, S.J. (2003). Targeting metastatic prostate cancer with radiolabeled monoclonal antibody J591 to the extracellular domain of prostate specific membrane antigen. J Urol *170*, 1717-1721.

Banerjee, S.R., Foss, C.A., Horhota, A., Pullambhatla, M., McDonnell, K., Zale, S., and Pomper, M.G. (2017). (111)In- and IRDye800CW-Labeled PLA-PEG Nanoparticle for Imaging Prostate-Specific Membrane Antigen-Expressing Tissues. Biomacromolecules *18*, 201-209.

Barinka, C., Hlouchova, K., Rovenska, M., Majer, P., Dauter, M., Hin, N., Ko, Y.S., Tsukamoto, T., Slusher, B.S., Konvalinka, J.*, a kol.* (2008). Structural basis of interactions between human glutamate carboxypeptidase II and its substrate analogs. Journal of molecular biology *376*, 1438-1450.

Barinka, C., Rinnová, M., Sácha, P., Rojas, C., Majer, P., Slusher, B.S., and Konvalinka, J. (2002). Substrate specificity, inhibition and enzymological analysis of recombinant human glutamate carboxypeptidase II. J Neurochem *80*, 477-487.

Barinka, C., Rovenská, M., Mlcochová, P., Hlouchová, K., Plechanovová, A., Majer, P., Tsukamoto, T., Slusher, B.S., Konvalinka, J., and Lubkowski, J. (2007a). Structural insight into the pharmacophore pocket of human glutamate carboxypeptidase II. Journal of medicinal chemistry *50*, 3267-3273.

Barinka, C., Sácha, P., Sklenár, J., Man, P., Bezouska, K., Slusher, B.S., and Konvalinka, J. (2004). Identification of the N-glycosylation sites on glutamate carboxypeptidase II necessary for proteolytic activity. Protein science : a publication of the Protein Society *13*, 1627-1635.

Barinka, C., Starkova, J., Konvalinka, J., and Lubkowski, J. (2007b). A high-resolution structure of ligand-free human glutamate carboxypeptidase II. Acta crystallographica Section F, Structural biology and crystallization communications *63*, 150-153.

Baum, V., Bühler, P., Gierschner, D., Herchenbach, D., Fiala, G.J., Schamel, W.W., Wolf, P., and Elsässer-Beile, U. (2013). Antitumor activities of PSMA×CD3 diabodies by redirected T-cell lysis of prostate cancer cells. Immunotherapy *5*, 27-38.

Becker, I., Lodder, J., Gieselmann, V., and Eckhardt, M. (2010). Molecular characterization of N-acetylaspartylglutamate synthetase. J Biol Chem *285*, 29156-29164.

Beckett, M.L., Cazares, L.H., Vlahou, A., Schellhammer, P.F., and Wright, G.L. (1999). Prostate-specific Membrane Antigen Levels in Sera from Healthy Men and Patients with Benign Prostate Hyperplasia or Prostate Cancer. Clinical Cancer Research *5*, 4034.

Behnam Azad, B., Banerjee, S.R., Pullambhatla, M., Lacerda, S., Foss, C.A., Wang, Y., Ivkov, R., and Pomper, M.G. (2015). Evaluation of a PSMA-targeted BNF nanoparticle construct. Nanoscale *7*, 4432-4442.

Bendell, J., Saleh, M., Rose, A.A., Siegel, P.M., Hart, L., Sirpal, S., Jones, S., Green, J., Crowley, E., Simantov, R.*, a kol.* (2014). Phase I/II study of the antibody-drug conjugate glembatumumab vedotin in patients with locally advanced or metastatic breast cancer. J Clin Oncol *32*, 3619-3625.

Berger, U.V., Carter, R.E., and Coyle, J.T. (1995). The immunocytochemical localization of N-acetylaspartyl glutamate, its hydrolysing enzyme NAALADase, and the NMDAR-1 receptor at a vertebrate neuromuscular junction. Neuroscience *64*, 847-850.

Berger, U.V., Luthi-Carter, R., Passani, L.A., Elkabes, S., Black, I., Konradi, C., and Coyle, J.T. (1999). Glutamate carboxypeptidase II is expressed by astrocytes in the adult rat nervous system. J Comp Neurol *415*, 52-64.

Binz, H.K., Stumpp, M.T., Forrer, P., Amstutz, P., and Plückthun, A. (2003). Designing repeat proteins: well-expressed, soluble and stable proteins from combinatorial libraries of consensus ankyrin repeat proteins. Journal of molecular biology *332*, 489-503.

Blasco, H., Mavel, S., Corcia, P., and Gordon, P.H. (2014). The glutamate hypothesis in ALS: pathophysiology and drug development. Current medicinal chemistry *21*, 3551-3575.

Boarman, D.M., and Allegra, C.J. (1992). Intracellular metabolism of 5-formyl tetrahydrofolate in human breast and colon cell lines. Cancer research *52*, 36-44.

Bois, F., Noirot, C., Dietemann, S., Mainta, I.C., Zilli, T., Garibotto, V., and Walter, M.A. (2020). [(68)Ga]Ga-PSMA-11 in prostate cancer: a comprehensive review. Am J Nucl Med Mol Imaging *10*, 349-374.

Bostwick, D.G., Pacelli, A., Blute, M., Roche, P., and Murphy, G.P. (1998). Prostate specific membrane antigen expression in prostatic intraepithelial neoplasia and adenocarcinoma. Cancer *82*, 2256-2261.

Bouhlal, H., Blondin, C., Haeffner-Cavaillon, N., and Goldschmidt, P. (2002). [N acetyl-aspartyl glutamic acid (NAAGA) inhibits the adhesion of leukocytes to activated endothelial cells and down-modulates the cytokine-induced expression of adhesion molecules]. Journal francais d'ophtalmologie *25*, 993-1000.

Brignole-Baudouin, F., Robert, P.Y., Creuzot-Garcher, C., Olmiere, C., Delval, L., and Baudouin, C. (2009). [Evaluation of NAAGA efficacy in dry eye syndrome]. Journal francais d'ophtalmologie *32*, 613-620.

Bruno, V., Battaglia, G., Casabona, G., Copani, A., Caciagli, F., and Nicoletti, F. (1998a). Neuroprotection by glial metabotropic glutamate receptors is mediated by transforming growth factor-beta. J Neurosci *18*, 9594-9600.

Bruno, V., Wroblewska, B., Wroblewski, J.T., Fiore, L., and Nicoletti, F. (1998b). Neuroprotective activity of N-acetylaspartylglutamate in cultured cortical cells. Neuroscience *85*, 751-757.

Burlina, A.P., Ferrari, V., Burlina, A.B., Ermani, M., Boespflug-Tanguy, O., and Bertini, E. (2006). N-acetylaspartylglutamate (NAAG) in Pelizaeus-Merzbacher disease. Adv Exp Med Biol *576*, 353-359; discussion 361-353.

Butterworth, C.E., Jr., Baugh, C.M., and Krumdieck, C. (1969). A study of folate absorption and metabolism in man utilizing carbon-14--labeled polyglutamates synthesized by the solid phase method. J Clin Invest *48*, 1131-1142.

Bychkov, A., Vutrapongwatana, U., Tepmongkol, S., and Keelawat, S. (2017). PSMA expression by microvasculature of thyroid tumors - Potential implications for PSMA theranostics. Scientific reports *7*, 5202.

Cai, Z., Lin, S., and Rhodes, P.G. (2002). Neuroprotective effects of N-acetylaspartylglutamate in a neonatal rat model of hypoxia-ischemia. European journal of pharmacology *437*, 139-145.

Cangro, C.B., Namboodiri, M.A., Sklar, L.A., Corigliano-Murphy, A., and Neale, J.H. (1987). Immunohistochemistry and biosynthesis of N-acetylaspartylglutamate in spinal sensory ganglia. J Neurochem *49*, 1579-1588.

Cao, K.Y., Mao, X.P., Wang, D.H., Xu, L., Yuan, G.Q., Dai, S.Q., Zheng, B.J., and Qiu, S.P. (2007). High expression of PSM-E correlated with tumor grade in prostate cancer: a new alternatively spliced variant of prostate-specific membrane antigen. The Prostate *67*, 1791-1800.

Cao, K.Y., Xu, L., Zhang, D.M., Zhang, X.M., Zhang, T., He, X., Wang, Z., Feng, F.S., Qiu, S.P., and Shen, G.X. (2012). New alternatively spliced variant of prostate-specific membrane antigen PSM-E suppresses the proliferation, migration and invasiveness of prostate cancer cells. International journal of oncology *40*, 1977-1985.

Carlton, S.M., Hargett, G.L., and Coggeshall, R.E. (2001). Localization of metabotropic glutamate receptors 2/3 on primary afferent axons in the rat. Neuroscience *105*, 957-969.

Caromile, L.A., Dortche, K., Rahman, M.M., Grant, C.L., Stoddard, C., Ferrer, F.A., and Shapiro, L.H. (2017). PSMA redirects cell survival signaling from the MAPK to the PI3K-AKT pathways to promote the progression of prostate cancer. Science signaling *10*.

Cartmell, J., Monn, J.A., and Schoepp, D.D. (1999). The metabotropic glutamate 2/3 receptor agonists LY354740 and LY379268 selectively attenuate phencyclidine versus d-amphetamine motor behaviors in rats. The Journal of pharmacology and experimental therapeutics *291*, 161-170.

Collard, F., Stroobant, V., Lamosa, P., Kapanda, C.N., Lambert, D.M., Muccioli, G.G., Poupaert, J.H., Opperdoes, F., and Van Schaftingen, E. (2010). Molecular identification of N-acetylaspartylglutamate synthase and beta-citrylglutamate synthase. J Biol Chem *285*, 29826-29833.

Collard, F., Vertommen, D., Constantinescu, S., Buts, L., and Van Schaftingen, E. (2011). Molecular identification of β-citrylglutamate hydrolase as glutamate carboxypeptidase 3. J Biol Chem *286*, 38220-38230.

Colombatti, M., Grasso, S., Porzia, A., Fracasso, G., Scupoli, M.T., Cingarlini, S., Poffe, O., Naim, H.Y., Heine, M., Tridente, G.*, a kol.* (2009). The prostate specific membrane antigen regulates the expression of IL-6 and CCL5 in prostate tumour cells by activating the MAPK pathways. PloS one *4*, e4608.

Conway, R.E., Joiner, K., Patterson, A., Bourgeois, D., Rampp, R., Hannah, B.C., McReynolds, S., Elder, J.M., Gilfilen, H., and Shapiro, L.H. (2013). Prostate specific membrane antigen produces pro-angiogenic laminin peptides downstream of matrix metalloprotease-2. Angiogenesis *16*, 847-860.

Conway, R.E., Petrovic, N., Li, Z., Heston, W., Wu, D., and Shapiro, L.H. (2006). Prostate-specific membrane antigen regulates angiogenesis by modulating integrin signal transduction. Mol Cell Biol *26*, 5310-5324.

Conway, R.E., Rojas, C., Alt, J., Nováková, Z., Richardson, S.M., Rodrick, T.C., Fuentes, J.L., Richardson, N.H., Attalla, J., Stewart, S.*, a kol.* (2016). Prostate-specific membrane antigen (PSMA)-mediated laminin proteolysis generates a pro-angiogenic peptide. Angiogenesis *19*, 487-500.

Crowley, M.J., Scognamiglio, T., Liu, Y.F., Kleiman, D.A., Beninato, T., Aronova, A., Liu, H., Jhanwar, Y.S., Molina, A., Tagawa, S.T.*, a kol.* (2016). Prostate-Specific Membrane Antigen Is a Potential Antiangiogenic Target in Adrenocortical Carcinoma. The Journal of clinical endocrinology and metabolism *101*, 981-987.

Cummings, D., Dowling, K.F., Silverstein, N.J., Tanner, A.S., Eryilmaz, H., Smoller, J.W., and Roffman, J.L. (2017). A Cross-Sectional Study of Dietary and Genetic Predictors of Blood Folate Levels in Healthy Young Adults. Nutrients *9*.

Cunha, A.C., Weigle, B., Kiessling, A., Bachmann, M., and Rieber, E.P. (2006). Tissue-specificity of prostate specific antigens: comparative analysis of transcript levels in prostate and non-prostatic tissues. Cancer letters *236*, 229-238.

Czernin, J., and Calais, J. (2021). ¹⁷⁷Lu-PSMA617 and the VISION Trial: One of the Greatest Success Stories in the History of Nuclear Medicine. Journal of Nuclear Medicine *62*, 1025.

Damaraju, V.L., Cass, C.E., and Sawyer, M.B. (2008). Renal conservation of folates role of folate transport proteins. Vitamins and hormones *79*, 185-202.

Darcy-Vrillon, B., Selhub, J., and Rosenberg, I.H. (1988). Analysis of sequential events in intestinal absorption of folylpolyglutamate. The American journal of physiology *255*, G361-366.

Date, A.A., Rais, R., Babu, T., Ortiz, J., Kanvinde, P., Thomas, A.G., Zimmermann, S.C., Gadiano, A.J., Halpert, G., Slusher, B.S.*, a kol.* (2017). Local enema treatment to inhibit FOLH1/GCPII as a novel therapy for inflammatory bowel disease. Journal of controlled release : official journal of the Controlled Release Society *263*, 132-138.

Datz, B., Sieger, C., and Weibel, M.A. (1988). [NAAGA and cromoglycate. A comparison in the treatment of seasonal allergic rhinitis]. Laryngologie, Rhinologie, Otologie *67*, 300-303.

Deb, N., Goris, M., Trisler, K., Fowler, S., Saal, J., Ning, S., Becker, M., Marquez, C., and Knox, S. (1996). Treatment of hormone-refractory prostate cancer with 90Y-CYT-356 monoclonal antibody. Clinical cancer research : an official journal of the American Association for Cancer Research *2*, 1289-1297.

Deegen, P., Thomas, O., Nolan-Stevaux, O., Li, S., Wahl, J., Bogner, P., Aeffner, F., Friedrich, M., Liao, M.Z., Matthes, K.*, a kol.* (2021). The PSMA-targeting Half-life Extended BiTE Therapy AMG 160 has Potent Antitumor Activity in Preclinical Models of Metastatic Castration-resistant Prostate Cancer. Clinical cancer research : an official journal of the American Association for Cancer Research *27*, 2928-2937.

Denis, D., Bloch-Michel, E., Verin, P., Sebastiani, A., Tazartes, M., Helleboid, L., Di Giovanni, A., and Lecorvec, M. (1998). Treatment of common ocular allergic disorders; a comparison of lodoxamide and NAAGA. The British journal of ophthalmology *82*, 1135-1138.

Devlin, A.M., Clarke, R., Birks, J., Evans, J.G., and Halsted, C.H. (2006). Interactions among polymorphisms in folate-metabolizing genes and serum total homocysteine concentrations in a healthy elderly population. Am J Clin Nutr *83*, 708-713.

DeVos, L., Chanson, A., Liu, Z., Ciappio, E.D., Parnell, L.D., Mason, J.B., Tucker, K.L., and Crott, J.W. (2008). Associations between single nucleotide polymorphisms in folate uptake and metabolizing genes with blood folate, homocysteine, and DNA uracil concentrations. Am J Clin Nutr *88*, 1149-1158.

Dias, A.H., Holm Vendelbo, M., and Bouchelouche, K. (2017). Prostate-Specific Membrane Antigen PET/CT: Uptake in Lymph Nodes With Active Sarcoidosis. Clinical nuclear medicine *42*, e175-e176.

Diekmann, S., Henneke, M., Burckhardt, B.C., and Gärtner, J. (2010). Pelizaeus-Merzbacher-like disease is caused not only by a loss of connexin47 function but also by a hemichannel dysfunction. European journal of human genetics : EJHG *18*, 985-992.

DiPippo, V.A., Olson, W.C., Nguyen, H.M., Brown, L.G., Vessella, R.L., and Corey, E. (2015). Efficacy studies of an antibody-drug conjugate PSMA-ADC in patient-derived prostate cancer xenografts. The Prostate *75*, 303-313.

Doble, A. (1999). The role of excitotoxicity in neurodegenerative disease: implications for therapy. Pharmacology & therapeutics *81*, 163-221.

Ducker, G.S., and Rabinowitz, J.D. (2017). One-Carbon Metabolism in Health and Disease. Cell metabolism *25*, 27-42.

Duda, D.G., Fukumura, D., and Jain, R.K. (2004). Role of eNOS in neovascularization: NO for endothelial progenitor cells. Trends in molecular medicine *10*, 143-145.

Dumas, F., Gala, J.L., Berteau, P., Brasseur, F., Eschwège, P., Paradis, V., Lacour, B., Philippe, M., and Loric, S. (1999). Molecular expression of PSMA mRNA and protein in primary renal tumors. International Journal of Cancer *80*, 799-803.

Ellington, A.D., and Szostak, J.W. (1990). In vitro selection of RNA molecules that bind specific ligands. Nature *346*, 818-822.

Emmett, L., Metser, U., Bauman, G., Hicks, R.J., Weickhardt, A., Davis, I.D., Punwani, S., Pond, G., Chua, S., Ho, B.*, a kol.* (2019). Prospective, Multisite, International Comparison of (18)F-Fluoromethylcholine PET/CT, Multiparametric MRI, and (68)Ga-HBED-CC PSMA-11 PET/CT in Men with High-Risk Features and Biochemical Failure After Radical Prostatectomy: Clinical Performance and Patient Outcomes. Journal of nuclear medicine : official publication, Society of Nuclear Medicine *60*, 794-800.

Evazalipour, M., D'Huyvetter, M., Tehrani, B.S., Abolhassani, M., Omidfar, K., Abdoli, S., Arezumand, R., Morovvati, H., Lahoutte, T., Muyldermans, S.*, a kol.* (2014). Generation and characterization of nanobodies targeting PSMA for molecular imaging of prostate cancer. Contrast media & molecular imaging *9*, 211-220.

Fan, X., Guo, Y., Wang, L., Xiong, X., Zhu, L., and Fang, K. (2016). Diagnosis of prostate cancer using anti-PSMA aptamer A10-3.2-oriented lipid nanobubbles. International journal of nanomedicine *11*, 3939-3950.

Feuillard, J., Maillet, F., Goldschmidt, P., Weiss, L., and Kazatchkine, M.D. (1991). Comparative study of in vitro inhibition of activation of the classical and alternative pathways of human complement by the magnesium and sodium salts of the anti-inflammatory peptide N-acetyl-aspartyl-glutamic acid (NAAGA). Agents and actions *32*, 343-346.

Fielding, A.B., Schonteich, E., Matheson, J., Wilson, G., Yu, X., Hickson, G.R., Srivastava, S., Baldwin, S.A., Prekeris, R., and Gould, G.W. (2005). Rab11-FIP3 and FIP4 interact with Arf6 and the exocyst to control membrane traffic in cytokinesis. The EMBO journal *24*, 3389-3399.

Finch, C.E., and Girgis, F.G. (1974). Enlarged seminal vesicles of senescent C57BL-6J mice. Journal of gerontology *29*, 134-138.

Fong, M.Y., McDunn, J., and Kakar, S.S. (2011). Identification of metabolites in the normal ovary and their transformation in primary and metastatic ovarian cancer. PloS one *6*, e19963.

Foran, E., and Trotti, D. (2009). Glutamate transporters and the excitotoxic path to motor neuron degeneration in amyotrophic lateral sclerosis. Antioxid Redox Signal *11*, 1587-1602.

Foss, C.A., Mease, R.C., Cho, S.Y., Kim, H.J., and Pomper, M.G. (2012). GCPII imaging and cancer. Current medicinal chemistry *19*, 1346-1359.

Francis, J.S., Wojtas, I., Markov, V., Gray, S.J., McCown, T.J., Samulski, R.J., Bilaniuk, L.T., Wang, D.-J., De Vivo, D.C., Janson, C.G.*, a kol.* (2016). N-acetylaspartate supports the energetic demands of developmental myelination via oligodendroglial aspartoacylase. Neurobiol Dis *96*, 323-334.

Fricker, A.C., Mok, M.H., de la Flor, R., Shah, A.J., Woolley, M., Dawson, L.A., and Kew, J.N. (2009). Effects of N-acetylaspartylglutamate (NAAG) at group II mGluRs and NMDAR. Neuropharmacology *56*, 1060-1067.

Frigerio, B., Franssen, G., Luison, E., Satta, A., Seregni, E., Colombatti, M., Fracasso, G., Valdagni, R., Mezzanzanica, D., Boerman, O.*, a kol.* (2017). Full preclinical validation of the 123I-labeled anti-PSMA antibody fragment ScFvD2B for prostate cancer imaging. Oncotarget *8*, 10919-10930.

Frigerio, B., Morlino, S., Luison, E., Seregni, E., Lorenzoni, A., Satta, A., Valdagni, R., Bogni, A., Chiesa, C., Mira, M.*, a kol.* (2019). Anti-PSMA (124)I-scFvD2B as a new immuno-PET tool for prostate cancer: preclinical proof of principle. Journal of experimental & clinical cancer research : CR *38*, 326.

Gala, J.L., Loric, S., Guiot, Y., Denmeade, S.R., Gady, A., Brasseur, F., Heusterspreute, M., Eschwège, P., De Nayer, P., Van Cangh, P.*, a kol.* (2000). Expression of prostate-specific membrane antigen in transitional cell carcinoma of the bladder: prognostic value? Clinical cancer research : an official journal of the American Association for Cancer Research *6*, 4049-4054.

Gao, X.R., Huang, H., Nannini, D.R., Fan, F., and Kim, H. (2018). Genome-wide association analyses identify new loci influencing intraocular pressure. Human molecular genetics *27*, 2205-2213.

Gao, Y., Xu, S., Cui, Z., Zhang, M., Lin, Y., Cai, L., Wang, Z., Luo, X., Zheng, Y., Wang, Y.*, a kol.* (2015). Mice lacking glutamate carboxypeptidase II develop normally, but are less susceptible to traumatic brain injury. J Neurochem *134*, 340-353.

Gehl, L.M., Saab, O.H., Bzdega, T., Wroblewska, B., and Neale, J.H. (2004). Biosynthesis of NAAG by an enzyme-mediated process in rat central nervous system neurons and glia. J Neurochem *90*, 989-997.

Ghadge, G.D., Slusher, B.S., Bodner, A., Canto, M.D., Wozniak, K., Thomas, A.G., Rojas, C., Tsukamoto, T., Majer, P., Miller, R.J.*, a kol.* (2003). Glutamate carboxypeptidase II inhibition protects motor neurons from death in familial amyotrophic lateral sclerosis models. Proc Natl Acad Sci U S A *100*, 9554-9559.

Ghose, S., Wroblewska, B., Corsi, L., Grayson, D.R., De Blas, A.L., Vicini, S., and Neale, J.H. (1997). N-acetylaspartylglutamate stimulates metabotropic glutamate receptor 3 to regulate expression of the GABA(A) alpha6 subunit in cerebellar granule cells. J Neurochem *69*, 2326-2335.

Goldschmidt, P., and Luyckx, J. (1996). Effects of lodoxamide (LOD), disodium cromoglycate (DSCG) and N-acetyl-aspartyl-glutamate sodium salt (NAAGA) on ocular active anaphylaxis. Allergie et immunologie *28*, 124-126.

Good, D., Schwarzenberger, P., Eastham, J.A., Rhoads, R.E., Hunt, J.D., Collins, M., Batzer, M., Theodossiou, C., Kolls, J.K., and Grimes, S.R. (1999). Cloning and characterization of the prostate-specific membrane antigen promoter. Journal of cellular biochemistry *74*, 395-405.

Gordon, I.O., Tretiakova, M.S., Noffsinger, A.E., Hart, J., Reuter, V.E., and Al-Ahmadie, H.A. (2008). Prostate-specific membrane antigen expression in regeneration and repair. Modern Pathology *21*, 1421-1427.

Grant, C.L., Caromile, L.A., Ho, V., Durrani, K., Rahman, M.M., Claffey, K.P., Fong, G.H., and Shapiro, L.H. (2012). Prostate specific membrane antigen (PSMA) regulates angiogenesis independently of VEGF during ocular neovascularization. PloS one *7*, e41285.

Gulhane, B., Ramsay, S., and Fong, W. (2017). 68Ga-PSMA Uptake in Neurofibromas Demonstrated on PET/CT in a Patient With Neurofibromatosis Type 1. Clinical nuclear medicine *42*, 776-778.

Guo, J., Xie, H., Wang, J., Zhao, H., Wang, F., Liu, C., Wang, L., Lu, X., Bao, Y., Zou, J.*, a kol.* (2013). The maternal folate hydrolase gene polymorphism is associated with neural tube defects in a high-risk Chinese population. Genes & nutrition *8*, 191-197.

Haffner, M.C., Kronberger, I.E., Ross, J.S., Sheehan, C.E., Zitt, M., Mühlmann, G., Ofner, D., Zelger, B., Ensinger, C., Yang, X.J.*, a kol.* (2009). Prostate-specific membrane antigen expression in the neovasculature of gastric and colorectal cancers. Human pathology *40*, 1754-1761.

Halsted, C.H. (1991). Jejunal brush-border folate hydrolase. A novel enzyme. West J Med *155*, 605-609.

Halsted, C.H., Wong, D.H., Peerson, J.M., Warden, C.H., Refsum, H., Smith, A.D., Nygård, O.K., Ueland, P.M., Vollset, S.E., and Tell, G.S. (2007). Relations of glutamate carboxypeptidase II (GCPII) polymorphisms to folate and homocysteine concentrations and to scores of cognition, anxiety, and depression in a homogeneous Norwegian population: the Hordaland Homocysteine Study. Am J Clin Nutr *86*, 514-521.

Han, L., Picker, J.D., Schaevitz, L.R., Tsai, G., Feng, J., Jiang, Z., Chu, H.C., Basu, A.C., Berger-Sweeney, J., and Coyle, J.T. (2009). Phenotypic characterization of mice heterozygous for a null mutation of glutamate carboxypeptidase II. Synapse (New York, NY) *63*, 625-635.

Hanks, S.K., and Polte, T.R. (1997). Signaling through focal adhesion kinase. BioEssays : news and reviews in molecular, cellular and developmental biology *19*, 137-145.

Haseman, M.K., Reed, N.L., and Rosenthal, S.A. (1996). Monoclonal antibody imaging of occult prostate cancer in patients with elevated prostate-specific antigen. Positron emission tomography and biopsy correlation. Clinical nuclear medicine *21*, 704-713.

Haupt, K., and Mosbach, K. (1998). Plastic antibodies: developments and applications. Trends in biotechnology *16*, 468-475.

Hehnly, H., Chen, C.T., Powers, C.M., Liu, H.L., and Doxsey, S. (2012). The centrosome regulates the Rab11- dependent recycling endosome pathway at appendages of the mother centriole. Current biology : CB *22*, 1944-1950.

Heitkötter, B., Steinestel, K., Trautmann, M., Grünewald, I., Barth, P., Gevensleben, H., Bögemann, M., Wardelmann, E., Hartmann, W., Rahbar, K.*, a kol.* (2018). Neovascular PSMA expression is a common feature in malignant neoplasms of the thyroid. Oncotarget *9*, 9867-9874.

Heitkötter, B., Trautmann, M., Grünewald, I., Bögemann, M., Rahbar, K., Gevensleben, H., Wardelmann, E., Hartmann, W., Steinestel, K., and Huss, S. (2017). Expression of PSMA in tumor neovasculature of high grade sarcomas including synovial sarcoma, rhabdomyosarcoma, undifferentiated sarcoma and MPNST. Oncotarget *8*, 4268-4276.

Hermann, R.M., Djannatian, M., Czech, N., and Nitsche, M. (2016). Prostate-Specific Membrane Antigen PET/CT: False-Positive Results due to Sarcoidosis? Case reports in oncology *9*, 457-463.

Hlouchova, K., Barinka, C., Konvalinka, J., and Lubkowski, J. (2009). Structural insight into the evolutionary and pharmacologic homology of glutamate carboxypeptidases II and III. The FEBS journal *276*, 4448-4462.

Hlouchová, K., Navrátil, V., Tykvart, J., Sácha, P., and Konvalinka, J. (2012). GCPII variants, paralogs and orthologs. Current medicinal chemistry *19*, 1316-1322.

Hofman, M.S., Violet, J., Hicks, R.J., Ferdinandus, J., Thang, S.P., Akhurst, T., Iravani, A., Kong, G., Ravi Kumar, A., Murphy, D.G.*, a kol.* (2018). [(177)Lu]-PSMA-617 radionuclide treatment in patients with metastatic castration-resistant prostate cancer (LuPSMA trial): a single-centre, single-arm, phase 2 study. Lancet Oncol *19*, 825-833.

Hollinger, K.R., Alt, J., Riehm, A.M., Slusher, B.S., and Kaplin, A.I. (2016). Dose-dependent inhibition of GCPII to prevent and treat cognitive impairment in the EAE model of multiple sclerosis. Brain research *1635*, 105-112.

Holm, J., Hansen, S.I., and Høier-Madsen, M. (1993). High-affinity folate binding in human prostate. Bioscience reports *13*, 99-105.

Horoszewicz, J.S., Kawinski, E., and Murphy, G.P. (1987). Monoclonal antibodies to a new antigenic marker in epithelial prostatic cells and serum of prostatic cancer patients. Anticancer research *7*, 927-935.

Hrkach, J., Von Hoff, D., Mukkaram Ali, M., Andrianova, E., Auer, J., Campbell, T., De Witt, D., Figa, M., Figueiredo, M., Horhota, A.*, a kol.* (2012). Preclinical development and clinical translation of a PSMA-targeted docetaxel nanoparticle with a differentiated pharmacological profile. Science translational medicine *4*, 128ra139.

Huang, B., Otis, J., Joice, M., Kotlyar, A., and Thomas, T.P. (2014). PSMA-targeted stably linked "dendrimer-glutamate urea-methotrexate" as a prostate cancer therapeutic. Biomacromolecules *15*, 915-923.

Huang, C.T., Guo, X., Bařinka, C., Lupold, S.E., Pomper, M.G., Gabrielson, K., Raman, V., Artemov, D., and Hapuarachchige, S. (2020). Development of 5D3-DM1: A Novel Anti-Prostate-Specific Membrane Antigen Antibody-Drug Conjugate for PSMA-Positive Prostate Cancer Therapy. Mol Pharm *17*, 3392-3402.

Huang, X., Bennett, M., and Thorpe, P.E. (2004). Anti-tumor effects and lack of side effects in mice of an immunotoxin directed against human and mouse prostate-specific membrane antigen. The Prostate *61*, 1-11.

Chandler, C.J., Wang, T.T., and Halsted, C.H. (1986). Pteroylpolyglutamate hydrolase from human jejunal brush borders. Purification and characterization. J Biol Chem *261*, 928-933.

Chandran, S.S., Banerjee, S.R., Mease, R.C., Pomper, M.G., and Denmeade, S.R. (2008). Characterization of a targeted nanoparticle functionalized with a urea-based inhibitor of prostate-specific membrane antigen (PSMA). Cancer biology & therapy *7*, 974-982.

Chang, S.S., Reuter, V.E., Heston, W.D., Bander, N.H., Grauer, L.S., and Gaudin, P.B. (1999). Five different anti-prostate-specific membrane antigen (PSMA) antibodies confirm PSMA expression in tumor-associated neovasculature. Cancer research *59*, 3192-3198.

Chatalic, K.L., Veldhoven-Zweistra, J., Bolkestein, M., Hoeben, S., Koning, G.A., Boerman, O.C., de Jong, M., and van Weerden, W.M. (2015). A Novel ^{111}In-Labeled Anti-Prostate-Specific Membrane Antigen Nanobody for Targeted SPECT/CT Imaging of Prostate Cancer. Journal of nuclear medicine : official publication, Society of Nuclear Medicine *56*, 1094-1099.

Chen, J., Kyte, C., Valcin, M., Chan, W., Wetmur, J.G., Selhub, J., Hunter, D.J., and Ma, J. (2004). Polymorphisms in the one-carbon metabolic pathway, plasma folate levels and colorectal cancer in a prospective study. Int J Cancer *110*, 617-620.

Chen, S.R., Wozniak, K.M., Slusher, B.S., and Pan, H.L. (2002). Effect of 2-(phosphono-methyl)-pentanedioic acid on allodynia and afferent ectopic discharges in a rat model of neuropathic pain. The Journal of pharmacology and experimental therapeutics *300*, 662-667.

Chen, Z., Penet, M.F., Krishnamachary, B., Banerjee, S.R., Pomper, M.G., and Bhujwalla, Z.M. (2016). PSMA-specific theranostic nanoplex for combination of TRAIL gene and 5-FC prodrug therapy of prostate cancer. Biomaterials *80*, 57-67.

Cheng, Y., Schlosser, P., Hertel, J., Sekula, P., Oefner, P.J., Spiekerkoetter, U., Mielke, J., Freitag, D.F., Schmidts, M., Kronenberg, F.*, a kol.* (2021). Rare genetic variants affecting urine metabolite levels link population variation to inborn errors of metabolism. Nature communications *12*, 964.

Chigurupati, S., Son, T.G., Hyun, D.-H., Lathia, J.D., Mughal, M.R., Savell, J., Li, S.C., Nagaraju, G.P.C., Chan, S.L., Arumugam, T.V.*, a kol.* (2008). Lifelong running reduces oxidative stress and degenerative changes in the testes of mice. J Endocrinol *199*, 333-341.

Chopra, M., Yao, Y., Blake, T.J., Hampson, D.R., and Johnson, E.C. (2009). The Neuroactive Peptide N-Acetylaspartylglutamate Is Not an Agonist at the Metabotropic Glutamate Receptor Subtype 3 of Metabotropic Glutamate Receptor. Journal of Pharmacology and Experimental Therapeutics *330*, 212.

Israeli, R.S., Powell, C.T., Corr, J.G., Fair, W.R., and Heston, W.D. (1994). Expression of the prostate-specific membrane antigen. Cancer research *54*, 1807-1811.

Jambou, D., and Lapalus, P. (1990). Effect of N-acetyl-aspartyl-glutamate (Naaga) on in-vitro leukotriene synthesis by macrophage cell line P388D1. International journal of tissue reactions *12*, 273-280.

Janczura, K.J., Olszewski, R.T., Bzdega, T., Bacich, D.J., Heston, W.D., and Neale, J.H. (2013). NAAG peptidase inhibitors and deletion of NAAG peptidase gene enhance memory in novel object recognition test. European journal of pharmacology *701*, 27-32.

Jiao, Y., Xu, P., Luan, S., Wang, X., Gao, Y., Zhao, C., and Fu, P. (2021). Molecular imaging and treatment of PSMA-positive prostate cancer with (99m)Tc radiolabeled aptamer-siRNA chimeras. Nuclear medicine and biology *104-105*, 28-37.

Junghans, R.P., Ma, Q., Rathore, R., Gomes, E.M., Bais, A.J., Lo, A.S., Abedi, M., Davies, R.A., Cabral, H.J., Al-Homsi, A.S.*, a kol.* (2016). Phase I Trial of Anti-PSMA Designer CAR-T Cells in Prostate Cancer: Possible Role for Interacting Interleukin 2-T Cell Pharmacodynamics as a Determinant of Clinical Response. The Prostate *76*, 1257-1270.

Kahn, D., Austin, J.C., Maguire, R.T., Miller, S.J., Gerstbrein, J., and Williams, R.D. (1999). A phase II study of [90Y] yttrium-capromab pendetide in the treatment of men with prostate cancer recurrence following radical prostatectomy. Cancer biotherapy & radiopharmaceuticals *14*, 99-111.

Kahn, D., Williams, R.D., Seldin, D.W., Libertino, J.A., Hirschhorn, M., Dreicer, R., Weiner, G.J., Bushnell, D., and Gulfo, J. (1994). Radioimmunoscintigraphy with 111indium labeled CYT-356 for the detection of occult prostate cancer recurrence. J Urol *152*, 1490-1495.

Kasoha, M., Unger, C., Solomayer, E.F., Bohle, R.M., Zaharia, C., Khreich, F., Wagenpfeil, S., and Juhasz-Böss, I. (2017). Prostate-specific membrane antigen (PSMA) expression in breast cancer and its metastases. Clinical & experimental metastasis *34*, 479-490.

Kasten, B.B., Liu, T., Nedrow-Byers, J.R., Benny, P.D., and Berkman, C.E. (2013). Targeting prostate cancer cells with PSMA inhibitor-guided gold nanoparticles. Bioorganic & medicinal chemistry letters *23*, 565-568.

Keam, S.J. (2021). Piflufolastat F 18: Diagnostic First Approval. Molecular diagnosis & therapy *25*, 647-656.

Kim, D., Jeong, Y.Y., and Jon, S. (2010a). A drug-loaded aptamer-gold nanoparticle bioconjugate for combined CT imaging and therapy of prostate cancer. ACS Nano *4*, 3689-3696.

Kim, M.J., Chae, S.S., Koh, Y.H., Lee, S.K., and Jo, S.A. (2010b). Glutamate carboxypeptidase II: an amyloid peptide-degrading enzyme with physiological function in the brain. FASEB journal : official publication of the Federation of American Societies for Experimental Biology *24*, 4491-4502.

Kinoshita, Y., Kuratsukuri, K., Landas, S., Imaida, K., Rovito, P.M., Jr., Wang, C.Y., and Haas, G.P. (2006). Expression of prostate-specific membrane antigen in normal and malignant human tissues. World journal of surgery *30*, 628-636.

Kloss, C.C., Lee, J., Zhang, A., Chen, F., Melenhorst, J.J., Lacey, S.F., Maus, M.V., Fraietta, J.A., Zhao, Y., and June, C.H. (2018). Dominant-Negative TGF-β Receptor Enhances PSMA-Targeted Human CAR T Cell Proliferation And Augments Prostate Cancer Eradication. Molecular therapy : the journal of the American Society of Gene Therapy *26*, 1855-1866.

Knedlík, T., Navrátil, V., Vik, V., Pacík, D., Šácha, P., and Konvalinka, J. (2014). Detection and quantitation of glutamate carboxypeptidase II in human blood. The Prostate *74*, 768-780.

Kobe, C., Maintz, D., Fischer, T., Drzezga, A., and Chang, D.H. (2015). Prostate-Specific Membrane Antigen PET/CT in Splenic Sarcoidosis. Clinical nuclear medicine *40*, 897-898.

Kolishetti, N., Dhar, S., Valencia, P.M., Lin, L.Q., Karnik, R., Lippard, S.J., Langer, R., and Farokhzad, O.C. (2010). Engineering of self-assembled nanoparticle platform for precisely controlled combination drug therapy. Proceedings of the National Academy of Sciences *107*, 17939.

Kopecek, J., and Kopecková, P. (2010). HPMA copolymers: origins, early developments, present, and future. Advanced drug delivery reviews *62*, 122-149.

Kozikowski, A.P., Zhang, J., Nan, F., Petukhov, P.A., Grajkowska, E., Wroblewski, J.T., Yamamoto, T., Bzdega, T., Wroblewska, B., and Neale, J.H. (2004). Synthesis of urea-based inhibitors as active site probes of glutamate carboxypeptidase II: efficacy as analgesic agents. Journal of medicinal chemistry *47*, 1729-1738.

Kratochwil, C., Giesel, F.L., Stefanova, M., Benešová, M., Bronzel, M., Afshar-Oromieh, A., Mier, W., Eder, M., Kopka, K., and Haberkorn, U. (2016). PSMA-Targeted Radionuclide Therapy of Metastatic Castration-Resistant Prostate Cancer with 177Lu-Labeled PSMA-617. Journal of nuclear medicine : official publication, Society of Nuclear Medicine *57*, 1170-1176.

Kuroda, K., Liu, H., Kim, S., Guo, M., Navarro, V., and Bander, N.H. (2010). Saporin toxin-conjugated monoclonal antibody targeting prostate-specific membrane antigen has potent anticancer activity. The Prostate *70*, 1286-1294.

Lane, Z., Hansel, D.E., and Epstein, J.I. (2008). Immunohistochemical expression of prostatic antigens in adenocarcinoma and villous adenoma of the urinary bladder. The American journal of surgical pathology *32*, 1322-1326.

Lea, P.M.t., Wroblewska, B., Sarvey, J.M., and Neale, J.H. (2001). beta-NAAG rescues LTP from blockade by NAAG in rat dentate gyrus via the type 3 metabotropic glutamate receptor. J Neurophysiol *85*, 1097-1106.

Leamon, C.P., Reddy, J.A., Bloomfield, A., Dorton, R., Nelson, M., Vetzel, M., Kleindl, P., Hahn, S., Wang, K., and Vlahov, I.R. (2019). Prostate-Specific Membrane Antigen-Specific Antitumor Activity of a Self-Immolative Tubulysin Conjugate. Bioconjug Chem *30*, 1805-1813.

Leconet, W., Liu, H., Guo, M., Le Lamer-Déchamps, S., Molinier, C., Kim, S., Vrlinic, T., Oster, M., Liu, F., Navarro, V.*, a kol.* (2018). Anti-PSMA/CD3 Bispecific Antibody Delivery and Antitumor Activity Using a Polymeric Depot Formulation. Molecular cancer therapeutics *17*, 1927-1940.

Lee, S.J., Lee, K., Yang, X., Jung, C., Gardner, T., Kim, H.S., Jeng, M.H., and Kao, C. (2003). NFATc1 with AP-3 site binding specificity mediates gene expression of prostate-specific-membrane-antigen. Journal of molecular biology *330*, 749-760.

Lee, S.K., Kim, H., Cheong, Y.H., Kim, M.J., Jo, S.A., Youn, H.S., and Park, S.I. (2013). S1 pocket of glutamate carboxypeptidase II: a new binding site for amyloid-β degradation. Biochemical and biophysical research communications *438*, 765-771.

Leonardi, A., Bremond-Gignac, D., Bortolotti, M., Violato, D., Pouliquen, P., Delval, L., Grouin, J.M., and Fregona, I.A. (2007). Clinical and biological efficacy of preservative-free NAAGA eye-drops versus levocabastine eye-drops in vernal keratoconjunctivitis patients. The British journal of ophthalmology *91*, 1662-1666.

Lievers, K.J., Kluijtmans, L.A., Boers, G.H., Verhoef, P., den Heijer, M., Trijbels, F.J., and Blom, H.J. (2002). Influence of a glutamate carboxypeptidase II (GCPII) polymorphism (1561C-->T) on plasma homocysteine, folate and vitamin B(12) levels and its relationship to cardiovascular disease risk. Atherosclerosis *164*, 269-273.

Liu, H., Moy, P., Kim, S., Xia, Y., Rajasekaran, A., Navarro, V., Knudsen, B., and Bander, N.H. (1997). Monoclonal antibodies to the extracellular domain of prostate-specific membrane antigen also react with tumor vascular endothelium. Cancer research *57*, 3629-3634.

Liu, H., Rajasekaran, A.K., Moy, P., Xia, Y., Kim, S., Navarro, V., Rahmati, R., and Bander, N.H. (1998). Constitutive and antibody-induced internalization of prostate-specific membrane antigen. Cancer research *58*, 4055-4060.

Liu, T., Jabbes, M., Nedrow-Byers, J.R., Wu, L.Y., Bryan, J.N., and Berkman, C.E. (2011). Detection of prostate-specific membrane antigen on HUVECs in response to breast tumor-conditioned medium. International journal of oncology *38*, 1349-1355.

Lodder-Gadaczek, J., Becker, I., Gieselmann, V., Wang-Eckhardt, L., and Eckhardt, M. (2011). N-acetylaspartylglutamate synthetase II synthesizes N-acetylaspartylglutamylglutamate. The Journal of biological chemistry *286*, 16693-16706.

Lodder-Gadaczek, J., Gieselmann, V., and Eckhardt, M. (2013). Vesicular uptake of N-acetylaspartylglutamate is catalysed by sialin (SLC17A5). The Biochemical journal *454*, 31-38.

Lopes, A.D., Davis, W.L., Rosenstraus, M.J., Uveges, A.J., and Gilman, S.C. (1990). Immunohistochemical and pharmacokinetic characterization of the site-specific immunoconjugate CYT-356 derived from antiprostate monoclonal antibody 7E11-C5. Cancer research *50*, 6423-6429.

Lu, X.M., Tang, Z., Liu, W., Lin, Q., and Slusher, B.S. (2000). N-acetylaspartylglutamate protects against transient focal cerebral ischemia in rats. European journal of pharmacology *408*, 233-239.

Lu, Z.R. (2010). Molecular imaging of HPMA copolymers: visualizing drug delivery in cell, mouse and man. Advanced drug delivery reviews *62*, 246-257.

Ma, Q., Gomes, E.M., Lo, A.S., and Junghans, R.P. (2014). Advanced generation anti-prostate specific membrane antigen designer T cells for prostate cancer immunotherapy. The Prostate *74*, 286-296.

Ma, S., Li, X., Wang, X., Cheng, L., Li, Z., Zhang, C., Ye, Z., and Qian, Q. (2019). Current Progress in CAR-T Cell Therapy for Solid Tumors. Int J Biol Sci *15*, 2548-2560.

Machulkin, A.E., Uspenskaya, A.A., Zyk, N.Y., Nimenko, E.A., Ber, A.P., Petrov, S.A., Shafikov, R.R., Skvortsov, D.A., Smirnova, G.B., Borisova, Y.A.*, a kol.* (2022). PSMA-targeted small-molecule docetaxel conjugate: Synthesis and preclinical evaluation. European journal of medicinal chemistry *227*, 113936.

Manyak, M.J., Hinkle, G.H., Olsen, J.O., Chiaccherini, R.P., Partin, A.W., Piantadosi, S., Burgers, J.K., Texter, J.H., Neal, C.E., Libertino, J.A.*, a kol.* (1999). Immunoscintigraphy with indium-111-capromab pendetide: evaluation before definitive therapy in patients with prostate cancer. Urology *54*, 1058-1063.

Matsuda, M., Ishikawa, E., Yamamoto, T., Hatano, K., Joraku, A., Iizumi, Y., Masuda, Y., Nishiyama, H., and Matsumura, A. (2018). Potential use of prostate specific membrane antigen (PSMA) for detecting the tumor neovasculature of brain tumors by PET imaging with (89)Zr-Df-IAB2M anti-PSMA minibody. Journal of neuro-oncology *138*, 581-589.

McDevitt, M.R., Barendswaard, E., Ma, D., Lai, L., Curcio, M.J., Sgouros, G., Ballangrud, A.M., Yang, W.H., Finn, R.D., Pellegrini, V.*, a kol.* (2000). An alpha-particle emitting antibody ([213Bi]J591) for radioimmunotherapy of prostate cancer. Cancer research *60*, 6095-6100.

McEnaney, P.J., Fitzgerald, K.J., Zhang, A.X., Douglass, E.F., Jr., Shan, W., Balog, A., Kolesnikova, M.D., and Spiegel, D.A. (2014). Chemically synthesized molecules with the targeting and effector functions of antibodies. J Am Chem Soc *136*, 18034-18043.

McNulty, H., and Pentieva, K. (2004). Folate bioavailability. The Proceedings of the Nutrition Society *63*, 529-536.

Melse-Boonstra, A., Lievers, K.J., Blom, H.J., and Verhoef, P. (2004). Bioavailability of polyglutamyl folic acid relative to that of monoglutamyl folic acid in subjects with different genotypes of the glutamate carboxypeptidase II gene. Am J Clin Nutr *80*, 700-704.

Meng, F.D., Wang, S., Jiang, Y.H., and Sui, C.G. (2016). Antitumor effect of dendritic cells transfected with prostate-specific membrane antigen recombinant adenovirus on prostate cancer: An in vitro study. Molecular medicine reports *13*, 2124-2134.

Meng, P., Dong, Q.C., Tan, G.G., Wen, W.H., Wang, H., Zhang, G., Wang, Y.Z., Jing, Y.M., Wang, C., Qin, W.J.*, a kol.* (2017). Anti-tumor effects of a recombinant anti-prostate specific membrane antigen immunotoxin against prostate cancer cells. BMC urology *17*, 14.

Mennini, T., and Bendotti, C. (2004). Excitotoxicity in Amyotrophic Lateral Sclerosis: Selective Vulnerability of Motor Neurons. In Excitotoxicity in Neurological Diseases: New Therapeutic Challenge, C. Ferrarese, and M.F. Beal, eds. (Boston, MA: Springer US), pp. 217-227.

Mesters, J.R., Barinka, C., Li, W., Tsukamoto, T., Majer, P., Slusher, B.S., Konvalinka, J., and Hilgenfeld, R. (2006). Structure of glutamate carboxypeptidase II, a drug target in neuronal damage and prostate cancer. The EMBO journal *25*, 1375-1384.

Mhawech-Fauceglia, P., Zhang, S., Terracciano, L., Sauter, G., Chadhuri, A., Herrmann, F.R., and Penetrante, R. (2007). Prostate-specific membrane antigen (PSMA) protein expression in normal and neoplastic tissues and its sensitivity and specificity in prostate adenocarcinoma: an immunohistochemical study using mutiple tumour tissue microarray technique. Histopathology *50*, 472-483.

Michalska, M., Schultze-Seemann, S., Bogatyreva, L., Hauschke, D., Wetterauer, U., and Wolf, P. (2016). In vitro and in vivo effects of a recombinant anti-PSMA immunotoxin in combination with docetaxel against prostate cancer. Oncotarget *7*, 22531-22542.

Milowsky, M.I., Galsky, M.D., Morris, M.J., Crona, D.J., George, D.J., Dreicer, R., Tse, K., Petruck, J., Webb, I.J., Bander, N.H.*, a kol.* (2016). Phase 1/2 multiple ascending dose trial of the prostate-specific membrane antigen-targeted antibody drug conjugate MLN2704 in metastatic castration-resistant prostate cancer. Urologic oncology *34*, 530.e515-530.e521.

Milowsky, M.I., Nanus, D.M., Kostakoglu, L., Vallabhajosula, S., Goldsmith, S.J., and Bander, N.H. (2004). Phase I trial of yttrium-90-labeled anti-prostate-specific membrane antigen monoclonal antibody J591 for androgen-independent prostate cancer. J Clin Oncol *22*, 2522-2531.

Minner, S., Wittmer, C., Graefen, M., Salomon, G., Steuber, T., Haese, A., Huland, H., Bokemeyer, C., Yekebas, E., Dierlamm, J.*, a kol.* (2011). High level PSMA expression is associated with early PSA recurrence in surgically treated prostate cancer. The Prostate *71*, 281-288.

Miyake, M., Kakimoto, Y., and Sorimachi, M. (1981). A gas chromatographic method for the determination of N-acetyl-L-aspartic acid, N-acetyl-alpha-aspartylglutamic acid and beta-citryl-L-glutamic acid and their distributions in the brain and other organs of various species of animals. J Neurochem *36*, 804-810.

Moghaddam, B., and Adams, B.W. (1998). Reversal of phencyclidine effects by a group II metabotropic glutamate receptor agonist in rats. Science *281*, 1349-1352.

Morin, I., Devlin, A.M., Leclerc, D., Sabbaghian, N., Halsted, C.H., Finnell, R., and Rozen, R. (2003). Evaluation of genetic variants in the reduced folate carrier and in glutamate carboxypeptidase II for spina bifida risk. Molecular genetics and metabolism *79*, 197-200.

Morris, M.J., Vogelzang, N.J., Sartor, O., Armour, A., Groaning, M., Robarts, A., Petrylak, D.P., Tolcher, A.W., Gordon, M.S., and Babiker, H.M. (2017). Phase 1 study of the PSMA-targeted small-molecule drug conjugate EC1169 in patients with metastatic castrate-resistant prostate cancer (mCRPC). Journal of Clinical Oncology *35*, 5038-5038.

Mukherjee, A., Darlington, T., Baldwin, R., Holz, C., Olson, S., Kulkarni, P., DeWeese, T.L., Getzenberg, R.H., Ivkov, R., and Lupold, S.E. (2014). Development and screening of a series of antibody-conjugated and silica-coated iron oxide nanoparticles for targeting the prostate-specific membrane antigen. ChemMedChem *9*, 1356-1360.

Nagesh, P.K.B., Johnson, N.R., Boya, V.K.N., Chowdhury, P., Othman, S.F., Khalilzad-Sharghi, V., Hafeez, B.B., Ganju, A., Khan, S., Behrman, S.W.*, a kol.* (2016). PSMA targeted docetaxel-loaded superparamagnetic iron oxide nanoparticles for prostate cancer. Colloids and surfaces B, Biointerfaces *144*, 8-20.

Namboodiri, A.M., Peethambaran, A., Mathew, R., Sambhu, P.A., Hershfield, J., Moffett, J.R., and Madhavarao, C.N. (2006). Canavan disease and the role of N-acetylaspartate in myelin synthesis. Molecular and cellular endocrinology *252*, 216-223.

Navrátil, M., Ptáček, J., Šácha, P., Starková, J., Lubkowski, J., Bařinka, C., and Konvalinka, J. (2014). Structural and biochemical characterization of the folyl-poly-γ-l-glutamate hydrolyzing activity of human glutamate carboxypeptidase II. The FEBS journal *281*, 3228-3242.

Navrátil, M., Tykvart, J., Schimer, J., Pachl, P., Navrátil, V., Rokob, T.A., Hlouchová, K., Rulíšek, L., and Konvalinka, J. (2016). Comparison of human glutamate carboxypeptidases II and III reveals their divergent substrate specificities. The FEBS journal *283*, 2528-2545.

Navrátil, V., Schimer, J., Tykvart, J., Knedlík, T., Vik, V., Majer, P., Konvalinka, J., and Šácha, P. (2017). DNA-linked Inhibitor Antibody Assay (DIANA) for sensitive and selective enzyme detection and inhibitor screening. Nucleic acids research *45*, e10-e10.

Nawaz, S., Mullen, G.E.D., Sunassee, K., Bordoloi, J., Blower, P.J., and Ballinger, J.R. (2017). Simple, mild, one-step labelling of proteins with gallium-68 using a tris(hydroxypyridinone) bifunctional chelator: a (68)Ga-THP-scFv targeting the prostate-specific membrane antigen. EJNMMI research *7*, 86.

Neale, J.H. (2011). N-acetylaspartylglutamate is an agonist at mGluR$_3$ in vivo and in vitro. Journal of neurochemistry *119*, 891-895.

Neale, J.H., Bzdega, T., and Wroblewska, B. (2000). N-Acetylaspartylglutamate: the most abundant peptide neurotransmitter in the mammalian central nervous system. J Neurochem *75*, 443-452.

Neale, J.H., and Olszewski, R. (2019). A role for N-acetylaspartylglutamate (NAAG) and mGluR3 in cognition. Neurobiology of learning and memory *158*, 9-13.

Neale, J.H., Olszewski, R.T., Gehl, L.M., Wroblewska, B., and Bzdega, T. (2005). The neurotransmitter N-acetylaspartylglutamate in models of pain, ALS, diabetic neuropathy, CNS injury and schizophrenia. Trends in pharmacological sciences *26*, 477-484.

Neale, J.H., and Yamamoto, T. (2020). N-acetylaspartylglutamate (NAAG) and glutamate carboxypeptidase II: An abundant peptide neurotransmitter-enzyme system with multiple clinical applications. Progress in neurobiology *184*, 101722.

Neels, O.C., Kopka, K., Liolios, C., and Afshar-Oromieh, A. (2021). Radiolabeled PSMA Inhibitors. Cancers (Basel) *13*, 6255.

Nguyen, D.P., Xiong, P.L., Liu, H., Pan, S., Leconet, W., Navarro, V., Guo, M., Moy, J., Kim, S., Ramirez-Fort, M.K.*, a kol.* (2016). Induction of PSMA and Internalization of an Anti-PSMA mAb in the Vascular Compartment. Molecular cancer research : MCR *14*, 1045-1053.

Nguyen, T., Kirsch, B.J., Asaka, R., Nabi, K., Quinones, A., Tan, J., Antonio, M.J., Camelo, F., Li, T., Nguyen, S.*, a kol.* (2019). Uncovering the Role of N-Acetyl-Aspartyl-Glutamate as a Glutamate Reservoir in Cancer. Cell Rep *27*, 491-501.e496.

Nomura, N., Pastorino, S., Jiang, P., Lambert, G., Crawford, J.R., Gymnopoulos, M., Piccioni, D., Juarez, T., Pingle, S.C., Makale, M.*, a kol.* (2014). Prostate specific membrane antigen (PSMA) expression in primary gliomas and breast cancer brain metastases. Cancer cell international *14*, 26.

Nord, K., Gunneriusson, E., Ringdahl, J., Ståhl, S., Uhlén, M., and Nygren, P.A. (1997). Binding proteins selected from combinatorial libraries of an alpha-helical bacterial receptor domain. Nature biotechnology *15*, 772-777.

Nordengen, K., Morland, C., Slusher, B.S., and Gundersen, V. (2020). Dendritic Localization and Exocytosis of NAAG in the Rat Hippocampus. Cerebral cortex (New York, NY : 1991) *30*, 1422-1435.

Noss, K.R., Wolfe, S.A., and Grimes, S.R. (2002). Upregulation of prostate specific membrane antigen/folate hydrolase transcription by an enhancer. Gene *285*, 247-256.

O'Keefe, D.S., Su, S.L., Bacich, D.J., Horiguchi, Y., Luo, Y., Powell, C.T., Zandvliet, D., Russell, P.J., Molloy, P.L., Nowak, N.J.*, a kol.* (1998). Mapping, genomic organization and promoter analysis of the human prostate-specific membrane antigen gene. Biochimica et biophysica acta *1443*, 113-127.

O'Keefe, D.S., Bacich, D.J., and Heston, W.D.W. (2001). Prostate Specific Membrane Antigen. In Prostate Cancer: Biology, Genetics, and the New Therapeutics, L.W.K. Chung, W.B. Isaacs, and J.W. Simons, eds. (Totowa, NJ: Humana Press), pp. 307-326.

Oliveira, D.S.M., Dzinic, S., Bonfil, A.I., Saliganan, A.D., Sheng, S., and Bonfil, R.D. (2016). The mouse prostate: a basic anatomical and histological guideline. Bosn J Basic Med Sci *16*, 8-13.

Olszewski, R.T., Janczura, K.J., Bzdega, T., Der, E.K., Venzor, F., O'Rourke, B., Hark, T.J., Craddock, K.E., Balasubramanian, S., Moussa, C.*, a kol.* (2017). NAAG Peptidase Inhibitors Act via mGluR3: Animal Models of Memory, Alzheimer's, and Ethanol Intoxication. Neurochemical research *42*, 2646-2657.

Packer, D. (2021). The history of the antibody as a tool. Acta Histochemica *123*, 151710.

Pandit-Taskar, N., O'Donoghue, J.A., Beylergil, V., Lyashchenko, S., Ruan, S., Solomon, S.B., Durack, J.C., Carrasquillo, J.A., Lefkowitz, R.A., Gonen, M.*, a kol.* (2014). ^{89}Zr-huJ591 immuno-PET imaging in patients with advanced metastatic prostate cancer. Eur J Nucl Med Mol Imaging *41*, 2093-2105.

Pandit-Taskar, N., O'Donoghue, J.A., Divgi, C.R., Wills, E.A., Schwartz, L., Gönen, M., Smith-Jones, P., Bander, N.H., Scher, H.I., Larson, S.M.*, a kol.* (2015). Indium 111-labeled J591 anti-PSMA antibody for vascular targeted imaging in progressive solid tumors. EJNMMI research *5*, 28-28.

Pangalos, M.N., Neefs, J.M., Somers, M., Verhasselt, P., Bekkers, M., van der Helm, L., Fraiponts, E., Ashton, D., and Gordon, R.D. (1999). Isolation and expression of novel human glutamate carboxypeptidases with N-acetylated alpha-linked acidic dipeptidase and dipeptidyl peptidase IV activity. J Biol Chem *274*, 8470-8483.

Patterson, J.T., Isaacson, J., Kerwin, L., Atassi, G., Duggal, R., Bresson, D., Zhu, T., Zhou, H., Fu, Y., and Kaufmann, G.F. (2017). PSMA-targeted bispecific Fab conjugates that engage T cells. Bioorganic & medicinal chemistry letters *27*, 5490-5495.

Pavlícek, J., Ptácek, J., and Barinka, C. (2012). Glutamate carboxypeptidase II: an overview of structural studies and their importance for structure-based drug design and deciphering the reaction mechanism of the enzyme. Current medicinal chemistry *19*, 1300-1309.

Pearse, B.M., Smith, C.J., and Owen, D.J. (2000). Clathrin coat construction in endocytosis. Current opinion in structural biology *10*, 220-228.

Perico, M.E., Grasso, S., Brunelli, M., Martignoni, G., Munari, E., Moiso, E., Fracasso, G., Cestari, T., Naim, H.Y., Bronte, V.*, a kol.* (2016). Prostate-specific membrane antigen (PSMA) assembles a macromolecular complex regulating growth and survival of prostate cancer cells "in vitro" and correlating with progression "in vivo". Oncotarget *7*, 74189-74202.

Perner, S., Hofer, M.D., Kim, R., Shah, R.B., Li, H., Möller, P., Hautmann, R.E., Gschwend, J.E., Kuefer, R., and Rubin, M.A. (2007). Prostate-specific membrane antigen expression as a predictor of prostate cancer progression. Human pathology *38*, 696-701.

Perry, T.L., Krieger, C., Hansen, S., and Eisen, A. (1990). Amyotrophic lateral sclerosis: amino acid levels in plasma and cerebrospinal fluid. Annals of neurology *28*, 12-17.

Peters, D., Norris, L., Dash, R., Brayton, C., Rais, R., and Slusher, B. (2019). P135 ORALLY ADMINISTERED FOLH1 /GCPII INHIBITORS AS NOVEL THERAPEUTICS IN INFLAMMATORY BOWEL DISEASE (IBD). Inflammatory Bowel Diseases *25*, S63-S63.

Petrylak, D.P., Kantoff, P., Vogelzang, N.J., Mega, A., Fleming, M.T., Stephenson, J.J., Jr., Frank, R., Shore, N.D., Dreicer, R., McClay, E.F.*, a kol.* (2019). Phase 1 study of PSMA ADC, an antibody-drug conjugate targeting prostate-specific membrane antigen, in chemotherapy-refractory prostate cancer. The Prostate *79*, 604-613.

Petrylak, D.P., Vogelzang, N.J., Chatta, K., Fleming, M.T., Smith, D.C., Appleman, L.J., Hussain, A., Modiano, M., Singh, P., Tagawa, S.T.*, a kol.* (2020). PSMA ADC monotherapy in patients with progressive metastatic castration-resistant prostate cancer following abiraterone and/or enzalutamide: Efficacy and safety in open-label single-arm phase 2 study. The Prostate *80*, 99-108.

Pienta, K.J., Gorin, M.A., Rowe, S.P., Carroll, P.R., Pouliot, F., Probst, S., Saperstein, L., Preston, M.A., Alva, A.S., Patnaik, A.*, a kol.* (2021). A Phase 2/3 Prospective Multicenter Study of the Diagnostic Accuracy of Prostate Specific Membrane Antigen PET/CT with (18)F-DCFPyL in Prostate Cancer Patients (OSPREY). The Journal of urology *206*, 52-61.

Plaitakis, A., and Constantakakis, E. (1993). Altered metabolism of excitatory amino acids, N-acetyl-aspartate and N-acetyl-aspartyl-glutamate in amyotrophic lateral sclerosis. Brain research bulletin *30*, 381-386.

Pouwels, P.J., and Frahm, J. (1997). Differential distribution of NAA and NAAG in human brain as determined by quantitative localized proton MRS. NMR in biomedicine *10*, 73-78.

Ptacek, J., Nedvedova, J., Navratil, M., Havlinova, B., Konvalinka, J., and Barinka, C. (2018). The calcium-binding site of human glutamate carboxypeptidase II is critical for dimerization, thermal stability, and enzymatic activity. Protein science : a publication of the Protein Society *27*, 1575-1584.

Qiu, A., Min, S.H., Jansen, M., Malhotra, U., Tsai, E., Cabelof, D.C., Matherly, L.H., Zhao, R., Akabas, M.H., and Goldman, I.D. (2007). Rodent intestinal folate transporters (SLC46A1):

secondary structure, functional properties, and response to dietary folate restriction. Am J Physiol Cell Physiol *293*, C1669-1678.

Rahbar, K., Afshar-Oromieh, A., Jadvar, H., and Ahmadzadehfar, H. (2018). PSMA Theranostics: Current Status and Future Directions. Mol Imaging *17*, 1536012118776068-1536012118776068.

Rais, R., Jiang, W., Zhai, H., Wozniak, K.M., Stathis, M., Hollinger, K.R., Thomas, A.G., Rojas, C., Vornov, J.J., Marohn, M.*, a kol.* (2016). FOLH1/GCPII is elevated in IBD patients, and its inhibition ameliorates murine IBD abnormalities. JCI Insight *1*, e88634.

Rajasekaran, A.K., Anilkumar, G., and Christiansen, J.J. (2005). Is prostate-specific membrane antigen a multifunctional protein? American Journal of Physiology-Cell Physiology *288*, C975-C981.

Rajasekaran, S.A., Anilkumar, G., Oshima, E., Bowie, J.U., Liu, H., Heston, W., Bander, N.H., and Rajasekaran, A.K. (2003). A novel cytoplasmic tail MXXXL motif mediates the internalization of prostate-specific membrane antigen. Molecular biology of the cell *14*, 4835-4845.

Rajasekaran, S.A., Christiansen, J.J., Schmid, I., Oshima, E., Ryazantsev, S., Sakamoto, K., Weinstein, J., Rao, N.P., and Rajasekaran, A.K. (2008). Prostate-specific membrane antigen associates with anaphase-promoting complex and induces chromosomal instability. Molecular cancer therapeutics *7*, 2142-2151.

Reisenauer, A.M., Krumdieck, C.L., and Halsted, C.H. (1977). Folate conjugase: two separate activities in human jejunum. Science *198*, 196-197.

Ren, H., Zhang, H., Wang, X., Liu, J., Yuan, Z., and Hao, J. (2014). Prostate-specific membrane antigen as a marker of pancreatic cancer cells. Medical oncology (Northwood, London, England) *31*, 857.

Renneberg, H., Friedetzky, A., Konrad, L., Kurek, R., Weingärtner, K., Wennemuth, G., Tunn, U.W., and Aumüller, G. (1999). Prostate specific membrane antigen (PSM) is expressed in various human tissues: implication for the use of PSM reverse transcription polymerase chain reaction to detect hematogenous prostate cancer spread. Urological research *27*, 23-27.

Renno, W.M., Lee, J.H., and Beitz, A.J. (1997). Light and electron microscopic immunohistochemical localization of N-acetylaspartylglutamate (NAAG) in the olivocerebellar pathway of the rat. Synapse (New York, NY) *26*, 140-154.

Robinson, M.B., Blakely, R.D., Couto, R., and Coyle, J.T. (1987). Hydrolysis of the brain dipeptide N-acetyl-L-aspartyl-L-glutamate. Identification and characterization of a novel N-acetylated alpha-linked acidic dipeptidase activity from rat brain. J Biol Chem *262*, 14498-14506.

Roffman, J.L., Lamberti, J.S., Achtyes, E., Macklin, E.A., Galendez, G.C., Raeke, L.H., Silverstein, N.J., Smoller, J.W., Hill, M., and Goff, D.C. (2013). Randomized multicenter investigation of folate plus vitamin B12 supplementation in schizophrenia. JAMA psychiatry *70*, 481-489.

Rogers, O.C., Rosen, D.M., Antony, L., Harper, H.M., Das, D., Yang, X., Minn, I., Mease, R.C., Pomper, M.G., and Denmeade, S.R. (2021). Targeted delivery of cytotoxic proteins to prostate cancer via conjugation to small molecule urea-based PSMA inhibitors. Scientific reports *11*, 14925.

Rochon, Y.P., Horoszewicz, J.S., Boynton, A.L., Holmes, E.H., Barren, R.J., 3rd, Erickson, S.J., Kenny, G.M., and Murphy, G.P. (1994). Western blot assay for prostate-specific membrane antigen in serum of prostate cancer patients. The Prostate *25*, 219-223.

Romei, C., Raiteri, M., and Raiteri, L. (2013). Glycine release is regulated by metabotropic glutamate receptors sensitive to mGluR2/3 ligands and activated by N-acetylaspartylglutamate (NAAG). Neuropharmacology *66*, 311-316.

Rosenberg, I.H., Streiff, R.R., Godwin, H.A., and Castle, W.B. (1969). Absorption of polyglutamic folate: participation of deconjugating enzymes of the intestinal mucosa. N Engl J Med *280*, 985-988.

Rothstein, J.D., Tsai, G., Kuncl, R.W., Clawson, L., Cornblath, D.R., Drachman, D.B., Pestronk, A., Stauch, B.L., and Coyle, J.T. (1990). Abnormal excitatory amino acid metabolism in amyotrophic lateral sclerosis. Annals of neurology *28*, 18-25.

Rovenská, M., Hlouchová, K., Sácha, P., Mlcochová, P., Horák, V., Zámecník, J., Barinka, C., and Konvalinka, J. (2008). Tissue expression and enzymologic characterization of human prostate specific membrane antigen and its rat and pig orthologs. The Prostate *68*, 171-182.

Sácha, P., Zámecník, J., Barinka, C., Hlouchová, K., Vícha, A., Mlcochová, P., Hilgert, I., Eckschlager, T., and Konvalinka, J. (2007). Expression of glutamate carboxypeptidase II in human brain. Neuroscience *144*, 1361-1372.

Salas Fragomeni, R.A., Menke, J.R., Holdhoff, M., Ferrigno, C., Laterra, J.J., Solnes, L.B., Javadi, M.S., Szabo, Z., Pomper, M.G., and Rowe, S.P. (2017). Prostate-Specific Membrane Antigen-Targeted Imaging With [18F]DCFPyL in High-Grade Gliomas. Clinical nuclear medicine *42*, e433-e435.

Samplaski, M.K., Heston, W., Elson, P., Magi-Galluzzi, C., and Hansel, D.E. (2011). Folate hydrolase (prostate-specific membrane [corrected] antigen) 1 expression in bladder cancer subtypes and associated tumor neovasculature. Modern pathology : an official journal of the United States and Canadian Academy of Pathology, Inc *24*, 1521-1529.

Sancey, L., Lucie, S., Garanger, E., Elisabeth, G., Foillard, S., Stéphanie, F., Schoehn, G., Guy, S., Hurbin, A., Amandine, H.*, a kol.* (2009). Clustering and internalization of integrin alphavbeta3 with a tetrameric RGD-synthetic peptide. Molecular therapy : the journal of the American Society of Gene Therapy *17*, 837-843.

Sanna, V., Singh, C.K., Jashari, R., Adhami, V.M., Chamcheu, J.C., Rady, I., Sechi, M., Mukhtar, H., and Siddiqui, I.A. (2017). Targeted nanoparticles encapsulating (-)-epigallocatechin-3-gallate for prostate cancer prevention and therapy. Scientific reports *7*, 41573.

Santoro, S.P., Kim, S., Motz, G.T., Alatzoglou, D., Li, C., Irving, M., Powell, D.J., Jr., and Coukos, G. (2015). T cells bearing a chimeric antigen receptor against prostate-specific membrane antigen mediate vascular disruption and result in tumor regression. Cancer Immunol Res *3*, 68-84.

Sartor, O., de Bono, J., Chi, K.N., Fizazi, K., Herrmann, K., Rahbar, K., Tagawa, S.T., Nordquist, L.T., Vaishampayan, N., El-Haddad, G.*, a kol.* (2021). Lutetium-177-PSMA-617 for Metastatic Castration-Resistant Prostate Cancer. N Engl J Med *385*, 1091-1103.

Sartori, S., Burlina, A.B., Salviati, L., Trevisson, E., Toldo, I., Laverda, A.M., and Burlina, A.P. (2008). Increased level of N-acetylaspartylglutamate (NAAG) in the CSF of a patient with Pelizaeus-Merzbacher-like disease due to mutation in the GJA12 gene. European journal of

paediatric neurology : EJPN : official journal of the European Paediatric Neurology Society *12*, 348-350.

Scaglione, F., and Panzavolta, G. (2014). Folate, folic acid and 5-methyltetrahydrofolate are not the same thing. Xenobiotica; the fate of foreign compounds in biological systems *44*, 480-488.

Serganova, I., Moroz, E., Cohen, I., Moroz, M., Mane, M., Zurita, J., Shenker, L., Ponomarev, V., and Blasberg, R. (2017). Enhancement of PSMA-Directed CAR Adoptive Immunotherapy by PD-1/PD-L1 Blockade. Molecular therapy oncolytics *4*, 41-54.

Severic, M., Ma, G., Pereira, S.G.T., Ruiz, A., Cheung, C.C.L., and Al-Jamal, W.T. (2021). Genetically-engineered anti-PSMA exosome mimetics targeting advanced prostate cancer in vitro and in vivo. Journal of Controlled Release *330*, 101-110.

Shafizadeh, T.B., and Halsted, C.H. (2007). gamma-Glutamyl hydrolase, not glutamate carboxypeptidase II, hydrolyzes dietary folate in rat small intestine. The Journal of nutrition *137*, 1149-1153.

Shaw, P.J., and Ince, P.G. (1997). Glutamate, excitotoxicity and amyotrophic lateral sclerosis. Journal of neurology *244 Suppl 2*, S3-14.

Schmidt, L.H., Heitkötter, B., Schulze, A.B., Schliemann, C., Steinestel, K., Trautmann, M., Marra, A., Hillejan, L., Mohr, M., Evers, G.*, a kol.* (2017). Prostate specific membrane antigen (PSMA) expression in non-small cell lung cancer. PloS one *12*, e0186280.

Schmittgen, T.D., Teske, S., Vessella, R.L., True, L.D., and Zakrajsek, B.A. (2003a). Expression of prostate specific membrane antigen and three alternatively spliced variants of PSMA in prostate cancer patients. Int J Cancer *107*, 323-329.

Schmittgen, T.D., Zakrajsek, B.A., Hill, R.E., Liu, Q., Reeves, J.J., Axford, P.D., Singer, M.J., and Reed, M.W. (2003b). Expression pattern of mouse homolog of prostate-specific membrane antigen (FOLH1) in the transgenic adenocarcinoma of the mouse prostate model. The Prostate *55*, 308-316.

Schülke, N., Varlamova, O.A., Donovan, G.P., Ma, D., Gardner, J.P., Morrissey, D.M., Arrigale, R.R., Zhan, C., Chodera, A.J., Surowitz, K.G.*, a kol.* (2003). The homodimer of prostate-specific membrane antigen is a functional target for cancer therapy. Proc Natl Acad Sci U S A *100*, 12590-12595.

Silver, D.A., Pellicer, I., Fair, W.R., Heston, W.D., and Cordon-Cardo, C. (1997). Prostate-specific membrane antigen expression in normal and malignant human tissues. Clinical cancer research : an official journal of the American Association for Cancer Research *3*, 81-85.

Simons, B.W., Turtle, N.F., Ulmert, D.H., Abou, D.S., and Thorek, D.L.J. (2019). PSMA expression in the Hi-Myc model; extended utility of a representative model of prostate adenocarcinoma for biological insight and as a drug discovery tool. The Prostate *79*, 678-685.

Singhal, N.K., Huang, H., Li, S., Clements, R., Gadd, J., Daniels, A., Kooijman, E.E., Bannerman, P., Burns, T., Guo, F.*, a kol.* (2017). The neuronal metabolite NAA regulates histone H3 methylation in oligodendrocytes and myelin lipid composition. Experimental brain research *235*, 279-292.

Slusher, B.S., Vornov, J.J., Thomas, A.G., Hurn, P.D., Harukuni, I., Bhardwaj, A., Traystman, R.J., Robinson, M.B., Britton, P., Lu, X.C.*, a kol.* (1999). Selective inhibition of NAALADase, which converts NAAG to glutamate, reduces ischemic brain injury. Nat Med *5*, 1396-1402.

Sokoloff, R.L., Norton, K.C., Gasior, C.L., Marker, K.M., and Grauer, L.S. (2000). A dual-monoclonal sandwich assay for prostate-specific membrane antigen: levels in tissues, seminal fluid and urine. The Prostate *43*, 150-157.

Spreux-Varoquaux, O., Bensimon, G., Lacomblez, L., Salachas, F., Pradat, P.F., Le Forestier, N., Marouan, A., Dib, M., and Meininger, V. (2002). Glutamate levels in cerebrospinal fluid in amyotrophic lateral sclerosis: a reappraisal using a new HPLC method with coulometric detection in a large cohort of patients. Journal of the neurological sciences *193*, 73-78.

Su, S.L., Huang, I.P., Fair, W.R., Powell, C.T., and Heston, W.D. (1995). Alternatively spliced variants of prostate-specific membrane antigen RNA: ratio of expression as a potential measurement of progression. Cancer research *55*, 1441-1443.

Tagawa, S.T., Beltran, H., Vallabhajosula, S., Goldsmith, S.J., Osborne, J., Matulich, D., Petrillo, K., Parmar, S., Nanus, D.M., and Bander, N.H. (2010). Anti-prostate-specific membrane antigen-based radioimmunotherapy for prostate cancer. Cancer *116*, 1075-1083.

Tagawa, S.T., Milowsky, M.I., Morris, M., Vallabhajosula, S., Christos, P., Akhtar, N.H., Osborne, J., Goldsmith, S.J., Larson, S., Taskar, N.P.*, a kol.* (2013). Phase II study of Lutetium-177-labeled anti-prostate-specific membrane antigen monoclonal antibody J591 for metastatic castration-resistant prostate cancer. Clinical cancer research : an official journal of the American Association for Cancer Research *19*, 5182-5191.

Tagawa, S.T., Milowsky, M.I., Morris, M.J., Vallabhajosula, S., Goldsmith, S., Matulich, D., Kaplan, J., Berger, F., Scher, H.I., Bander, N.H.*, a kol.* (2008). Phase II trial of 177Lutetium radiolabeled anti-prostate-specific membrane antigen (PSMA) monoclonal antibody J591 (177Lu- J591) in patients (pts) with metastatic castrate-resistant prostate cancer (metCRPC). Journal of Clinical Oncology *26*, 5140-5140.

Thomas, A.G., Liu, W., Olkowski, J.L., Tang, Z., Lin, Q., Lu, X.C., and Slusher, B.S. (2001a). Neuroprotection mediated by glutamate carboxypeptidase II (NAALADase) inhibition requires TGF-beta. European journal of pharmacology *430*, 33-40.

Thomas, A.G., Olkowski, J.L., and Slusher, B.S. (2001b). Neuroprotection afforded by NAAG and NAALADase inhibition requires glial cells and metabotropic glutamate receptor activation. European journal of pharmacology *426*, 35-38.

Tian, J.-y., Chi, C.-l., Bian, G., Xing, D., Guo, F.-j., and Wang, X.-q. (2021). PSMA conjugated combinatorial liposomal formulation encapsulating genistein and plumbagin to induce apoptosis in prostate cancer cells. Colloids and Surfaces B: Biointerfaces *203*, 111723.

Tieman, S.B., Cangro, C.B., and Neale, J.H. (1987). N-acetylaspartylglutamate immunoreactivity in neurons of the cat's visual system. Brain research *420*, 188-193.

Tolkach, Y., Gevensleben, H., Bundschuh, R., Koyun, A., Huber, D., Kehrer, C., Hecking, T., Keyver-Paik, M.D., Kaiser, C., Ahmadzadehfar, H.*, a kol.* (2018). Prostate-specific membrane antigen in breast cancer: a comprehensive evaluation of expression and a case report of radionuclide therapy. Breast cancer research and treatment *169*, 447-455.

Tortella, F.C., Lin, Y., Ved, H., Slusher, B.S., and Dave, J.R. (2000). Neuroprotection produced by the NAALADase inhibitor 2-PMPA in rat cerebellar neurons. European journal of pharmacology *402*, 31-37.

Trover, J.K., Beckett, M.L., and Wright Jr., G.L. (1995). Detection and characterization of the prostate-specific membrane antigen (PSMA) in tissue extracts and body fluids. International Journal of Cancer *62*, 552-558.

Troyer, J.K., Beckett, M.L., and Wright, G.L., Jr. (1995). Detection and characterization of the prostate-specific membrane antigen (PSMA) in tissue extracts and body fluids. Int J Cancer *62*, 552-558.

Tsai, B., Gilbert, J.M., Stehle, T., Lencer, W., Benjamin, T.L., and Rapoport, T.A. (2003a). Gangliosides are receptors for murine polyoma virus and SV40. The EMBO journal *22*, 4346-4355.

Tsai, G., and Coyle, J.T. (2002). Glutamatergic mechanisms in schizophrenia. Annual review of pharmacology and toxicology *42*, 165-179.

Tsai, G., Dunham, K.S., Drager, U., Grier, A., Anderson, C., Collura, J., and Coyle, J.T. (2003b). Early embryonic death of glutamate carboxypeptidase II (NAALADase) homozygous mutants. Synapse (New York, NY) *50*, 285-292.

Tsai, G., Forloni, G., Robinson, M.B., Stauch, B.L., and Coyle, J.T. (1988). Calcium-dependent evoked release of N-[3H]acetylaspartylglutamate from the optic pathway. J Neurochem *51*, 1956-1959.

Tsai, G.C., Stauch-Slusher, B., Sim, L., Hedreen, J.C., Rothstein, J.D., Kuncl, R., and Coyle, J.T. (1991). Reductions in acidic amino acids and N-acetylaspartylglutamate in amyotrophic lateral sclerosis CNS. Brain research *556*, 151-156.

Tykvart, J., Sácha, P., Bařinka, C., Knedlík, T., Starková, J., Lubkowski, J., and Konvalinka, J. (2012). Efficient and versatile one-step affinity purification of in vivo biotinylated proteins: expression, characterization and structure analysis of recombinant human glutamate carboxypeptidase II. Protein expression and purification *82*, 106-115.

Van Den Bosch, L., Van Damme, P., Bogaert, E., and Robberecht, W. (2006). The role of excitotoxicity in the pathogenesis of amyotrophic lateral sclerosis. Biochimica et Biophysica Acta (BBA) - Molecular Basis of Disease *1762*, 1068-1082.

Vargas-Martinez, C., Ordovas, J.M., Wilson, P.W., and Selhub, J. (2002). The glutamate carboxypeptidase gene II (C>T) polymorphism does not affect folate status in the Framingham Offspring cohort. The Journal of nutrition *132*, 1176-1179.

Viola-Villegas, N.T., Sevak, K.K., Carlin, S.D., Doran, M.G., Evans, H.W., Bartlett, D.W., Wu, A.M., and Lewis, J.S. (2014). Noninvasive Imaging of PSMA in prostate tumors with (89)Zr-Labeled huJ591 engineered antibody fragments: the faster alternatives. Mol Pharm *11*, 3965-3973.

Von Hoff, D.D., Mita, M.M., Ramanathan, R.K., Weiss, G.J., Mita, A.C., LoRusso, P.M., Burris, H.A., 3rd, Hart, L.L., Low, S.C., Parsons, D.M.*, a kol.* (2016). Phase I Study of PSMA-Targeted Docetaxel-Containing Nanoparticle BIND-014 in Patients with Advanced Solid Tumors. Clinical cancer research : an official journal of the American Association for Cancer Research *22*, 3157-3163.

Vorlova, B., Knedlik, T., Tykvart, J., and Konvalinka, J. (2019). GCPII and its close homolog GCPIII: from a neuropeptidase to a cancer marker and beyond. Frontiers in bioscience (Landmark edition) *24*, 648-687.

Vornov, J.J., Wozniak, K., Lu, M., Jackson, P., Tsukamoto, T., Wang, E., and Slusher, B. (1999). Blockade of NAALADase: a novel neuroprotective strategy based on limiting glutamate and elevating NAAG. Annals of the New York Academy of Sciences *890*, 400-405.

Walder, K.K., Ryan, S.B., Bzdega, T., Olszewski, R.T., Neale, J.H., and Lindgren, C.A. (2013). Immunohistological and electrophysiological evidence that N-acetylaspartylglutamate is a co-

transmitter at the vertebrate neuromuscular junction. The European journal of neuroscience *37*, 118-129.

Wang, T.T., Chandler, C.J., and Halsted, C.H. (1986). Intracellular pteroylpolyglutamate hydrolase from human jejunal mucosa. Isolation and characterization. J Biol Chem *261*, 13551-13555.

Wang, X., Ma, D., Olson, W.C., and Heston, W.D. (2011). In vitro and in vivo responses of advanced prostate tumors to PSMA ADC, an auristatin-conjugated antibody to prostate-specific membrane antigen. Molecular cancer therapeutics *10*, 1728-1739.

Ward, J.H., Kushner, J.P., and Kaplan, J. (1982). Transferrin receptors of human fibroblasts. Analysis of receptor properties and regulation. Biochemical Journal *208*, 19-26.

Watt, F., Martorana, A., Brookes, D.E., Ho, T., Kingsley, E., O'Keefe, D.S., Russell, P.J., Heston, W.D., and Molloy, P.L. (2001). A tissue-specific enhancer of the prostate-specific membrane antigen gene, FOLH1. Genomics *73*, 243-254.

Wernicke, A.G., Edgar, M.A., Lavi, E., Liu, H., Salerno, P., Bander, N.H., and Gutin, P.H. (2011). Prostate-specific membrane antigen as a potential novel vascular target for treatment of glioblastoma multiforme. Archives of pathology & laboratory medicine *135*, 1486-1489.

Wernicke, A.G., Varma, S., Greenwood, E.A., Christos, P.J., Chao, K.S., Liu, H., Bander, N.H., and Shin, S.J. (2014). Prostate-specific membrane antigen expression in tumor-associated vasculature of breast cancers. APMIS : acta pathologica, microbiologica, et immunologica Scandinavica *122*, 482-489.

Williams, A.J., Lu, X.M., Slusher, B., and Tortella, F.C. (2001). Electroencephalogram analysis and neuroprotective profile of the N-acetylated-alpha-linked acidic dipeptidase inhibitor, GPI5232, in normal and brain-injured rats. The Journal of pharmacology and experimental therapeutics *299*, 48-57.

Williams, T., and Kole, R. (2006). Analysis of prostate-specific membrane antigen splice variants in LNCap cells. Oligonucleotides *16*, 186-195.

Williamson, L.C., and Neale, J.H. (1988). Ultrastructural localization of N-acetylaspartylglutamate in synaptic vesicles of retinal neurons. Brain research *456*, 375-381.

Wilson, G.M., Fielding, A.B., Simon, G.C., Yu, X., Andrews, P.D., Hames, R.S., Frey, A.M., Peden, A.A., Gould, G.W., and Prekeris, R. (2005). The FIP3-Rab11 Protein Complex Regulates Recycling Endosome Targeting to the Cleavage Furrow during Late Cytokinesis. Molecular biology of the cell *16*, 849-860.

Wolf, N.I., Willemsen, M.A., Engelke, U.F., van der Knaap, M.S., Pouwels, P.J., Harting, I., Zschocke, J., Sistermans, E.A., Rating, D., and Wevers, R.A. (2004). Severe hypomyelination associated with increased levels of N-acetylaspartylglutamate in CSF. Neurology *62*, 1503-1508.

Wolf, P. (2021). Targeted Toxins for the Treatment of Prostate Cancer. Biomedicines *9*, 986.

Wolf, P., Alt, K., Bühler, P., Katzenwadel, A., Wetterauer, U., Tacke, M., and Elsässer-Beile, U. (2008). Anti-PSMA immunotoxin as novel treatment for prostate cancer? High and specific antitumor activity on human prostate xenograft tumors in SCID mice. The Prostate *68*, 129-138.

Wolf, P., Freudenberg, N., Bühler, P., Alt, K., Schultze-Seemann, W., Wetterauer, U., and Elsässer-Beile, U. (2010). Three conformational antibodies specific for different PSMA

epitopes are promising diagnostic and therapeutic tools for prostate cancer. The Prostate *70*, 562-569.

Wright, A.J., Dainty, J.R., and Finglas, P.M. (2007). Folic acid metabolism in human subjects revisited: potential implications for proposed mandatory folic acid fortification in the UK. The British journal of nutrition *98*, 667-675.

Wright, G.L., Jr., Haley, C., Beckett, M.L., and Schellhammer, P.F. (1995). Expression of prostate-specific membrane antigen in normal, benign, and malignant prostate tissues. Urologic oncology *1*, 18-28.

Wroblewska, B., Santi, M.R., and Neale, J.H. (1998). N-acetylaspartylglutamate activates cyclic AMP-coupled metabotropic glutamate receptors in cerebellar astrocytes. Glia *24*, 172-179.

Wroblewska, B., Wegorzewska, I.N., Bzdega, T., Olszewski, R.T., and Neale, J.H. (2006). Differential negative coupling of type 3 metabotropic glutamate receptor to cyclic GMP levels in neurons and astrocytes. J Neurochem *96*, 1071-1077.

Wroblewska, B., Wroblewski, J.T., Pshenichkin, S., Surin, A., Sullivan, S.E., and Neale, J.H. (1997). N-acetylaspartylglutamate selectively activates mGluR3 receptors in transfected cells. J Neurochem *69*, 174-181.

Wulff, G. (1995). Molecular Imprinting in Cross-Linked Materials with the Aid of Molecular Templates— A Way towards Artificial Antibodies. Angewandte Chemie International Edition in English *34*, 1812-1832.

Xing, Y., Xu, K., Li, S., Cao, L., Nan, Y., Li, Q., Li, W., and Hong, Z. (2021). A Single-Domain Antibody-Based Anti-PSMA Recombinant Immunotoxin Exhibits Specificity and Efficacy for Prostate Cancer Therapy. International journal of molecular sciences *22*.

Xu, X., Wu, J., Liu, Y., Saw, P.E., Tao, W., Yu, M., Zope, H., Si, M., Victorious, A., Rasmussen, J.*, a kol.* (2017). Multifunctional Envelope-Type siRNA Delivery Nanoparticle Platform for Prostate Cancer Therapy. ACS Nano *11*, 2618-2627.

Yamamoto, T., Kozikowski, A., Zhou, J., and Neale, J.H. (2008). Intracerebroventricular administration of N-acetylaspartylglutamate (NAAG) peptidase inhibitors is analgesic in inflammatory pain. Molecular pain *4*, 31.

Yamamoto, T., Nozaki-Taguchi, N., and Sakashita, Y. (2001a). Spinal N-acetyl-alpha-linked acidic dipeptidase (NAALADase) inhibition attenuates mechanical allodynia induced by paw carrageenan injection in the rat. Brain research *909*, 138-144.

Yamamoto, T., Nozaki-Taguchi, N., Sakashita, Y., and Inagaki, T. (2001b). Inhibition of spinal N-acetylated-alpha-linked acidic dipeptidase produces an antinociceptive effect in the rat formalin test. Neuroscience *102*, 473-479.

Yamamoto, T., Saito, O., Aoe, T., Bartolozzi, A., Sarva, J., Zhou, J., Kozikowski, A., Wroblewska, B., Bzdega, T., and Neale, J.H. (2007). Local administration of N-acetylaspartylglutamate (NAAG) peptidase inhibitors is analgesic in peripheral pain in rats. European Journal of Neuroscience *25*, 147-158.

Yang, D., Holt, G.E., Velders, M.P., Kwon, E.D., and Kast, W.M. (2001). Murine six-transmembrane epithelial antigen of the prostate, prostate stem cell antigen, and prostate-specific membrane antigen: prostate-specific cell-surface antigens highly expressed in prostate cancer of transgenic adenocarcinoma mouse prostate mice. Cancer research *61*, 5857-5860.

Yao, V., and Bacich, D.J. (2006). Prostate specific membrane antigen (PSMA) expression gives prostate cancer cells a growth advantage in a physiologically relevant folate environment in vitro. The Prostate *66*, 867-875.

Yao, V., Berkman, C.E., Choi, J.K., O'Keefe, D.S., and Bacich, D.J. (2010). Expression of prostate-specific membrane antigen (PSMA), increases cell folate uptake and proliferation and suggests a novel role for PSMA in the uptake of the non-polyglutamated folate, folic acid. The Prostate *70*, 305-316.

Yari, H., Nkepang, G., and Awasthi, V. (2019). Surface Modification of Liposomes by a Lipopolymer Targeting Prostate Specific Membrane Antigen for Theranostic Delivery in Prostate Cancer. Materials (Basel) *12*, 756.

You, J., O'Hara, S.D., Velupillai, P., Castle, S., Levery, S., Garcea, R.L., and Benjamin, T. (2015). Ganglioside and Non-ganglioside Mediated Host Responses to the Mouse Polyomavirus. PLoS pathogens *11*, e1005175.

Younes, A., Bartlett, N.L., Leonard, J.P., Kennedy, D.A., Lynch, C.M., Sievers, E.L., and Forero-Torres, A. (2010). Brentuximab vedotin (SGN-35) for relapsed CD30-positive lymphomas. N Engl J Med *363*, 1812-1821.

Zackova Suchanova, J., Neburkova, J., Spanielova, H., Forstova, J., and Cigler, P. (2017). Retargeting Polyomavirus-Like Particles to Cancer Cells by Chemical Modification of Capsid Surface. Bioconjugate Chemistry *28*, 307-313.

Zeng, C., Ke, Z.F., Yang, Z., Wang, Z., Yang, S.C., Luo, C.Q., and Wang, L.T. (2012). Prostate-specific membrane antigen: a new potential prognostic marker of osteosarcoma. Medical oncology (Northwood, London, England) *29*, 2234-2239.

Zhang, A.X., Murelli, R.P., Barinka, C., Michel, J., Cocleaza, A., Jorgensen, W.L., Lubkowski, J., and Spiegel, D.A. (2010). A Remote Arene-Binding Site on Prostate Specific Membrane Antigen Revealed by Antibody-Recruiting Small Molecules. Journal of the American Chemical Society *132*, 12711-12716.

Zhang, F., Shan, L., Liu, Y., Neville, D., Woo, J.H., Chen, Y., Korotcov, A., Lin, S., Huang, S., Sridhar, R.*, a kol.* (2013). An anti-PSMA bivalent immunotoxin exhibits specificity and efficacy for prostate cancer imaging and therapy. Advanced healthcare materials *2*, 736-744.

Zhang, T., Song, B., Zhu, W., Xu, X., Gong, Q.Q., Morando, C., Dassopoulos, T., Newberry, R.D., Hunt, S.R., and Li, E. (2012). An ileal Crohn's disease gene signature based on whole human genome expression profiles of disease unaffected ileal mucosal biopsies. PloS one *7*, e37139.

Zhao, J., Ramadan, E., Cappiello, M., Wroblewska, B., Bzdega, T., and Neale, J.H. (2001). NAAG inhibits KCl-induced [(3)H]-GABA release via mGluR3, cAMP, PKA and L-type calcium conductance. The European journal of neuroscience *13*, 340-346.

Zhao, R., Matherly, L.H., and Goldman, I.D. (2009). Membrane transporters and folate homeostasis: intestinal absorption and transport into systemic compartments and tissues. Expert Rev Mol Med *11*, e4-e4.

Zhong, C., Zhao, X., Van, K.C., Bzdega, T., Smyth, A., Zhou, J., Kozikowski, A.P., Jiang, J., O'Connor, W.T., Berman, R.F.*, a kol.* (2006). NAAG peptidase inhibitor increases dialysate NAAG and reduces glutamate, aspartate and GABA levels in the dorsal hippocampus following fluid percussion injury in the rat. Journal of Neurochemistry *97*, 1015-1025.

Zhu, C., Bandekar, A., Sempkowski, M., Banerjee, S.R., Pomper, M.G., Bruchertseifer, F., Morgenstern, A., and Sofou, S. (2016). Nanoconjugation of PSMA-Targeting Ligands

Enhances Perinuclear Localization and Improves Efficacy of Delivered Alpha-Particle Emitters against Tumor Endothelial Analogues. Molecular cancer therapeutics *15*, 106-113.

Zink, C.F., Barker, P.B., Sawa, A., Weinberger, D.R., Wang, M., Quillian, H., Ulrich, W.S., Chen, Q., Jaffe, A.E., Kleinman, J.E.*, a kol.* (2020). Association of Missense Mutation in FOLH1 With Decreased NAAG Levels and Impaired Working Memory Circuitry and Cognition. The American journal of psychiatry *177*, 1129-1139.

Zollinger, M., Amsler, U., Do, K.Q., Streit, P., and Cuénod, M. (1988). Release of N-acetylaspartylglutamate on depolarization of rat brain slices. J Neurochem *51*, 1919-1923.

Zuccolotto, G., Penna, A., Fracasso, G., Carpanese, D., Montagner, I.M., Dalla Santa, S., and Rosato, A. (2021). PSMA-Specific CAR-Engineered T Cells for Prostate Cancer: CD28 Outperforms Combined CD28-4-1BB "Super-Stimulation". Frontiers in oncology *11*, 708073.

9. Přílohy

1. **Příloha 1:** Tykvart J, Navrátil V, **Sedlák F**, Corey E, Colombatti M, Fracasso G, Koukolík F, Bařinka C, Šácha P, Konvalinka J. **Comparative analysis of monoclonal antibodies against prostate-specific membrane antigen (PSMA).** *Prostate.* 2014 Dec;74(16):1674-90. ..... **98**
2. **Příloha 2:** Šácha P, Knedlík T, Schimer J, Tykvart J, Parolek J, Navrátil V, Dvořáková P, **Sedlák F**, Ulbrich K, Strohalm J, Majer P, Šubr V, Konvalinka J. **iBodies: Modular Synthetic Antibody Mimetics Based on Hydrophilic Polymers Decorated with Functional Moieties.** *Angew Chem Int Ed Engl.* 2016 Feb 12;55(7):2356-60. ..... **114**
3. **Příloha 3:** Knedlík T, Vorlová B, Navrátil V, Tykvart J, **Sedlák F**, Vaculín Š, Franěk M, Šácha P, Konvalinka J.: **Mouse glutamate carboxypeptidase II (GCPII) has a similar enzyme activity and inhibition profile but a different tissue distribution to human GCPII.** *FEBS Open Bio*. 2017 Aug 29;7(9):1362-1378. ..... **119**
4. **Příloha 4:** Vorlová B, **Sedlák F**, Kašpárek P, Šrámková K, Malý M, Zámečník J, Šácha P, Konvalinka J.: **A novel PSMA/GCPII-deficient mouse model shows enlarged seminal vesicles upon aging.** *Prostate.* 2019 Feb;79(2):126-139. ..... **136**
5. **Příloha 5:** **Sedlák F**, Šácha P, Blechová M, Březinová A, Šafařík M, Šebestík J, Konvalinka J. **Glutamate carboxypeptidase II does not process amyloid-β peptide.** *FASEB J.* 2013 Jul;27(7):2626-32. ..... **143**
6. **Příloha 6:** Neburková J, **Sedlák F**, Žáčková Suchanová J, Kostka L, Šácha P, Šubr V, Etrych T, Šimon P, Bařinková J, Kryštufek R, Španielová H, Forstová J, Konvalinka J, Cígler P: **Inhibitor-GCPII Interaction: Selective and Robust System for Targeting Cancer Cells with Structurally Diverse Nanoparticles.** *Mol Pharm.* 2018 Aug 6;15(8):2932-2945. ..... **157**

Příloha 1

The Prostate 74:1674–1690 (2014)

Comparative Analysis of Monoclonal Antibodies Against Prostate-Specific Membrane Antigen (PSMA)

J. Tykvart,[1,2] V. Navrátil,[1,2] F. Sedlák,[1,3] E. Corey,[4] M. Colombatti,[5] G. Fracasso,[5] F. Koukolík,[6] C. Bařinka,[7] P. Šácha,[1,2] and J. Konvalinka[1,2]*

[1]Gilead Sciences and IOCB Research Centre, Institute of Organic Chemistry and Biochemistry, Academy of Sciences of the Czech Republic, Czech Republic
[2]Department of Biochemistry, Faculty of Natural Science, Charles University, Czech Republic
[3]First Faculty of Medicine, Charles University in Prague, Czech Republic
[4]Genitourinary Cancer Research Laboratory, Department of Urology, University of Washington, Seattle
[5]Department of Pathology and Diagnostics, Section of Immunology, University of Verona, Verona, Italy
[6]Department of Pathology and Molecular Medicine, Thomayer Teaching Hospital, Czech Republic
[7]Institute of Biotechnology, Academy of Sciences of the Czech Republic, Czech Republic

BACKGROUND. Prostate-specific membrane antigen (PSMA), also known as glutamate carboxypeptidase II (GCPII), is generally recognized as a diagnostic and therapeutic cancer antigen and a molecular address for targeted imaging and drug delivery studies. Due to its significance in cancer research, numerous monoclonal antibodies (mAbs) against GCPII have been described and marketed in the past decades. Unfortunately, some of these mAbs are poorly characterized, which might lead to their inappropriate use and misinterpretation of the acquired results.

METHODS. We collected the 13 most frequently used mAbs against GCPII and quantitatively characterized their binding to GCPII by enzyme-linked immunosorbent assay (ELISA) and surface plasmon resonance (SPR). Using a peptide library, we mapped epitopes recognized by a given mAb. Finally, we assessed the applicability of these mAbs to routine experimental setups, including Western blotting, immunohistochemistry, and flow cytometry.

RESULTS. ELISA and SPR analyses revealed that mAbs J591, J415, D2B, 107-1A4, GCP-05, and 2G7 bind preferentially to GCPII in native form, while mAbs YPSMA-1, YPSMA-2, GCP-02, GCP-04, and 3E6 bind solely to denatured GCPII. mAbs 24.4E6 and 7E11-C5.3 recognize both forms of GCPII. Additionally, we determined that GCP-02 and 3E6 cross-react with mouse GCPII, while GCP-04 recognizes GCPII and GCPIII proteins from both human and mouse.

CONCLUSION. This comparative analysis provides the first detailed quantitative characterization of the most commonly used mAbs against GCPII and can serve as a guideline for the scientific community to use them in a proper and efficient way. *Prostate 74: 1674–1690, 2014.*

Grant sponsor: The Czech Republic; Grant number: P304-12-0847; Grant sponsor: Project InterBioMed; Grant number: LO1302; Grant sponsor: The GACR; Grant number: 301/12/1513; Grant sponsor: BIOCEV; Grant number: CZ.1.05/1.1.00/02.0109.

*Correspondence to: Jan Konvalinka, Institute of Organic Chemistry and Biochemistry, ASCR, v.v.i. Flemingovo n. 2, Prague 6, 166 10, Czech Republic
E-mail: jan.konvalinka@uochb.cas.cz
Received 27 June 2014; Accepted 5 August 2014
DOI 10.1002/pros.22887
Published online 27 September 2014 in Wiley Online Library (wileyonlinelibrary.com).

KEY WORDS: **glutamate carboxypeptidase II; prostate-specific membrane antigen; folate hydrolase; NAALADase; Western blot; immunohistochemistry; ELISA; flow cytometry; surface plasmon resonance**

INTRODUCTION

Over the past 20 years, prostate specific membrane antigen (PSMA), also known as glutamate carboxypeptidase II (GCPII), has been investigated for use in cancer diagnostics and targeted drug delivery due to its elevated and highly restricted expression in prostate adenocarcinoma [1]. In 1997, GCPII was also found to be expressed in the neovasculature of newly formed solid tumors [2–3]. This finding turned GCPII into an even more attractive target for diagnostic and therapeutic applications [4]. Furthermore, GCPII has become widely used as a model molecular address for various targeted drug delivery strategies due to its favorable features, including its topology (it is a transmembrane protein with the majority of the molecule facing outside of the cell [5]), ability to internalize ligands upon binding [6] and restricted tissue expression [7–11].

Several laboratories are currently studying GCPII from various perspectives, and the majority of them routinely use monoclonal antibodies (mAbs) in a variety of experimental methods [12–15]. There is a large pool of available anti-GCPII mAbs produced by both academia and industry. Unfortunately, some of them are not sufficiently well characterized to allow appropriate use and interpretation of results. This may occasionally lead to inconsistent or even contradictory results. For example, numerous research groups intensively studied the expression profile of GCPII in the human body. The researchers utilized several detection methods (immunohistochemistry (IHC) [2–3,16–22], Western blot (WB) [23–24], enzyme-linked immunosorbent assay (ELISA) [25]) and various mAbs (7E11-C5.3 [3,18–20,24–25], J591 [2,18], PEQ226.5 [18,25], 24.4E6 [20], YPSMA-1 [21], 3D16 [16], PM2J004.5 [17–18], GCP-04 [23], and 3E6 [22]). Taken together, the studies provided some clear and consistent results (e.g., GCPII was detected in prostate tissue in all studies) but also yielded some major inconsistencies and contradictions (e.g., expression of GCPII in tumor-associated neovasculature was detected by some scientists [16–17,22] but not others [20–21]; the expression of GCPII in brain was confirmed in some studies [20–21,24] but not others [3,18–19]).

Therefore, our objective was to gather the most frequently used mAbs against GCPII and perform their thorough analysis and comparison. These mAbs are listed in Table I.

Two mAbs from our collected panel are either in clinical use or advanced stage of clinical trials. 7E11-C5.3 was the first mouse mAb developed against GCPII. It was generated in 1987 by immunizing mice with crude LNCaP cell lysate, and it recognizes the intracellular portion of GCPII [29]. The ^{111}In radioconjugate of 7E11-C5.3 (ProstaScint^{TM}) is currently the only anti-GCPII agent employed in clinical practice. It is used for detection of prostate cancer recurrence and metastases [26–28].

J591 is a second-generation mAb that recognizes the extracellular portion of GCPII. It was prepared and characterized in 1997 by Liu et al. J591 recognizes viable LNCaP cells expressing GCPII and enables visualization of GCPII in frozen tissue sections [2]. J591 has been intensively investigated for potential use in the clinic. Various conjugates of this mAb have been prepared and characterized as potential diagnostic and therapeutic agents, and some are now being tested in phase II clinical trials [31–39].

We could not possibly cover all available mAbs against GCPII, but we believe that we included most of those that are commonly used. The notable exceptions involve a panel of mAbs prepared in the laboratory of Dr. Ursula Elsässer-Beile (Universitätsklinikum Freiburg, Experimentelle Urologie, Germany) [61] and a panel of mAbs developed by Progenics [62–63]. These mAbs were unfortunately not provided to us for the purpose of this study.

We believe the results of this study will help clarify the inconsistent results published in the GCPII literature. We also hope that our observations will help scientists choose the most appropriate mAbs for their experiments and plan them in the most effective manner (e.g., information about the binding affinity of a particular mAb would enable facile estimation of its working concentration). Finally, we point out some misconceptions and the erroneous performances of some of the methods involving these mAbs, specifically Western blot and immunohistochemistry.

MATERIALS AND METHODS

Purification of Recombinant Avi-tagged Proteins

The extracellular portion of human GCPII with an N-terminal Avi-tag (Avi-GCPII) was prepared as previously described [64]. Human GCPII homologs (human GCPIII, mouse GCPII and mouse GCPIII) were prepared and denoted in a similar fashion. See Supplementary Material for more details.

mouse Avi-GCPIII were used in a similar fashion as human GCPII. For mAb 7E11-C5.3, intraGCPII peptide in native binding buffer was used instead of human Avi-GCPII. Then, solutions of various mAbs prepared by 2× serial dilution (11 concentrations in total) were added into the wells, followed by addition of HRP-conjugated goat anti-mouse polyclonal antibody. The chemiluminiscent substrate was added into each well, and the chemiluminiscence was measured. See Supplementary Material for more details.

Epitope Determination Assay

The protocol described for the native GCPII ELISA assay was also used for this experiment. A library of 83 biotinylated 18-mer peptides was synthesized. These peptides, which cover the entire sequence of human GCPII, were immobilized on a 96-well plate via neutravidin and then treated with the appropriate mAb. Experiments without any primary antibody and with indifferent mouse IgG were also performed as negative controls. See Supplementary Material for more details.

Characterization of mAb Binding by SPR

All SPR measurements were performed on a four-channel SPR sensor platform (PLASMON IV) developed at the Institute of Photonics and Electronics (IPE) of the Academy of Sciences of the Czech Republic, Prague [65–66]. First, a gold chip was functionalized with alkanethiols containing carboxylic terminal groups (Prochimia) in pure ethanol and then mounted to the prism on the SPR sensor. All experiments were performed at 25°C. Activation of carboxylic terminal groups on the sensor surface was performed in situ by injecting a solution of N-hydroxysuccinimide and N-ethyl-N-(dimethylaminopropyl) carbodiimide in pure water. Then, neutravidin was covalently immobilized on the chip surface, followed by a high ionic strength solution and ethanolamine to wash out non-covalently bound neutravidin and deactivate residual carboxylic groups, respectively. Recombinant human Avi-GCPII in PBS was immobilized to the prepared layer, followed by injection of an appropriate mAb (D2B, J591, J415, 107-1A4 or 2G7). Four different mAb concentrations in PBS were used for each experiment (association phase). Then, PBS was loaded to the chip to wash out the bound mAb (dissociation phase).

TraceDrawer 1.5 (Ridgeview Instruments AB) was used to calculate k_{on} and k_{off} parameters of mAb binding. Measurements were performed twice for each mAb. See Supplementary Material for more details.

Western Blotting

Western blots were performed using standard procedures and overnight incubation with appropriate mAbs, namely GCP-02, GCP-04, YPSMA-1, YPSMA-2, 3E6, 24.4E6, J591 (1 μg/ml) and D2B (10 μg/ml). See Supplementary Material for more details.

Immunohistochemistry

A prostate adenocarcinoma sample (Gleason score 3 + 4) was obtained by radical prostatectomy at Thomayer's Hospital in Prague. Patient consent and local ethical commission approval were obtained. Formalin-fixed paraffin-embedded tissues (3-μm-thick slides) were used for IHC that was performed according to a standard procedure with overnight incubation of the anti-GCPII mAbs at 4°C. The mAb concentration differed depending on the particular experiment, ranging from 0.01 μg/ml to 10 μg/ml. For visualization of antibody–antigen complexes, the slides were incubated with Histofine® Simple Stain™ MAX PO (MULTI) (Nichirei Biosciences Inc.). See Supplementary Material for more details.

Flow Cytometry

LNCaP and PC3 cells were grown under standard tissue culture conditions. After reaching 80% confluence, the cells were trypsinized, harvested, counted and diluted in 10% FBS/PBS to a final concentration 4×10^6 cells/ml.

The experiments were performed in a 96-well plate format with 2×10^5 cells in each well. All subsequent procedures were performed strictly at 4°C to prevent internalization of a bound primary antibody. An appropriate mAb was added into each well to reach a final concentration of 10 μg/ml. After 1 hour, cells were washed several times and incubated for another hour with secondary F(ab') fragment donkey anti-mouse IgG (H + L) antibody conjugated with phycoerythrin (Jackson ImmunoResearch). Finally, the cells were diluted in 10% FBS/PBS, and single cell suspensions were measured on a BD LSRFortessa™ cell analyzer (Becton, Dickinson and Company). All experiments (all mAbs and both cell lines) were measured in triplicate. See Supplementary Material for more details.

RESULTS

We sorted the mAbs based on the nature of the antigen they recognize (i.e., GCPII in native or denatured form) since this feature predetermines mAb effectiveness in all the methods tested. Throughout

this manuscript, we use the term "GCPII in native form" to refer to the biophysical properties of GCPII, that is, properly folded and enzymatically active protein. We use the term "GCPII in denatured form" to refer to protein that has been heat-denatured in the presence of the detergents.

In this study, we used GCPII of two different origins. For ELISA, SPR, and WB experiments, we used the extracellular portion of recombinant human GCPII (Avi-GCPII) or its three homologs (human Avi-GCPIII, mouse Avi-GCPII, and mouse Avi-GCPIII) produced in insect cells with N-terminal biotin (covalently attached to the Avi-tag^{TM}) [64] while for FC, IHC, and WB experiments, we used GCPII endogenously expressed in LNCaP cells or prostate adenocarcinoma tissue.

Quantitative Analysis

The affinities of mAbs for Avi-GCPII were determined by ELISA and SPR. First, we used ELISA to qualitatively test the ability of the mAbs to bind Avi-GCPII in its native or denatured form. Based on these results, we measured a titration curve for each mAb and its appropriate antigen. From these measurements, we obtained the 50% saturation binding value, which describes the affinity of the mAb, and the maximal saturation signal value, which corresponds to the overall output signal of the mAb.

Using ELISA, we also tested mAb binding to three GCPII homologs (human Avi-GCPIII, mouse Avi-GCPII, and mouse Avi-GCPIII). Additionally, to gain an even better understanding of the binding event, we used SPR to determine the kinetic profile of binding for the tight-binding mAbs against Avi-GCPII in native form.

TABLE II. Characteristics of mAb Binding to Human Avi-GCPII in Native Form

Antibody	50% saturation	Maximal signal	#
D2B	0.072 ± 0.013 nM	4.8	2
J415	0.163 ± 0.022 nM	3.9	3
J591	1.40 ± 0.27 nM	6.9	3
2G7	2.89 ± 0.25 nM	1.0	2
107-1A4	3.81 ± 0.43 nM	2.6	2
24.4E6	365 ± 77 nM	NC	4
GCP-05	550 ± 130 nM	NC	2

ELISA experiments under native conditions were performed with various mAbs to measure their saturation binding curves to Avi-GCPII. "50% saturation" indicates the mAb concentration at which 50% of the maximal saturation signal was obtained. "#" stands for the number of measurements performed. "Maximal signal" shows the ratio of maximal saturation signals among all mAbs (the lowest maximal saturation signal was taken as the standard). The maximal signal values for GCP-05 and 24.4E6 were not calculated (NC) because a different amount of immobilized Avi-GCPII was used in those experiments. 50% saturation values are shown as arithmetic means with weighted standard errors calculated from the individual measurements. The saturation curves for each mAb are shown in Fig. S1 in the Supplementary Material.

ELISA Using Avi-GCPII in Native Form

mAbs that bind to Avi-GCPII in native form are listed in Table II. Our results show that mAbs 2G7, J415, J591, D2B and 107-1A4 bind Avi-GCPII very tightly (with nanomolar to high picomolar 50% saturation values), while GCP-05 and 24.4E6 bind Avi-GCPII much weakly (with submicromolar 50% saturation values). Moreover, a comparison of the maximal saturation values of the tight-binding mAbs showed an almost sevenfold difference in maximal signal output (2G7 vs. J591).

ELISA Using Denatured Avi-GCPII and mAb Epitope Mapping

mAbs that bind Avi-GCPII in denatured form are listed in Table III. The results show a wide range of 50%

TABLE III. Characteristics of mAb Binding to Denatured Human Avi-GCPII

Antibody	50% saturation	Maximal signal	Epitope	#
GCP-04	0.628 ± 0.066 nM	54	91–108	2
J591	3.06 ± 0.89 nM	1	ND	3
GCP-02	5.2 ± 1.2 nM	40	271–288	4
3E6	9.8 ± 1.7 nM	9	118–135	2
7E11-C5.3	9.9 ± 3.0 nM	NC	1–21	2
YPSMA-1	61 ± 17 nM	7	469–486	2
YPSMA-2	216 ± 55 nM	42	469–486	3
24.4E6	267 ± 49 nM	5	640–657	2

ELISA experiments under denaturing conditions were performed with various mAbs to measure their binding to Avi-GCPII (for 7E11-C5.3, a synthetic biotinylated peptide was used). "50% saturation" indicates the mAb concentration at which 50% of the maximal saturation signal was obtained. "#" stands for the number of measurements performed. "Maximal signal" shows the ratio of maximal saturation signals among all mAbs (the lowest maximal saturation signal was taken as standard). "Epitope" indicates the sequence of the biotinylated peptide used in the epitope determination assay. Positions of mAb epitopes refer to the GCPII sequence of accession number Q04609-1. The assay did not provide any positive results for J591. In the case of 7E11-C5.3, the sequence of intraGCPII peptide, which was used for measurement of saturation binding curve, is stated. The maximal signal value for 7E11-C5.3 was not calculated (NC) because a different amount of immobilized antigen was used in the experiment. 50% saturation values are shown as arithmetic means with weighted standard errors calculated from the individual measurements. The saturation curves for each mAb are shown in Fig. S1 in the Supplementary Material.

saturation values (from subnanomolar for GCP-04 to submicromolar for 24.4E6 and YPSMA-2). The variation in the maximal saturation signals is even higher, with a 54-fold difference between mAbs GCP-04 and J591. In addition to the mAbs listed in Table III, we also observed detectable binding of D2B to denatured Avi-GCPII. However, due to the very low signal, we were unable to obtain an appropriate saturation-binding curve to characterize this interaction (data not shown). For measurements with 7E11-C5.3, we used a synthetic peptide (intraGCPII peptide) as antigen because the 7E11-C5.3 epitope lies within the intracellular portion of GCPII, which is not included in Avi-GCPII.

To further characterize the epitopes of the mAbs tested, we used a library of biotinylated peptides that cover the entire GCPII sequence. Using this library, we identified the epitopes of all tested mAbs except J591 and D2B. For 7E11-C5.3, GCP-04 and 24.4E6, we confirmed already known epitopes, and for 3E6, we substantially narrowed the previously suggested epitope. Furthermore, we identified the epitopes of YPSMA-1 (aa 469–486), YPSMA-2 (aa 469–486), and GCP-02 (aa 271–288).

ELISA Using Avi-GCPII Homologs

None of the tested mAbs recognize human GCPII homologs (human Avi-GCPIII, mouse Avi-GCPII, and mouse Avi-GCPIII) in native form. On the other hand, three of the 13 mAbs tested cross-react with the denatured form of the human GCPII homologs (see Table IV). GCP-02 and 3E6 recognize mouse Avi-GCPII with similar affinity as human Avi-GCPII, but GCP-02 has a much lower maximal saturation signal value toward the mouse enzyme. GCP-04 recognizes all tested homologs, binding to mouse Avi-GCPII with similar affinity as to human Avi-GCPII and recognizing both Avi-GCPIII proteins with approximately 10-fold lower affinity and threefold lower maximal saturation signal compared to their Avi-GCPII counterparts.

SPR Using Avi-GCPII in Native Form

To further characterize binding of the tested mAbs to Avi-GCPII, we determined their binding kinetics using SPR. Due to persistent problems with preparation of a stable denatured Avi-GCPII layer, we were only able to analyze mAb binding to Avi-GCPII in its native form. We performed this kinetic analysis for mAbs J415, J591, 107-1A4, D2B, and 2G7. GCP-05 and 24.4E6 did not provide sufficient signal for proper measurement.

The results (summarized in Table V) show similar kinetic profiles for mAbs J591 and 2G7, with dissociation constants (K_D values) in the subnanomolar range. 107-1A4 had a very high association rate (k_{on} value) but also the highest dissociation rate (k_{off} value) leading to a similar K_D as those calculated for J591 and 2G7. J415 and D2B showed high k_{on} and very low k_{off} values. The k_{off} values were under the detection limit of our SPR instrument. However, our results indicate that the K_D

TABLE IV. Characteristics of mAb Binding to Denatured Avi-GCPII Homologs

Antibody	50% saturation	Maximal signal	Antigen	#
GCP-02	5.2 ± 1.2 nM	16.3	human GCPII	2
	2.52 ± 0.44 nM	1.0	mouse GCPII	3
3E6	9.8 ± 1.7 nM	1.0	human GCPII	2
	28.6 ± 3.0 nM	1.3	mouse GCPII	2
GCP-04	0.628 ± 0.066 nM	3.4	human GCPII	2
	2.62 ± 0.13 nM	2.9	mouse GCPII	2
	50.4 ± 9.3 nM	1.0	human GCPIII	2
	29.3 ± 3.3 nM	1.3	mouse GCPIII	3

ELISA experiments were performed under denaturing conditions with various mAbs to determine their binding affinity toward human Avi-GCPIII, mouse Avi-GCPII and mouse Avi-GCPIII. "50% saturation" indicates the antibody concentration at which 50% of maximal saturation signal was obtained. "#" stands for the number of measurements performed. "Maximal signal" shows the ratio of maximal saturation signals for one mAb and several GCPII homologs (the lowest maximal saturation signal was taken as the standard). 50% saturation values are shown as arithmetic means with weighted standard errors calculated from the individual measurements. The saturation curves for each mAb are shown in Fig. S1 in the Supplementary Material.

TABLE V. Kinetic Parameters of mAb Binding to Avi-GCPII in Native Form

Antibody	k_{on} $[10^4\ (M^*s)^{-1}]$	k_{off} $[10^{-5}\ s^{-1}]$	K_D $[10^{-9}\ M]$
J415	110.5 ± 3.5	< 2	< 0.018
D2B	49.2 ± 3.1	< 2	< 0.041
107-1A4	46.1 ± 1.3	10.2 ± 3.8	0.221 ± 0.083
2G7	11.45 ± 0.78	4.1 ± 1.5	0.36 ± 0.13
J591	11.15 ± 0.64	8.4 ± 1.5	0.75 ± 0.14

Recombinant human Avi-GCPII was immobilized via biotin to the SPR chip. Four different concentrations of each mAb were applied to the layer, and their association and dissociation curves were measured. Each measurement was performed twice. The k_{on} and k_{off} values represent the average of both measurements with the deviation from the mean. The k_{off} values of J415 and 107-1A4 were below the detection limit of our SPR sensor and thus could not be reliably determined. The fitted binding curves for each mAb are shown in Figure S2 in the Supplementary Material.

values for these two mAbs are in the picomolar range. The SPR results are in agreement with the results from ELISA experiments, in which mAbs J415 and D2B displayed the lowest 50% saturation values.

Qualitative Analysis

To obtain additional information about the characteristics of the tested mAbs, we compared them using three basic techniques: Western blot (WB), immunohistochemistry (IHC) and flow cytometry (FC). In the WB analysis, the protein samples are denatured; therefore, we analyzed only those mAbs capable of binding to denatured GCPII. In the other two methods, we exploited a larger pool of mAbs because the methods can be performed under both native and denaturing conditions.

Comparison of mAbs in Western Blot

We used mAbs GCP-02, GCP-04, 3E6, YPSMA-1, YPSMA-2, 24.4E6, J591, D2B, and 7E11-C5.3 to detect GCPII by Western blot (see Fig. 1). Our sample set contained a dilution series of purified human Avi-GCPII and its three homologs, lysate from LNCaP cells (a cell line endogenously expressing GCPII) and lysate from prostate adenocarcinoma tissue (only the latter two samples were used with 7E11-C5.3 because this mAb has an intracellular epitope and thus does not recognize the recombinant protein constructs).

Our results show that all the mAbs are able to detect GCPII under WB conditions. Based on signal strength, the mAbs can be divided into three groups: (a) GCP-02, GCP-04 and YPSMA-1, yielding a strong signal even for low amounts of Avi-GCPII and lysates; (b) 3E6, YPSMA-2 and 7E11-C5.3, providing an average signal for detection of GCPII in lysates and the highest concentration of Avi-GCPII; and (c) 24.4E6, J591 and D2B, showing weak signals (for D2B, we had to increase the mAb concentration to obtain a detectable signal). Additionally, only mAbs GCP-02, GCP-04, and 3E6 were able to detect some of the human Avi-GCPII homologs, which is in agreement with

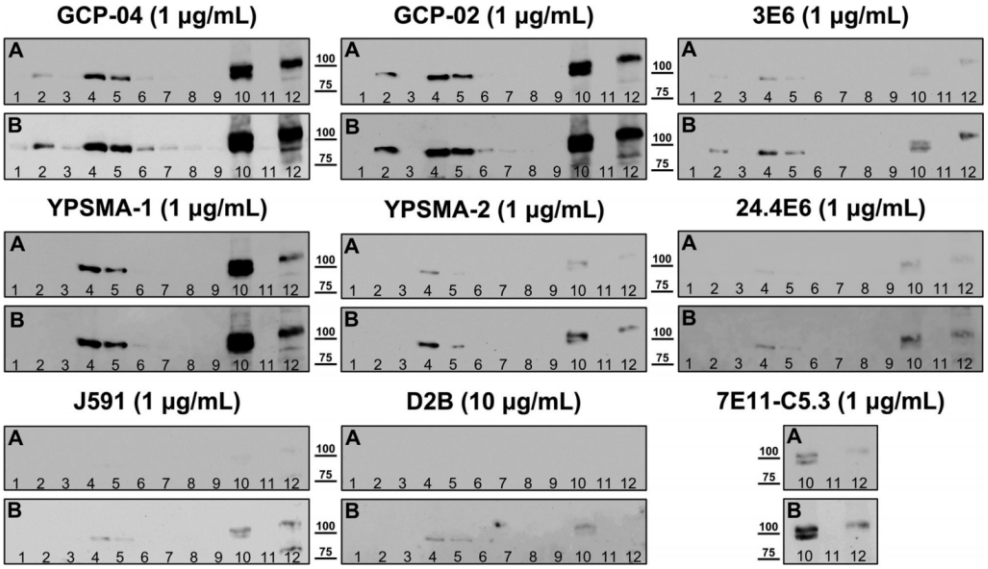

Fig. 1. Western blot detection of human GCPII and its homologs by anti-GCPII mAbs. Samples of purified human Avi-GCPII and its homologs (human Avi-GCPIII, mouse Avi-GCPII and Avi-GCPIII), lysate from LNCaP cells and lysate from prostate adenocarcinoma tissue were resolved by SDS-PAGE, blotted onto nitrocellulose membranes and incubated with various mAbs. Sample legend: 1. mouse Avi-GCPIII – 10 ng, 2. mouse Avi-GCPII – 10 ng, 3. human Avi-GCPIII – 10 ng, 4. human Avi-GCPII – 10 ng, 5. human Avi-GCPII – 5 ng, 6. human Avi-GCPII – 1 ng, 7. human Avi-GCPII – 500 pg, 8. human Avi-GCPII – 200 pg, 9. empty line, 10. LNCaP lysate – 20 µg total protein 11. empty line, 12. prostate adenocarcinoma lysate – 50 µg total protein. The chemiluminiscence detection was performed identically for all mAbs. **A:** Figures were not processed with a graphical editor. **B:** Contains the same figures as in panels A, but processed with a graphical editor (changes in color contrast and levels) to highlight the chemiluminiscence signal.

results from ELISA. In Figure 1, panels "A" serve for proper comparison of the signal outputs of the tested mAbs (images were not processed with a graphical editor), while panels "B" show images that were individually processed with a graphical editor to highlight the chemiluminiscence signal.

Comparison of mAbs in Immunohistochemistry

We prepared formalin-fixed paraffin-embedded tissue sections (this preparation method leads to complete denaturation of the sample proteins) from high-grade prostate adenocarcinoma and tested the ability of our mAb panel to visualize GCPII. We tested the mAbs at a concentration of 10 μg/ml. As shown in Figure 2, only mAbs GCP-02, GCP-04, YPSMA-1, YPSMA-2, 3E6, and 24.4E6 provide visible staining of GCPII in tissue sections. Even though the strength of staining is different among these six mAbs, they all provided clear visualization of GCPII.

Additionally, we performed an experiment with these mAbs to map the dependence of the output signal on the mAb working concentration. As shown in Figure 3, all tested mAbs were able to visualize GCPII in tissue sections at a concentration 0.1 μg/ml, and GCP-04 was effective even at concentration 0.01 μg/ml.

Comparison of mAbs in Flow Cytometry

To assess the ability of the tested mAbs to bind GCPII in native form, we used flow cytometry and evaluated their binding to two prostate cancer cell lines: one endogenously expressing GCPII (LNCaP) and one lacking this expression (PC3). We incubated live cells with mAbs (10 μg/ml final concentration) and investigated the potential binding.

Results from these experiments are summarized in Figure 4. Based on the overall fluorescent signal of the cells, the mAbs can be divided into two groups: a) mAbs that bind to LNCaP but not to PC3: J591, D2B, 107-1A4, J415, GCP-05, and 2G7 and b) mAbs that do not bind either LNCaP or PC3 cells: 24.4E6, GCP-02, GCP-04, 7E11-C5.3, YPMSA-1, YPSMA-2, and 3E6 (see Fig. 4A).

Additionally, the mAbs binding to LNCaP cells can be further divided based on their ability to distinguish the LNCaP and PC3 cell populations. J591, D2B, 107-1A4, GCP-05, and J415 are able to separate these populations quantitatively, while 2G7 provides approximately 60% separation of these populations (see Fig. 4B).

The results from all our presented experiments are summarized in a simplified form in Table VI. All tested mAbs are marked with "+/−" signs to indicate their efficacy in the appropriate method ("+++" meaning the highest efficacy and "−" meaning not working at all).

TABLE VI. Summary of Basic Characteristics of Anti-GCPII mAbs

	GCPII in native form		GCPII in denatured form		
Antibody	ELISA	FC	ELISA	WB	IHC-P
J591	+++	+++	+	+	−
J415	+++	+++	−	−	−
D2B	+++	+++	+	+	−
107-1A4	+++	+++	−	−	−
2G7	++	++	−	−	−
GCP-05	+	+++	−	−	−
7E11-C5.3*	++	−	++	++	−
GCP-02	−	−	+++	+++	+++
GCP-04	−	−	+++	+++	+++
YPSMA-1	−	−	++	+++	+++
YPSMA-2	−	−	++	++	+++
3E6	−	−	++	++	++
24.4E6	+	−	+	+	++

*for this mAb the intraGCPII peptide was used as antigen instead of GCPII protein. ELISA, enzyme-linked immunosorbent assay; WB, Western blot; FC, flow cytometry performed under native conditions; IHC-P, immunohistochemistry performed on paraffin-embedded tissue sections.

Discussion

The form of the antigen (native or denatured) that a mAb recognizes and its appropriate binding constants are the two features that should suffice for the proper utilization of a given mAb. Therefore, in our study we did not aim to compare the efficacies of all mAbs in all applicable methods, but rather quantitatively analyze the binding of collected mAbs to their antigens. Our results, together with the understanding of a particular method's principles and some basic biochemical knowledge, should allow researchers to select the best mAb and conditions for their particular experiments.

Evaluation of Quantitative Analysis Data

The data obtained from quantitative analysis of mAbs from ELISA experiments can be used to estimate the efficacies of the mAbs in other methods, such as WB, IHC, and FC. We can evaluate this assumption based on the results presented in this study, including the 50% saturation value (which reflects binding affinity) and the maximal saturation signal obtained from ELISA analysis. Comparing

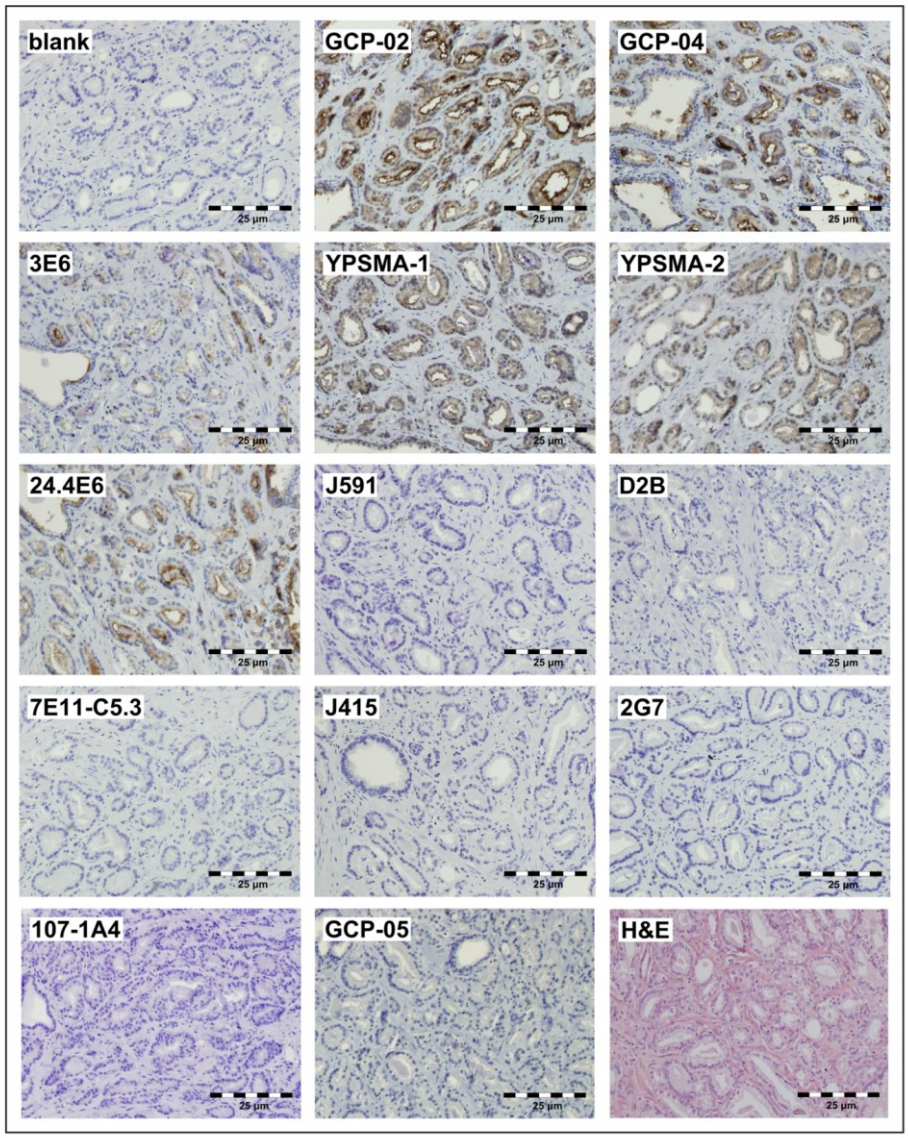

Fig. 2. Immunohistological staining of prostate adenocarcinoma tissue sections with anti-GCPII mAbs. Formalin-fixed paraffin-embedded sections were subjected to the panel of mAbs (all at 10 µg/ml concentration) to compare their abilities to visualize GCPII. The immunoperoxidase method was used for visualization of antibody-antigen complexes, followed by counterstaining with Harris' hematoxylin. Routine hematoxylin and eosin staining (H&E) was also performed to determine the morphological features of the cancer tissue. The specificity of staining was confirmed by processing one slide with omission of the primary antibody (blank).

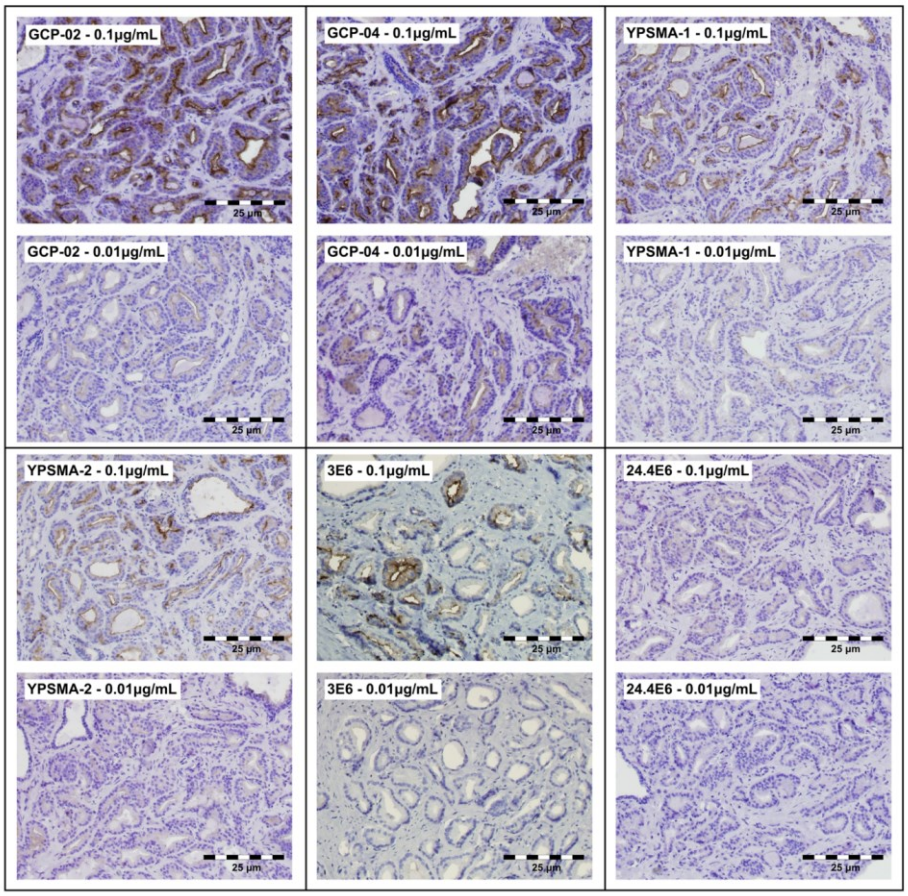

Fig. 3. Immunohistological staining of prostate adenocarcinoma tissue sections by different concentration of various anti-GCPII mAbs. Formalin-fixed paraffin-embedded tissue sections were subjected to two different concentrations (0.1 µg/ml and 0.01 µg/ml) of GCP-02, GCP-04, YPSMA-1, YPSMA-2, 3E6 and 24.4E6. The immunoperoxidase method was used for visualization of bound mAbs, followed by counterstaining with Harris' hematoxylin.

the 50% saturation value to the working mAb concentration used in a certain method (e.g., WB) indicates whether the mAb is saturated with the particular antigen. The maximal saturation signal provides an estimate of the maximal signal output given by the mAb in a particular method. However, it is important to keep in mind that these are only rough estimates because the conditions used for the method studied (e.g., WB) differ slightly from the conditions used for quantitative analysis (e.g., ELISA).

GCP-02 and GCP-04 should provide the best WB results based on the ELISA experiments, and they are indeed the most sensitive mAbs from the panel. YPSMA-2 has a high maximal saturation signal as well, but also a high 50% saturation value (the working concentration of mAbs in WB was approximately 7 nM). Therefore, it did not provide a very strong signal. In this case, increasing the mAb concentration should significantly improve the signal output. On the other hand, increasing the mAb concentration is unlikely to greatly improve the results for J591 and

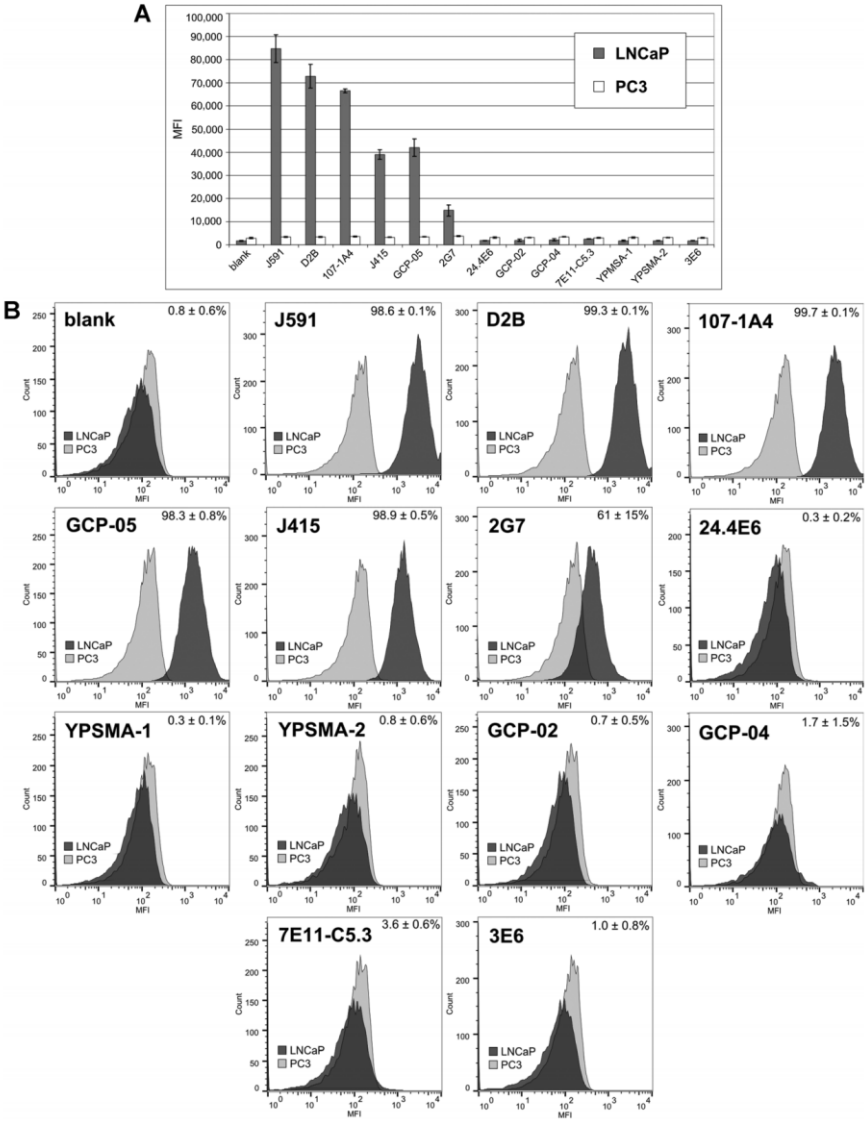

Fig. 4. Flow cytometry analysis of mAb binding efficacy to viable prostate cancer cell lines. Single cell suspensions of cell lines that possess (LNCaP) or lack (PC3) endogenous GCPII expression were mixed with the tested mAbs. The antibody-antigen complex was subsequently visualized by phycoerythrin-conjugated secondary antibody followed by flow cytometry analysis. For each measurement, 10,000 events (gated to analyze only living cells) were processed. **A:** Graph showing the mean fluorescent intensity (MFI) of each mAb for either LNCaP or PC3 cells. Each experiment was run in triplicate, and error bars represent the standard deviation. **B:** A series of histograms for each mAb showing the population distribution based on the fluorescent intensity. Each histogram was created from a single representative experiment. The LNCaP population is shown in dark grey and the PC3 population in light grey. The number in the top right corner of each histogram indicates the percentage of the LNCaP population that has a higher MFI signal than the highest 5% of the PC3 population. This number was calculated for each measurement (performed in triplicate), and the mean ± SEM is presented.

3E6 because they already have very low 50% saturation values, and their weak signals are likely caused by their low maximal saturation values.

A quantitative comparison of IHC staining is very difficult to perform. Nevertheless, it appears that GCP-02 and GCP-04 provided the strongest signals (see Fig. 2). The working concentration of mAbs in IHC was approximately 70 nM. Such a concentration should, based on the results from ELISA, provide the maximal saturation signal for all mAbs except YPSMA-1, YPSMA-2, and 24.4E6. For those mAbs, an additional increase in concentration should improve the signal output obtained upon staining. Even though we showed that many of the tested mAbs also work at lower concentrations (as low as 0.07 nM for GCP-04), it should be noted that we analyzed a sample of high-grade prostate adenocarcinoma with very high expression of GCPII; the expression will likely be much lower in other tissues. Therefore, we recommend following the 50% saturation values determined by ELISA (concentrations 10-fold higher than the 50% saturation value should provide the highest signal output) to estimate an appropriate mAb concentration for IHC experiments.

Interestingly, the mAb 7E11-C5.3 did not provide any visible staining in our IHC experiments, even though there is clear and repeated evidence of its expected "positive" performance throughout the literature (see references in Table I). To elucidate this result, we performed an additional experiment with two different antigen retrieval buffers (acidic and basic). This experiment showed that even though basic retrieval buffer slightly improved the staining, 7E11-C5.3 still provides very weak to no signal (see Fig. S3). This might indicate that the intracellular epitope of GCPII was not accessible under our experimental conditions (perhaps due to the cross-linking with the surrounding intracellular proteins during the fixation step by formaldehyde), suggesting that the IHC protocol would require additional optimization to work efficiently for this particular mAb. This result favors mAbs with epitopes located in the extracellular portion of GCPII (e.g., GCP-04 or YPSMA-1) over 7E11-C5.3, because these mAbs likely do not require such stringent and optimized experimental conditions to work efficiently.

Data from FC experiments are in general agreement with the estimations made from the ELISA results. J591, J415, D2B, and 107-1A4 provided the highest signals and full separation of the GCPII-positive and GCPII-negative cell populations. 2G7 showed average separation, which is probably caused by its low maximal signal value. mAb 7E11-C5.3 did not bind to viable LNCaP cells because the mAb was likely unable to access its intracellular epitope in our experimental setup. Both 24.4E6 and 7E11-C5.3 were also tested in FC at a higher concentration (100 μg/ml), yielding the same negative results (data not shown).

Discrepancies in Proposed mAb Efficacies

Taken together, the results of our quantitative analysis can be used to estimate mAb efficacy in other methods. Nevertheless, we observed several examples of poor data correlation; namely, 7E11-C5.3 efficacy in IHC and FC, GCP-05 and 24.4E6 efficacy in FC and YPSMA-1 efficacy in WB. As discussed earlier, 7E11-C5.3 behaved differently than other tested mAbs mainly due to its different epitope localization (intracellular vs. extracellular).

GCP-05, which bound to Avi-GCPII weakly in ELISA, provided very good results in FC experiments. On the other hand mAb 24.4E6, which showed similar affinity to Avi-GCPII as GCP-05 in the ELISA assay, did not work in FC at all. There are at least two potential explanations for these discrepancies. First, there is a difference in experimental conditions (e.g., working with immobilized antigen in ELISA vs. working in solution in FC and use of different secondary antibodies or different binding buffers). This problem cannot be overcome and must always be taken into account. Second, the antigens used for ELISA and FC originate from different sources. We performed the ELISA experiments with recombinant Avi-GCPII protein expressed in insect cells, while FC was performed with human cell lines. Even though it has been repeatedly shown that the extracellular portion of GCPII produced in insect cells is properly folded, enzymatically active protein [64,67], there is a difference in the protein's post-translational modification, namely N-glycosylation, compared to that of its mammalian counterpart.

There is little information about the epitopes of mAbs binding to GCPII in native form and therefore we can only speculate about the influence of N-glycosylation on the binding of GCP-05. On the other hand, we have determined the approximate epitopes of mAbs that bind to denatured Avi-GCPII. As shown in Fig. S4, the epitope of 24.4E6 does not contain an N-glycosylation site, and therefore the discrepant results obtained from ELISA and FC experiments cannot be explained by this phenomenon. Contrary to 24.4E6 the determined epitope sequences of YPSMA-1, YPSMA-2, and 3E6 contain Asn residue which is N-glycosylated suggesting that these three mAbs could bound differently to GCPII expressed in insect and mammalian cells. However, the results from WB experiment where both recombinant Avi-GCPII from insect cells and endogenous GCPII were detected (see Fig. 1) shows that these mAbs recognize both forms of GCPII with similar affinity and

thus N-glycosylation does not play role in the recognition of GCPII by these mAbs.

Specificity of mAbs Against Different Forms of GCPII

Our results suggest that most mAbs recognize GCPII either in its native or denatured form. The exceptions are 24.4E6 and 7E11-C5.3 because their epitopes probably adopt the same conformation regardless of the GCPII state. Additionally, we observed binding of J591 and D2B to denatured GCPII, but in comparison to their affinity toward the native protein, this binding was negligible. We hypothesize that the process of denaturation in some methods was incomplete, and a small portion of the protein (or at least the appropriate antibody epitope) remained in the native state. This hypothesis is supported by the fact that epitope determination assays using the panel of synthetic peptides were inconclusive for J591 and D2B. This would suggest that these mAbs require some additional structural motive (secondary structure) for efficient binding and they do not bind to a single unstructured polypeptide chain.

On the other hand, 24.4E6 showed very similar binding to Avi-GCPII in both native and denaturing ELISA setups. Since for this particular mAb the amount of immobilized Avi-GCPII was identical (10 ng per well) in both experiments, the incomplete denaturation of Avi-GCPII in the denaturing ELISA setup or partial denaturation of Avi-GCPII in the native ELISA setup would not explain the observed binding. In addition, the epitope determination assay provided a positive result for 24.4E6, unlike J591 and D2B. Both facts support the finding that 24.4E6 can bind to both the native and denatured forms of Avi-GCPII.

Results from the epitope determination assay were also helpful in predicting and validating the cross-reactivities of the mAbs with close GCPII homologs in denatured form. In this case, cross-reactivity is exclusively dependent on the protein sequence similarity. Therefore, it was not surprising to observe cross-reactivity of 3E6 with mouse Avi-GCPII because the 3E6 epitope sequences of mouse and human GCPII are identical (see Fig. S4). We can also turn this approach around and narrow the determined 18 aa epitope for YPSMA-1 and YPSMA-2, which do not recognize mouse Avi-GCPII. Because the only difference between human and mouse GCPII in this region is Lys482, which is a Gln residue in mouse GCPII, the epitopes of these mAbs are likely located around this residue. Interestingly, the determined epitope for YPSMA-1 does not correspond to the suggested epitope (aa 716–723; information taken from Abcam datasheet). To address this discrepancy, we tested two different batches of YPSMA-1, from Anogen and Abcam. Both these mAbs provided identical results in our epitope determination assay.

Advantages and Disadvantages of the Comparative Analysis Approach

Finally, we should note that we performed all qualitative experiments with the same mAb concentrations (with the exception of D2B in WB) because we focused primarily on comparative analysis of the tested mAbs. The consequence of this approach was that in some cases we performed an experiment with a mAb concentration that was too low compared to its corresponding 50% saturation value (e.g., YPSMA-2 in WB) and thus did not obtain optimal results.

Additionally, direct comparison of our results with those presented in the literature is difficult because use of different instrumentation and protocols can influence the results. Therefore, we decided to perform a large-scale comparative study of anti-GCPII mAbs rather than characterize only mAbs developed in our lab. For example, our results do not disprove the fact that J591 can recognize GCPII with sufficient sensitivity in WB if the experiment is performed with a different blotting device or by using a different blotting membrane or secondary antibody compared to our WB protocol [2] (in that study, 100 nM J591 was used). On the other hand, the result suggesting that J591 works with similar efficacy as GCP-04 in WB as presented by Wang et al. is quite surprising in light of our observations [58].

General Remarks on the Lack of Experimental Details in the Scientific Literature

Because comparative studies of mAbs in this field are lacking, it is very challenging to compare published results and determine their biological and/or clinical relevance. The situation is further complicated by the fact that the experimental sections of published papers often lack sufficient and precise descriptions of the experimental setups. For example, the amount of protein sample loaded onto a WB or the exact concentration of primary antibody used is often not mentioned in the figure legend or Methods section [20,39,48]. Sometimes, even the name of the mAb is not stated clearly and a generalized denotation, such as "antibody purchased from Abcam," is given instead (Abcam currently provides more than 30 different mAbs against GCPII) [68].

It is even more complicated for methods such as IHC or ICC, because these methods can generally be

performed under either native or denaturing conditions. Therefore, even if the mAb is suggested for use in IHC or ICC by its manufacturer, the researcher should always attempt to check the exact experimental conditions. For example, IHC from frozen tissue sections is generally thought to visualize antigen in its native form. But the experimental protocol often includes fixation with acetone or methanol, which leads to complete denaturation of the sample and therefore requires different mAbs for proper visualization. If these seemingly minor differences are not stated explicitly, it may lead to confusion. In the case of YPSMA-1, several manufacturers state that it works in ICC and IHC-Fr. These methods are generally thought to visualize native proteins. Therefore, it is not surprising that some studies used YPSMA-1 in experimental setups in which GCPII in native form was targeted, even though based on our results YPSMA-1 binds solely to denatured GCPII [10,69].

To avoid such pitfalls, precise description of experimental details is essential. Unfortunately, this is not the case for many studies, which use mAbs to visualize GCPII. For example, the dilution rather than the working concentration of 3E6, the most frequently used mAb for visualizing GCPII in IHC experiments, is almost exclusively stated in the literature [22,49–51]. Unfortunately, 3E6 is provided as dialyzed supernatant with its concentration determined by the producer, and this concentration varies batch-to-batch. For example, we used two batches of 3E6 (#10041132 and #10067501, which were provided at concentrations of 283 μg/ml and 81 μg/ml, respectively) in our study. With such a difference in concentrations between the batches, it is not surprising that the dilution of 3E6 used varies from 1:20 to 1:200 in the literature [22,51]. Clearly, in this case there is no way to calculate the actual working concentration of 3E6. It is also worth noting that the customer purchases a volume of supernatant, so the actual amount of mAb purchased differs for each batch.

The lack of detailed information regarding experimental procedures may be partially caused by the ongoing efforts of scientific journals to reduce the length of published articles as much as possible; the Materials and Methods sections are most often the first choice for truncation. Even though this effort is understandable, it should not be done at the expense of scientific accuracy. The authors may try to overcome this issue by providing a simplified method description in the main text and full detailed experimental descriptions in the Supplementary Material (as is already suggested by some of scientific journals, e.g., *Science*).

CONCLUSION

We performed a thorough comparative analysis of 13 mAbs against GCPII. We divided them based on their abilities to bind GCPII in either native or denatured form and compared their efficacies in basic molecular biology methods (WB, IHC, and FC). We believe that our observations will help dissect some of the discrepancies in the published results and that they will be useful in helping researchers choose the most appropriate mAb for their experimental setup. We also dare to hope that the common inaccuracies in method descriptions that we pointed out will become less frequent in the future.

ACKNOWLEDGEMENT

The authors would like to acknowledge Jana Starková and Karolína Šrámková for their excellent technical support, Mirka Blechová for preparation of intraGCPII peptide and Hillary Hoffman for language editing. We would like to thank Dr. Neil H. Bander (Weill Cornell Medical College, NY, USA), who generously provided purified J415 and J591, and also Dr. Ching Y. Wang (SUNY Upstate Medical University, NY, USA), who kindly provided the supernatant of 24.4E6. This work was supported by grant P304-12-0847 from the Grant Agency of the Czech Republic and Project InterBioMed LO1302 from Ministry of Education of the Czech Republic. C.B. acknowledges the support from the GACR (grant No 301/12/1513). This publication is in part supported by the project "BIOCEV" (CZ.1.05/1.1.00/02.0109), from the ERDF.

REFERENCES

1. Ghosh A, Heston WD. Tumor target prostate specific membrane antigen (PSMA) and its regulation in prostate cancer. J Cell Biochem 2004;91(3):528–539.
2. Liu H, Moy P, Kim S, Xia Y, Rajasekaran A, Navarro V, Knudsen B, Bander NH. Monoclonal antibodies to the extracellular domain of prostate-specific membrane antigen also react with tumor vascular endothelium. Cancer Res 1997;57(17):3629–3634.
3. Silver DA, Pellicer I, Fair WR, Heston WD, Cordon-Cardo C. Prostate-specific membrane antigen expression in normal and malignant human tissues. Clin Cancer Res 1997;3(1):81–85.
4. Foss CA, Mease RC, Cho SY, Kim HJ, Pomper MG. GCPII imaging and cancer. Curr Med Chem 2012;19(9):1346–1359.
5. Mesters JR, Barinka C, Li W, Tsukamoto T, Majer P, Slusher BS, Konvalinka J, Hilgenfeld R. Structure of glutamate carboxypeptidase II, a drug target in neuronal damage and prostate cancer. EMBO J 2006;25(6):1375–1384.
6. Liu H, Rajasekaran AK, Moy P, Xia Y, Kim S, Navarro V, Rahmati R, Bander NH. Constitutive and antibody-induced

36. Kampmeier F, Williams JD, Maher J, Mullen GE, Blower PJ. Design and preclinical evaluation of a 99mTc-labelled diabody of mAb J591 for SPECT imaging of prostate-specific membrane antigen (PSMA). EJNMMI Res 2014;4(1):13.

37. Bandekar A, Zhu C, Jindal R, Bruchertseifer F, Morgenstern A, Sofou S. Anti-prostate-specific membrane antigen liposomes loaded with 225Ac for potential targeted antivascular alpha-particle therapy of cancer. J Nucl Med 2014;55(1):107–114.

38. Zhang F, Shan L, Liu Y, Neville D, Woo JH, Chen Y, Korotcov A, Lin S, Huang S, Sridhar R, Liang W, Wang PC. An anti-PSMA bivalent immunotoxin exhibits specificity and efficacy for prostate cancer imaging and therapy. Adv Healthc Mater 2013;2(5):736–744.

39. Baiz D, Hassan S, Choi YA, Flores A, Karpova Y, Yancey D, Pullikuth A, Sui G, Sadelain M, Debinski W, Kulik G. Combination of the PI3K inhibitor ZSTK474 with a PSMA-targeted immunotoxin accelerates apoptosis and regression of prostate cancer. Neoplasia 2013;15(10):1172–1183.

40. Lutje S, Rijpkema M, Franssen GM, Fracasso G, Helfrich W, Eek A, Oyen WJ, Colombatti M, Boerman OC. Dual-modality image-guided surgery of prostate cancer with a radiolabeled fluorescent anti-psma monoclonal antibody. J Nucl Med 2014.

41. Colombatti M, Grasso S, Porzia A, Fracasso G, Scupoli MT, Cingarlini S, Poffe O, Naim HY, Heine M, Tridente G, Mainiero F, Ramarli D. The prostate specific membrane antigen regulates the expression of IL-6 and CCL5 in prostate tumour cells by activating the MAPK pathways. PLoS One 2009;4(2): e4608.

42. Frigerio B, Fracasso G, Luison E, Cingarlini S, Mortarino M, Coliva A, Seregni E, Bombardieri E, Zuccolotto G, Rosato A, Colombatti M, Canevari S, Figini M. A single-chain fragment against prostate specific membrane antigen as a tool to build theranostic reagents for prostate cancer. Eur J Cancer 2013;49(9): 2223–2232.

43. Schmidt S, Fracasso G, Colombatti M, Naim HY. Cloning and characterization of canine prostate-specific membrane antigen. Prostate 2013;73(6):642–650.

44. Schmidt S, Gericke B, Fracasso G, Ramarli D, Colombatti M, Naim HY. Discriminatory role of detergent-resistant membranes in the dimerization and endocytosis of prostate-specific membrane antigen. PLoS One 2013;8(6):e66193.

45. Lutje S, van Rij CM, Franssen GM, Fracasso G, Helfrich W, Eek A, Oyen WJ, Colombatti M, Boerman OC. Targeting human prostate cancer with In-labeled D2B IgG, F(ab') and Fab fragments in nude mice with PSMA-expressing xenografts. Contrast Media Mol Imaging 2014.

46. Brown LG, Wegner SK, Wang H, Buhler KR, Arfman EW, Lange PH, Vessella RL. A novel monoclonal antibody 107-1A4 with high prostate specificity: Generation, characterization of antigen expression, and targeting of human prostate cancer xenografts. Prostate Cancer Prostatic Dis 1998;1(4):208–215.

47. Wang S, Diamond DL, Hass GM, Sokoloff R, Vessella RL. Identification of prostate specific membrane antigen (PSMA) as the target of monoclonal antibody 107-1A4 by proteinchip; array, surface-enhanced laser desorption/ionization (SELDI) technology. Int J Cancer 2001;92(6):871–876.

48. Mincheff M, Zoubak S, Altankova I, Tchakarov S, Makogonenko Y, Botev C, Ignatova I, Dimitrov R, Madarzhieva K, Hammett M, Pomakov Y, Meryman H, Lissitchkov T. Human dendritic cells genetically engineered to express cytosolically retained fragment of prostate-specific membrane antigen prime cytotoxic T-cell responses to multiple epitopes. Cancer Gene Ther 2003; 10(12):907–917.

49. Chaux A, Eifler J, Karram S, Al-Hussain T, Faraj S, Pomper M, Rodriguez R, Netto GJ. Focal positive prostate-specific membrane antigen (PSMA) expression in ganglionic tissues associated with prostate neurovascular bundle: Implications for novel intraoperative PSMA-based fluorescent imaging techniques. Urol Oncol 2013;31(5):572–575.

50. Minner S, Wittmer C, Graefen M, Salomon G, Steuber T, Haese A, Huland H, Bokemeyer C, Yekebas E, Dierlamm J, Balabanov S, Kilic E, Wilczak W, Simon R, Sauter G, Schlomm T. High level PSMA expression is associated with early PSA recurrence in surgically treated prostate cancer. Prostate 2011; 71(3):281–288.

51. Perner S, Hofer MD, Kim R, Shah RB, Li H, Moller P, Hautmann RE, Gschwend JE, Kuefer R, Rubin MA. Prostate-specific membrane antigen expression as a predictor of prostate cancer progression. Hum Pathol 2007;38(5):696–701.

52. Murphy GPS, WA), Boynton, Alton L. (Redmond, WA), Holmes, Eric H. (Bothell, WA), Tino, William Thomas (Redmond, WA); Northwest Biotherapeutics, Inc. (Seattle, WA), assignee. Monoclonal antibodies specific for the extracellular domain of prostate-specific membrane antigen. United States. 2000.

53. Knedlik T, Navratil V, Vik V, Pacik D, Sacha P, Konvalinka J. Detection and quantitation of glutamate carboxypeptidase II in human blood. Prostate 2014.

54. Kinoshita Y, Kuratsukuri K, Newman N, Rovito PM, Kaumaya PT, Wang CY, Haas GP. Targeting epitopes in prostate-specific membrane antigen for antibody therapy of prostate cancer. Prostate Cancer Prostatic Dis 2005;8(4):359–363.

55. Barinka C, Mlcochova P, Sacha P, Hilgert I, Majer P, Slusher BS, Horejsi V, Konvalinka J. Amino acids at the N- and C-termini of human glutamate carboxypeptidase II are required for enzymatic activity and proper folding. Eur J Biochem 2004;271(13):2782–2790.

56. Barinka C, Sacha P, Sklenar J, Man P, Bezouska K, Slusher BS, Konvalinka J. Identification of the N-glycosylation sites on glutamate carboxypeptidase II necessary for proteolytic activity. Protein Sci 2004;13(6):1627–1635.

57. Sacha P, Zamecnik J, Barinka C, Hlouchova K, Vicha A, Mlcochova P, Hilgert I, Eckschlager T, Konvalinka J. Expression of glutamate carboxypeptidase II in human brain. Neuroscience 2007;144(4):1361–1372.

58. Wang X, Ma D, Olson WC, Heston WD. In vitro and in vivo responses of advanced prostate tumors to PSMA ADC, an auristatin-conjugated antibody to prostate-specific membrane antigen. Mol Cancer Ther 2011;10(9):1728–1739.

59. Chen Z, Penet MF, Nimmagadda S, Li C, Banerjee SR, Winnard PT Jr, Artemov D, Glunde K, Pomper MG, Bhujwalla ZM. PSMA-targeted theranostic nanoplex for prostate cancer therapy. ACS Nano 2012;6(9):7752–7762.

60. Mlcochova P, Barinka C, Tykvart J, Sacha P, Konvalinka J. Prostate-specific membrane antigen and its truncated form PSM'. Prostate 2009;69(5):471–479.

61. Elsasser-Beile U, Wolf P, Gierschner D, Buhler P, Schultze-Seemann W, Wetterauer U. A new generation of monoclonal and recombinant antibodies against cell-adherent prostate specific membrane antigen for diagnostic and therapeutic targeting of prostate cancer. Prostate 2006;66(13):1359–1370.

62. Schulke N, Varlamova OA, Donovan GP, Ma D, Gardner JP, Morrissey DM, Arrigale RR, Zhan C, Chodera AJ, Surowitz KG, Maddon PJ, Heston WD, Olson WC. The homodimer of prostate-

specific membrane antigen is a functional target for cancer therapy. Proc Natl Acad Sci U S A 2003;100(22):12590–12595.

63. Ma D, Hopf CE, Malewicz AD, Donovan GP, Senter PD, Goeckeler WF, Maddon PJ, Olson WC. Potent antitumor activity of an auristatin-conjugated, fully human monoclonal antibody to prostate-specific membrane antigen. Clin Cancer Res 2006; 12(8):2591–2596.
64. Tykvart J, Sacha P, Barinka C, Knedlik T, Starkova J, Lubkowski J, Konvalinka J. Efficient and versatile one-step affinity purification of in vivo biotinylated proteins: Expression, characterization and structure analysis of recombinant human glutamate carboxypeptidase II. Protein Expr Purif 2012;82(1):106–115.
65. Hegnerova K, Bockova M, Vaisocherova H, Kristofikova Z, Ricny J, Ripova D, Homola J. Surface plasmon resonance biosensors for detection of Alzheimer disease biomarker. Sensor Actuat B-Chem 2009;139(1):69–73.
66. Pimkova K, Bockova M, Hegnerova K, Suttnar J, Cermak J, Homola J, Dyr JE. Surface plasmon resonance biosensor for the detection of VEGFR-1–a protein marker of myelodysplastic syndromes. Anal Bioanal Chem 2012;402(1):381–387.
67. Barinka C, Rinnova M, Sacha P, Rojas C, Majer P, Slusher BS, Konvalinka J. Substrate specificity, inhibition and enzymological analysis of recombinant human glutamate carboxypeptidase II. J Neurochem 2002;80(3):477–487.
68. Liu N, Liang W, Ma X, Li X, Ning B, Cheng C, Ou G, Wang B, Zhang J, Gao Z. Simultaneous and combined detection of multiple tumor biomarkers for prostate cancer in human serum by suspension array technology. Biosens Bioelectron 2013;47:92–98.
69. Conway RE, Petrovic N, Li Z, Heston W, Wu D, Shapiro LH. Prostate-specific membrane antigen regulates angiogenesis by modulating integrin signal transduction. Mol Cell Biol 2006; 26(14):5310–5324.

SUPPORTING INFORMATION

Additional Supporting Information may be found in the online version of this article at the publisher's web-site

internalization of prostate-specific membrane antigen. Cancer Res 1998;58(18):4055–4060.

7. Javier DJ, Nitin N, Levy M, Ellington A, Richards-Kortum R. Aptamer-targeted gold nanoparticles as molecular-specific contrast agents for reflectance imaging. Bioconjug Chem 2008;19(6):1309–1312.
8. Kasten BB, Liu T, Nedrow-Byers JR, Benny PD, Berkman CE. Targeting prostate cancer cells with PSMA inhibitor-guided gold nanoparticles. Bioorg Med Chem Lett 2013;23(2):565–568.
9. Schol D, Fleron M, Greisch JF, Jaeger M, Frenz M, De Pauw E, De Pauw-Gillet MC. Anti-PSMA antibody-coupled gold nanorods detection by optical and electron microscopies. Micron 2013;50:68–74.
10. Wang L, Li L, Guo Y, Tong H, Fan X, Ding J, Huang H. Construction and in vitro/in vivo targeting of PSMA-targeted nanoscale microbubbles in prostate cancer. Prostate 2013;73(11): 1147–1158.
11. Xu W, Siddiqui IA, Nihal M, Pilla S, Rosenthal K, Mukhtar H, Gong S. Aptamer-conjugated and doxorubicin-loaded unimolecular micelles for targeted therapy of prostate cancer. Biomaterials 2013;34(21):5244–5253.
12. Osborne JR, Akhtar NH, Vallabhajosula S, Anand A, Deh K, Tagawa ST. Prostate-specific membrane antigen-based imaging. Urol Oncol 2013;31(2):144–154.
13. Vacchelli E, Aranda F, Eggermont A, Galon J, Sautes-Fridman C, Zitvogel L, Kroemer G, Galluzzi L. Trial watch: Tumor-targeting monoclonal antibodies in cancer therapy. Oncoimmunology 2014;3(1):e27048.
14. Vacchelli E, Vitale I, Tartour E, Eggermont A, Sautes-Fridman C, Galon J, Zitvogel L, Kroemer G, Galluzzi L. Trial watch: Anticancer radioimmunotherapy. Oncoimmunology 2013;2(9):e25595.
15. Vacchelli E, Eggermont A, Galon J, Sautes-Fridman C, Zitvogel L, Kroemer G, Galluzzi L. Trial watch: Monoclonal antibodies in cancer therapy. Oncoimmunology 2013;2(1):e22789.
16. Al-Ahmadie HA, Olgac S, Gregor PD, Tickoo SK, Fine SW, Kondagunta GV, Scher HI, Morris MJ, Russo P, Motzer RJ, Reuter VE. Expression of prostate-specific membrane antigen in renal cortical tumors. Mod Pathol 2008;21(6):727–732.
17. Baccala A, Sercia L, Li J, Heston W, Zhou M. Expression of prostate-specific membrane antigen in tumor-associated neovasculature of renal neoplasms. Urology 2007;70(2):385–390.
18. Chang SS, Reuter VE, Heston WD, Bander NH, Grauer LS, Gaudin PB. Five different anti-prostate-specific membrane antigen (PSMA) antibodies confirm PSMA expression in tumor-associated neovasculature. Cancer Res 1999;59(13):3192–3198.
19. Lopes AD, Davis WL, Rosenstraus MJ, Uveges AJ, Gilman SC. Immunohistochemical and pharmacokinetic characterization of the site-specific immunoconjugate CYT-356 derived from antiprostate monoclonal antibody 7E11-C5. Cancer Res 1990;50(19):6423–6429.
20. Kinoshita Y, Kuratsukuri K, Landas S, Imaida K, Rovito PM Jr, Wang CY, Haas GP. Expression of prostate-specific membrane antigen in normal and malignant human tissues. World J Surg 2006;30(4):628–636.
21. Mhawech-Fauceglia P, Zhang S, Terracciano L, Sauter G, Chadhuri A, Herrmann FR, Penetrante R. Prostate-specific membrane antigen (PSMA) protein expression in normal and neoplastic tissues and its sensitivity and specificity in prostate adenocarcinoma: An immunohistochemical study using mutiple tumour tissue microarray technique. Histopathology 2007;50(4): 472–483.
22. Haffner MC, Kronberger IE, Ross JS, Sheehan CE, Zitt M, Muhlmann G, Ofner D, Zelger B, Ensinger C, Yang XJ, Geley S, Margreiter R, Bander NH. Prostate-specific membrane antigen expression in the neovasculature of gastric and colorectal cancers. Hum Pathol 2009;40(12):1754–1761.
23. Rovenska M, Hlouchova K, Sacha P, Mlcochova P, Horak V, Zamecnik J, Barinka C, Konvalinka J. Tissue expression and enzymologic characterization of human prostate specific membrane antigen and its rat and pig orthologs. Prostate 2008; 68(2): 171–182.
24. Troyer JK, Beckett ML, Wright GL Jr. Detection and characterization of the prostate-specific membrane antigen (PSMA) in tissue extracts and body fluids. Int J Cancer 1995;62(5):552–558.
25. Sokoloff RL, Norton KC, Gasior CL, Marker KM, Grauer LS. A dual-monoclonal sandwich assay for prostate-specific membrane antigen: Levels in tissues, seminal fluid and urine. Prostate 2000;43(2):150–157.
26. Ellis RJ, Kaminsky DA, Zhou EH, Fu P, Chen WD, Brelin A, Faulhaber PF, Bodner D. Ten-year outcomes: The clinical utility of single photon emission computed tomography/computed tomography capromab pendetide (Prostascint) in a cohort diagnosed with localized prostate cancer. Int J Radiat Oncol Biol Phys 2011;81(1):29–34.
27. Han M, Partin AW. Current clinical applications of the in-capromab pendetide scan (prostascint(r) scan, cyt-356). Rev Urol 2001;3(4):165–171.
28. Hinkle GH, Burgers JK, Neal CE, Texter JH, Kahn D, Williams RD, Maguire R, Rogers B, Olsen JO, Badalament RA. Multicenter radioimmunoscintigraphic evaluation of patients with prostate carcinoma using indium-111 capromab pendetide. Cancer 1998; 83(4):739–747.
29. Horoszewicz JS, Kawinski E, Murphy GP. Monoclonal antibodies to a new antigenic marker in epithelial prostatic cells and serum of prostatic cancer patients. Anticancer Res 1987;7(5B):927–935.
30. Troyer JK, Feng Q, Beckett ML, Wright GL Jr. Biochemical characterization and mapping of the 7E11-C5. 3 epitope of the prostate-specific membrane antigen. Urol Oncol 1995;1(1):29–37.
31. Tagawa ST, Milowsky MI, Morris M, Vallabhajosula S, Christos P, Akhtar NH, Osborne J, Goldsmith SJ, Larson S, Taskar NP, Scher HI, Bander NH, Nanus DM. Phase II study of Lutetium-177-labeled anti-prostate-specific membrane antigen monoclonal antibody J591 for metastatic castration-resistant prostate cancer. Clin Cancer Res 2013;19(18):5182–5191.
32. Tagawa ST, Akhtar NH, Nikolopoulou A, Kaur G, Robinson B, Kahn R, Vallabhajosula S, Goldsmith SJ, Nanus DM, Bander NH. Bone marrow recovery and subsequent chemotherapy following radiolabeled anti-prostate-specific membrane antigen monoclonal antibody j591 in men with metastatic castration-resistant prostate cancer. Front Oncol 2013;3:214.
33. Holland JP, Divilov V, Bander NH, Smith-Jones PM, Larson SM, Lewis JS. 89Zr-DFO-J591 for immunoPET of prostate-specific membrane antigen expression in vivo. J Nucl Med 2010;51(8): 1293–1300.
34. Moffatt S, Papasakelariou C, Wiehle S, Cristiano R. Successful in vivo tumor targeting of prostate-specific membrane antigen with a highly efficient J591/PEI/DNA molecular conjugate. Gene Ther 2006;13(9):761–772.
35. Patri AK, Myc A, Beals J, Thomas TP, Bander NH, Baker JR Jr. Synthesis and in vitro testing of J591 antibody-dendrimer conjugates for targeted prostate cancer therapy. Bioconjug Chem 2004;15(6):1174–1181.

Příloha 2

GDCh Communications Angewandte International Edition Chemie

Antibody Mimetics

International Edition: DOI: 10.1002/anie.201508642
German Edition: DOI: 10.1002/ange.201508642

iBodies: Modular Synthetic Antibody Mimetics Based on Hydrophilic Polymers Decorated with Functional Moieties

Pavel Šácha[+], Tomáš Knedlík[+], Jiří Schimer, Jan Tykvart, Jan Parolek, Václav Navrátil, Petra Dvořáková, František Sedlák, Karel Ulbrich, Jiří Strohalm, Pavel Majer, Vladimír Šubr, and Jan Konvalinka**

Abstract: *Antibodies are indispensable tools for biomedicine and anticancer therapy. Nevertheless, their use is compromised by high production costs, limited stability, and difficulty of chemical modification. The design and preparation of synthetic polymer conjugates capable of replacing antibodies in biomedical applications such as ELISA, flow cytometry, immunocytochemistry, and immunoprecipitation is reported. The conjugates, named "iBodies", consist of an HPMA copolymer decorated with low-molecular-weight compounds that function as targeting ligands, affinity anchors, and imaging probes. We prepared specific conjugates targeting several proteins with known ligands and used these iBodies for enzyme inhibition, protein isolation, immobilization, quantification, and live-cell imaging. Our data indicate that this highly modular and versatile polymer system can be used to produce inexpensive and stable antibody substitutes directed toward virtually any protein of interest with a known ligand.*

The discovery of antibodies specifically targeting biologically relevant molecules revolutionized the life sciences. Nevertheless, the use of antibodies has several disadvantages, such as limited stability, difficulty of chemical modification, and difficulty targeting proteins in mouse models. To address these limitations, researchers have developed alternative molecular recognition tools capable of replacing antibodies in biomedical research applications (antibody mimetics). These include affibodies,[1] designed ankyrin repeat proteins (DARPins),[2] and aptamers.[3] Recently, chemically synthesized small molecules that fulfill some functions of antibodies have been described.[4] Polymers capable of molecular recognition of other molecules were described several decades ago. These molecularly imprinted polymers (MIPs) are based on structure complementarity with the target molecules and are used as molecular biosensors and binders.[5]

We set out to develop novel antibody mimetics based on *N*-(2-hydroxypropyl)methacrylamide (HPMA) copolymer conjugates decorated with three different low-molecular-weight ligands. We chose water-soluble and biocompatible HPMA copolymers since they have been used for the development of drug delivery vectors, imaging agents, and polymer drugs.[6] The HPMA copolymers are multivalent synthetic macromolecules that carry a number of reactive groups that enable covalent attachment of various ligands such as fluorescent probes, therapeutics, proteins, and oligonucleotides.[7]

Specific recognition, immobilization, and imaging of a protein of interest require a specific targeting ligand (e.g., an inhibitor), an affinity anchor, and an imaging probe attached to the polymer backbone (Figure 1a). As an affinity tag, we chose biotin because it can be readily used for high-affinity immobilization on a variety of commercially available resins (Figure 1b). As an imaging probe, we chose the fluorophore ATTO488 (Figure 1c). The choice of targeting ligand depends on the protein of interest; we developed and tested these antibody mimetics with glutamate carboxypeptidase II, HIV-1 protease, pepsin, and His-tagged proteins (Figure 1d–g). To reflect functional similarity to antibodies and the use of inhibitors as targeting ligands, we propose the name iBodies for these polymer conjugates. All prepared iBodies were characterized in terms of chemical identity and the content of individual ligands, and their characteristics are summarized in Table 1 and Table S2 in the Supporting Information. We assume statistical distribution of the attached moieties, since each ligand terminates with the same sterically unhindered reactive moiety ($-CH_2CH_2NH_2$). The synthesis and characteristics of the conjugates are described in detail in the Supporting Information.

For developing the technique, we chose human glutamate carboxypeptidase II (GCPII; also known as prostate-specific membrane antigen or PSMA). GCPII is a transmembrane metallopeptidase that is strongly expressed in the brain and

[*] Dr. P. Šácha,[+] T. Knedlík,[+] Dr. J. Schimer, Dr. J. Tykvart, J. Parolek, V. Navrátil, P. Dvořáková, Dr. F. Sedlák, Dr. P. Majer, Dr. J. Konvalinka
Institute of Organic Chemistry and Biochemistry
Academy of Science of the Czech Republic
Flemingovo n. 2, 16610 Prague 6 (Czech Republic)
E-mail: konval@uochb.cas.cz

Prof. K. Ulbrich, Dr. J. Strohalm, Dr. V. Šubr
Institute of Macromolecular Chemistry
Academy of Science of the Czech Republic
Heyrovského n. 2, 16206 Prague 6 (Czech Republic)
E-mail: subr@imc.cas.cz

Dr. P. Šácha,[+] T. Knedlík,[+] Dr. J. Schimer, Dr. J. Tykvart, J. Parolek, V. Navrátil, Dr. J. Konvalinka
Department of Biochemistry, Faculty of Science, Charles University
Hlavova 8, 12843 Prague 2 (Czech Republic)

Dr. F. Sedlák
First Faculty of Medicine, Charles University
Kateřinská 32, 12108 Prague 2 (Czech Republic)

[+] These authors contributed equally to this work.

Supporting information for this article is available on the WWW under http://dx.doi.org/10.1002/anie.201508642.

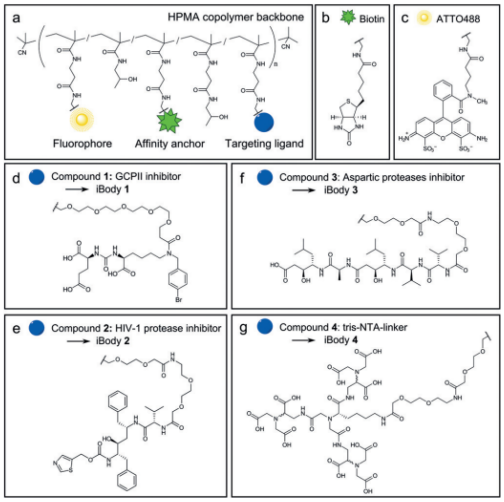

Figure 1. Structures of the iBodies and their functional modules. a) HPMA copolymer decorated with functional molecules. b) The affinity anchor biotin. c) ATTO488 fluorophore. d) GCPII inhibitor. e) HIV-1 protease inhibitor. f) A class-specific inhibitor of aspartic proteases. g) A nitrilotriacetic acid (NTA)-based ligand for binding the His-tag.

Table 1: The composition and basic characteristics of the iBodies.

Conjugate (M_n)	Target	No. of inhibitor moieties	No. of ATTO488 units	No. of biotin units	K_i [nM]
iBody **1** (148 800)[a]	GCPII	19	7	51	0.0043 ± 0.0005
iBody **2** (40 600)[a]	HIV-1 protease	6	–	7	7.9 ± 0.5
iBody **3** (42 100)[a]	Aspartic proteases	7	–	9	18.9 ± 0.2[b]
iBody **4** (135 800)[a]	His-tag sequence	12	7	46	3.5 ± 0.1[c]
iBody **5** (108 100)[a]	–	–	6	41	–
iBody **6** (37 800)[a]	–	–	–	8	–

[a] M_n = number-average molecular weight. For full molecular characteristics of the conjugates, see Table S2–S4 and Figure S8 in Supporting Information. [b] K_i value was determined for wild-type HIV-1 protease. [c] For iBody **4**, a dissociation constant K_D is shown instead of an inhibition constant K_i.

prostate; its expression is markedly increased in prostate carcinoma.[8]

The polymer conjugate targeting GCPII (iBody **1**, Figure S1 in the Supporting Information) contains a tight-binding GCPII inhibitor as a targeting ligand. To avoid steric hindrance between GCPII and the polymer molecules, the previously described inhibitor (called compound **22a**,[9] Table S1) was modified with a PEG_5 linker to yield compound **1** (Figure 1d). As a negative control, we prepared the corresponding conjugate lacking the GCPII inhibitor (iBody **5**; Figure S2).

The utility of iBody **1** for the inhibition, binding, and visualization of GCPII was tested with a variety of common biochemical methods in which antibodies are normally used: immunoprecipitation and affinity pull-downs, flow cytometry, immunocytochemistry, and ELISA.

First, we tested whether iBody **1** inhibits the enzymatic activity of GCPII and determined K_i values for compound **1** and iBody **1** (Figure 2a). Interestingly, attachment of several molecules of compound **1** to the HPMA copolymer led to a significant drop in the K_i value [K_i(compound **1**) = 2.0 nM vs. K_i(iBody **1**) = 4.3 pM]. This nearly three-order-of-magnitude decrease in K_i can be explained by the synergic effect of several inhibitor molecules on the polymer scaffold and increased local inhibitor concentration (19 inhibitor molecules per polymer chain).

The binding of iBody **1** to GCPII was further evaluated by surface plasmon resonance (SPR), which revealed an extremely high association rate and a low dissociation rate (Figure 2b). The dissociation constant ($K_D < 20$ pM) is comparable to that of the tightest-binding anti-GCPII antibodies available.

To analyze the utility of iBody **1** for visualizing GCPII-expressing cells, we incubated LNCaP cells (a cell line that endogenously expresses GCPII) and PC3 cells (which do not express GCPII) with iBody **1**. As controls, we used iBody **5** (which lacks a GCPII inhibitor) and a fluorescently labeled anti-GCPII monoclonal antibody 2G7[10] (mAb 2G7-ATTO488). iBody **1** and the anti-GCPII mAb bound specifically to LNCaP cells and not to PC3 cells, while iBody **5** did not bind to either LNCaP or PC3 cells. iBody **1** and the mAb were taken up into the cells through internalization of membrane-embedded GCPII as expected.[11] Additionally, binding of iBody **1** to LNCaP cells was blocked by 2-(phosphonomethyl)pentanedioic acid (2-PMPA), a specific GCPII inhibitor (Figure 2c).

To analyze the potential use of iBodies in flow cytometry, LNCaP and PC3 cells were first incubated with iBody **1**, iBody **5**, or 2G7-ATTO488[10] and then analyzed by flow cytometry. The results indicate that both iBody **1** and the anti-GCPII mAb specifically recognize GCPII-expressing cells (LNCaP) and enable their separation from GCPII-negative cells (PC3). Moreover, iBody **1** and iBody **5** exhibited very low non-specific binding to PC3 cells, which was approximately 5-fold lower than that of mAb 2G7-ATTO488 (Figure 2d).

Furthermore, we used iBody **1** to isolate GCPII from cell lysates. iBodies **1** and **5** were immobilized on Streptavidin Sepharose resin, and GCPII was pulled down from LNCaP cell lysate (Figure 2e). An anti-GCPII mAb (J591[12]) bound to Protein G Sepharose was used as a positive control. As shown by subsequent western blot analysis, the amount of GCPII immunoprecipitated when using iBody **1** was comparable to that obtained with mAb J591. These findings suggest that iBodies could also be useful for the isolation of target proteins from complex biological materials such as tissue lysates or blood samples.

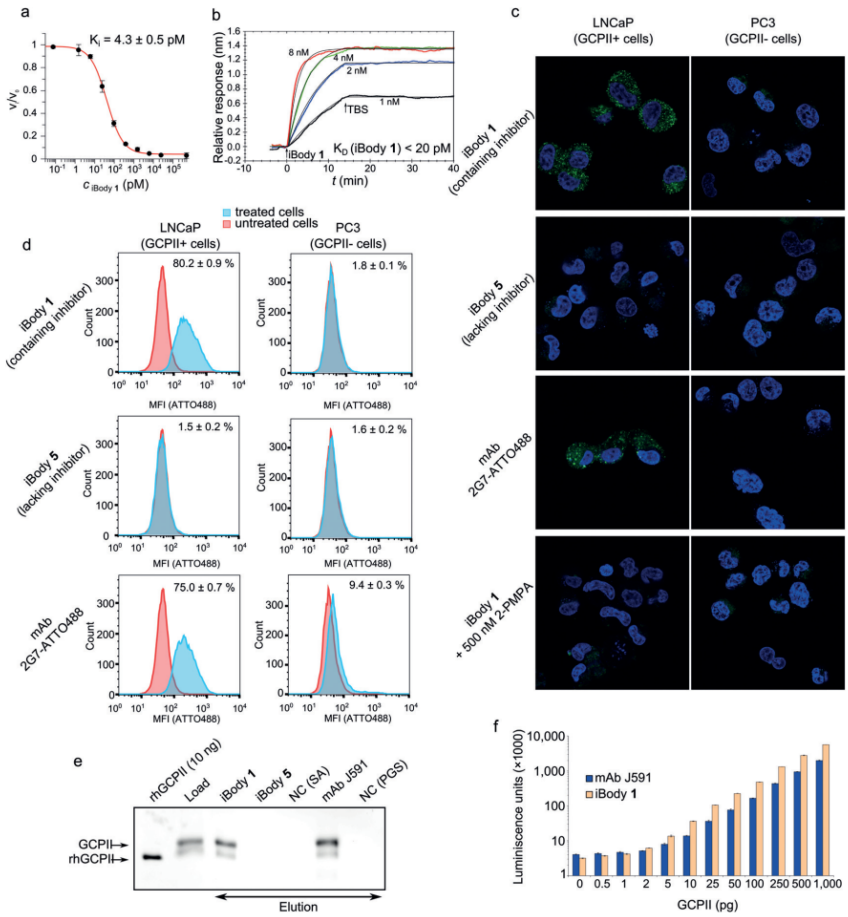

Figure 2. Application of iBody **1**, which targets glutamate carboxypeptidase II (GCPII). a) The inhibition potency of iBody **1** in terms of GCPII hydrolytic activity. b) SPR analysis of iBody **1** binding to immobilized GCPII ($K_D < 20$ pM). c) Confocal microscopy of cells positive (LNCaP) and negative (PC3) for GCPII expression. Cells were stained with iBody **1**; to compare iBody staining with antibody staining, the anti-GCPII monoclonal antibody (mAb) 2G7[10] labeled with ATTO488 (2G7-ATTO488) was used. Binding of iBody **1** to LNCaP cells can be blocked by using 2-PMPA, a specific GCPII inhibitor. d) Flow cytometry analysis of LNCaP and PC3 cells incubated with iBody **1**, iBody **5** (which lacks the targeting module), or 2G7-ATTO488. e) Western blot analysis of affinity isolation of GCPII from LNCaP cell lysate using iBody **1** or the anti-GCPII mAb J591. iBody **5**, blank Streptavidin Agarose (NC (SA)), and blank Protein G Sepharose (NC (PGS)) were used as negative controls. rhGCPII is a recombinant extracellular GCPII. Load = LNCaP cell lysate. f) Sandwich ELISA with the anti-GCPII capture mAb 2G7 and either the biotinylated anti-GCPII mAb J591 or iBody **1** used as the detecting agent.

Finally, we used iBodies for the quantitative detection of GCPII. We employed a sandwich ELISA in which the detecting anti-GCPII mAb was replaced with iBody **1**. The detection limit was as low as 0.5 pg GCPII; furthermore, the signal was linear over a nearly three-order-of-magnitude concentration range (Figure 2 f).

To demonstrate versatility of iBodies, we also developed iBodies targeting the aspartic proteases HIV-1 and pepsin. HIV-1 protease plays a crucial role in viral replication[13] and a number of specific inhibitors are available. As aspartic proteases, both HIV-1 protease and pepsin are also efficiently inhibited by the peptidic inhibitor pepstatin A.[14]

The polymer conjugate targeted towards HIV-1 protease (iBody **2**; Figure S3) contains compound **2**, a specific HIV-1 protease inhibitor derived from the commercially available inhibitor ritonavir (Figure 1 e), as a targeting ligand. The analogous iBody **3** (Figure S4) contains compound **3** (Figure 1 f), a derivative of the class-specific aspartic protease inhibitor pepstatin A, as a targeting ligand. As a negative control, we prepared the corresponding conjugate lacking an

inhibitor (iBody **6**; Figure S5). We successfully used iBody **2** and iBody **3** to pull down HIV-1 protease from an LNCaP cell lysate spiked with HIV-1 protease (Figure S7a).

Besides HIV-1 protease, another aspartic protease, pepsin, was also successfully pulled down from LNCaP lysate (spiked with pepsin) by using iBody **3** (Figure S7b), thus showing the general applicability of this iBody. In both experiments, iBody **6** (which contains only biotin and no inhibitor) was used as a negative control. This iBody was unable to pull down either HIV-1 protease or pepsin from an LNCaP cell lysate (Figure S7a,b).

Finally, the use of iBodies is not limited to enzymes. Theoretically, iBodies can be designed to target any molecule of interest for which a ligand is known. To demonstrate this general principle, we set out to target proteins containing a polyhistidine tag (His-tag), the most common affinity tag used for protein purification and visualization. Because the His-tag is bound by nickel-loaded nitrilotriacetic acid (NTA) derivatives, we prepared tris-NTA connected to a linker[15] (compound **4**, Figure 1 g) and subsequently iBody **4** (Figure S6). iBody **4** was decorated with the fluorophore ATTO488 for visualization and biotin for both visualization and immobilization. As a negative control, iBody **5**, which bears only the fluorophore ATTO488 and biotin, was used.

We compared the sensitivity and specificity of iBody **4** with that of commercially available peroxidase-conjugated anti-polyhistidine antibody by western blot. iBody **4** exhibited slightly increased sensitivity and equal specificity in comparison to the commercial antibody (Figure 3 a, b). When using iBody **4**, we detected as little as 100 pg of the His-tagged DNA damage protein 1 (Ddi1-His). Additionally, we specifically pulled down the protein from an *E. coli* lysate (Figure 3 c). To quantify the binding, we analyzed the interaction between iBody **4** and Ddi1-His by SPR, which indicated K_D = 3.5 nM (Figure 3 d).

Our approach has two major advantages. First, the system is remarkably modular: any compound, functional group, or tag for any specific purpose can be added to form the final polymer conjugate. For the targeting of a specific protein with an iBody, simple replacement of the targeting moiety (the inhibitor) is sufficient to yield a new specific polymer conjugate. To some extent, this resembles the concept of molecularly imprinted polymers (MIPs). MIPs rely on lock-and-key interaction with the target, which makes them more suitable for the extraction of target compounds/proteins, even though the targeting of proteins on the cell surface has been reported.[16] Second, the system is truly versatile: a single iBody can be used for several methods, as we have shown for GCPII. One potential limitation of the system is the need for a ligand that specifically binds to the target protein. Moreover, for attachment to the polymer backbone, the ligand must be modified with a linker that does not significantly compromise its binding affinity. Nonetheless, if a potent ligand is known and the attachment of the linker does not lead to a dramatic loss of potency, the preparation of a specific iBody is rather straightforward.

In summary, we have developed inexpensive, stable, and modular synthetic conjugates called iBodies for use as antibody mimetics. The presented data demonstrate that the prepared iBodies targeting various proteins of interest are efficient substitutes for the corresponding antibodies in standard immunochemical methods. Overall, iBodies offer an inexpensive, non-animal-based alternative for antibodies in biochemical methods involving the isolation and visualization of proteins, cells, and tissues.

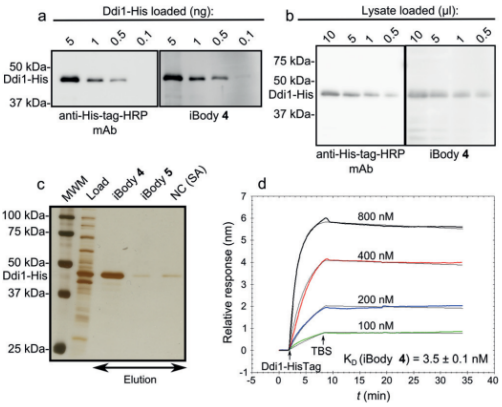

Figure 3. Application of iBody **4**, which targets His-tagged proteins. a) Comparison of iBody **4** and anti-polyhistidine antibody sensitivity for the visualization of purified Ddi1-His by western blot. b) Comparison of iBody **4** and the anti-polyhistidine antibody for the visualization of Ddi1-His in a cell lysate by western blot. c) Affinity isolation of Ddi1-His by using iBody **4**. iBody **5** (which does not possess the tris-NTA ligand), and blank resin (NC) were used as negative controls. MWM = molecular-weight marker. d) Binding of Ddi1-His to immobilized iBody **4** as analyzed by SPR.

Acknowledgements

We thank Jana Starková and Karolína Šrámková for their technical support, Marco Colombatti for the D2B antibody, Michal Svoboda for expression of Ddi1-His and Stanislava Matějková for ICP-OES analysis. This work was supported by Grant No. P208-12-G016 (Center of Excellence) from the Grant Agency of the Czech Republic and InterBioMed project LO 1302 from the Ministry of Education of the Czech Republic.

Keywords: antibody mimetics · HPMA · molecular recognition · polymer conjugates · protein targeting

How to cite: *Angew. Chem. Int. Ed.* **2016**, *55*, 2356–2360
Angew. Chem. **2016**, *128*, 2402–2406

[1] K. Nord, E. Gunneriusson, J. Ringdahl, S. Stahl, M. Uhlen, P. A. Nygren, *Nat. Biotechnol.* **1997**, *15*, 772.
[2] H. K. Binz, M. T. Stumpp, P. Forrer, P. Amstutz, A. Pluckthun, *J. Mol. Biol.* **2003**, *332*, 489.
[3] A. D. Ellington, J. W. Szostak, *Nature* **1990**, *346*, 818.
[4] P. J. McEnaney, K. J. Fitzgerald, A. X. Zhang, E. F. Douglass, Jr., W. Shan, A. Balog, M. D. Kolesnikova, D. A. Spiegel, *J. Am. Chem. Soc.* **2014**, *136*, 18034.

[5] a) Y. Hoshino, H. Koide, T. Urakami, H. Kanazawa, T. Kodama, N. Oku, K. J. Shea, *J. Am. Chem. Soc.* **2010**, *132*, 6644; b) G. Wulff, *Angew. Chem. Int. Ed. Engl.* **1995**, *34*, 1812; *Angew. Chem.* **1995**, *107*, 1958.
[6] a) R. Haag, F. Kratz, *Angew. Chem. Int. Ed.* **2006**, *45*, 1198; *Angew. Chem.* **2006**, *118*, 1218; b) J. Kopeček, P. Kopečková, *Adv. Drug Delivery Rev.* **2010**, *62*, 122.
[7] V. Šubr, L. Kostka, J. Strohalm, T. Etrych, K. Ulbrich, *Macromolecules* **2013**, *46*, 2100.
[8] a) R. G. Lapidus, C. W. Tiffany, J. T. Isaacs, B. S. Slusher, *Prostate* **2000**, *45*, 350; b) M. B. Robinson, R. D. Blakely, R. Couto, J. T. Coyle, *J. Biol. Chem.* **1987**, *262*, 14498.
[9] J. Tykvart, J. Schimer, J. Barinkova, P. Pachl, L. Postova-Slavetinska, P. Majer, J. Konvalinka, P. Sacha, *Bioorg. Med. Chem.* **2014**, *22*, 4099.
[10] T. Knedlík, V. Navratil, V. Vik, D. Pacik, P. Sacha, J. Konvalinka, *Prostate* **2014**, *74*, 768.
[11] H. Liu, A. K. Rajasekaran, P. Moy, Y. Xia, S. Kim, V. Navarro, R. Rahmati, N. H. Bander, *Cancer Res.* **1998**, *58*, 4055.
[12] H. Liu, P. Moy, S. Kim, Y. Xia, A. Rajasekaran, V. Navarro, B. Knudsen, N. H. Bander, *Cancer Res.* **1997**, *57*, 3629.
[13] H. G. Krausslich, R. H. Ingraham, M. T. Skoog, E. Wimmer, P. V. Pallai, C. A. Carter, *Proc. Natl. Acad. Sci. USA* **1989**, *86*, 807.
[14] J. Eder, U. Hommel, F. Cumin, B. Martoglio, B. Gerhartz, *Curr. Pharm. Des.* **2007**, *13*, 271.
[15] Z. Huang, P. Hwang, D. S. Watson, L. Cao, F. C. Szoka, Jr., *Bioconjugate Chem.* **2009**, *20*, 1667.
[16] a) Y. Ma, G. Q. Pan, Y. Zhang, X. Z. Guo, H. Q. Zhang, *Angew. Chem. Int. Ed.* **2013**, *52*, 1511; *Angew. Chem.* **2013**, *125*, 1551; b) S. Shinde, Z. El-Schich, A. Malakpour, W. Wan, N. Dizeyi, R. Mohammadi, K. Rurack, A. Gjorloff Wingren, B. Sellergren, *J. Am. Chem. Soc.* **2015**, *137*, 13908.

Received: September 18, 2015
Published online: January 8, 2016

Příloha 3

FEBS openbio

FEBS PRESS science publishing by scientists

Mouse glutamate carboxypeptidase II (GCPII) has a similar enzyme activity and inhibition profile but a different tissue distribution to human GCPII

Tomáš Knedlík[1,2], Barbora Vorlová[1,3], Václav Navrátil[1,2], Jan Tykvart[1,2,†], František Sedlák[1,3,4], Šimon Vaculín[5], Miloslav Franěk[5], Pavel Šácha[1] and Jan Konvalinka[1,2]

1 Institute of Organic Chemistry and Biochemistry of the Czech Academy of Sciences, Prague, Czech Republic
2 Department of Biochemistry, Faculty of Science, Charles University, Prague, Czech Republic
3 First Faculty of Medicine, Charles University, Prague, Czech Republic
4 Department of Genetics and Microbiology, Faculty of Science, Charles University, Prague, Czech Republic
5 Department of Normal, Pathological and Clinical Physiology, Third Faculty of Medicine, Charles University, Prague, Czech Republic

Keywords
glutamate carboxypeptidase II; mouse animal model; neuronal disorders; prostate cancer; prostate-specific membrane antigen

Correspondence
J. Konvalinka, Institute of Organic Chemistry and Biochemistry of the CAS, v.v.i., Flemingovo n. 2, Prague 6, 16610, Czech Republic
Fax: +420 220 183 578
Tel: +420 220 183 218
E-mail: konval@uochb.cas.cz

†Present address
Donnelly Centre for Cellular and Biomolecular Research, University of Toronto, Toronto, ON, Canada

(Received 18 April 2017, revised 23 June 2017, accepted 19 July 2017)

doi:10.1002/2211-5463.12276

Glutamate carboxypeptidase II (GCPII), also known as prostate-specific membrane antigen (PSMA) or folate hydrolase, is a metallopeptidase expressed predominantly in the human brain and prostate. GCPII expression is considerably increased in prostate carcinoma, and the enzyme also participates in glutamate excitotoxicity in the brain. Therefore, GCPII represents an important diagnostic marker of prostate cancer progression and a putative target for the treatment of both prostate cancer and neuronal disorders associated with glutamate excitotoxicity. For the development of novel therapeutics, mouse models are widely used. However, although mouse GCPII activity has been characterized, a detailed comparison of the enzymatic activity and tissue distribution of the mouse and human GCPII orthologs remains lacking. In this study, we prepared extracellular mouse GCPII and compared it with human GCPII. We found that mouse GCPII possesses lower catalytic efficiency but similar substrate specificity compared with the human protein. Using a panel of GCPII inhibitors, we discovered that inhibition constants are generally similar for mouse and human GCPII. Furthermore, we observed highest expression of GCPII protein in the mouse kidney, brain, and salivary glands. Importantly, we did not detect GCPII in the mouse prostate. Our data suggest that the differences in enzymatic activity and inhibition profile are rather small; therefore, mouse GCPII can approximate human GCPII in drug development and testing. On the other hand, significant differences in GCPII tissue expression must be taken into account when developing novel GCPII-based anticancer and therapeutic methods, including targeted anticancer drug delivery systems, and when using mice as a model organism.

Glutamate carboxypeptidase II (GCPII; EC 3.4.17.21) is a membrane metalloprotease that has been studied intensively over the past 20 years in three different scientific fields: neuroscience, prostate oncology, and dietology. In humans, GCPII is expressed predominantly in the brain [1,2], prostate [3,4], small intestine

Abbreviations
Avi-hGCPII, recombinant extracellular human GCPII; Avi-mGCPII, recombinant extracellular mouse GCPII; GCPII, glutamate carboxypeptidase II; GCPIII, glutamate carboxypeptidase III; NAAG, *N*-acetyl-L-aspartyl-L-glutamate; PSMA, prostate-specific membrane antigen.

FEBS Open Bio **7** (2017) 1362–1378

[5], and kidney [4,6]. Because GCPII plays different physiological roles in these tissues, three alternative names for the enzyme have historically been used: *N*-acetylated alpha-linked acidic dipeptidase (NAALADase) [7], prostate-specific membrane antigen (PSMA) [8], and folate hydrolase [5]. The close GCPII homolog GCPIII [9,10], recently identified as β-citryl-glutamate hydrolase [11], is also expressed in human tissues.

In the human central nervous system, GCPII hydrolyzes the most abundant peptide neurotransmitter, *N*-acetyl-L-aspartyl-L-glutamate (NAAG), into *N*-acetyl-L-aspartate and glutamate [7]. Inhibition of this proteolytic activity with selective GCPII inhibitors has been shown to be neuroprotective in experiments with mouse models [12]; NAAG activation of metabotropic glutamate type 3 receptors exerts neuroprotective effects toward glutamate-mediated excitotoxicity caused by elevated levels of glutamate released during stroke, traumatic brain injury, and other pathological conditions [13–15]. In addition to the brain, GCPII is expressed on the human jejunal brush border [5,16], where it cleaves the terminal glutamates from poly-γ-glutamylated folates, enabling their transport across the intestinal mucosa (folate absorption) [17]. On the other hand, the function of GCPII in the human prostate is unknown. GCPII is overexpressed in prostate cancer [3,18]; therefore, it has been suggested as a promising target for prostate cancer diagnosis and treatment using targeted strategies [19–21].

An appropriate animal model is necessary for the development and testing of novel therapeutics. Mice, rats, and pigs are among the most promising candidates to become such a model for GCPII research. Several years ago, our laboratory conducted a study comparing human GCPII with its porcine and rat orthologs [22]. The orthologs showed similarity in their enzymatic properties, but considerable differences in terms of their tissue distribution [22]. However, mouse GCPII was not included in the study, even though mice now are the most widely used preclinical models for GCPII-targeted research (stroke [12], traumatic brain injury [23,24], amyotrophic lateral sclerosis [25], inflammatory, and neuropathic pain [26,27], reviewed in Refs [13,28]). Therefore, a comparative analysis of mouse GCPII characterization is needed.

Mouse GCPII shares 91% amino acid similarity with human GCPII and preserves the internalization signal MXXXL, despite low similarity in the intracellular domain [29]. Mouse GCPII also possesses both NAAG-hydrolyzing and folate hydrolase activities [29]. In contrast to the expression pattern of human GCPII, mouse GCPII is expressed in largest amounts in the kidney and, surprisingly, is absent in the mouse prostate [29]. Results from studies with GCPII-knockout mice have been contradictory: some reports have described normal development to adulthood [9,30] and others have noted early embryonic death [31,32].

In the current study, we prepared and characterized recombinant mouse GCPII and compared it with its human counterpart. We put a strong focus on distribution of GCPII in mouse tissues, as this information is highly relevant for the development of novel GCPII-based anticancer and neuroprotective therapies using mouse models.

Results

Efficient one-step purification method yields purified recombinant mouse GCPII (Avi-mGCPII)

As recombinant extracellular human GCPII was shown to correctly represent the endogenous full-length GCPII [33,34], we prepared the recombinant extracellular part of mouse GCPII (Avi-mGCPII) using a *Drosophila* S2 expression system, according to the protocol previously established in our laboratory [34]. Avi-mGCPII has a TEV cleavable Avi-tag sequence attached to the N terminus of the mouse GCPII extracellular domain (amino acids 45–752), enabling fast one-step purification (Fig. 1A).

Avi-mGCPII was purified from the conditioned medium of cells stably transfected with Avi-mGCPII by affinity chromatography based on the biotin–streptavidin interaction [34], yielding 3 mg of pure protein from 1 L conditioned medium (Fig. 1B).

Mouse GCPII has lower catalytic efficiency than human GCPII

To characterize the enzyme activity of Avi-mGCPII, we determined kinetic parameters (K_M and k_{cat}) for cleavage of both substrates: *N*-acetyl-L-aspartyl-L-glutamate (NAAG) and pteroyl-di-L-glutamate (Table 1). The data revealed that the catalytic efficiency of Avi-mGCPII is lower than that of its human counterpart. The enzymes had similar turnover numbers but differed in their K_M values. The differences were more pronounced for pteroyl-di-L-glutamate than for NAAG. Surprisingly, both enzymes had higher catalytic efficiencies for cleavage of pteroyl-di-L-glutamate than for NAAG (Table 1).

Furthermore, to analyze the inhibition profile of Avi-mGCPII, we determined K_i values for several commonly used GCPII inhibitors (using pteroyl-di-L-glutamate as a substrate). The set of GCPII inhibitors included 2-(phosphonomethyl)pentanedioic acid

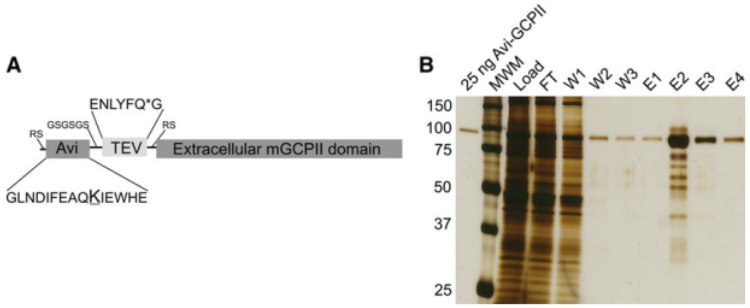

Fig. 1. Schematic structure of Avi-mGCPII and affinity purification. (A) Schematic structure of Avi-mGCPII containing an Avi sequence (the biotinylated lysine residue is enlarged and underlined) and TEV protease cleavage sequence (the cleavage site is marked with an asterisk). (B) Silver-stained SDS/PAGE gel showing affinity purification of Avi-mGCPII expressed in *Drosophila* S2 cells. MWM, molecular weight marker; load, concentrated S2 cell medium; FT, flow-through; W1–W3, wash fractions; E1–E4, elution fractions. Ten microliter samples was loaded onto the gel, except for the E2 fraction (1 μL was loaded).

Table 1. Kinetic parameters of recombinant mouse and human GCPII (Avi-mGCPII and Avi-hGCPII, respectively) for their substrates. Kinetic parameters (K_M and k_{cat}) of *N*-acetyl-L-aspartyl-L-glutamate (NAAG) and pteroyl-di-L-glutamate cleavage were determined using radioenzymatic [34] and HPLC assays [39], respectively. The values shown are mean ± standard deviation of duplicate measurements.

	NAAG			Pteroyl-di-L-glutamate		
Enzymes	K_M [nM]	k_{cat} [s^{-1}]	k_{cat}/K_M [× 10^7 s^{-1} M]	K_M [nM]	k_{cat} [s^{-1}]	k_{cat}/K_M [× 10^7 s^{-1} M]
Avi-mGCPII	1900 ± 100	1.44 ± 0.02	0.077 ± 0.001	290 ± 20	3.63 ± 0.09	1.26 ± 0.08
Avi-hGCPII	550 ± 60	1.45 ± 0.04	0.265 ± 0.007	39 ± 2	5.09 ± 0.09	13.2 ± 0.8

(2-PMPA) [35], (S)-2-(3-((S)-1-carboxy-3-methylbutyl) ureido)pentanedioic acid (ZJ-43) [36], (*S*)-2-(3-((*S*)-1-carboxy-(4-iodobenzamido)pentyl)ureido)pentanedioic acid (DCIBzL) [37], quisqualate, DKFZ-PSMA-11 [38], and beta-citryl-L-glutamate (Table 2). We also tested three compounds recently prepared in our laboratory: JB-352 and JB-277 (originally reported as compounds **3** and **22a** [39]) and JS-686 (originally compound **7** [40]).

Mouse and human GCPII exhibit similar substrate specificities

To obtain information about the substrate specificity of Avi-mGCPII, we screened 19 different dipeptide libraries of the general formula *N*-Ac-A-X [where A represents a given single N-terminal amino acid and X represents a mixture of 19 proteinogenic amino acids (all except for cysteine)]. The *N*-acetylated dipeptide libraries were incubated with the enzymes, and the cleaved amino acids were analyzed by HPLC [41]. As a negative control, the potent and selective GCPII inhibitor 2-PMPA was used to block the specific enzyme activity.

Overall, we found no significant differences in hydrolysis of dipeptide substrates between mouse and human GCPII, as illustrated by heat maps showing mouse and human GCPII processing of individual *N*-acetylated dipeptides (Fig. 2). The enzymes exhibited a clear preference for glutamate in the C-terminal position (i.e., glutamate carboxypeptidase activity); mouse GCPII possesses higher selectivity toward the C-terminal glutamate.

GCPII is highly expressed in mouse kidney, brain, and major salivary glands

To analyze GCPII distribution in mouse tissues, we collected tissues samples from six mice (three females and three males) and analyzed them by western blot using the anti-GCPII antibody GCP-04 [2,42].

Mouse GCPII was expressed predominantly in the mouse kidney and brain (Fig. 3), which is in agreement with previous data [9]. Interestingly, we observed high and variable expression in the mouse major salivary glands. The different apparent molecular weights are likely caused by different glycosylation of GCPII in the tissues.

We also determined the NAAG-hydrolyzing activity in the tissue lysate samples using tritium-labeled NAAG as a substrate and compared these results with

Table 2. Inhibition of recombinant mouse and human GCPII (Avi-mGCPII and Avi-hGCPII, respectively) by a panel of GCPII inhibitors. Inhibition constants (K_i values) were determined using an HPLC-based assay using pteroyl-di-L-glutamate as a substrate. The values shown are mean ± standard deviation of duplicate measurements.

Compound		K_i (Avi-mGCPII) (nM)	K_i (Avi-hGCPII) (nM)
Quisqualate	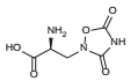	580 ± 60	520 ± 80
2-PMPA	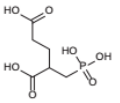	0.56 ± 0.05	0.26 ± 0.03
ZJ-43	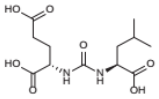	5.9 ± 0.9	0.58 ± 0.07
JB-352	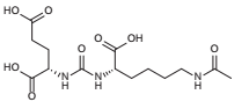	0.66 ± 0.06	0.17 ± 0.04
β-citryl-L-glutamate	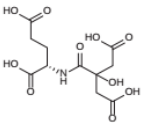	24 000 ± 3000	16 000 ± 5000
DCIBzL	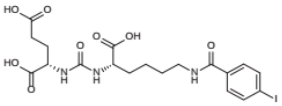	0.028 ± 0.003	0.017 ± 0.002
JB-277	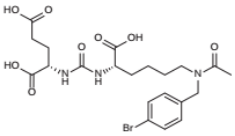	0.68 ± 0.07	0.05 ± 0.02
DKFZ-PSMA-11	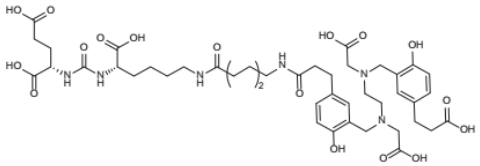	0.10 ± 0.01	0.018 ± 0.002
JS-686	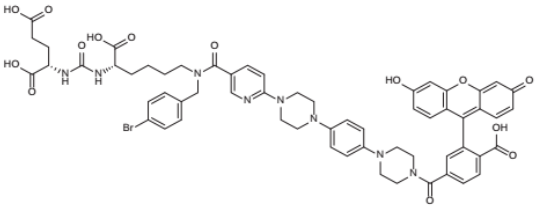	0.049 ± 0.005	0.021 ± 0.004

the data obtained by western blot analysis. Recombinant mouse GCPII was used as a standard, and the observed levels of NAAG-hydrolyzing activity were converted to amounts of GCPII, which were then normalized to the total protein concentrations in the homogenates (Fig. 4).

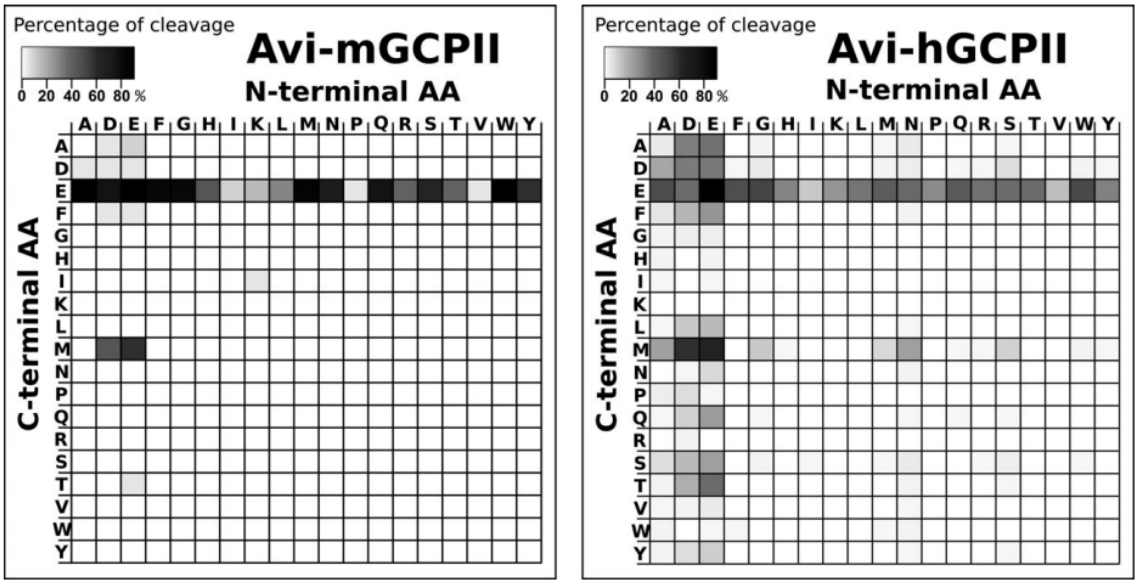

Fig. 2. Heat maps representing the substrate specificities of mouse and human GCPII. Recombinant mouse and human GCPII (Avi-mGCPII and Avi-hGCPII, respectively) were incubated with 19 dipeptide libraries of the general formula *N*-Ac-A-X-OH [where A represents a given single N-terminal amino acid and X represents a mixture of 19 proteinogenic amino acids (all except for cysteine)]. The samples were incubated for 1.5 h at 37 °C, and the cleaved C-terminal amino acids were quantified using HPLC. As negative controls, experiments either with the GCPII-specific inhibitor 2-PMPA or without Avi-mGCPII/Avi-hGCPII were performed. The grayscale key represents the percentage of conversion of the particular amino acid in the reaction mixture.

The results confirmed high expression of GCPII in the kidney, brain, and major salivary glands. We did not detect GCPII in the mouse prostate (Fig. 4).

To further examine the location of GCPII in the highly expressing tissues, we performed immunohistochemistry using the anti-GCPII antibody GCP-04 [2,42]. We found relatively high expression in the white matter in the brain, on luminal side of proximal tubules in the kidney and in the abluminal cells in the major salivary glands (mainly in the sublingual gland) (Fig. 5).

mRNA expression profile differentiates GCPII and GCPIII expression levels in mouse tissues

The GCP-04 antibody cross-reacts with GCPIII, which also cleaves NAAG [11,43]. Therefore, we decided to further analyze the tissue distribution of both homologs by quantitative RNA determination (qPCR). For these analyses, we used either commercially available panels of mouse tissue cDNA libraries (Fig. 6A) or cDNA libraries prepared from mouse tissues (female 1 and male 1; Fig. 6B,C).

The results from commercial cDNA libraries represent the average tissue distribution of both transcripts in the mouse population. Each library was pooled from several hundred mice and normalized by the vendor to several different housekeeping genes (beta-actin, G3PDH, phospholipase A2, and ribosomal protein S29). The highest expression of mouse GCPII mRNA was in the kidney, brain, and testis, while mouse GCPIII mRNA was predominantly expressed in the testis, heart, lung, and skeletal muscle (Fig. 6A).

To gain insight into expression of both transcripts in individual mice, we also quantified mRNA transcripts in cDNA libraries prepared from mouse tissues dissected from one female and one male mouse. The results were normalized to the starting amount of total RNA and are in good agreement with findings from the pooled libraries (Fig. 6B,C).

Discussion

GCPII is a potential pharmaceutical target for a number of pathological conditions caused by glutamate excitotoxicity in the central nervous system, including stroke and traumatic brain injury. Moreover, GCPII has been intensively studied as a target for diagnosis and treatment of prostate cancer, as it is overexpressed in the malignant prostate. In last two decades, a large

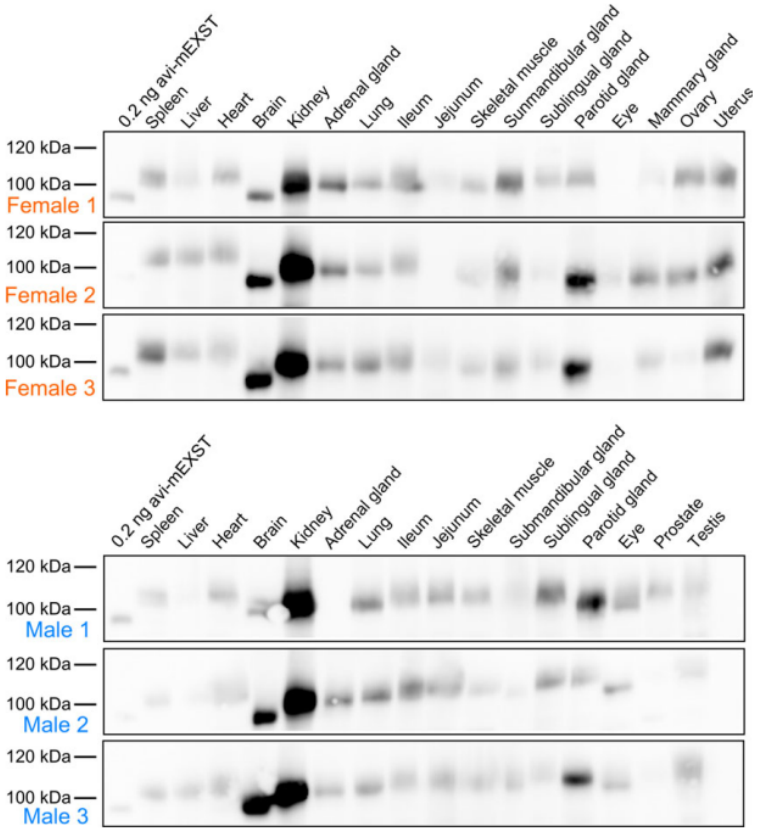

Fig. 3. Western blot analysis of GCPII expression in a panel of mouse tissues. Mouse tissue samples (from three males and three females) were homogenized, and lysates were resolved by SDS/PAGE (50 μg of total protein per lane). Mouse GCPII was visualized using the anti-GCPII primary antibody GCP-04 [2] and HRP-conjugated goat anti-mouse secondary antibody.

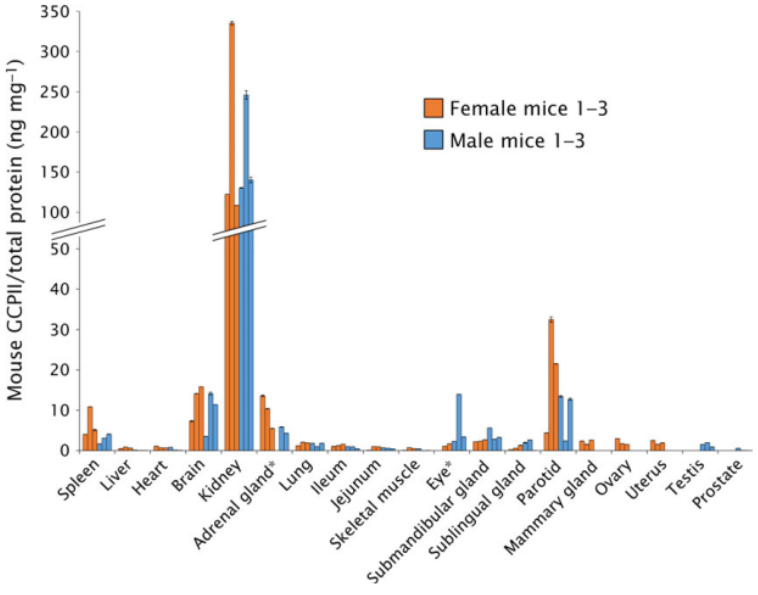

Fig. 4. GCPII expression in mouse tissues determined by radioenzymatic assay. The amount of GCPII in mouse tissues was determined by radioenzymatic assay using [^{3}H]NAAG as a substrate and recombinant mouse GCPII (Avi-mGCPII) as a standard. Each tissue sample was measured in duplicate using 1–50 μg total protein in the reaction; the amount of mouse GCPII was normalized to total protein concentration (ng GCPII per mg total protein). The assay was performed with the same tissue samples used in the western blot analysis. *Not determined (adrenal gland: sample M1; eye: sample F1).

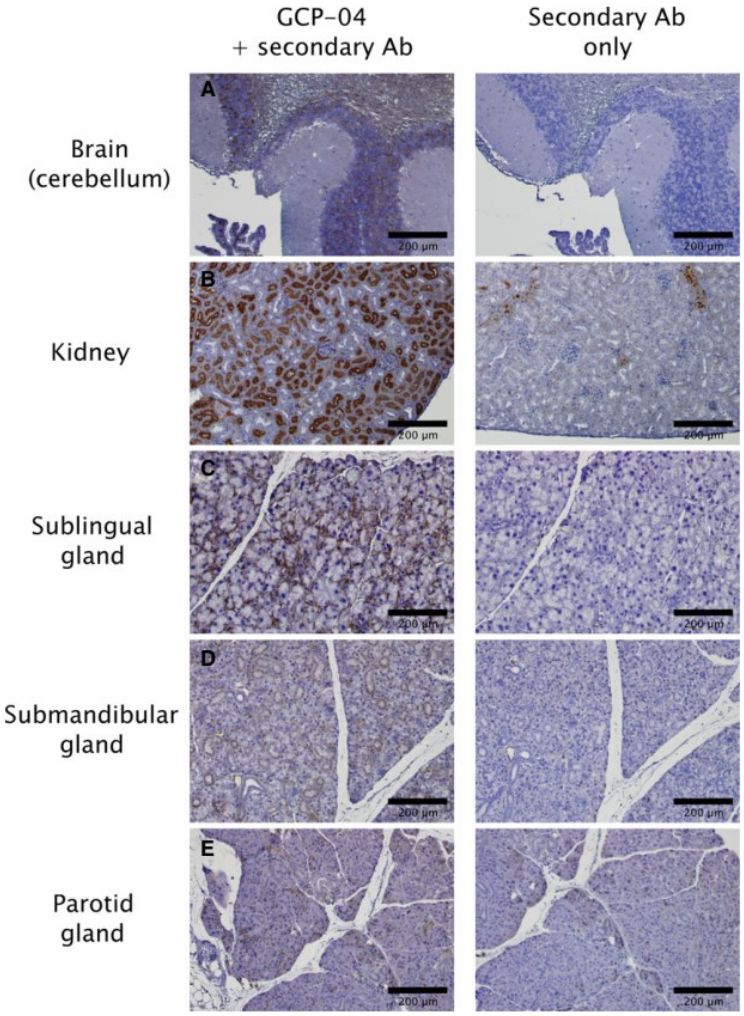

Fig. 5. Immunohistochemical staining of chosen mouse tissue sections. Formalin-fixed, paraffin-embedded mouse tissue sections were incubated with anti-GCPII antibody GCP-04 (at 10 µg·mL^{-1} concentration) to visualize and localize mouse GCPII expression [42]. (A) Brain (cerebellum): positive choroid plexus, stratum granulare, white matter. (B) Kidney: positive luminal side of proximal tubules, Bowman capsule; little crossreactivity of secondary anti-mouse antibody with capillaries and blood vessels could be seen in the negative control. (C) Sublingual gland: positive staining of abluminal cells (probably myoepitelial cells). (D) Submandibular gland: faint staining of intercallated ducts and some non-glandular abluminal cells. (E) Parotid gland: faint staining of some non-glandular abluminal cells.

number of papers have been published describing novel GCPII inhibitors acting as neuroprotective drugs [28,44] and GCPII inhibitor-based tools for imaging and/or treating prostate cancer [19,20,45–47]. Most of these compounds and methods were evaluated using mouse models. However, there has been no direct comparison of mouse and human GCPII, which would provide important information to assess the usefulness of such mouse models. Therefore, we set out to perform a systematic and detailed study to compare the enzymatic properties of mouse and human GCPII, as well as tissue distributions on both the mRNA and protein levels.

We expressed the recombinant extracellular part of mouse GCPII with an N-terminal Avi-tag (Avi-mGCPII), which enables fast and efficient one-step purification [34]. Even though GCPII is a transmembrane enzyme, its extracellular domain is the catalytically active portion and correctly represents endogenous full-length GCPII [33]. To compare the enzymatic properties of mouse and human GCPII, we analyzed the cleavage of their substrates: *N*-acetyl-L-aspartyl-L-glutamate (NAAG), which is cleaved by GCPII in the brain, and pteroyl-di-L-glutamate, which is a model substrate for poly-gamma-glutamylated folates hydrolyzed by GCPII in the small intestine. Because mouse and human GCPII have high sequence similarity (86% identity and 97% similarity in the extracellular part; Fig. 7), we did not expect to find any significant differences in their enzymatic

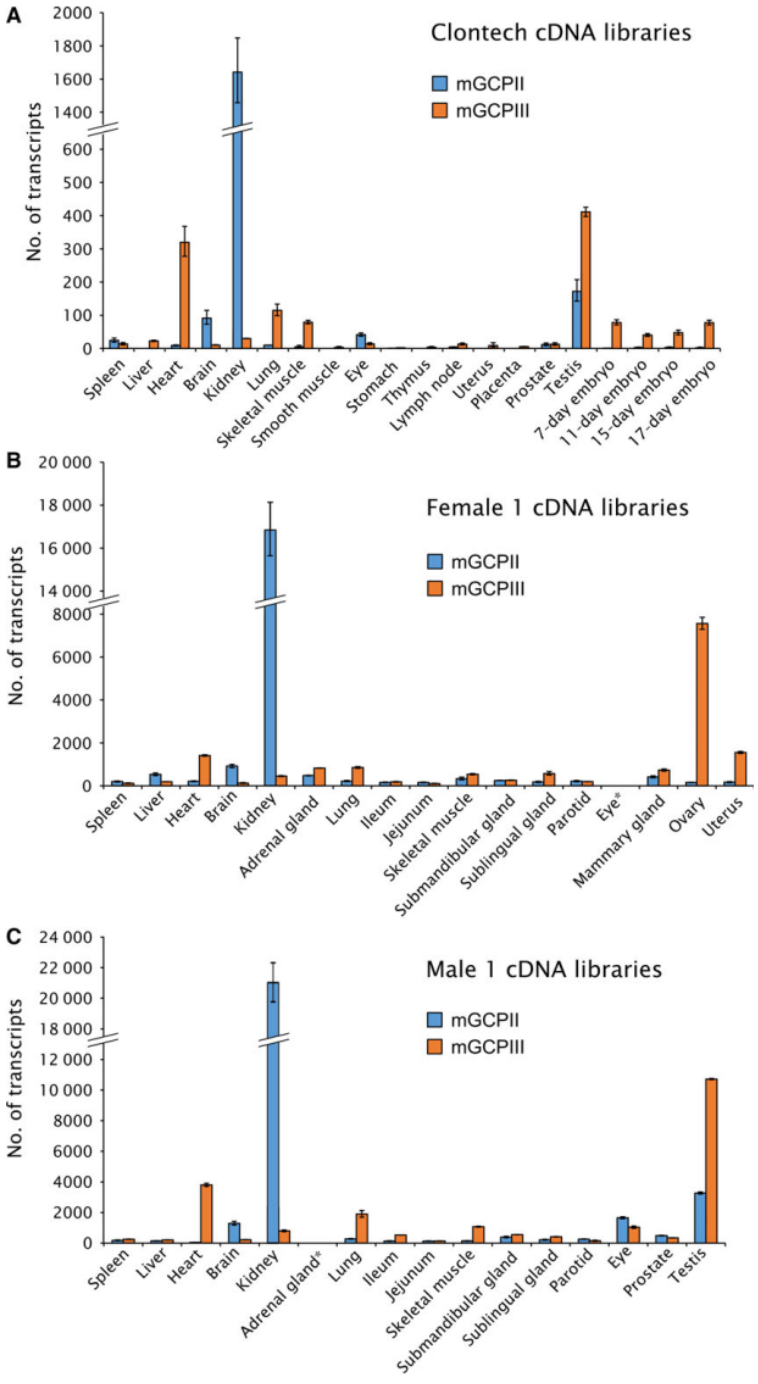

Fig. 6. Quantification of mouse GCPII and GCPIII (mGCPII and mGCPIII, respectively) transcripts using qPCR. (A) Quantification of mGCPII and mGCPIII transcripts using qPCR in commercial mouse tissue cDNA libraries from Clontech. The 'number of transcripts' corresponds to the amount of transcripts in 1.0 μL of 10-fold diluted cDNA libraries (for experimental details, see Experimental procedures). Error bars show standard deviations from triplicate measurements. (B, C) Quantification of mGCPII and mGCPIII transcripts using qPCR in cDNA libraries prepared from mouse tissues dissected from one female (B) and one male mouse (C). The 'number of transcripts' corresponds to the amount of transcripts per 10 ng of total RNA as a starting material for cDNA synthesis (for experimental details, see Experimental procedures). Error bars show standard deviations from triplicate measurements. *Not determined.

properties. In fact, we found that while the enzymes are quite similar in NAAG-hydrolyzing activity, there is an order-of-magnitude difference in their catalytic efficiencies for cleavage of pteroyl-di-L-glutamate. This difference lies in the K_M values of mouse and human GCPII (290 vs. 39 nM for pteroyl-di-L-glutamate and

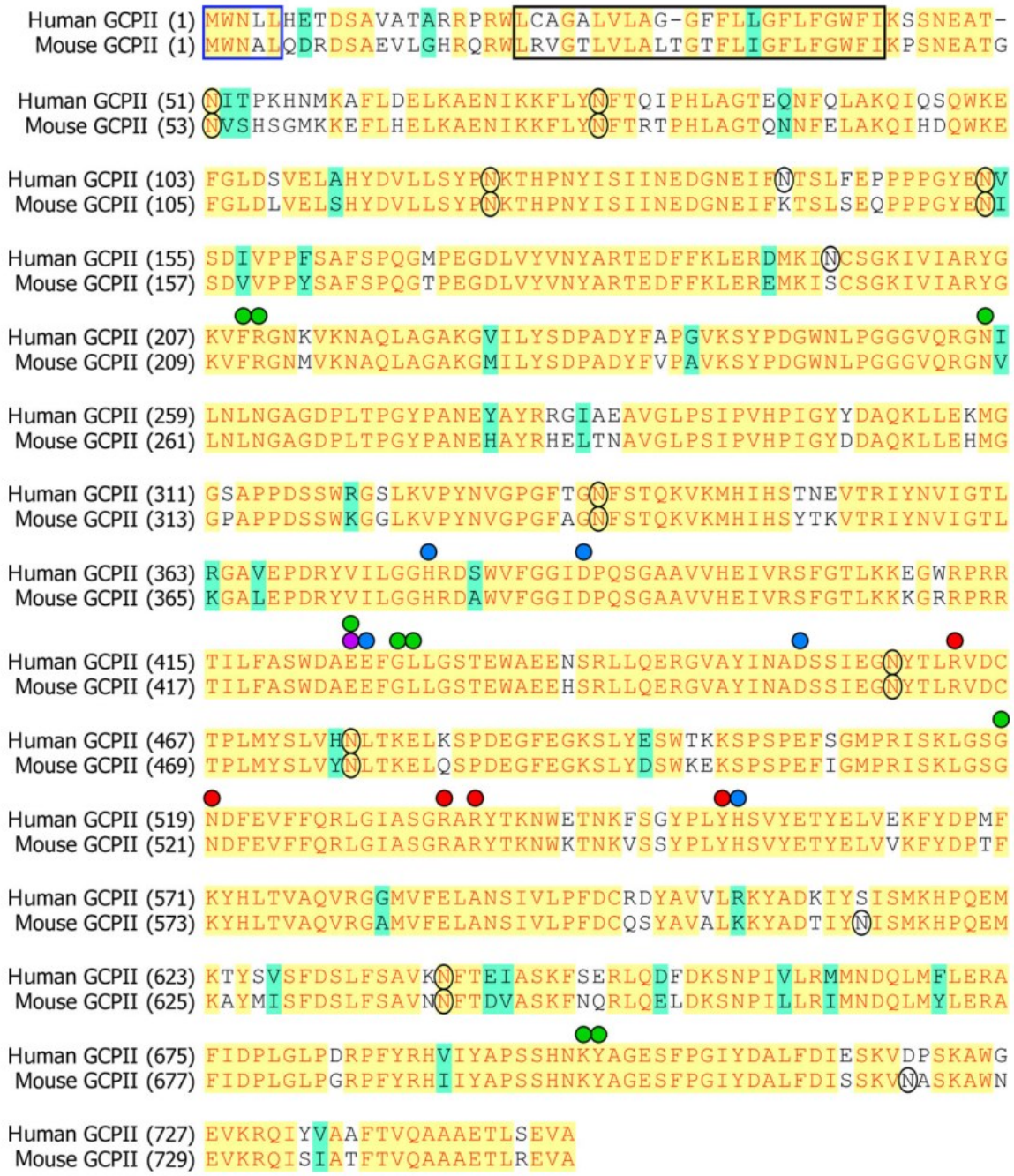

Fig. 7. Sequence alignment of the mouse and human GCPII proteins. Identical amino acid residues are highlighted in yellow, similar residues in green, and different residues in white. A blue frame marks the internalization signal MXXXL [54], and a black frame corresponds to predicted GCPII transmembrane domain (predicted by TMHMM Server v. 2.0). Black circles denote potential N-glycosylation sites ('N-X-S/T'). Green spheres: residues defining the S1′ pocket [49]; red spheres: residues forming the S1 pocket [48]; purple sphere: proton shuttle catalytic base [55]; blue spheres: zinc ligands [56,57].

1900 vs. 550 nM for NAAG). Their turnover numbers are quite similar (3.6 vs. 5.1 s^{-1} and 1.4 vs. 1.5 s^{-1}, respectively) (see Table 1). Slightly surprisingly, our data revealed that the catalytic efficiency of NAAG cleavage by mouse and human GCPII is significantly lower than that of pteroyl-di-L-glutamate cleavage (20-fold and 50-fold, respectively) (see Table 1).

Additionally, we analyzed the inhibition profile of Avi-mGCPII using several GCPII inhibitors commonly used in research, including 2-PMPA, ZJ-43, DCIBzL, DKFZ-PSMA-11, and quisqualate. We also tested several other inhibitors that were prepared in our laboratory. Generally, we did not observe considerable differences in the K_i values obtained for mouse and human GCPII. However, inhibitors ZJ-43 and JB-277 were exceptions; the K_i values for Avi-mGCPII were 10-fold higher (Table 2). Both compounds belong to the urea-based group of GCPII inhibitors, together with DCIBzL. Surprisingly, the K_i value of DCIBzL was identical for both enzymes. As seen in Fig. 7, mouse and human GCPII are highly similar and key amino acid residues participating in substrate binding and hydrolysis are identical [48–50]. Thus, in the absence of an experimentally determined structure of mouse GCPII, it is difficult to explain the observed differences in inhibitor binding and catalytic efficiency.

Next, we assessed the substrate specificity of Avi-mGCPII. We screened dipeptide libraries covering almost all *N*-acetylated dipeptide substrates, not including cysteine-containing dipeptides. Unsurprisingly, mouse GCPII exhibited a strong preference for glutamate in the P1′ position, cleaving almost any dipeptide with a C-terminal glutamate (i.e., glutamate carboxypeptidase activity). It also cleaves dipeptides with methionine in the P1′ position and an acidic amino acid (aspartate or glutamate) in the P1 position. Dipeptides containing any other C-terminal amino acid were not hydrolyzed by mouse GCPII. The substrate specificity of mouse GCPII thus seems to be even more pronounced than that of the human enzyme (Fig. 2).

In addition to the enzymatic properties of mouse GCPII, its tissue distribution is a relevant aspect both to understand the physiological function of the enzyme and to assess the use of mouse models for targeted drug delivery and GCPII inhibition experiments. Therefore, we set out to elucidate GCPII expression in mouse tissues. To see individual differences, we collected tissue samples from six mice (three females and three males).

To assess GCPII expression on the protein level, we prepared mouse tissue lysates and detected mouse GCPII by western blot using the anti-GCPII antibody GCP-04, which was raised against human GCPII [2,42]. Because GCP-04 recognizes a linear epitope in the GCPII primary structure (amino acids 100–104: WKEFG [22]), which is conserved in the mouse GCPII sequence, the antibody can be used for selective and sensitive detection of mouse GCPII as well. We confirmed very high expression of GCPII in the mouse kidney and high expression in the mouse brain, which is in agreement with high GCPII expression in the corresponding human tissues [22]. Furthermore, we observed high expression of GCPII in the mouse major salivary glands. Relatively high variability among individual samples of major salivary glands is probably caused by close association of salivary glands that are macroscopically quite similar. This makes the proper dissection of topographically complicated ventral cervical region particularly cumbersome and might lead to cross-contamination. Therefore, we localized GCPII expression by immunohistochemistry using anti-GCPII antibody GCP-04. We observed GCPII expression in all three salivary glands (sublingual, submandibular, and parotid); however, GCPII is expressed predominantly in the sublingual gland, while the expression in the submandibular and parotid glands is lower (Fig. 5).

Mouse prostate contains negligible levels of GCPII, which is consistent with previous findings [9] and in contrast with human prostate, which expresses large amounts of GCPII [6,22,51]. Additionally, as human and mouse prostates differ considerably in their morphology, we dissected a mouse prostate into its individual parts (anterior, dorsal, and lateral prostate) and searched for potential GCPII expression in each part separately. Nevertheless, we did not detect GCPII expression in any of the tested parts of mouse prostate. Our data suggest that GCPII might also be absent in the mouse jejunum, a tissue where human GCPII cleaves off glutamates from glutamylated folates [17]. Rat jejunum and ileum were shown not to contain GCPII, in contrast to the corresponding human tissues, which express large amounts of GCPII [22]. Folates in rat intestine are hydrolyzed by γ-glutamyl hydrolase, not GCPII [52], and the situation in mice may be thus similar.

Furthermore, we verified GCPII tissue distribution obtained by western blot analysis by quantification of NAAG-hydrolyzing activity in mouse tissues. The activity-based GCPII expression profile correlated well with the western blot results, confirming strong GCPII expression in the mouse kidney, brain, and salivary glands and no expression in mouse prostate and jejunum.

GCPIII is a close GCPII homolog found both in humans and in mouse. The GCP-04 antibody also

recognizes GCPIII but is roughly 10-fold less sensitive toward GCPIII than toward GCPII [42]. Moreover, GCPIII also hydrolyzes NAAG, although with a lower catalytic efficiency [10,11,43]. Therefore, GCPII distribution in mouse tissues obtained by western blot analysis with GCP-04 and activity assay based on NAAG hydrolysis could be distorted by a high amount of GCPIII and low amount of GCPII in a particular tissue. Because there is no specific antibody against GCPIII, we explored GCPII/GCPIII expression in mouse tissues on the mRNA level to differentiate between the two homologs. We quantified GCPII and GCPIII transcripts in both commercially available mouse tissue cDNA libraries and cDNA libraries we prepared from isolated mouse tissues (Fig. 6). Taking these qPCR data into account, GCPIII appears to be the source of the NAAG-hydrolyzing activity in the mouse ovary, uterus, and heart. GCPIII was most strongly expressed in the testis but was accompanied by rather high quantities of GCPII.

To conclude, we prepared and characterized recombinant mouse GCPII and compared it with human GCPII. We found that the differences in enzymatic activity, inhibition profile, and substrate specificity between mouse and human GCPII are rather small; therefore, mouse GCPII can serve as a suitable substitute for human GCPII in enzymological studies.

Due to the observed lack of GCPII expression in the mouse prostate, mouse might not seem to be an ideal model for the development of prostate cancer diagnostic/therapeutic agents. However, most such studies employ human tumor xenografts in mouse models. For this purpose, mice are generally suitable, because the distribution of GCPII in other tissues is quite similar to that in humans. Therefore, mouse GCPII appears to be a good model for the development of GCPII-targeted drugs for treatment of prostate cancer and neuronal disorders.

Experimental procedures

Cloning of mouse GCPII (Avi-mGCPII)

The pIRES/mGCPII plasmid encoding full-length mouse GCPII (amino acids 1-752) was a kind gift from Warren Heston (Cleveland Clinic, USA).

Because the sequence contained two conflicts compared to the annotated mouse GCPII sequence, we performed site-directed mutagenesis to remove them (G240A and E287N). The primers 5′-gctgactactttgttcctGCGgtgaagtc ctatcc-3′ and 5′-ggataggacttcacCGCaggaacaaagtagtcagc-3′ were used to remove the sequence conflict at position 240, and the primers 5′-catgagttgacaAACgctgttggccttc-3′ and 5′-gaaggccaacagcGTTtgtcaactcatg-3′ to remove the sequence conflict at position 287 (changed deoxyribonucleotides are underlined, changed codons capitalized). The mutagenesis was carried out according to the manufacturer's protocol (QuikChange™ Site-Directed Mutagenesis; Stratagene, San Diego, CA, USA).

Then, the sequence corresponding to the extracellular part of mouse GCPII (amino acids 45-752) was amplified by PCR using primers 5′-aaaagatctaaaccttccaatgaagctactgg-3′ and 5′-aaactcgagttaagctacttccctcagagtc-3′ (restriction sites introduced into the sequence are underlined; the primers introduced a *Bgl*II site at the 5′ end and an *Xho*I site at the 3′ end). The resulting DNA fragment was cleaved with *Bgl*II and *Xho*I and ligated into pMT/BiP/AviTEV/rhGCPII plasmid [34] cleaved with the same endonucleases. The correct sequence of the resulting plasmid pMT/BiP/Avi-mGCPII was verified by DNA sequencing.

Transfection of *Drosophila* S2 cells and expression of Avi-mGCPII

Drosophila S2 cells expressing BirA biotin-protein ligase localized in the endoplasmic reticulum (described in Ref. [34]) were used to prepare stable Avi-mGCPII transfectants. The cells were transfected using Calcium Phosphate Transfection Kit (Invitrogen, Waltham, MA, USA) with 9 μg of pMT/BiP/Avi-mGCPII together with 0.5 μg of pCoBlast (Invitrogen), as previously described [10]. The transfected cells were cultivated in the presence of both blasticidin (5 $\mu g \cdot mL^{-1}$, Invitrogen) and hygromycin B (300 $\mu g \cdot mL^{-1}$; Invitrogen).

To express Avi-mGCPII, approximately 2×10^6 stably transfected cells was transferred into a 35-mm Petri dish supplemented with 2 mL SF900II medium (Invitrogen). The following day, protein expression was induced by adding $CuSO_4$ (Sigma-Aldrich, St. Louis, MO, USA) to a final concentration of 1 mM. After three days, cells were harvested by centrifugation, and the medium was analyzed by western blot.

The large-scale expression of Avi-mGCPII was performed as previously described [33]. The final volume of cell suspension was 1000 mL.

Purification of Avi-mGCPII

Purification of Avi-mGCPII was performed as previously described [34]. Briefly, cell medium (1000 mL) containing secreted biotinylated Avi-mGCPII was centrifuged at 3400 ***g*** for 45 min. Then, it was concentrated 10-fold using a LabScale TFF System (Merck Millipore, Billerica, MA, USA) with a Pellicon® XL 50 Cassette, Biomax 100. The concentrated medium was centrifuged again at 3400 ***g*** for 20 min and equilibrated with 300 mM Tris/HCl, 450 mM NaCl, pH 7.2 in a 2 : 1 ratio. The equilibrated

concentrated Avi-mGCPII medium was then mixed with 1 mL Streptavidin Mutein Matrix (Roche, Basel, Switzerland) and incubated with gentle shaking at 6 °C for 15 h. Afterward, the resin was washed with 50 column volumes of 100 mM Tris/HCl, 150 mM NaCl, pH 7.2. Bound biotinylated proteins were eluted with 5 mL of 100 mM Tris/HCl, 150 mM NaCl, 2 mM D-biotin, pH 7.2, in five consecutive elution fractions (after the first elution fraction, the resin was incubated with elution buffer for 1 h). After regeneration of the resin, the flow-through fraction was again mixed with the resin, and the purification procedure was repeated.

Determination of kinetic parameters by radioenzymatic assay

Kinetic parameters (K_M and k_{cat}) of *N*-acetyl-L-aspartyl-L-glutamate (NAAG) cleavage by Avi-mGCPII were determined as previously described [34], with a minor modification: The reactions were performed in a 96-well plate, and appropriate amounts of Avi-mGCPII were mixed with 25 mM Bis-Tris propane, 150 mM NaCl, 0.001% octaethylene glycol monododecyl ether (Affymetrix, Santa Clara, CA, USA), pH 7.4.

Determination of kinetic and inhibition constants by HPLC

Kinetic parameters (K_M and k_{cat}) of pteroyl-di-L-glutamate cleavage by Avi-mGCPII, as well as K_i values for all inhibitors, were determined as previously described [39]. Briefly, in a 96-well plate, Avi-mGCPII was mixed with 25 mM Bis-Tris propane, 150 mM NaCl, 0.001% octaethylene glycol monododecyl ether (Affymetrix), pH 7.4 (and tested inhibitor, if used), into a final volume of 90 μL. Reactions were started by adding 10 μL of 4 μM pteroyl-di-L-glutamate and incubated at 37 °C for 20 min. The reactions were stopped with 20 μL of 25 μM 2-PMPA and subsequently analyzed on an Agilent 1200 Series system using an Acquity UPLC HSS T3 1.8 μm column (2.1 × 100 mm; Waters, Milford, MA, USA).

Animals and tissue isolation

Six C57BL/GJ mice (three males (M) and three females (F)) were sacrificed by cervical dislocation with agreement of the local ethical commission. The ages of the mice were as follows: M1: 5 months; M2: 8 months; M3: 12 months; F1: 8 months; F2 and F3: 12 months. Samples of tissues (for preparation of tissue lysates) were immediately transferred into microtubes and frozen at −80 °C. Samples of tissues (for qPCR quantification) were immediately transferred into RNAlater, impregnated with it for 2 days at 4 °C, and then stored at −80 °C.

Tissue lysate sample preparation

A small piece of tissue (approx. 30 mg) was transferred into 250 μL of 50 mM Tris/HCl, 100 mM NaCl, pH 7.4, in a 2-mL microtube. Tissue samples were homogenized using TissueLyser II (30 Hz, 3 min). The homogenates were then diluted with 250 μL of the lysis buffer. Octaethylene glycol monododecyl ether (Affymetrix) was added to reach 1% final concentration, and the homogenate was sonicated in a water bath for 5 min at 0 °C. Finally, the samples were centrifuged at 600 ***g*** for 15 min, and the resulting supernatant was stored at −80 °C until further use. The lysate protein concentration was determined using Bradford 1 × Dye Reagent (Bio-Rad, Hercules, CA, USA).

Radioenzymatic determination of NAAG-hydrolyzing activity in mouse tissues

The determination of NAAG-hydrolyzing activity in mouse tissues was performed as previously described [53]. A sample of tissue lysate was mixed with 20 mM Tris/HCl, 150 mM NaCl, 0.1% Tween 20, pH 7.4, to a final volume of 90 μL. Reactions were started by adding 10 μL of 1 μM NAAG (containing 50 nM tritium-labeled NAAG), and incubated at 37 °C for 15 h. The reactions were stopped with 100 μL of ice-cold 200 mM KH_2PO_4, 2 mM 2-mercaptoethanol, pH 7.4. The released glutamate was separated from the unreacted substrate using ion-exchange AG1-X resin (Bio-Rad). The radioactivity of the sample was quantified by liquid scintillation using the Rotiszint ECO Plus scintillation cocktail (Roth) in a Tri-Carb Liquid Scintillation Counter (Perkin-Elmer, Waltham, MA, USA). The samples were measured in duplicate.

SDS/PAGE and western blotting

Protein samples were resolved by reducing SDS/PAGE. Proteins were electroblotted onto a nitrocellulose membrane (wet blotting: 100 V/1 h). After blotting, the membrane was blocked with 0.55% (w/v) casein solution in PBS (Casein Buffer 20X-4X Concentrate, SDT, Baesweiler, Germany) at room temperature for 1 h. To visualize GCPII, the blots were probed with the antibody GCP-04 (described in [2]) for 12 h at 4 °C (200 $ng \cdot mL^{-1}$; diluted in 0.55% casein solution), washed three times with PBS containing 0.05% Tween 20 (PBST buffer), and incubated with goat anti-mouse antibody conjugated with horseradish peroxidase (Thermo Scientific, Waltham, MA, USA; diluted in 0.55% casein solution, 1 : 25 000). The blots were then washed three times with PBST to remove unbound antibodies and developed with SuperSignal West Femto Chemiluminescent Substrate (Thermo Scientific).

Chemiluminescence was captured with a ChemiDoc-It™ 600 Imaging System (UVP, Upland, CA, USA).

Immunohistochemistry

Immunohistochemistry was performed according to the protocol described previously using anti-GCPII antibody GCP-04 [2] with minor modifications [42]. Briefly, after standard histological processing (fixation, dehydration, embedding into paraffin, cutting, paraffin removal, rehydration), heat antigen retrieval was performed using 10 mM sodium citrate, 0.1% Tween 20, pH 6.0 buffer and heating to 110 °C for 15 min in an autoclave. Afterward, samples were incubated in 1.5% hydrogen peroxide solution for 20 min to reduce endogenous peroxidase activity and in 10% fetal bovine serum in PBS to block unspecific interactions. The slides were then stained by primary anti-GCPII antibody GCP-04 (10 $\mu g \cdot mL^{-1}$ in 4 °C, overnight), followed by extensive washing (five times with PBS containing 0.1% Tween 20) and incubation with secondary antibody Histofine® Simple Stain™ MAX PO (MULTI) (Nichirei Bioscience Inc., Tokyo, Japan) diluted 1 : 2 with 10% fetal bovine serum in PBS at room temperature for 1 h. After further extensive washing (five times with PBS containing 0.1% Tween 20), GCPII was visualized using DAB/Plus kit (Diagnostic BioSystems, Pleasanton, CA, USA, 60 s). The slides were counterstained with Harris' hematoxylin and mounted in polyvinyl alcohol-based media.

Carboxypeptidase activity assay

Carboxypeptidase activity (i.e., substrate specificity) of mouse GCPII was determined using *N*-Ac-A-X peptide libraries according to a previously published method [41]. Briefly, 1.2 μg Avi-mGCPII was diluted into 25 mM Bis-Tris propane, 150 mM NaCl, 0.001% octaethylene glycol monododecyl ether (Affymetrix), pH 7.4, and incubated in the presence of 25 μM dipeptide for 1.5 h at 37 °C. As negative controls, reactions without the enzyme and in the presence of 1 mM 2-PMPA, a highly selective GCPII inhibitor, were performed. The reaction mixture was then analyzed using HPLC, as previously described [41].

Total RNA isolation and reverse transcription

First, tissue samples were transferred from RNA later solution (Invitrogen, #AM7021) to RLT buffer (part of the RNEasy Mini Kit, Qiagen, Hilden, Germany, #74106) supplied with β-mercaptoethanol and homogenized with 5-mm steel beads (Qiagen; #69989) using TissueLyser II (#85300; Qiagen). Total RNA was isolated using RNeasy Mini Kit according to the manufacturer's instructions. The concentration and purity of isolated RNA were determined spectrophotometrically using a Nanodrop ND-1000 spectrophotometer. The integrity of each RNA sample was analyzed using the Agilent RNA 6000 Nano kit run on an Agilent 2100 Bioanalyzer. Only samples without significant degradation were used for subsequent steps.

RNA was then reverse-transcribed using M-MLV (#28025013; Invitrogen) according to the manufacturer's instructions. Each 20 μL reaction contained up to 2 μg total RNA, 2.5 μM oligo$(dT)_{20}$ primers (#18418020; Invitrogen), 50 ng random hexamers (100 ng if more than 1 μg RNA was transcribed), 40 units of RNAseOUT, 200 units of M-MLV reverse transcriptase, and other components as specified by the manufacturer.

Quantitative PCR (qPCR) analysis

All qPCRs were carried out in triplicate in FrameStar 480/96 multiwell plates (#4ti-0951; 4titude, Wotton, UK) sealed with adhesive optical foil (#4729692001; Roche) using a LightCycler 480 II instrument (Roche) in a total volume of 10 μL. Each reaction consisted of LightCycler 480 Probe Master (Roche) diluted according to the manufacturer's instructions, forward and reverse primers (1 μM final concentration each), fluorescent probe (see description of individual assays for final concentration), and 1 μL of sample or template DNA (positive and nontemplate controls as well as interplate calibrators were included on each plate). Initial denaturation for 3 min at 95 °C was followed by 45 cycles of 10 s at 95 °C, 30 s at 66 °C, and 30 s at 72 °C. The threshold cycle numbers (C_q) were then determined from fluorescence intensities acquired during the qPCR runs by the second-derivative maximum method using LightCycler 480 software (Roche). The presence and size of PCR products were analyzed by agarose gel electrophoresis.

The amount of mouse GCPII (encoded by the gene Folh1) was quantified by an assay set of forward and reverse primers (sequences 5′-gattgccagatatgggaaagtg-3′ and 5′-cctgccagttgagcattttt-3′) and fluorescent hydrolysis probe #6 from the Roche Universal Probe Library (LNA octamer sequence 5′-cagaggaa-3′; final concentration 100 nM). This set was designed to amplify nucleotides 714–773 in mouse GCPII transcript NM_016770 to yield an amplified product of 60 bps, which spans the region of exons 5 and 6 and corresponds to amino acids 202–223 in the longest open reading frame (ORF). This assay should not amplify genomic sequence because it spans a 1029-bp intron.

The amount of mouse GCPIII transcript (encoded by the gene Naalad2) was quantified by an assay set of forward and reverse primers (sequences 5′-aatgatgcagagagactattacgc-3′ and 5′-ccagcttttgtctggtggag-3′) and fluorescent hydrolysis probe #52 from the Roche Universal Probe Library (LNA octamer sequence 5′-gggaggag-3′; final concentration 50 nM). This set was designed to amplify nucleotides 922–981 in mouse GCPIII transcript NM_028279 to yield an amplified product of 60 bps, which spans the region of exons 7 and 8 and corresponds to

amino acids 289–309 in the longest ORF. This assay should not amplify genomic sequence because it spans a 880-bp intron.

As a standard for absolute quantification, serial 10-fold dilutions covering concentrations from 10^8 to 10^2 copies per reaction of either pcDNA4 plasmid with subcloned coding sequence of full-length mouse GCPII (longest ORF from NM_016770 coding amino acids 1–752) or pMT/BiP plasmid with subcloned coding sequence of extracellular part of mouse GCPIII (part of longest ORF from NM_028279 coding amino acids 36–740) were amplified with the corresponding assay set. The initial concentration of plasmid DNA (purified by QIAprep Spin Miniprep Kit, #27106; Qiagen) prior to dilution was determined spectrophotometrically at 260 nm (Nanodrop ND-1000; Thermo Scientific).

To enable precise absolute comparison between the determined amounts of both transcripts, obtained calibration curves were further normalized against each other by quantification of a common region of both plasmids. The region containing the ampicillin resistance gene was quantified by a set of primers with sequences 5′-gcagaagtggtcctgcaact-3′ and 5′-agcttcccggcaacaatta-3′ and fluorescent hydrolysis probe #58 from the Roche Universal Probe Library (final concentration 50 nM). In this way, two calibration curves were obtained for each plasmid, one for the amplification of target transcript and one for the common sequence. Finally, the slope and intercept values of both curves were transformed for each plasmid so that the transformed slope and intercept values of the curves for the common sequence were equal between the two plasmids and corresponded to the average value between the two plasmids.

The amount of both transcripts was determined in the prepared tissue cDNA libraries. In each qPCR, an amount of cDNA corresponding to the starting amount of total RNA of 5–10 ng was used, and the amount of GCPII and GCPIII transcripts were normalized to the total amount of RNA. Both transcripts were also quantified in 1.0 μL of 10-fold diluted commercial tissue cDNA libraries (Mouse MTC Panels I and III supplied by Clontech, Mountain View, CA, USA, #636745 and 636757), which had been normalized to several control genes by the vendor (beta-actin, G3PDH, phospholipase A2, and ribosomal protein S29).

Statistical analysis

All values are presented as the mean ± standard deviation.

Acknowledgements

We would like to thank Warren Heston (Lerner Research Institute, Cleveland Clinic) for providing us with a plasmid encoding mouse GCPII, Jana Starková and Karolína Šrámková for their excellent technical support, Radko Souček for HPLC analyses, and Hillary Hoffman for language editing. This work was supported by Grant No. GA16-02938S from the Grant Agency of the Czech Republic and InterBioMed Project LO 1302 from the Ministry of Education of the Czech Republic.

Author contributions

The manuscript was written through contributions of all authors. All authors have given approval to the final version of the manuscript. JK and PS conceived the project and analyzed data, TK, BV, JT, VN, PS and JK wrote the manuscript, TK, BV, VN, JT, FS, SV and MF designed, performed and interpreted the experiments.

References

1 Berger UV, Carter RE, Mckee M and Coyle JT (1995) N-acetylated alpha-linked acidic dipeptidase is expressed by non-myelinating Schwann-cells in the peripheral nervous-system. *J Neurocytol* **24**, 99–109.

2 Sacha P, Zamecnik J, Barinka C, Hlouchova K, Vicha A, Mlcochova P, Hilgert I, Eckschlager T and Konvalinka J (2007) Expression of glutamate carboxypeptidase II in human brain. *Neuroscience* **144**, 1361–1372.

3 Bostwick DG, Pacelli A, Blute M, Roche P and Murphy GP (1998) Prostate specific membrane antigen expression in prostatic intraepithelial neoplasia and adenocarcinoma: a study of 184 cases. *Cancer* **82**, 2256–2261.

4 Silver DA, Pellicer I, Fair WR, Heston WD and Cordon-Cardo C (1997) Prostate-specific membrane antigen expression in normal and malignant human tissues. *Clin Cancer Res* **3**, 81–85.

5 Pinto JT, Suffoletto BP, Berzin TM, Qiao CH, Lin SL, Tong WP, May F, Mukherjee B and Heston WDW (1996) Prostate-specific membrane antigen: a novel folate hydrolase in human prostatic carcinoma cells. *Clin Cancer Res* **2**, 1445–1451.

6 Kinoshita Y, Kuratsukuri K, Landas S, Imaida K, Rovito PM Jr, Wang CY and Haas GP (2006) Expression of prostate-specific membrane antigen in normal and malignant human tissues. *World J Surg* **30**, 628–636.

7 Robinson MB, Blakely RD, Couto R and Coyle JT (1987) Hydrolysis of the brain dipeptide N-acetyl-L-aspartyl-L-glutamate. Identification and characterization of a novel N-acetylated alpha-linked acidic dipeptidase activity from rat brain. *J Biol Chem* **262**, 14498–14506.

8 Horoszewicz JS, Kawinski E and Murphy GP (1987) Monoclonal-antibodies to a new antigenic marker in epithelial prostatic cells and serum of prostatic-cancer patients. *Anticancer Res* **7**, 927–936.
9 Bacich DJ, Ramadan E, O'Keefe DS, Bukhari N, Wegorzewska I, Ojeifo O, Olszewski R, Wrenn CC, Bzdega T, Wroblewska B *et al.* (2002) Deletion of the glutamate carboxypeptidase II gene in mice reveals a second enzyme activity that hydrolyzes N-acetylaspartylglutamate. *J Neurochem* **83**, 20–29.
10 Hlouchova K, Barinka C, Klusak V, Sacha P, Mlcochova P, Majer P, Rulisek L and Konvalinka J (2007) Biochemical characterization of human glutamate carboxypeptidase III. *J Neurochem* **101**, 682–696.
11 Collard F, Vertommen D, Constantinescu S, Buts L and Van Schaftingen E (2011) Molecular identification of beta-citrylglutamate hydrolase as glutamate carboxypeptidase 3. *J Biol Chem* **286**, 38220–38230.
12 Slusher BS, Vornov JJ, Thomas AG, Hurn PD, Harukuni I, Bhardwaj A, Traystman RJ, Robinson MB, Britton P, Lu XCM *et al.* (1999) Selective inhibition of NAALADase, which converts NAAG to glutamate, reduces ischemic brain injury. *Nat Med* **5**, 1396–1402.
13 Neale JH, Olszewski RT, Gehl LM, Wroblewska B and Bzdega T (2005) The neurotransmitter N-acetylaspartylglutamate in models of pain, ALS, diabetic neuropathy, CNS injury and schizophrenia. *Trends Pharmacol Sci* **26**, 477–484.
14 Wroblewska B, Wroblewski JT, Pshenichkin S, Surin A, Sullivan SE and Neale JH (1997) N-acetylaspartylglutamate selectively activates mGluR3 receptors in transfected cells. *J Neurochem* **69**, 174–181.
15 Bruno V, Wroblewska B, Wroblewski JT, Fiore L and Nicoletti F (1998) Neuroprotective activity of N-acetylaspartylglutamate in cultured cortical cells. *Neuroscience* **85**, 751–757.
16 Halsted CH, Ling EH, Luthi-Carter R, Villanueva JA, Gardner JM and Coyle JT (1998) Folylpoly-gamma-glutamate carboxypeptidase from pig jejunum – molecular characterization and relation to glutamate carboxypeptidase II. *J Biol Chem* **273**, 20417–20424.
17 Chandler CJ, Wang TT and Halsted CH (1986) Pteroylpolyglutamate hydrolase from human jejunal brush borders. Purification and characterization. *J Biol Chem* **261**, 928–933.
18 Mhawech-Fauceglia P, Zhang S, Terracciano L, Sauter G, Chadhuri A, Herrmann FR and Penetrante R (2007) Prostate-specific membrane antigen (PSMA) protein expression in normal and neoplastic tissues and its sensitivity and specificity in prostate adenocarcinoma: an immunohistochemical study using multiple tumour tissue microarray technique. *Histopathology* **50**, 472–483.
19 Chen Z, Penet MF, Nimmagadda S, Li C, Banerjee SR, Winnard PT Jr, Artemov D, Glunde K, Pomper MG and Bhujwalla ZM (2012) PSMA-targeted theranostic nanoplex for prostate cancer therapy. *ACS Nano* **6**, 7752–7762.
20 Heck MM, Retz M, D'Alessandria C, Rauscher I, Scheidhauer K, Maurer T, Storz E, Janssen F, Schottelius M, Wester HJ *et al.* (2016) Systemic radioligand therapy with (177)Lu labeled prostate specific membrane antigen ligand for imaging and therapy in patients with metastatic castration resistant prostate cancer. *J Urol* **196**, 382–391.
21 Hrkach J, Von Hoff D, Ali MM, Andrianova E, Auer J, Campbell T, De Witt D, Figa M, Figueiredo M, Horhota A *et al.* (2012) Preclinical development and clinical translation of a PSMA-targeted docetaxel nanoparticle with a differentiated pharmacological profile. *Sci Transl Med* **4**, 128ra39.
22 Rovenska M, Hlouchova K, Sacha P, Mlochova P, Horak V, Zamecnik J, Barinka C and Konvalinka J (2008) Tissue expression and enzymologic characterization of human prostate specific membrane antigen and its rat and pig orthologs. *Prostate* **68**, 171–182.
23 Zhong C, Zhao X, Van KC, Bzdega T, Smyth A, Zhou J, Kozikowski AP, Jiang J, O'Connor WT, Berman RF *et al.* (2006) NAAG peptidase inhibitor increases dialysate NAAG and reduces glutamate, aspartate and GABA levels in the dorsal hippocampus following fluid percussion injury in the rat. *J Neurochem* **97**, 1015–1025.
24 Zhong CL, Zhao XR, Sarva J, Kozikowski A, Neale JH and Lyeth BG (2005) NAAG peptidase inhibitor reduces acute neuronal degeneration and astrocyte damage following lateral fluid percussion TBI in rats. *J Neurotraum* **22**, 266–276.
25 Ghadge GD, Slusher BS, Bodner A, Canto MD, Wozniak K, Thomas AG, Rojas C, Tsukamoto T, Majer P, Miller RJ *et al.* (2003) Glutamate carboxypeptidase II inhibition protects motor neurons from death in familial amyotrophic lateral sclerosis models. *Proc Natl Acad Sci USA* **100**, 9554–9559.
26 Chen SR, Wozniak KM, Slusher BS and Pan HL (2002) Effect of 2-(phosphono-methyl)-pentanedioic acid on allodynia and afferent ectopic discharges in a rat model of neuropathic pain. *J Pharmacol Exp Ther* **300**, 662–667.
27 Nagel J, Belozertseva I, Greco S, Kashkin V, Malyshkin A, Jirgensons A, Shekunova E, Eilbacher B, Bespalov A and Danysz W (2006) Effects of NAAG peptidase inhibitor 2-PMPA in model chronic pain – relation to brain concentration. *Neuropharmacology* **51**, 1163–1171.
28 Zhou J, Neale JH, Pomper MG and Kozikowski AP (2005) NAAG peptidase inhibitors and their potential

for diagnosis and therapy. *Nat Rev Drug Discov* **4**, 1015–1026.
29 Bacich DJ, Pinto JT, Tong WP and Heston WD (2001) Cloning, expression, genomic localization, and enzymatic activities of the mouse homolog of prostate-specific membrane antigen/NAALADase/folate hydrolase. *Mamm Genome* **12**, 117–123.
30 Gao Y, Xu SY, Cui ZW, Zhang MK, Lin YY, Cai L, Wang ZG, Luo XG, Zheng Y, Wang Y *et al.* (2015) Mice lacking glutamate carboxypeptidase II develop normally, but are less susceptible to traumatic brain injury. *J Neurochem* **134**, 340–353.
31 Tsai G, Dunham KS, Drager U, Grier A, Anderson C, Collura J and Coyle JT (2003) Early embryonic death of glutamate carboxypeptidase II (NAALADase) homozygous mutants. *Synapse* **50**, 285–292.
32 Han LQ, Picker JD, Schaevitz LR, Tsai GC, Feng JM, Jiang ZC, Chu HC, Basu AC, Berger-Sweeney J and Coyle JT (2009) Phenotypic characterization of mice heterozygous for a null mutation of glutamate carboxypeptidase II. *Synapse* **63**, 625–635.
33 Barinka C, Rinnova M, Sacha P, Rojas C, Majer P, Slusher BS and Konvalinka J (2002) Substrate specificity, inhibition and enzymological analysis of recombinant human glutamate carboxypeptidase II. *J Neurochem* **80**, 477–487.
34 Tykvart J, Sacha P, Barinka C, Knedlik T, Starkova J, Lubkowski J and Konvalinka J (2012) Efficient and versatile one-step affinity purification of in vivo biotinylated proteins: expression, characterization and structure analysis of recombinant human glutamate carboxypeptidase II. *Protein Expr Purif* **82**, 106–115.
35 Jackson PF, Cole DC, Slusher BS, Stetz SL, Ross LE, Donzanti BA and Trainor DA (1996) Design, synthesis, and biological activity of a potent inhibitor of the neuropeptidase N-acetylated alpha-linked acidic dipeptidase. *J Med Chem* **39**, 619–622.
36 Kozikowski AP, Zhang J, Nan FJ, Petukhov PA, Grajkowska E, Wroblewski JT, Yamamoto T, Bzdega T, Wroblewska B and Neale JH (2004) Synthesis of urea-based inhibitors as active site probes of glutamate carboxypeptidase II: efficacy as analgesic agents. *J Med Chem* **47**, 1729–1738.
37 Chen Y, Foss CA, Byun Y, Nimmagadda S, Pullambahatla M, Fox JJ, Castanares M, Lupold SE, Babich JW, Mease RC *et al.* (2008) Radiohalogenated prostate-specific membrane antigen (PSMA)-based ureas as imaging agents for prostate cancer. *J Med Chem* **51**, 7933–7943.
38 Eder M, Schafer M, Bauder-Wust U, Hull WE, Wangler C, Mier W, Haberkorn U and Eisenhut M (2012) Ga-68-complex lipophilicity and the targeting property of a urea-based PSMA inhibitor for PET imaging. *Bioconjug Chem* **23**, 688–697.
39 Tykvart J, Schimer J, Barinkova J, Pachl P, Postova-Slavetinska L, Majer P, Konvalinka J and Sacha P (2014) Rational design of urea-based glutamate carboxypeptidase II (GCPII) inhibitors as versatile tools for specific drug targeting and delivery. *Bioorg Med Chem* **22**, 4099–4108.
40 Tykvart J, Schimer J, Jancarik A, Barinkova J, Navratil V, Starkova J, Sramkova K, Konvalinka J, Majer P and Sacha P (2015) Design of highly potent urea-based, exosite-binding inhibitors selective for glutamate carboxypeptidase II. *J Med Chem* **58**, 4357–4363.
41 Tykvart J, Barinka C, Svoboda M, Navratil V, Soucek R, Hubalek M, Hradilek M, Sacha P, Lubkowski J and Konvalinka J (2015) Structural and biochemical characterization of a novel aminopeptidase from human intestine. *J Biol Chem* **290**, 11321–11336.
42 Tykvart J, Navratil V, Sedlak F, Corey E, Colombatti M, Fracasso G, Koukolik F, Barinka C, Sacha P and Konvalinka J (2014) Comparative analysis of monoclonal antibodies against prostate-specific membrane antigen (PSMA). *Prostate* **74**, 1674–1690.
43 Navratil M, Tykvart J, Schimer J, Pachl P, Navratil V, Rokob TA, Hlouchova K, Rulisek L and Konvalinka J (2016) Comparison of human glutamate carboxypeptidases II and III reveals their divergent substrate specificities. *FEBS J* **283**, 2528–2545.
44 Majer P, Jancarik A, Krecmerova M, Tichy T, Tenora L, Wozniak K, Wu Y, Pommier E, Ferraris D, Rais R *et al.* (2016) Discovery of orally available prodrugs of the glutamate carboxypeptidase II (GCPII) inhibitor 2-phosphonomethylpentanedioic acid (2-PMPA). *J Med Chem* **59**, 2810–2819.
45 Chen Y, Dhara S, Banerjee SR, Byun Y, Pullambhatla M, Mease RC and Pomper MG (2009) A low molecular weight PSMA-based fluorescent imaging agent for cancer. *Biochem Biophys Res Commun* **390**, 624–629.
46 Gorin MA, Pomper MG and Rowe SP (2016) PSMA-targeted imaging of prostate cancer: the best is yet to come. *BJU Int* **117**, 715–716.
47 Yang X, Mease RC, Pullambhatla M, Lisok A, Chen Y, Foss CA, Wang Y, Shallal H, Edelman H, Hoye AT *et al.* (2016) [(18)F]Fluorobenzoyllysinepentanedioic acid carbamates: new scaffolds for positron emission tomography (PET) imaging of prostate-specific membrane antigen (PSMA). *J Med Chem* **59**, 206–218.
48 Barinka C, Hlouchova K, Rovenska M, Majer P, Dauter M, Hin N, Ko YS, Tsukamoto T, Slusher BS, Konvalinka J *et al.* (2008) Structural basis of interactions between human glutamate carboxypeptidase II and its substrate analogs. *J Mol Biol* **376**, 1438–1450.
49 Barinka C, Rovenska M, Mlcochova P, Hlouchova K, Plechanovova A, Majer P, Tsukamoto T, Slusher BS, Konvalinka J and Lubkowski J (2007) Structural

insight into the pharmacophore pocket of human glutamate carboxypeptidase II. *J Med Chem* **50**, 3267–3273.

50 Mlcochova P, Plechanovova A, Barinka C, Mahadevan D, Saldanha JW, Rulisek L and Konvalinka J (2007) Mapping of the active site of glutamate carboxypeptidase II by site-directed mutagenesis. *FEBS J* **274**, 4731–4741.

51 O'Keefe DS, Bacich DJ and Heston WD (2004) Comparative analysis of prostate-specific membrane antigen (PSMA) versus a prostate-specific membrane antigen-like gene. *Prostate* **58**, 200–210.

52 Shafizadeh TB and Halsted CH (2007) Gamma-glutamyl hydrolase, not glutamate carboxypeptidase II, hydrolyzes dietary folate in rat small intestine. *J Nutr* **137**, 1149–1153.

53 Knedlik T, Navratil V, Vik V, Pacik D, Sacha P and Konvalinka J (2014) Detection and quantitation of glutamate carboxypeptidase II in human blood. *Prostate* **74**, 768–780.

54 Rajasekaran SA, Anilkumar G, Oshima E, Bowie JU, Liu H, Heston W, Bander NH and Rajasekaran AK (2003) A novel cytoplasmic tail MXXXL motif mediates the internalization of prostate-specific membrane antigen. *Mol Biol Cell* **14**, 4835–4845.

55 Klusak V, Barinka C, Plechanovova A, Mlcochova P, Konvalinka J, Rulisek L and Lubkowski J (2009) Reaction mechanism of glutamate carboxypeptidase II revealed by mutagenesis, X-ray crystallography, and computational methods. *Biochemistry* **48**, 4126–4138.

56 Mesters JR, Barinka C, Li WX, Tsukamoto T, Majer P, Slusher BS, Konvalinka J and Hilgenfeld R (2006) Structure of glutamate carboxypeptidase II, a drug target in neuronal damage and prostate cancer. *EMBO J* **25**, 1375–1384.

57 Speno HS, Luthi-Carter R, Macias WL, Valentine SL, Joshi ART and Coyle JT (1999) Site-directed mutagenesis of predicted active site residues in glutamate carboxypeptidase II. *Mol Pharmacol* **55**, 179–185.

Příloha 4

The FASEB Journal article fj.12-225094. Published online March 23, 2013.

The FASEB Journal • Research Communication

Glutamate carboxypeptidase II does not process amyloid-β peptide

František Sedlák,[*,†] Pavel Šácha,[*,†,‡] Miroslava Blechová,[*,†] Anna Březinová,[*,†] Martin Šafařík,[*,†] Jaroslav Šebestík,[*,†] and Jan Konvalinka[*,†,‡,1]

[*]Gilead Sciences and [†]Institute of Organic Chemistry and Biochemistry (IOCB) Research Center, IOCB, Academy of Sciences of the Czech Republic, Prague, Czech Republic; and [‡]Department of Biochemistry, Faculty of Science, Charles University, Prague, Czech Republic

ABSTRACT **The accumulation of amyloid-β (Aβ) peptide is thought to be a major causative mechanism of Alzheimer's disease. Aβ accumulation could be caused by dysregulated processing of amyloid precursor protein, yielding excessive amounts of Aβ, and/or by inefficient proteolytic degradation of the peptide itself. Several proteases have been described as Aβ degradation enzymes, most notably metalloendopeptidases, aspartic endopeptidases, and some exopeptidases. Recently a report suggested that another metallopeptidase, glutamate carboxypeptidase II (GCPII), can also cleave Aβ. GCPII is a zinc exopeptidase that cleaves glutamate from *N*-acetyl-L-aspartyl-L-glutamate in the central nervous system and from pteroylpoly-γ-glutamate in the jejunum. GCPII has been proposed as a promising therapeutic target for disorders caused by glutamate neurotoxicity. However, an Aβ-degrading activity of GCPII would compromise potential pharmaceutical use of GCPII inhibitors, because the enzyme inhibition might lead to increased Aβ levels and consequently to Alzheimer's disease. Therefore, we analyzed the reported Aβ-degrading activity of GCPII using highly purified recombinant enzyme and synthetic Aβ. We did not detect any Aβ degradation activity of GCPII or its homologue even under prolonged incubation at a high enzyme to substrate ratio. These results are in good agreement with the current detailed structural understanding of the substrate specificity and enzyme-ligand interactions of GCPII.—Sedlák, F., Šácha, P., Blechová, M., Březinová, A., Šafařík, M., Šebestík, J., Konvalinka, J. Glutamate carboxypeptidase II does not process amyloid-β peptide. *FASEB J.* 27, 000–000 (2013). www.fasebj.org**

Key Words: PSMA · Alzheimer's disease · disaggregation · exopeptidase · substrate specificity · depsipeptide

ALZHEIMER'S DISEASE (AD) is one of the most common causes of senile dementia (1). AD is a serious and widespread medical problem. According to 2011 estimates, 5.4 million Americans are affected by AD, and the prevalence is expected to increase as the population ages (2).

The key histological feature of AD is the presence of neuritic plaques and tangles in the brain tissue. The plaques are composed of amyloid-β (Aβ) peptide, which originates from sequential cleavage of amyloid precursor protein by β- and γ-secretases (3). The pathogenesis of AD is not completely understood, but an association between amyloid precursor protein (APP) processing disorders and AD incidence has been identified. Mutations of APP or presenilins (part of the γ-secretase complex) may lead to AD by increasing production of Aβ (4).

Lower clearance of Aβ might also increase the risk of AD development. There are two mechanisms of Aβ clearance (5). One is the efflux of Aβ from the brain to the blood, and the second is clearance by *in situ* proteolysis. Several proteases are capable of cleaving Aβ. Most of these are zinc-binding metalloendopeptidases, such as neprilysin, insulin-degrading enzyme, and endotelin converting enzymes 1 and 2 (5–8); others belong to the serine endopeptidase (plasmin, tissue plasminogen activator, acylpeptide hydrolase; refs. 7, 9) or aspartic endopeptidase (cathepsin D) family (10). Furthermore, Aβ can act as a substrate for the metalloexopeptidase angiotensin-converting enzyme (5, 7). Recently, glutamate carboxypeptidase II (GCPII) was also reported to degrade Aβ *in vitro* (11). Kim *et al.* (11) conducted matrix-assisted laser desorp-

Abbreviations: 2-PMPA, 2-(phosphonomethyl)pentanedioic acid; 3D, 3-dimensional; Aβ, amyloid β; AD, Alzheimer's disease; APP, amyloid precursor protein; Avi-GCPII, *in vivo* specifically biotinylated glutamate carboxypeptidase II; DCM, dichloromethane; DIC, diisopropylcarbodiimide; DMF, dimethylformamide; GCPII, glutamate carboxypeptidase II; GCPIII, glutamate carboxypeptidase III; HBTU, [2-(1H-benzotriazole-1-yl)-1,1,3,3]-tetramethyluronium hexafluorophosphate; HFIP, hexafluoroisopropanol; HOBT, 1-hydroxybenzotriazole monohydrate; HPLC, high-performance liquid chromatography; LC-MS, liquid chromatography mass spectrometry; MALDI, matrix-assisted laser desorption/ionization; NAAG, *N*-acetyl-L-aspartyl-L-glutamate; rhGCPII, recombinant human glutamate carboxypeptidase II; SDS-PAGE, sodium dodecyl sulfate–polyacrylamide gel electrophoresis; TFA, trifluoroacetic acid; TOF, time of flight

[1] Correspondence: Institute of Organic Chemistry and Biochemistry, Flemingovo n. 2, 166 10, Prague 6, Czech Republic. E-mail: konval@uochb.cas.cz

doi: 10.1096/fj.12-225094

tion/ionization (MALDI) time-of-flight (TOF) mass spectrometry analysis of reaction mixtures and showed that recombinant human GCPII cleaves $A\beta_{1-40}$ and $A\beta_{1-42}$ monomers at their C termini, producing smaller fragments, including an $A\beta_{1-14}$ fragment. The researchers also reported that GCPII degrades soluble oligomers and fibrils. The authors corroborated their findings in tissue culture experiments showing that overexpression of GCPII in either HEK293-APP Swedish cells or primary neurons and glial cells reduces levels of secreted or exogenously supplemented Aβ. Furthermore, they reported that treatment of transgenic mice with a specific GCPII inhibitor increases cerebral Aβ content.

GCPII is a Zn^{2+}-dependent, transmembrane, homodimeric metalloproteinase with a large ectodomain possessing carboxypeptidase activity and short transmembrane and intracellular domains. GCPII is also known as prostate-specific membrane antigen and folate hydrolase I. In the brain, this enzyme cleaves the neurotransmitter *N*-acetyl-L-aspartyl-L-glutamate (NAAG) into *N*-acetyl-L-aspartate and free glutamate. It also possesses a folate hydrolase activity, liberating γ-linked glutamates from folyl-poly-γ-glutamates, and it may play a role in folate absorption in the small intestine (12).

GCPII expression is elevated in prostate carcinoma and in the cancer-associated neovasculature of most solid tumors (12). In the nervous system, GCPII inhibition increases the NAAG concentration, leading to neuroprotection in animal models of brain injury, amyotrophic lateral sclerosis, and neuropathic pain (13). GCPII is thus a very promising target for the treatment of diseases caused by glutamate excitotoxicity and for cancer diagnostics, imaging, and targeted delivery of anticancer drugs. The reported ability of GCPII to degrade Aβ is very relevant to the potential pharmaceutical use of GCPII inhibitors, as the use of such compounds might lead to elevated accumulation of Aβ in patient brains, increasing the risk of AD development.

The observation that GCPII is capable of degrading Aβ (11) is quite surprising. GCPII is an exopeptidase with exquisite specificity. Glutamate, aspartate, or a similar dicarboxylic residue is required at the P1′ position for efficient substrate hydrolysis (14). Several other amino acids, both natural (methionine, alanine) and non-natural (harboring aliphatic side chains; refs. 15, 16), are also tolerated, yet substrates with these amino acids in the P1′ position have lower susceptibility to cleavage. No protein or large peptide substrate has ever before been described for GCPII, and the structure of the binding cleft does not allow for endoproteolytic activity (17). Therefore, we set out to analyze potential Aβ cleavage by GCPII using highly purified recombinant GCPII and $A\beta_{1-42}$ prepared by chemical synthesis.

MATERIALS AND METHODS

Preparation of $A\beta_{1-42}$ by solid-phase synthesis

The peptide sequence was assembled in an ABI 433A solid-phase synthesizer (Applied Biosystems, Foster City, CA, USA) by stepwise coupling of the corresponding Fmoc amino acids to the growing chain on Fmoc-Ala-Wang resin LL (0.34 mmol/g). Fully protected peptide resin was synthesized according to a standard procedure involving cleavage of the N^{α}-Fmoc-protecting group with 20% piperidine in *N*-methylpyrrolidone and coupling mediated by mixtures of the coupling reagents [2-(1H-benzotriazole-1-yl)-1,1,3,3]-tetramethyluronium hexafluorophosphate (HBTU) and 1-hydroxybenzotriazole monohydrate (HOBT) in dimethylformamide (DMF). On completion of the syntheses, deprotection and detachment of linear peptides from the resins were carried out simultaneously, using a trifluoroacetic acid (TFA)/thioanisole/1,2-ethanedithiol/anisole (90:5:3:2) mixture. The resin was washed with dichloromethane, and the combined TFA filtrates were evaporated at room temperature. The peptides were precipitated with *tert*-butyl-methyl ether, collected by suction, dissolved in acetonitrile/H_2O (50:50), and dried.

The peptide was further purified by reverse-phase high-performance liquid chromatography (HPLC) on a semi-preparative C18 column (MAG 3 10×250 mm, 10 μm; Labio a.s., Prague, Czech Republic) with an acetonitrile/H_2O gradient with TFA additive at high temperature (60°C). Purified fractions were frozen in liquid nitrogen and lyophilized.

$A\beta_{1-42}$ disaggregation and analysis

The lyophilized Aβ powder was disaggregated by a previously described method with some modifications (18). Aβ was dissolved in neat TFA in an approximate 1:5 (mg:ml) ratio, followed by 10 min sonication at 25°C and centrifugation (16,100 *g*, 5 min, 25°C). Insoluble aggregates were discarded. TFA was then evaporated under dry nitrogen gas. The remaining TFA was removed by addition of hexafluoroisopropanol (HFIP) and sonication. HFIP was subsequently evaporated using a gaseous nitrogen stream. The HFIP procedure was repeated twice. The purity of the synthesized peptide was analyzed by analytical HPLC and MALDI-TOF mass spectrometry. Samples were portioned into aliquots and stored at −80°C under a nitrogen atmosphere. Peptide quantity was determined by amino acid analysis.

Synthesis of $A\beta_{1-42}$ by isomerization of depsi(25,26)$A\beta_{1-42}$

The depsipeptide was prepared according to a modification of a published procedure (19). Briefly Boc-Ser(Fmoc-Gly)-OH (0.04 mmol, 19.5 mg), HOBT (0.04 mmol, 5.5 mg), and diisopropylcarbodiimide (DIC; 0.044 mmol, 6.8 μl) were activated in a DMF-dichloromethane (DCM) mixture (0.6 ml, 1:9) (20). The preactivated mixture was loaded into a syringe with Aβ27–42-HMPB-ChemMatrix resin assembled by an ABI 433A automatic solid-phase synthesizer (Applied Biosystems) from H-Ala-HMPB ChemMatrix resin (100 mg, S 0.1 mmol/g, 0.01 mmol; PCAS BioMatrix, Saint-Jean-sur-Richelieu, QC, Canada) using the FastMoc 0.1 mmol program (SynthAssist 3.1; Applied Biosystems) with a double coupling (10-Eq excess of protected amino acids and HBTU coupling reagent and 20-Eq excess of *N,N*-diisopropylethylamine). The progress of depsipeptide coupling was monitored by Kaiser's test (21, 22). After 16 h coupling, recoupling with Boc-Ser(Fmoc-Gly)-OH (0.05 mmol, 24.2 mg), HOBT (0.05 mmol, 6.8 mg), DIC (0.055 mmol, 8.5 μl), and *N,N*-diisopropylethylamine (0.11 mmol, 19 μl) in a DMF-DCM mixture (0.6 ml, 1:1) was carried out for 0.5 h. The remaining peptide sequence was assembled by an ABI 433A automatic solid-phase synthesizer. Final Fmoc cleavage was carried out with 20% piperidine/DMF (3×1 ml) for 5, 25, and 25 min. The resin was washed extensively with DMF, isopropyl alcohol, and DCM and dried

in a vacuum drying box (Salvis AG; Emmenbrücke, Lucerne, Switzerland) at room temperature for 16 h. Depsi(25,26)Aβ_{1-42} peptide was detached from the resin using a TFA/H_2O/1,2-ethanedithiol/thioanisole/triisopropylsilane mixture (4 ml, 89.5:3:3:3:1.5) for 4 h. The TFA was evaporated by a stream of gaseous nitrogen, and the peptide was precipitated with cold ether. The crude peptide was purified by semipreparative HPLC (Spectra Physics SP8800 pump with a TSP Chrom Jet SP4290 integrator and a Spectra 100 UV detector; Newport Corp., Praha, Czech Republic) with a Vydac RP-18, 25 × 1 cm, 10 μm column (Separations Group, Hesperia, CA, USA). Purification was carried out using a flow rate of 3 ml/min in a gradient of 20–100% acetonitrile in 0.05% aqueous TFA over 35 min with detection at 220 nm. The final depsipeptide was obtained in 32 mg yield with 96% purity according to analytical HPLC (Agilent 1200; Agilent Technologies, Santa Clara, CA, USA) with a reverse-phase PoroShell 120 SB-C_{18} column (Agilent Technologies). The molecular weight was determined by mass spectrometry using MALDI-TOF spectra, recorded on a Lasermat mass spectrometer (Finnigan, San Jose, CA, USA) with Lasermat 2000 program. MALDI-MS *m/z* 4512.1 ($M+H^+$; expected molecular weight for $C_{203}H_{311}N_{55}O_{60}S$, 4511.27).

Recombinant human GCPII (rhGCPII) expression and purification

The extracellular part of human GCPII (aa residues 44–750) was prepared as described previously (14) with minor modifications. The procedure involved heterologous expression in stable transfected Schneider 2 (S2) cells and subsequent purification by ion-exchange chromatography, affinity chromatography, and size-exclusion chromatography. Briefly, the conditioned medium was dialyzed against 20 mM Tris HCl (pH 6.7) applied to QAE-Sephadex A50 (Pharmacia, Piscataway, NJ, USA) in the same buffer. Filtered flow-through fraction was applied to a Source 15S column (HR10/10; Pharmacia). The column was washed with 20 mM MOPS (pH 6.5) containing 20 mM NaCl, and the protein was eluted with a gradient of 0–0.5 M NaCl in 20 mM MOPS (pH 6.5). Next, affinity chromatography using lentil lectin-Sepharose (Sigma, St. Louis, MO, USA) was employed: Pooled purified fractions from the previous step were mixed with an equal volume of 0.1 M Tris-HCl (pH 7.4) containing 0.8 M NaCl, 2 mM $CaCl_2$, and 2 mM $MnCl_2$ and applied to the lentil lectin-Sepharose. Elution with 20 mM Tris-HCl, pH 7.4, containing 0.5 M NaCl and 0.3 M Met-α-D-Man (Sigma), was performed after several washes with 20 mM Tris-HCl (pH 7.4) containing 0.5 M NaCl, 1 mM $CaCl_2$, and 1 mM $MnCl_2$. rhGCPII-containing fractions were pooled and dialyzed against 20 mM MOPS (pH 7.4) containing 150 mM NaCl. Finally, concentrated pooled fractions were subjected to gel permeation chromatography on a Superdex HR200 column (16/60; Pharmacia) using the dialysis buffer.

The specifically *in vivo* biotinylated human ectodomain of GCPII (Avi-GCPII), with virtually identical activity to the nontagged variant (23), was expressed in S2 cells and purified as described previously (23). Briefly, 19× concentrated conditioned medium from S2 cells containing Avi-GCPII was mixed with equilibration buffer (450 mM NaCl and 300 mM Tris-HCl, pH 7.2) in a 2:1 ratio and incubated overnight with mutein resin. The resin was separated from the medium with a disposable gravity column (Thermo Fisher Scientific, Rockford, IL, USA) and washed by 50 column volumes with 100 mM Tris-HCl (pH 7.2) containing 150 mM NaCl. The protein was then eluted with 100 mM Tris-HCl (pH 7.2) containing 150 mM NaCl and 2 mM D-biotin.

Preparation of image of structural insight into active site of GCPII

The image was prepared using a structure of GCPII in complex with a urea-based inhibitor (PDB code 3D7H) using the PyMOL Molecular Graphics System (version 0.99rc6, Schrödinger, Portland, OR, USA).

GCPII activity determination

GCPII activity was analyzed using a radioenzymatic assay with [^{3}H]-Ac-Asp-Glu (radiolabeled on the glutamate; Perkin-Elmer, Waltham, MA, USA) according to the previously described protocol (24) with minor modifications. Briefly, 10 ng of purified rhGCPII or Avi-GCPII was diluted in reaction buffer (25 mM Tris-HCl, 50 mM NaCl, and 1 mM $CaCl_2$, pH 8) to a final volume of 90 μl and preincubated for 5 min at 37°C. The reaction was started by addition of 10 μl substrate solution (final concentrations were 5 nM radiolabeled N-Ac-Asp-Glu and a 95 nM unlabeled N-Ac-Asp-Glu). As a negative control, a separate reaction containing 500 nM 2-(phosphonomethyl)pentanedioic acid (2-PMPA), a specific GCPII inhibitor, was performed. The reactions were incubated at 37°C for 80 min and stopped by addition of 100 μl 2 mM β-mercaptoethanol in 200 mM sodium phosphate (pH 7.4). The free glutamate was then separated by anion exchange chromatography, Rotiszint ECO Plus scintillation cocktail (Carl Roth, Karlsruhe, Germany) was added, and the radiolabeled hydrolysis product was quantified by a TriCarb 2900TR liquid scintillation counter (PerkinElmer).

Active site titration of Avi-GCPII

An active site titration was performed as described previously (23). Briefly, reaction mixtures containing buffer (20 mM NaCl and 20 mM MOPS, pH 7.4), 2-PMPA (final concentration from 0 to 500 nM), and the amount of enzyme necessary for 10–15% substrate turnover were preincubated for 10 min at 37°C. Reactions were started by addition of substrate (N-Ac-Asp-Met in final concentration 100 μM), incubated for 10 min at 37°C and terminated by addition of ice-cold stopping buffer (0.2 M sodium borate, pH 10.0, and 4 μM L-glutamate as an internal standard). The amount of formed L-methionine was determined after *o*-phtaldialdehyde derivatization by HPLC (Agilent 1200 series, Agilent Technologies; AccQ-Tag Ultra column 2.1×100 mm, Waters, Milford, MA, USA). The active site concentrations were calculated using the GraFit program (Erithacus Software, Horley, UK).

Sodium dodecyl sulfate–polyacrylamide gel electrophoresis (SDS-PAGE)

The purity of enzyme samples was established by SDS-PAGE. Samples were diluted in reducing buffer with final concentration 58.3 mM Tris-HCl, 5% glycerol (v/v), 1.6% SDS (w/v), and 0.66% mercaptoethanol (v/v) and denatured by heating to 95°C for 5 min. The proteins were then resolved on 11% polyacrylamide gel (w/v) and silver stained.

Proteolytic digestion of Aβ_{1-42}

An aliquot of disaggregated Aβ_{1-42} was dissolved in 2 mM NaOH immediately before performing digestion to prevent isoelectric precipitation (25). After 10 min, the pH was adjusted to 8.1 by adding an equal volume of 50 mM Tris-HCl

(pH 8.0) containing 100 mM NaCl and 2 mM $CaCl_2$. The final concentration of the reaction mixture was 25 mM Tris, 50 mM NaCl, 1 mM $CaCl_2$, and 26 μM $A\beta_{1-42}$.

The freshly prepared solution of $A\beta_{1-42}$ (~2.6 nmol/reaction) was subjected to digestion by Avi-GCPII (molar ratio $A\beta_{1-42}$/Avi-GCPII of 80:1). As positive controls for amyloid peptide cleavage, the $A\beta_{1-42}$ was digested by chymotrypsin (ref. 26; Roche Applied Science, Penzberg, Germany; molar ratio $A\beta_{1-42}$/chymotrypsin of 81:1). All samples were incubated at 37°C for 12 h.

In situ preparation of $A\beta_{1-42}$

To prevent substrate aggregation prior to proteolytic digestion, an alternative approach using *in situ* generation of Aβ monomer from the depsipeptide precursor was used. A fresh aliquot of depsi(25,26)$A\beta_{1-42}$ was mixed with buffer to yield a final concentration of 25 mM Tris, 50 mM NaCl, 1 mM $CaCl_2$, and 50 μM depsi(25,16)$A\beta_{1-42}$ (pH 8.0). The self-isomerization was complete after incubation at 37°C for 1 h. Isomerization was confirmed by HPLC analysis (data not shown).

The $A\beta_{1-42}$ substrate (~3.75 nmol/reaction) was digested by rhGCPII, Avi-GCPII, and chymotrypsin as described above with slightly modified molar ratios ($A\beta_{1-42}$/Avi-GCPII, 120:1; $A\beta_{1-42}$/rhGCPII, 140:1; $A\beta_{1-42}$/chymotrypsin, 117:1). Recombinant glutamate carboxypeptidase III (GCPIII; molar ratio $A\beta_{1-42}$/GCPIII of 100:1) and neprilysin (R&D Systems, Minneapolis, USA, molar ratio $A\beta_{1-42}$/neprilysin of 100:1) were used as further controls. Corresponding controls without added substrate or enzyme were performed under identical conditions. All samples were incubated at 37°C for 12 h.

Analysis of the reaction mixtures by liquid chromatography mass spectrometry (LC-MS) analysis

LC-MS analysis was performed using an LCQ Fleet instrument (Thermo Fisher Scientific), which is a 3-dimensional (3D) ion-trap mass spectrometer coupled to HPLC by a 1:4 splitter. The HPLC was performed on a C8 reverse-phase column (Phenomenex, Torrance, CA, USA) with 1 ml/min flow using an acetonitrile/water gradient (5–52.6% in 30 min) with 0.1% formic acid and 0.4% HFIP additives at high temperature (80°C). Samples after proteolytic digestion were either analyzed immediately or stored on ice prior analysis to prevent excessive aggregation. Each analysis was performed with 30% of the reaction volume.

RESULTS

To analyze the potential processing of Aβ by GCPII, we used 2 independent recombinant protein preparations. First, we used a highly purified recombinant GCPII ectodomain spanning aa 44–750, expressed and purified as published (denominated rhGCPII; ref. 14), which includes the complete extracellular part of the enzyme in which the proteolytic activity of GCPII resides (14). Alternatively, we used the same GCPII ectodomain with a short peptide tag (biotin acceptor peptide) introduced to the N terminus of the protein (23). This tag was biotinylated by *E. coli* biotin ligase *in vivo*, and the active recombinant enzyme was expressed in *Drosophila* Schneider 2 cells as a secreted protein and

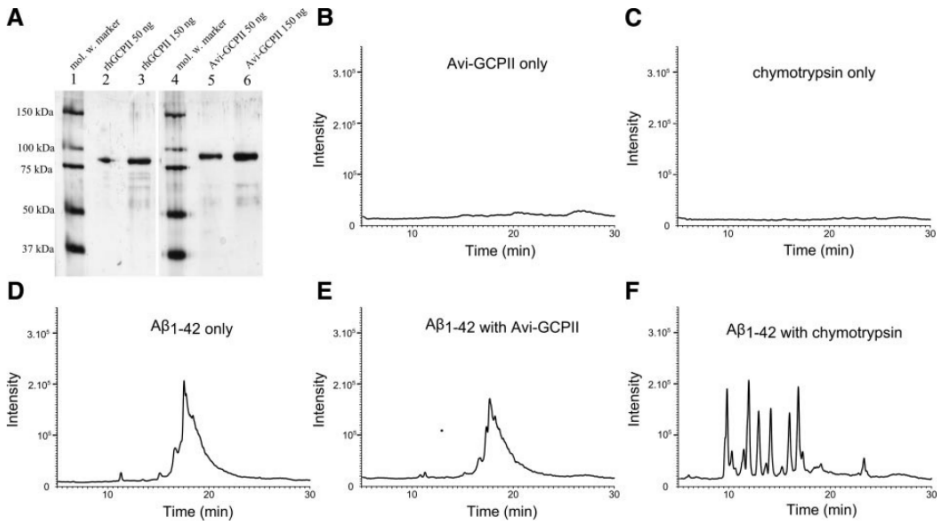

Figure 1. HPLC-MS analysis (total ion current chromatograms) of reaction mixtures and controls of hydrolysis of $A\beta_{1-42}$ generated *in situ* (~3.75 nmol/reaction). *A*) SDS-PAGE showing the purity of GCPII preparations used in this study. Lanes 1 and 4, molecular weight markers; lanes 2 and 5, 50 ng of rhGCPII or Avi-GCPII, respectively; lanes 3 and 6, 150 ng of rhGCPII or Avi-GCPII, respectively. *B–F*) Reaction mixtures contained Avi-GCPII only (*B*), chymotrypsin only (*C*), $A\beta_{1-42}$ only (*D*), $A\beta_{1-42}$ with Avi-GCPII (*E*), and $A\beta_{1-42}$ with chymotrypsin (*F*). All reactions were performed in buffer containing 25 mM Tris-HCl, 50 mM NaCl, and 1 mM $CaCl_2$. Reaction mixtures were incubated at 37°C for 12 h.

purified to homogeneity by affinity chromatography (denominated Avi GCPII; see **Fig. 1*A***).

GCPII activity in the reaction buffer (25 mM Tris-HCl, 50 mM NaCl, 1 mM $CaCl_2$) was confirmed by radioenzymatic assay, based on hydrolysis of radiolabeled N-Ac-Asp-Glu substrate and subsequent detection of free glutamate. While in the presence of a specific GCPII inhibitor the substrate showed almost no hydrolysis (2%), the conversion of noninhibited reaction reached 67.5% (see Supplemental Fig. S3). This is in good agreement with our previous analysis showing that the pH optimum for GCPII activity is in the mild alkaline region (27). The enzymatically active fraction of purified Avi-GCPII was determined by active site titration by tight binding inhibitor to be 102 ± 2%. Because commercially available preparations of Aβ were in our hands either not sufficiently pure or prone to rapid aggregation preventing further analysis (data not shown), we synthesized $A\beta_{1-42}$ by 2 independent methods. In one method, $A\beta_{1-42}$ was prepared by standard stepwise coupling of the corresponding Fmoc-amino acids on Fmoc-Ala-Wang resin. The peptide was purified by reverse-phase HPLC, and the pooled fractions corresponding to the purified product were immediately frozen in liquid nitrogen and lyophilized. Because even this peptide product was prone to rapid aggregation, the peptide was subjected to a disaggregation procedure (18). Freshly prepared disaggregated $A\beta_{1-42}$ was dissolved in 2 mM NaOH immediately before proteolytic digestion to prevent isoelectric precipitation (25). The pH of the solution was adjusted to 8.1, and the reaction was started by addition of Avi-GCPII or chymotrypsin as a positive control. Chymotrypsin has been reported to degrade Aβ peptide efficiently *in vivo* (26). All samples were incubated at 37°C for 12 h, and the resulting reaction mixtures were analyzed with a 3D ion-trap mass spectrometer coupled to HPLC. HPLC analysis showed only traces of $A\beta_{1-42}$ substrate in the mixture and no peptide fragments corresponding to the presumed cleavage products, while the control experiments using chymotrypsin showed significant $A\beta_{1-42}$ degradation (data not shown). This experiment showed no indication of proteolytic degradation of $A\beta_{1-42}$ by GCPII. However, the rapid substrate aggregation depleted most of the substrate monomer from the reaction mixture, which made the subsequent HPLC/MS analysis cumbersome (26).

To improve the solubility of $A\beta_{1-42}$ and slow down its aggregation, we prepared $A\beta_{1-42}$ by *in situ* isomerization of depsi(25,26)$A\beta_{1-42}$ synthesized on solid support using a modification of an established protocol (19). The protocol was improved by introduction of a building block with a preformed depsipeptide linkage, rather than forming the linkage *in situ*. This procedure yields final peptide product from a more soluble depsipeptide precursor by *N-O* acyl shift in weakly basic pH *in situ*, just prior to the proteolytic digestion (see Supplemental Fig. S1). The completeness of the isomerization was confirmed by HPLC analysis (data not shown). Using this procedure, we were able to prepare milligram quantities of pure, soluble $A\beta_{1-42}$ that could be subjected to hydrolysis by proteases in a standard biochemical setup.

Using this soluble substrate, we performed a series of digestions of $A\beta_{1-42}$ at 37°C for 12 h with Avi-GCPII or rhGCPII and bovine chymotrypsin as a positive control. The enzyme:substrate molar ratios were 1:117 for Avi-GCPII and 1:140 for rhGCPII, ensuring that even a weak hydrolytic activity would be identified. Corresponding digestions in the absence of substrate or enzyme were performed under identical conditions. The reaction mixtures were subsequently analyzed by reverse-phase HPLC-MS, summarized in Fig. 1. The data (total ion current spectra obtained from LC-MS analysis of the reaction mixtures) show no substrate degradation by rhGCPII (data not shown) or Avi-GCPII (Fig. 1*B, E*), while chymotrypsin cleaves $A\beta_{1-42}$ peptide very efficiently under identical conditions (Fig. 1*C, F*), and the molecular masses of the products correspond to theoretical predictions (28). We conclude that GCPII does not degrade $A\beta_{1-42}$ *in vitro*.

To ensure specificity of the cleavage, the proper conformation of amyloid peptide substrate and rule out possible involvement of a a homologue of GCPII in the putative degradation of $A\beta_{1-42}$, we analyzed the proteolytic degradation of the substrate with neprilysin, a known $A\beta_{1-42}$ processing enzyme, and recombinant human glutamate carboxypeptidase III (GCPIII), the closest homologue of GCPII (27). While neprilysin effectively processed $A\beta_{1-42}$, no hydrolysis was observed even after prolonged incubation with excess of recombinant human GCPIII (Supplemental Fig. S2).

DISCUSSION

To analyze potential proteolytic degradation of any peptide or protein, pure soluble preparations of the enzyme and the substrate are required. The report (11) describing the surprising observation that GCPII cleaves Aβ *in vitro* does not provide the reaction conditions in which the hydrolysis was performed. Therefore, in our experiments, we used highly purified, well-characterized enzyme and substrate preparations under conditions as favorable to possible proteolytic cleavage as possible. We used two different recombinant enzyme preparations: GCPII ectodomain spanning aa 44–750, which includes the whole extracellular part of the enzyme, and the same sequence cloned with a short peptide tag encompassing a biotin acceptor peptide that enables *in vivo* biotinylation of the recombinant protein for facile affinity purification. This procedure yields milligram quantities of soluble, crystallizable recombinant protein with enzymatic activity identical to that of the native protein. Our previously published experiments confirmed that the affinity tag does not affect the activity, 3D structure, or any biophysical properties of its fusion partner (23). Both procedures yielded recombinant proteins of identical purity and specific activity against cognate substrate of

GCP II, *N*-acetylaspartyl glutamate. In analogy, the substrate was also prepared by 2 independent methods. First, it was synthesized by standard stepwise approach on solid resin using Fmoc-protected amino acids, yielding pure Aβ peptide that in aqueous conditions rapidly aggregated. Second, we prepared the same $A\beta_{1-42}$ by *in situ* isomerization of corresponding depsi(25,26)$A\beta_{1-42}$, also synthesized on solid support. This approach yields pure, soluble peptide that could be subjected to enzymatic hydrolysis prior to aggregation. Regardless of the preparation method, no degradation of the peptide substrate by pure recombinant GCPII was observed using LC-MS detection, while the control digestion by chymotrypsin or specific $A\beta_{1-42}$-degrading enzyme neprilysin yielded almost completely degraded peptide substrate. The closest homologue of GCPII, human glutamate carboxypeptidase III, also did not show any hydrolysis of $A\beta_{1-42}$ even after prolonged incubation with excess enzyme.

Interestingly, under prolonged, overnight incubation of the substrate with very high concentration of both rhGCPII and Avi GCPII, we observed minor cleavage of the N-terminal Asp residue from the Aβ. This minor aminopeptidase activity was sensitive to 2-PMPA, a specific inhibitor of GCPII, and was confirmed using shorter peptide with N-terminal Asp (data not shown). Minor aminopeptidase activity of GCPII is not entirely unexpected: The enzyme belongs to the M28 metallopeptidase family, and its closest structural homologue is an aminopeptidase from *Streptomyces griseus* (29). However, this very minor side activity could not have any physiological consequence and cannot be responsible for Aβ degradation reported by (11).

Kim *et al.* (11) attributed the $A\beta_{1-42}$-hydrolyzing activity of GCPII to an unknown, alternative catalytic mechanism of the enzyme, noting that the observed activity was partially inhibited by 2-PMPA, a very potent GCPII inhibitor. This suggestion is, however, incompatible with the currently available, very detailed structural information about the mechanism of action of GCPII (12, 30, 31). GCPII possesses a single active site, and a major structural change leading to an alternative mechanism of action is difficult to imagine.

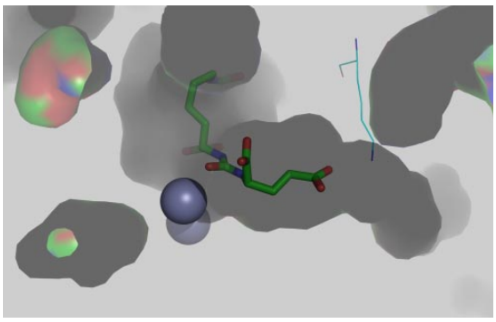

Figure 2. Structural insight into the active site of GCPII. The active site cavity of GCPII is shown in surface representation, the inhibitor *N*-{[(1*S*)-1-carboxy-5-{[(4-iodophenyl)carbonyl]amino}pentyl]carbamoyl}-L-glutamic acid inside the active site in stick representation, and Lys 699 that closes the bottom of the subsite binding pocket in line representation. Nitrogen atoms are depicted in blue, carbon atoms in green, and oxygen atoms in red. The 2 zinc ions are shown as gray spheres.

Furthermore, the distribution of fragments reported by Kim *et al.* ($A\beta_{1-X}$, X=14–20, 33, 34, and 38; ref. 11) suggests that GCPII acts as an endopeptidase. Again, the available structural data does not support such a notion, because the architecture of the binding cleft would have to undergo a very dramatic structural change (see **Fig. 2**).

In summary, we provide experimental evidence that GCPII does not degrade $A\beta_{1-42}$ peptide, and we also show that there are fundamental structural reasons for the lack of endoproteolytic activity of the enzyme. Therefore, there is no direct causative link between the GCPII inhibition and the amyloid formation *in vivo*, suggested by Kim *et al.* (11). FJ

The authors thank Tomáš Knedlík for the GCPII activity determination by radioenzymatic assay and Radko Souček for skillful amino acid analysis of $A\beta_{1-42}$ samples. This research was funded by grant P304/12/0847 from the Grant Agency of the Czech Republic.

REFERENCES

1. Plassman, B. L., Langa, K. M., Fisher, G. G., Heeringa, S. G., Weir, D. R., Ofstedal, M. B., Burke, J. R., Hurd, M. D., Potter, G. G., Rodgers, W. L., Steffens, D. C., Willis, R. J., and Wallace, R. B. (2007) Prevalence of dementia in the United States: the aging, demographics, and memory study. *Neuroepidemiology* **29,** 125–132
2. Thies, W., and Bleiler, L. (2011) 2011 Alzheimer's disease facts and figures. *Alzheimers Dement.* **7,** 208–244
3. O'Brien, R. J., and Wong, P. C. (2011) Amyloid precursor protein processing and Alzheimer's disease. *Annu. Rev. Neurosci.* **34,** 185–204
4. Selkoe, D. J. (1999) Translating cell biology into therapeutic advances in Alzheimer's disease. *Nature* **399,** A23–A31
5. Wang, Y. J., Zhou, H. D., and Zhou, X. F. (2006) Clearance of amyloid-beta in Alzheimer's disease: progress, problems and perspectives. *Drug Discov. Today* **11,** 931–938
6. Carson, J. A., and Turner, A. J. (2002) Beta-amyloid catabolism: roles for neprilysin (NEP) and other metallopeptidases? *J. Neurochem.* **81,** 1–8
7. Wang, D. S., Dickson, D. W., and Malter, J. S. (2006) Beta-amyloid degradation and Alzheimer's disease. *J. Biomed. Biotechnol.* **2006,** 58406
8. Selkoe, D. J., Xia, W., Kimberly, W. T., Vekrellis, K., Walsh, D., Esler, W. P., and Wolfe, M. S. (2001) Mechanisms of Aβ production and Aβ degradation: routes to the treatment of Alzheimer's disease. In *Alzheimer's Disease: Advances in Etiology, Pathology, and Therapeutics* (Iqbal, K., Sisodia, S. S., and Winblad, B., eds) pp. 421–432, John Wiley & Sons, New York
9. Yamin, R., Zhao, C., O'Connor, P. B., McKee, A. C., and Abraham, C. R. (2009) Acyl peptide hydrolase degrades monomeric and oligomeric amyloid-beta peptide. *Mol. Neurodegener.* **4,** 33
10. Hamazaki, H. (1996) Cathepsin D is involved in the clearance of Alzheimer's beta-amyloid protein. *FEBS Lett.* **396,** 139–142
11. Kim, M. J., Chae, S. S., Koh, Y. H., Lee, S. K., and Jo, S. A. (2010) Glutamate carboxypeptidase II: an amyloid peptide-degrading enzyme with physiological function in the brain. *FASEB J.* **24,** 4491–4502
12. Hlouchová, K., Barinka, C., and Konvalinka, J. (2012) Glutamate carboxypeptidase II as a therapeutic target. In *Proteinases as Drug*

Targets (Dunn, B. M., ed) pp. 63–95, Royal Society of Chemistry Publishing, Cambridge, UK
13. Barinka, C., Rojas, C., Slusher, B., and Pomper, M. (2012) Glutamate carboxypeptidase II in diagnosis and treatment of neurologic disorders and prostate cancer *Curr. Med. Chem.* **19,** 856–870
14. Barinka, C., Rinnova, M., Sacha, P., Rojas, C., Majer, P., Slusher, B. S., and Konvalinka, J. (2002) Substrate specificity, inhibition and enzymological analysis of recombinant human glutamate carboxypeptidase II. *J. Neurochem.* **80,** 477–487
15. Barinka, C., Mlcochova, P., Sacha, P., Hilgert, I., Majer, P., Slusher, B. S., Horejsi, V., and Konvalinka, J. (2004) Amino acids at the N- and C-termini of human glutamate carboxypeptidase II are required for enzymatic activity and proper folding. *Eur. J. Biochem.* **271,** 2782–2790
16. Plechanovova, A., Byun, Y., Alquicer, G., Skultetyova, L., Mlcochova, P., Nemcova, A., Kim, H. J., Navratil, M., Mease, R., Lubkowski, J., Pomper, M., Konvalinka, J., Rulisek, L., and Barinka, C. (2011) Novel substrate-based inhibitors of human glutamate carboxypeptidase II with enhanced lipophilicity. *J. Med. Chem.* **54,** 7535–7546
17. Barinka, C., Hlouchova, K., Rovenska, M., Majer, P., Dauter, M., Hin, N., Ko, Y. S., Tsukamoto, T., Slusher, B. S., Konvalinka, J., and Lubkowski, J. (2008) Structural basis of interactions between human glutamate carboxypeptidase II and its substrate analogs. *J. Mol. Biol.* **376,** 1438–1450
18. Zagorski, M. G., Yang, J., Shao, H. Y., Ma, K., Zeng, H., and Hong, A. (1999) Methodological and chemical factors affecting amyloid beta peptide amyloidogenicity. *Methods Enzymol.* **309,** 189–204
19. Carpino, L. A., Krause, E., Sferdean, C. D., Schumann, M., Fabian, H., Bienert, M., and Beyermann, M. (2004) Synthesis of 'difficult' peptide sequences: application of a depsipeptide technique to the Jung-Redemann 10- and 26-mers and the amyloid peptide A beta(1–42). *Tetrahedron Lett.* **45,** 7519–7523
20. Fields, G. B., and Noble, R. L. (1990) Solid-phase peptide-synthesis utilizing 9-fluorenylmethoxycarbonyl amino-acids. *Int. J. Peptide Protein Res.* **35,** 161–214
21. Kaiser, E., Colescot.Rl, Bossinge.Cd, and Cook, P. I. (1970) Color test for detection of free terminal amino groups in solid-phase synthesis of peptides. *Anal. Biochem.* **34,** 595–598
22. Sarin, V. K., Kent, S. B. H., Tam, J. P., and Merrifield, R. B. (1981) Quantitative monitoring of solid-phase peptide-synthesis by the ninhydrin reaction. *Anal. Biochem.* **117,** 147–157
23. Tykvart, J., Sacha, P., Barinka, C., Knedlik, T., Starkova, J., Lubkowski, J., and Konvalinka, J. (2012) Efficient and versatile one-step affinity purification of in vivo biotinylated proteins: expression, characterization and structure analysis of recombinant human glutamate carboxypeptidase II. *Protein Express Purification* **82,** 106–115
24. Robinson, M. B., Blakely, R. D., Couto, R., and Coyle, J. T. (1987) Hydrolysis of the brain dipeptide N-acetyl-L-aspartyl-L-glutamate—identification and characterization of a novel N-acetylated alpha-linked acidic dipeptidase activity from rat-brain. *J. Biol. Chem.* **262,** 14498–14506
25. O'Nuallain, B., Thakur, A. K., Williams, A. D., Bhattacharyya, A. M., Chen, S. M., Thiagarajan, G., and Wetzel, R. (2006) Kinetics and thermodynamics of amyloid assembly using a high-performance liquid chromatography-based sedimentation assay. *Methods Enzymol.* **413,** 34–74
26. Numata, K., and Kaplan, D. L. (2010) Mechanisms of enzymatic degradation of amyloid beta microfibrils generating nanofilaments and nanospheres related to cytotoxicity. *Biochemistry* **49,** 3254–3260
27. Hlouchova, K., Barinka, C., Klusak, V., Sacha, P., Mlcochova, P., Majer, P., Rulisek, L., and Konvalinka, J. (2007) Biochemical characterization of human glutamate carboxypeptidase III. *J. Neurochemi.* **101,** 682–696
28. Wilkins, M. R., Lindskog, I., Gasteiger, E., Bairoch, A., Sanchez, J. C., Hochstrasser, D. F., and Appel, R. D. (1997) Detailed peptide characterization using PEPTIDEMASS—a World-Wide-Web-accessible tool. *Electrophoresis* **18,** 403–408
29. Yoo, C., Ahn, K., Park, J. E., Kim, M. J., and Jo, S. A. (2010) An aminopeptidase from *Streptomyces* sp. KK565 degrades beta amyloid monomers, oligomers, and fibrils. *FEBS Lett.* **584,** 4157–4162
30. Klusak, V., Barinka, C., Plechanovova, A., Mlcochova, P., Konvalinka, J., Rulisek, L., and Lubkowski, J. (2009) Reaction mechanism of glutamate carboxypeptidase II revealed by mutagenesis, x-ray crystallography, and computational methods. *Biochemistry* **48,** 4126–4138
31. Hlouchova, K., Navratil, V., Tykvart, J., Sacha, P., and Konvalinka, J. (2012) GCPII Variants, paralogs and orthologs. *Curr. Med. Chem.* **19,** 1316–1322

Received for publication December 19, 2012.
Accepted for publication March 11, 2013.

Příloha 5

Received: 8 June 2018 | Accepted: 21 August 2018
DOI: 10.1002/pros.23717

ORIGINAL ARTICLE

WILEY The Prostate

A novel PSMA/GCPII-deficient mouse model shows enlarged seminal vesicles upon aging

Barbora Vorlová MSc[1,2] | František Sedlák MD[1,2,3] | Petr Kašpárek PhD[4,5] | Karolína Šrámková MSc[1] | Marek Malý PhD[6] | Josef Zámečník MD, PhD[7] | Pavel Šácha PhD[1] | Jan Konvalinka PhD[1,8]

[1] Institute of Organic Chemistry and Biochemistry of the Czech Academy of Sciences, Prague 6, Czech Republic

[2] First Faculty of Medicine, Charles University, Prague 2, Czech Republic

[3] Faculty of Science, Department of Genetics and Microbiology, Charles University, Prague 2, Czech Republic

[4] Laboratory of Transgenic Models of Diseases, Institute of Molecular Genetics of the Czech Academy of Sciences, Vestec, Czech Republic

[5] Czech Centre for Phenogenomics, Institute of Molecular Genetics of the Czech Academy of Sciences, Vestec, Czech Republic

[6] National Institute of Public Health, Prague 10, Czech Republic

[7] Department of Pathology and Molecular Medicine, Second Faculty of Medicine, Charles University and Motol University Hospital, Prague 5, Czech Republic

[8] Department of Biochemistry, Faculty of Science, Charles University, Prague 2, Czech Republic

Correspondence
Jan Konvalinka, Institute of Organic Chemistry and Biochemistry of the CAS, v.v.i, Flemingovo n. 2, 16610 Prague 6, Czech Republic.
Email: konval@uochb.cas.cz

Funding information
Czech Republic, Grant number: GA16-02938S; Ministry of Education, Youth and Sports of the Czech Republic, Grant numbers: LO1302, LM20150400; Academy of Sciences of the Czech Republic, Grant number: RVO 68378050

Background: Prostate-specific membrane antigen (PSMA), also known as glutamate carboxypeptidase II (GCPII), is an important diagnostic and therapeutic target in prostate cancer. PSMA/GCPII is also expressed in many healthy tissues, but its function has only been established in the brain and small intestine. Several research groups have attempted to produce PSMA/GCPII-deficient mice to study the physiological role of PSMA/GCPII in detail. The outcomes of these studies differ dramatically, ranging from embryonic lethality to production of viable PSMA/GCPII-deficient mice without any obvious phenotype.

Methods: We produced PSMA/GCPII-deficient mice (hereafter also referred as Folh1$^{-/-}$ mice) by TALEN-mediated mutagenesis on a C57BL/6NCrl background. Using Western blot and an enzyme activity assay, we confirmed the absence of PSMA/GCPII in our Folh1$^{-/-}$ mice. We performed anatomical and histopathological examination of selected tissues with a focus on urogenital system. We also examined the PSMA/GCPII expression profile within the mouse urogenital system using an enzyme activity assay and confirmed the presence of PSMA/GCPII in selected tissues by immunohistochemistry.

Results: Our Folh1$^{-/-}$ mice are viable, breed normally, and do not show any obvious phenotype. Nevertheless, aged Folh1$^{-/-}$ mice of 69-72 weeks exhibit seminal vesicle dilation, which is caused by accumulation of luminal fluid. This phenotype was also observed in Folh1$^{+/-}$ mice; the overall difference between our three cohorts (Folh1$^{-/-}$, Folh1$^{+/-}$, and Folh1$^{+/+}$) was highly significant ($P < 0.002$). Of all studied tissues of the mouse urogenital system, only the epididymis appeared to have a physiologically relevant level of PSMA/GCPII expression. Additional experiments demonstrated that PSMA/GCPII is also present in the human epididymis.

Conclusions: In this study, we provide the first evidence characterizing the reproductive tissue phenotype of PSMA/GCPII-deficient mice. These findings will help lay the groundwork for future studies to reveal PSMA/GCPII function in human reproduction.

KEYWORDS
dilated seminal vesicles, Folh1, glutamate carboxypeptidase II, knockout mice, prostate-specific membrane antigen

1 | INTRODUCTION

Prostate-specific membrane antigen (PSMA),[1] also known as glutamate carboxypeptidase II (GCPII),[2,3] is a transmembrane glycoprotein that is overexpressed in prostate cancer[4,5] and is regarded as an important diagnostic target and suitable molecular address for anticancer drug delivery.[6,7] PSMA/GCPII consists of short intracellular and transmembrane domains and a large extracellular domain with carboxypeptidase activity.[8,9] Under physiological conditions, PSMA/GCPII is primarily expressed in the prostate, brain, small intestine, and kidney.[4,10–14] However, the function of the enzyme has only been established in the brain and small intestine. In the brain, it cleaves the most abundant peptide neurotransmitter, N-acetyl-L-aspartyl-L-glutamate (NAAG), to yield N-acetyl-L-aspartate and L-glutamate, an important neurotransmitter.[15,16] In the small intestine, PSMA/GCPII cleaves poly-gamma-glutamylated folates and thus enables folate absorption.[1,17] The role of PSMA/GCPII in other tissues, most notably in the urogenital system, remains enigmatic.

PSMA/GCPII has several homologues in the human genome.[18] The only one with similar enzymatic activity is glutamate carboxypeptidase III (GCPIII),[19,20] which shares 67% amino acid identity and 81% amino acid similarity with PSMA/GCPII.[19,21] While the protein expression profile of GCPIII in human tissues has been addressed in only one report, it seems to be similar to that of PSMA/GCPII.[22] The most notable differences were found in the urogenital system. While GCPIII was detected in the highest amounts in human testis, its expression level in the prostate was much lower than that of PSMA/GCPII.

To understand the physiological role of PSMA/GCPII in more detail, several independent research groups have studied the consequences of inactivating the PSMA/GCPII-encoding gene *Folh1* in mice.[23–26] Surprisingly, the outcomes of these studies differ markedly. While some studies concluded that the PSMA/GCPII knockout is embryonically lethal,[24,25] others found that inactivating *Folh1* results in viable PSMA/GCPII-deficient mice with normal breeding performance and no obvious phenotype.[23,26]

Viable PSMA/GCPII-deficient mice have been used in studies to evaluate PSMA/GCPII function in the nervous system.[23,26–28] Although no significant differences between PSMA/GCPII-deficient and wild-type (WT) mice were observed in standard neurological behavioral tests, PSMA/GCPII-deficient mice showed lower susceptibility to peripheral neuropathies and traumatic brain injury, as well as improved long-term behavioral outcomes after traumatic brain injury.[26,27] Recently, the International Mouse Phenotyping Consortium (IMPC) incorporated PSMA/GCPII-deficient mice into the primary phenotyping pipeline and published the first results.[29] No clear phenotype has been revealed to date, but the set of phenotyping data is still not complete.

It remains unclear why such different outcomes of *Folh1* gene inactivation in mice have been observed. All attempts to date to prepare transgenic animals with impaired PSMA/GCPII have been performed by embryonic stem (ES) cell manipulation. The main methodological differences lie in the design of the targeting cassette. Embryonic lethality resulted after deletion of either exons 1 and 2 or exons 9 and 10 within the *Folh1* gene.[24,25] On the other hand, insertion of three stop codons between exons 1 and 2, deletion of exons 3-5, or deletion of exon 3 within the *Folh1* gene led to production of viable mice.[23,26,29] Of all the *Folh1* inactivation attempts, only one study has aimed to disrupt the active site of PSMA/GCPII (by deletion of exons 9 and 10) and thus avoid possible preservation of PSMA/GCPII enzyme activity by alternative mRNA splicing.[24] However, this attempt did not result in production of viable PSMA/GCPII-deficient mice.

Here, we describe production of PSMA/GCPII-deficient mice (hereafter also referred as Folh1$^{-/-}$ mice) by disrupting the PSMA/GCPII active site using a strategy different than ES cell manipulation—manipulation of mouse zygotes by targeted nucleases. We designed transcription activator-like effector nucleases (TALENs) that specifically cleave exon 11 of the *Folh1* gene within the sequence encoding the PSMA/GCPII active site. This strategy led to full loss of PSMA/GCPII protein expression in Folh1$^{-/-}$ mice. Our Folh1$^{-/-}$ mice were viable, able to breed normally, and did not show any obvious phenotype. As PSMA/GCPII function in the brain has been thoroughly studied using PSMA/GCPII-deficient mice by others, we focused on the mouse urogenital system. We found that aged Folh1$^{-/-}$ mice have an increased propensity for enlarged seminal vesicles compared with their WT littermates, and we explored the possible source of this phenomenon.

2 | MATERIALS AND METHODS

2.1 | Generation of Folh1$^{-/-}$ mice

All animal procedures were ethically reviewed and performed in accordance with European directive 2010/63/EU and were approved by the Czech Central Commission for Animal Welfare. Folh1$^{-/-}$ mice were generated by TALEN-mediated genome editing. TALENs were designed to target exon 11 of the *Folh1* gene, which encodes PSMA/GCPII. The following TALEN-repeat domain sequences were used: Left TALEN, NG NG NN HD NI NI NN HD NG NN NN NN NI NG NN; right TALEN, HD NI NN NG NI NN NI NI HD HD NI NI NN NI NI. TALEN RNA precursors were generated and microinjected into male nucleoli of zygotes isolated from C57BL/6NCrl mice as previously described.[30] These zygotes were subsequently implanted into pseudopregnant females. Tail biopsies from newborn pups were analyzed for the presence of TALEN-mediated mutations using Sanger sequencing. Briefly, chromosomal DNA was first isolated from tail biopsies using phenol-chloroform extraction. PCR with the primers F1 (5′-GGGCTATGCATTTTTCAGGA-3′) and R1 (5′-GCAGCAAGTGCCTTAACCAG-3′) was performed, generating fragments of approximately 500 bp (546 bp for the WT allele). PCR products were separated by agarose electrophoresis, isolated from the gel and ligated into pCRII-TOPO vector using TOPO TA Cloning Kit (Invitrogen, Carlsbad, CA). The resulting plasmids were sequenced using M13 Reverse primer supplied in the TOPO TA Cloning Kit. Founder mice carrying deletions of 3 bp (del3), 4 bp (del4), and 17 bp (del17) within exon 11 of the *Folh1* gene were bred with a WT C57Bl/6NCrl mice to obtain the F1 generation. The mice used in this study were offspring of the F2 generation or subsequent generations.

2.2 | Folh1$^{-/-}$ mice genotyping

Chromosomal DNA was isolated from tail biopsies using QuickExtract DNA Extraction Solution (Epicentre, Madison, WI). Genotyping was performed by nested PCR, which consisted of two successive rounds of PCR. In the first round, primers F1 and R1 (see above for sequences) were used to amplify a fragment of approximately 540 bp (546 bp for WT allele, 543 bp for del3 allele, 542 bp for del4 allele, and 529 bp for del17 allele). Reactions from the first round of PCR were diluted 200-fold and served as templates for the second round of PCR using primers F2 (5′-ATTTTGTTTGCAAGCTGG-3′) and R2 (5′-CACTCAGTAGAACCAAGAAGG-3′). Amplified fragments of specific length (56 bp for WT allele, 53 bp for del3 allele, 52 bp for del4 allele, 39 bp for del17 allele) were analyzed by DNA polyacrylamide gel electrophoresis in TBE followed by GelRed post-staining (Biotinum, Fremont, CA).

2.3 | Preparation of rm-GCPII

The extracellular portion of mouse GCPII (rm-GCPII) was prepared as previously described.[31] Briefly, large scale expression was performed using *Drosophila* S2 (BiP-BirA-KDEL) cells[32] stably transfected with a plasmid encoding rm-GCPII (pMT/BiP/AvimGCPII).[31] Biotinylated rm-GCPII was purified from S2 cell media using Streptavidin Mutein Matrix (Roche, Basel, Switzerland).[32] rm-GCPII protein solution containing D-biotin was subsequently purified by size-exclusion chromatography using a HiLoad™ Superdex™ 200 10/300 GL column (GE-Healthcare, Chicago, IL) as a solid phase and buffer consisting of 10 mM Tris-HCl, pH 7.4, 150 mM NaCl as a mobile phase. The protein concentration was determined using quantitative amino acid analysis (Biochrom, Cambridge, UK) following the manufacturer's protocol.

2.4 | Cloning of vector encoding rm-GCPIIdel17

Site-directed mutagenesis was carried out using pMT/BiP/AvimGCPII[31] as a template according to the manufacturer's protocol (Phusion Site-Directed Mutagenesis Kit, Thermo Fisher Scientific, Waltham, MA). Four consecutive mutageneses were performed. First, a deletion of 6 bp within pMT/BiP/AvimGCPII (pMT/BiP/AvimGCPIIdel6) was introduced using primers 5′-TGCAAGCTGGGATGCAGAAGGCCTTCTTGGTTCTACTG-3′ and 5′-CAGTAGAACCAAGAAGGCCTTCTGCATCCCAGCTTGCA-3′. Subsequently, pMT/BiP/AvimGCPII with a 9-bp deletion of was prepared from pMT/BiP/AvimGCPIIdel6 using primers 5′-TTTGTTTGCAAGCTGGGATGAAGGCCTTCTTGGTTCTACT-3′ and 5′-AGTAGAACCAAGAAGGCCTTCATCCCAGCTTGCAAACAAA-3′ followed by preparation of pMT/BiP/AvimGCPII with a deletion of 12 bp using primers 5′-TTTGTTTGCAAGCTGGGATGGCCTTCTTGGTTCTACTGAG-3′ and 5′-CTCAGTAGAACCAAGAAGGCCATCCCAGCTTGCAAACAAA-3′.
Finally, deletion of 17 bp within pMT/BiP/AvimGCPII (pMT/BiP/AvimGCPIIdel17) was prepared using pMT/BiP/AvimGCPIIdel12 as a template with primers 5′-CAATTTTGTTTGCAAGCTGGCCTTCTTGGTTCTACTGAGT-3′ and 5′-ACTCAGTAGAACCAAGAAGGCCAGCTTGCAAACAAAATTG-3′. To ensure that no other mutation was introduced into the vector during mutagenesis, the sequence of the resulting pMT/BiP/AvimGCPIIdel17 plasmid was verified by sequencing.

2.5 | Preparation of rm-GCPIIdel17

The recombinant protein rm-GCPIIdel17 was prepared similarly as previously described for rm-GCPII.[31] Briefly, *Drosophila* S2 (BiP-BirA-KDEL) cells[32] were co-transfected with the plasmids pMT/BiP/AvimGCPIIdel17 and pCoBlast (Invitrogen), followed by cell culture selection using cultivation of the transfectants in the presence of blasticidin (Invitrogen) and hygromycin B (Invitrogen). Prepared stably transfected cultures of S2 cells were tested for their ability to express rm-GCPIIdel17 using Western blot, and the cell culture expressing the highest amount of rm-GCPIIdel17 was used for large-scale expression. Large-scale expression was performed in a similar fashion as previously described for rh-GCPII.[33] Biotinylated rm-GCPIIdel17 was purified from S2 cell media by one-step purification using Streptavidin Mutein Matrix (Roche).[32] The protein concentration was determined using Bradford 1× Dye Reagent (Bio-Rad, Hercules, CA).

2.6 | Tissue lysate preparation

Mice were sacrificed by intraperitoneal anesthetic injection followed by cervical dislocation. The anesthetics used were a combination of either tiletamine (125 mg/kg), zolazepam (125 mg/kg), and xylazine (10 mg/kg) or ketamine (125 mg/kg), and xylazine (20 mg/kg). Tissues intended for Western blot and enzyme activity analysis were frozen on dry ice immediately after collection and stored at −80°C until further processing.

To ensure homogeneity during tissue lysis, whole organs were processed. The only exception was the brains, which were first split into two identical hemispheres, only one of which was subsequently used for the tissue lysis.

The mouse tissues were weighed and homogenized in lysis buffer (50 mM Tris-HCl, pH 7.4, 100 mM NaCl, 1× Roche cOmplete protease inhibitor cocktail; 3 µL of lysis buffer added per 1 mg of tissue) using TissueLyser II (Qiagen, Hilden, Germany). The homogenization process slightly differed between tissues. The kidneys and brains were first homogenized with TissueLyser II at 30 Hz for 3 min. A 120 µL aliquot of the tissue homogenate was subsequently diluted with 180 µL lysis buffer and further homogenized using TissueLyser II (30 Hz, 3 min). In contrast, tissues of the urogenital system were homogenized with TissueLyser II at 30 Hz once for 5 min.

All homogenates were mixed with lysis buffer containing an appropriate amount of Igepal CA-630 (Sigma-Aldrich, St. Louis, MO) to reach a final detergent concentration of 1%. The samples were sonicated in a water bath 4 × 1 min at 0°C. Finally, the samples were centrifuged at 16 000*g* for 30 min, and the supernatants were stored at −80°C until further use. The concentration of total protein in the lysates was determined right before Western blot or enzyme activity analysis using Bradford 1× Dye Reagent (Bio-Rad).

2.7 | Western blot analysis

A combination of reducing sodium dodecyl sulfate polyacrylamide gel electrophoresis (SDS-PAGE, Bio-Rad) and wet electroblotting (Bio-Rad)

was used for Western blot analysis. A total amount of protein per line was 100 µg. The antibody mixture consisted of the anti-mouse PSMA/GCPII GCP-04 (Exbio, Prague, Czechia) labeled with HRP and an anti-β-actin antibody (Mouse monoclonal anti-β-actin antibody, clone AC-15, Sigma-Aldrich) diluted in 0.55% casein solution. Conjugation of GCPII-04 with HRP was performed at pH 9.4 using the EZ-Link™ Plus Activated Peroxidase Kit (Thermo Fisher Scientific) according to the manufacturer's protocol. To visualize PSMA/GCPII, the blots were incubated with SuperSignal West Femto Chemiluminescent Substrate (Thermo Fisher Scientific), and chemiluminiscence was captured with a LAS-3000 CCD Camera (Fujifilm, Tokyo, Japan). To visualize β-actin, the blots were incubated with IRDye 680 RD goat anti-mouse antibody (LI-COR Biosciences, Lincoln, NE) and developed by an Odyssey CLx Infrared Imaging System (LI-COR Biosciences).

2.8 | Radioenzymatic assay

NAAG-hydrolyzing activity in mouse tissues was determined using ^{3}H-NAAG (radiolabeled on the terminal glutamate) as previously described[31] with minor modifications. A volume of tissue lysate corresponding to a selected amount of total protein was adjusted by addition of lysis buffer to 20 µL and mixed with 70 µL reaction buffer (20 mM Tris-HCl, pH 7.4, 150 mM NaCl, 0.1% Tween 20). Reactions were incubated with 10 µL of 1 µM NAAG (containing 50 nM ^{3}H-NAAG) at 37°C for 17 h (ie, overnight) or 6 h. The reactions were stopped by addition of 100 µL ice-cold stopping buffer (200 mM KH_2PO_4, 2 mM 2-mercaptoethanol, pH 7.4), and the released glutamate was separated from the uncleaved NAAG using AG1-X ion exchange resin (Bio-Rad). The eluate containing radioactive glutamate was mixed with Rotiszint ECO Plus scintillation cocktail (Roth), and the radioactivity of each sample was quantified by liquid scintillation using a Tri-Carb Liquid Scintillation Counter (PerkinElmer, Waltham, MA). The samples were measured in either duplicates or triplicates. A calibration curve of rm-GCPII (10 pg, 25 pg, 50 pg, 100 pg, 125 pg, and 250 pg of rm-GCPII per reaction) was included in each sample set.

2.9 | Gross anatomy of the urogenital system

Mice were sacrificed by intraperitoneal anesthetic injection followed by cervical dislocation. Ketamine (125 mg/kg) and xylazine (20 mg/kg) were used as anesthetics. The abdominal cavity was opened by midline laparotomy extending from the xiphoid process to the pubic symphysis. Seminal vesicles were localised, gently inverted, and pulled out of the abdominal cavity. Images of the seminal vesicles in front view with length scale were recorded. The seminal vesicle area was measured with ImageJ software[34] using the length scale as an internal standard.

2.10 | Histopathology and immunohistochemistry

Selected tissues from the mouse urogenital system were collected following gross anatomy examination. Unaffected human epididymis tissue samples were obtained from specimen surgically resected for testicular cancer ($n = 3$, average age—39 years). Tissues were immersed in 10% buffered formalin immediately after collection and stored at 4°C before further processing.

A standard histopathological examination of the seminal vesicles was performed. Briefly, after fixation in 10% buffered formalin, transverse sections of the tissues were dehydrated using graded ethanol followed by xylene immersion and embedded in paraffin. Five-micrometer slices were subsequently prepared and stained with hematoxylin-eosin.

Immunohistochemistry of human and mouse samples was performed as previously described[35] with minor modifications. After fixation in 10% buffered formalin, tissues were dehydrated using graded ethanol followed by xylene immersion and paraffin embedding. Five-micrometer serial slices were prepared, deparaffinized in xylene and rehydrated in graded ethanol. Heat antigen retrieval was performed in buffer containing 10 mM sodium citrate, pH 6.0, and 0.1% Tween 20 using an autoclave (110°C, 15 min). Endogenous peroxidase activity was blocked by incubation in a 1.5% hydrogen peroxide solution in PBS for 20 min at room temperature followed by incubation in 10% fetal bovine serum (FBS) in PBS for 1 h at room temperature to reduce nonspecific interactions. To block endogenous immunoglobulins in the mouse samples, the slices were incubated with AffiniPure Fab Fragment Goat Anti-Mouse IgG (H + L) (Jackson ImmunoResearch Laboratories, West Grove, PA, diluted to 50 µg/mL by 10% FBS in PBS) for 1 h at room temperature. The slides were then washed four times with PBS, and a solution of primary antibodies against mGCPII/hGCPII (GCP-04, Exbio, or GCP-02[36]) or hGCPII (YPSMA-1, Anogen, Toronto, Canada) diluted in 10% FBS in PBS to a concentration of 10 µg/mL was added to each slice. After overnight incubation at 4°C, the slides were washed five times with PBS containing 0.1% Tween 20, and each slice was incubated for 1 h at room temperature with the secondary antibody Histofine Simple Stain™ MAX PO (MULTI) (Nichirei Biosciences Inc., Tokyo, Japan), either undiluted (human samples) or diluted 1:2 with 10% FBS in PBS (mouse samples). Finally, the slides were washed five times with PBS containing 0.1% Tween 20, and mGCPII was visualized using the DAB/Plus kit (Diagnostic BioSystems, Pleasanton, CA). The slides were counterstained with Harris' hematoxylin and mounted in polyvinylalcohol-based media.

2.11 | Statistical analysis

All data from radioactive assays are presented as the mean of biological replicates ± standard deviation. Statistical analysis of mouse seminal vesicle enlargements was performed with the statistical software Stata, release 9.2 (Stata Corp LP, College Station, TX). A random-effects linear regression model with generalized least squares technique for estimating parameters was used to analyze the data. This approach allows estimation of within-animal variation as well as between-animal variation. It also takes into account the correlation between responses on paired organs from the same individual. Based on the result of the Shapiro-Wilk test for normality, the dependent variable (ie, area) was log-transformed to bring its distribution closer to normal. Group ($Folh1^{-/-}$ vs $Folh1^{+/-}$ vs $Folh1^{+/+}$) or age (<72 weeks old

vs >72 weeks old) entered the model as independent variables. All statistical tests were evaluated at a significance level of 0.05.

3 | RESULTS

3.1 | Folh1$^{-/-}$ mice generated by TALEN-mediated gene disruption are viable and devoid of PSMA/GCPII specific activity

To generate Folh1$^{-/-}$ mice, we designed TALENs that specifically cleaved exon 11 of the *Folh1* gene within the sequence encoding the PSMA/GCPII active site (Figure 1A). Two independent TALEN microinjections into male nuclei of C57BL/6NCrl zygotes were performed, resulting in 65 transgenic mice of the F0 generation. Gene sequencing was carried out on all F0 transgenic mice, and the chosen founder mice carrying deletions of 3 bp (del3), 4 bp (del4), and 17 bp (del17) within exon 11 of the *Folh1* gene were bred with WT C57BL/6NCrl mice to obtain the F1 generation. For facile monitoring of resulting genotypes, we established a reliable genotyping method based on nested PCR (Figure 1B).

Heterozygous mice bearing the *Folh1-del3*, *Folh1-del4*, or *Folh1-del17* variant bred normally and did not show any obvious phenotype. PSMA/GCPII mutant mice (mice homozygous for either *Folh1-del3* or *Folh1-del4* or *Folh1-del17*) were generated by intercrossing heterozygous mice of at least the F2 generation. Neither embryonic lethality nor any obvious phenotype was observed for the PSMA/GCPII mutant mice. Subsequent intercrossing of PSMA/GCPII mutant mice was consistent with the usual breeding performance of C57BL/6NCrl mice.

To confirm that the generated mutants could be considered as knockout, that is, possess functional gene ablations, we examined at first the PSMA/GCPII protein expression in the kidney and brain using Western blot (Figures 2A and 2C). No band corresponding to either full-length PSMA/GCPII or any truncated form of PSMA/GCPII was detected by Western blot, although the antibody against mouse PSMA/GCPII is able to recognize the potential protein products of *Folh1-del3*, *Folh1-del4*, and *Folh1-del17* gene expression. In addition, no version of PSMA/GCPII was detected in the insoluble fractions of lysates from PSMA/GCPII mutant mice (data not shown). Since all three mutants were devoid of PSMA/GCPII protein expression, they are hereafter collectively referred as Folh1$^{-/-}$ mice.

Next, we set out to determine if the Folh1$^{-/-}$ mice were devoid of specific PSMA/GCPII activity. We performed enzymatic activity assays with the brain and kidney lysates using NAAG, a physiologic substrate

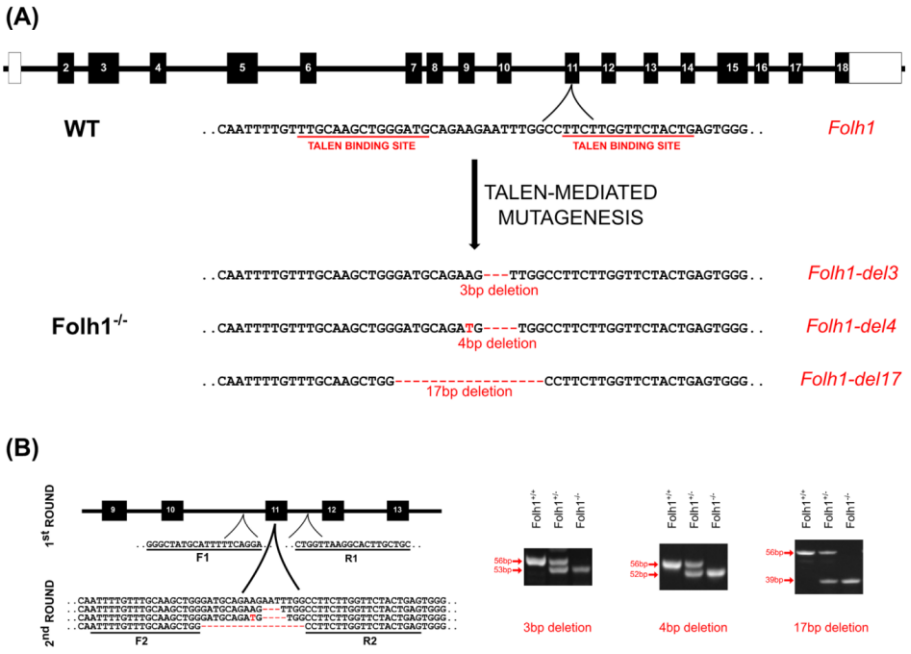

FIGURE 1 Generation and genotyping of Folh1$^{-/-}$ mice. A, Folh1$^{-/-}$ mice were generated on a C57BL/6NCrl background using TALEN technology. TALEN activity followed by non-homologous end joining generated several different mutations. Founder mice with deletions of 3 bp (*Folh1-del3*), 4 bp (*Folh1-del4*), and 17 bp (*Folh1-del17*) were chosen to establish PSMA/GCPII mutant mouse colonies. B, Mice were genotyped using nested PCR. The first round of PCR using F1 and R1 primers generated fragments of approximately 540 bp. The second round using F2 and R2 primers generated fragments with length depending on genotype. [Color figure can be viewed at wileyonlinelibrary.com]

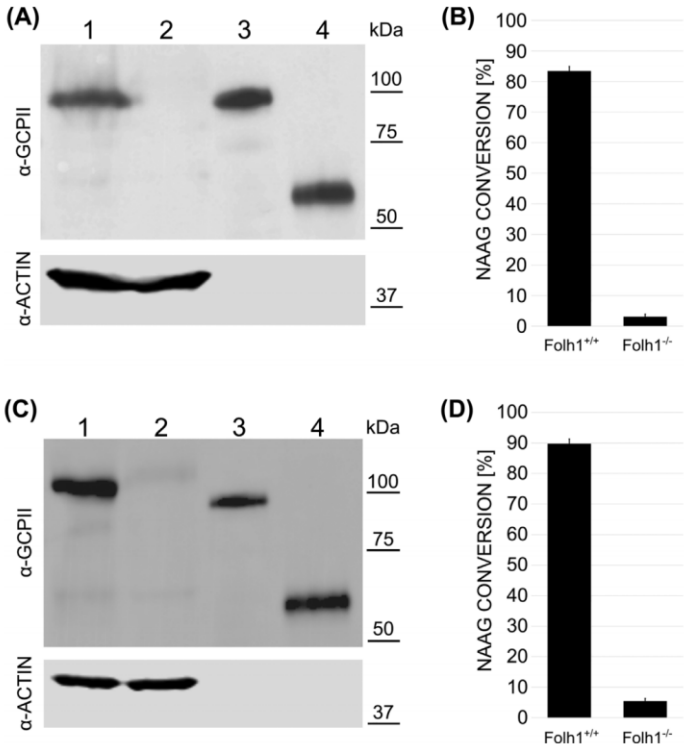

FIGURE 2 Characterization of Folh1$^{-/-}$ mice using brain and kidney lysates. A and C, Representative Western blot analysis of brain lysates (A) and kidney lysates (C). Western blot were performed with the anti-PSMA/GCPII antibody GCPII-04 (designated α-GCPII) and anti-β-actin antibody (designated α-ACTIN). Recombinant mouse GCPII (rm-GCPII)[31] and a truncated version corresponding to the extracellular part of the potential protein product of *Folh1-del17* gene expression (rm-GCPIIdel17) were used as mGCPII standards. 1-Folh1$^{+/+}$, 2-Folh1$^{-/-}$, 3-rm-GCPII WT, 4-rm-GCPII del17. B and D, NAAG cleavage activity analysis of brain lysates (B) and kidney lysates (D). Reactions were performed in 100 μg of total protein overnight. Error bars represent standard deviation of six biological replicates (8-week-old males)

of PSMA/GCPII (Figures 2B and 2D). Indeed, NAAG conversion after overnight incubation with Folh1$^{-/-}$ lysates did not exceed 6%.

3.2 | Aged Folh1$^{-/-}$ mice have an increased propensity for enlarged seminal vesicles

We focused on the urogenital system of aged mice to further examine possible phenotypic differences between Folh1$^{-/-}$ and Folh1$^{+/+}$ mice. We first performed gross anatomy analysis of the urogenital system of aged WT mice. Age-related changes were observed only in the seminal vesicles, which showed a tendency toward bilateral enlargement. Based on preliminary observations of a small cohort consisting of mice aged 63-82 weeks, we further studied two age groups—mice aged 69-72 weeks and mice aged 72.1-81 weeks. While the seminal vesicles of all WT mice aged 69-72 weeks were of a normal size (average stretched length of 1.5 cm and average area of 1 cm^2), the propensity for bilaterally enlarged seminal vesicles increased significantly in WT mice older than 72 weeks ($P < 0.001$, see Figure 3).

Based on these observations, we investigated possible PSMA/GCPII-mediated changes in the urogenital system in mice aged 69-72 weeks. Interestingly, we observed a higher prevalence of bilaterally enlarged seminal vesicles in Folh1$^{-/-}$ mice compared with Folh1$^{+/+}$ mice. Typical gross anatomy of the seminal vesicles of both Folh1$^{+/+}$ and Folh1$^{-/-}$ mice is depicted in Figure 4A. Histopathological examination using hematoxylin-eosin staining did not show any substantial differences between the seminal vesicles of Folh1$^{+/+}$ and Folh1$^{-/-}$ mice (Figures 4B and 4C). Nevertheless, "dilated" parts of the seminal vesicles were present to a greater extent in Folh1$^{-/-}$ mice than in their WT counterparts. Moreover, loosening of mucosal folds and decreasing epithelial thickness were also more prominent in Folh1$^{-/-}$ seminal vesicles. No epithelial hyperplasia, tumor or infection was observed.

To investigate the statistical significance of our observations, we performed gross anatomy analysis of a sufficient number of Folh1$^{-/-}$, Folh1$^{+/-}$, and Folh1$^{+/+}$ mice (at least nine mice per group, Figure 5A). Linear regression analysis of logarithmically transformed seminal

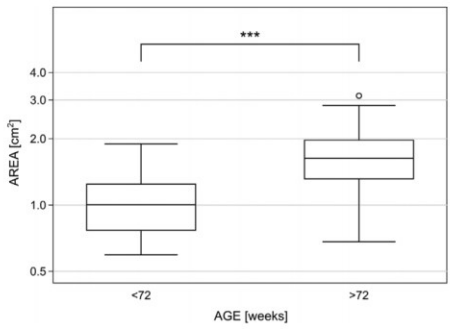

FIGURE 3 Age-related enlargement of mouse seminal vesicles. The WT mice were divided into two age groups based on preliminary observations of a small cohort consisting of mice aged 63-82 weeks. The group designated as <72 consisted of 20 mice aged 69-72 weeks. The group designated as >72 consisted of 11 mice aged 72.1-81 weeks. The difference in seminal vesicle area between the two groups was statistically significant ($P < 0.001$ as designated by ***)

vesicle areas showed that the overall difference between the three groups was highly statistically significant ($P < 0.002$). Comparisons of group pairs revealed a highly statistically significant difference between Folh1$^{-/-}$ and Folh1$^{+/+}$ mice ($P < 0.001$) and a statistically significant difference between Folh1$^{-/-}$ and Folh1$^{+/-}$ mice ($P = 0.028$). These data suggest that the propensity for enlarged seminal vesicles tends to increase with a decreasing number of PSMA/GCPII-expressing alleles.

We next investigated whether the amount of expressed PSMA/GCPII depends on the number of functional *Folh1* alleles in the aged mice. We prepared lysates from kidneys collected from 70-week-old mice with the three genotypes (Folh1$^{-/-}$, Folh1$^{+/-}$, Folh1$^{+/+}$) and analyzed them using two independent methods—Western blot and NAAG-hydrolyzing activity analysis (Figure 5B). Interestingly, the amount of PSMA/GCPII expressed in Folh1$^{+/-}$ mice was close to half that expressed in Folh1$^{+/+}$ mice, as determined by Western blot (Figure 5B). No PSMA/GCPII was detected in lysates from Folh1$^{-/-}$ mice. Moreover, NAAG conversion after incubation with kidney lysates from Folh1$^{+/-}$ mice was half of that observed after incubation

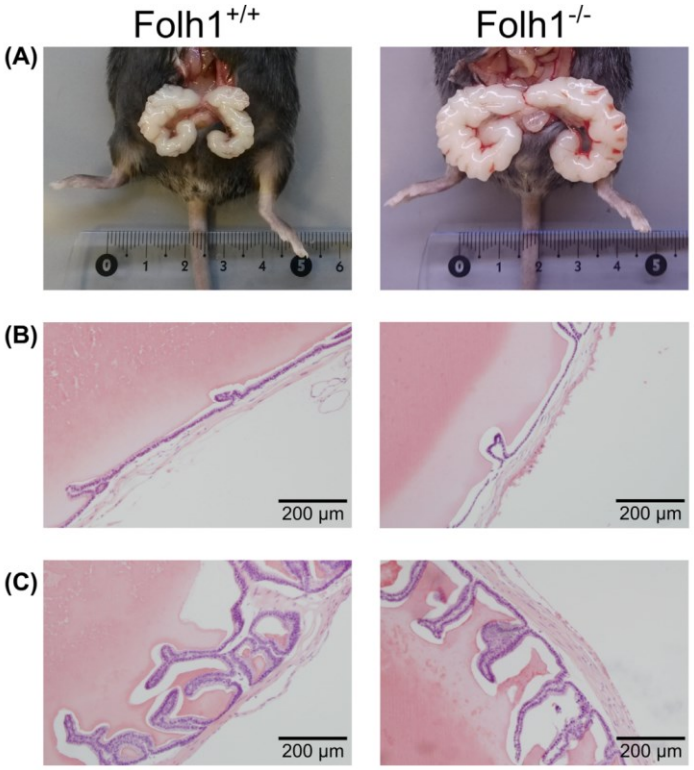

FIGURE 4 Images and histopathology of the seminal vesicles of typical Folh1$^{+/+}$ mice and some Folh1$^{-/-}$ mice. A, Images of mouse abdominal part. B, Histopathological images of mouse seminal vesicles showing "dilated" parts. C, Histopathological images of mouse seminal vesicles showing parts with normal seminal vesicle histology. [Color figure can be viewed at wileyonlinelibrary.com]

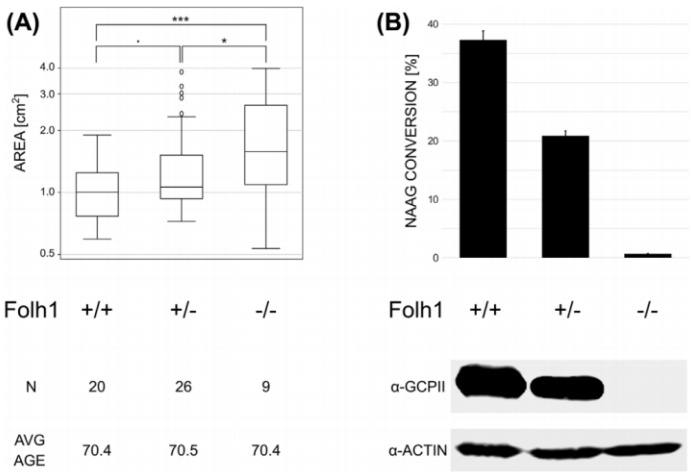

FIGURE 5 Statistical analysis of enlarged seminal vesicles and expression of PSMA/GCPII protein in kidneys of 70-week-old mice with distinct genotypes. A, Comparison of seminal vesicle areas of Folh1$^{+/+}$, Folh1$^{+/-}$, and Folh1$^{-/-}$ mice. AVG AGE indicates the average age of the mice in weeks. The difference in seminal vesicle area was highly statistically significant between Folh1$^{-/-}$ and Folh1$^{+/+}$ mice ($P < 0.001$, designated by ***), statistically significant between Folh1$^{-/-}$ and Folh1$^{+/-}$ mice ($P = 0.028$, designated by *) and on the border of significance between Folh1$^{+/-}$ and Folh1$^{+/+}$ mice ($P = 0.052$, designated by ·). B, NAAG cleavage and Western blot analysis of kidney lysates from Folh1$^{+/+}$, Folh1$^{+/-}$, and Folh1$^{-/-}$ mice. NAAG cleavage analysis was performed in 0.5 µg total protein for 6 h. Error bars represent standard deviation of 2 (for Folh1$^{-/-}$) or 3 (for Folh1$^{+/+}$ and Folh1$^{+/-}$) biological replicates. Western blot analysis of kidney lysates was performed using the anti-PSMA/GCPII antibody GCPII-04 (designated α-GCPII) and anti-β-actin antibody (designated α-ACTIN)

with kidney lysates from Folh1$^{+/+}$ mice (Figure 5B). As expected, almost no NAAG cleavage activity was observed in lysates from the kidneys of Folh1$^{-/-}$ mice.

3.3 | PSMA/GCPII is highly expressed in the epididymis

To investigate whether a possible source of seminal vesicle enlargement could be located within or close to the seminal vesicles, we examined the expression profile of PSMA/GCPII in male mouse urogenital tissues using the NAAG cleavage assay (Figure 6A). Among the tissues tested (30 µg total protein per reaction), only the kidney, spermatic cord, and epididymis reached at least 50% NAAG conversion after overnight incubation. Other tissues, including all four prostate glands and seminal vesicles, showed less than 25% NAAG conversion (Figure 6A). Assuming PSMA/GCPII is the only enzyme responsible for NAAG cleavage, this would correspond to less than 2.5 pg PSMA/GCPII per 1 µg total protein (as determined from our calibration curve, which was linear from 4% to 42% NAAG conversion, corresponding to 10 pg to 125 pg recombinant mouse GCPII). In addition, we examined PSMA/GCPII expression in the seminal vesicles using Western blot analysis. Even though a weak band of molecular weight similar to that of PSMA/GCPII was detected in the seminal vesicles of Folh1$^{+/+}$ mice, the same signal was also observed in the seminal vesicles of Folh1$^{-/-}$ mice (Figure 6B), suggesting possible cross-reactivity of the antibody. We thus further investigated only the spermatic cord and epididymis.

To filter out the possible contribution of other enzymes (such as mouse GCPIII) to NAAG hydrolysis, we analyzed lysates from the epididymis and spermatic cord of both Folh1$^{+/+}$ and Folh1$^{-/-}$ mice. While NAAG hydrolysis in the epididymis of Folh1$^{-/-}$ mice was negligible, NAAG conversion after incubation with spermatic cord lysates from Folh1$^{-/-}$ mice was more than half the WT value (Figure 6C). After taking into account the conversion from Folh1$^{-/-}$ mice, the amount of PSMA/GCPII in the spermatic cord appeared to be within the range of other tissues expressing low levels of PSMA/GCPII (Figure 6C). On the other hand, the amount of PSMA/GCPII in the epididymis was as high as 180 pg per 1 µg total protein. In comparison, we previously showed that the amount of PSMA/GCPII in the male kidney and brain is 100-250 pg and 2.5-10 pg in 1 µg total protein, respectively.[31] We thus visualized and localized PSMA/GCPII in the epididymis by immunohistochemistry using two different antibodies against mouse PSMA/GCPII—GCPII-02 and GCPII-04 (Figure 7). Cells expressing the protein were detected in all three parts of the epididymis—head, body, and tail.

Finally, we investigated whether PSMA/GCPII could be also detected in the human epididymis. For this purpose, we performed immunohistochemistry with tissue sections of the body of the epididymis collected from three patients using three different antibodies against human PSMA/GCPII—GCPII-02, GCPII-04, and YPSMA1. Interestingly, PSMA/GCPII-expressing cells were detected in all cases (Figure 8).

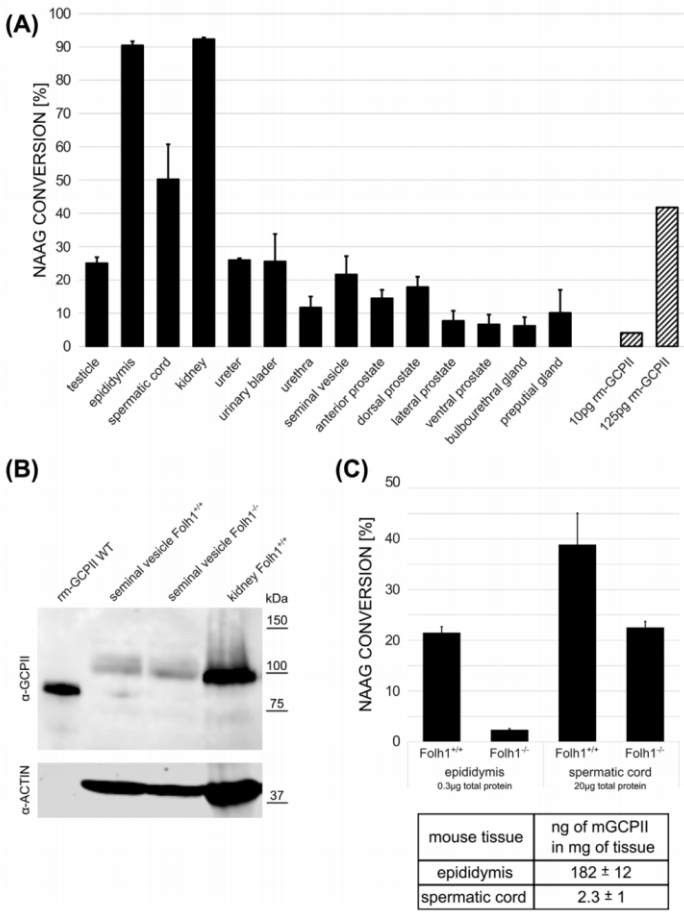

mouse tissue	ng of mGCPII in mg of tissue
epididymis	182 ± 12
spermatic cord	2.3 ± 1

FIGURE 6 NAAG cleavage activity in the male mouse urogenital system and Western blot analysis of the seminal vesicles. A, NAAG conversion performed overnight in 30 µg total protein of WT lysates compared to NAAG conversion performed overnight with 10 pg and 125 pg of recombinant mouse GCPII (rm-GCPII). Error bars of tissue lysate conversions represent standard deviations of biological replicates (from 3 to 5 mice of at least 2 of 3 different ages: 8 weeks, 17 weeks, and 30 weeks). Error bars of NAAG conversions by rm-GCPII represent standard deviations of 6 independent measurements. B, Representative Western blot analysis of seminal vesicle lysates. Western blots were performed with the anti-PSMA/GCPII antibody GCPII-04 (designated α-GCPII) and anti-β-actin antibody (designated α-ACTIN). Recombinant mouse GCPII (designated rm-GCPII WT)[31] was used as mGCPII standard. C, Comparison of overnight NAAG cleavage activity in selected reproductive tissues of Folh1$^{+/+}$ and Folh1$^{-/-}$ mice together with calculated amount of PSMA/GCPII (mGCPII) in mouse epididymis and spermatic cord after taking into account NAAG conversion in tissues from Folh1$^{-/-}$ mice. Error bars represent standard deviation of 4 biological replicates (8-week-old mice)

4 | DISCUSSION

Despite more than three decades of extensive research, the physiological function of PSMA/GCPII is still not fully understood. Several independent research groups have attempted to produce and characterize mice with disrupted PSMA/GCPII. However, the outcomes of these studies differ dramatically, ranging from embryonic lethality[24,25] to generation of viable mice without any obvious phenotype.[23,26] Viable PSMA/GCPII-deficient mice have been used to investigate PSMA/GCPII function in the nervous system[26–28] but not in other PSMA/GCPII-expressing tissues such as the urogenital system. In this study, we explored several issues that have not been addressed in the reports published to date.

First, in contrast to previous studies, which used ES cell manipulation to generate PSMA/GCPII-deficient mice, we inactivated the *Folh1* gene in mice using TALEN technology.[37,38] This strategy

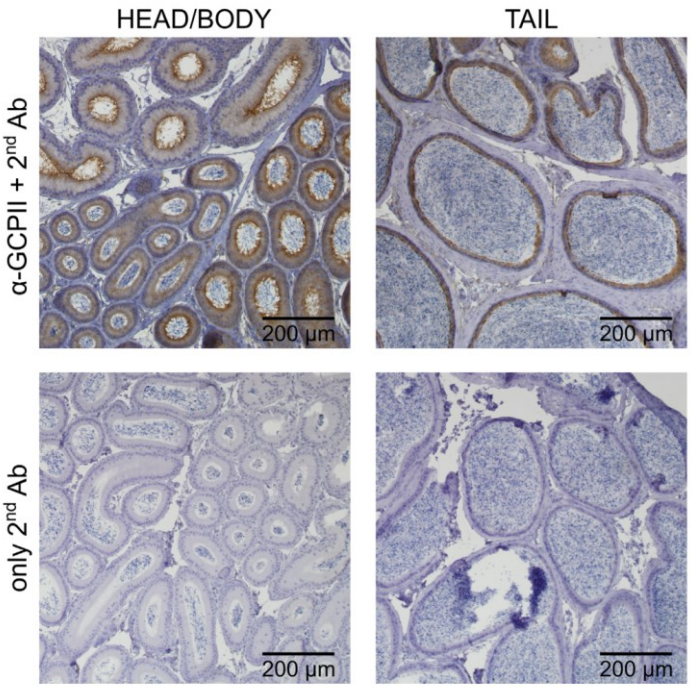

FIGURE 7 Representative immunohistochemical staining of the head, body, and tail of mouse epididymis. Formalin-fixed paraffin-embedded mouse epididymis tissue sections were incubated with the anti-PSMA/GCPII (α-GCPII) antibody GCP-04 (Exbio) to localize mouse PSMA/GCPII expression. As a negative control, immunohistochemistry using only secondary antibody (2nd Ab) Histofine Simple Stain™ MAX PO (MULTI) (Nichirei Biosciences Inc.) was performed. [Color figure can be viewed at wileyonlinelibrary.com]

enabled us to manipulate mouse zygotes with the same genetic background as the knockout colony that was being established. Therefore, potential phenotypic variations that could be caused by mixed genetic backgrounds[39] were eliminated. Moreover, our PSMA/GCPII-deficient mice do not contain the PGK-Neo cassette because TALEN technology does not require a selectable marker. When retained in the targeted loci, selectable marker cassettes such as PGK-Neo have been repeatedly shown to greatly influence the expression of neighboring genes within the locus, leading to unexpected phenotypes of null mutant mice.[40,41] Out of three PSMA/GCPII-deficient colonies established to date, only one (IMPC) had the PGK-Neo cassette removed using the Cre-Lox system before the mice were characterized.[29] The other two PSMA/GCPII-deficient colonies,[23,26] which are routinely used for diverse experiments,[28,42,43] likely do not contain any LoxP sites, and PGK-Neo cassette removal is thus not possible.

Second, when using TALENs to inactivate the *Folh1* gene, we intended to disrupt the active site of PSMA/GCPII. Several reports have shown that novel alternative splice variants can be detected in some knockout mice, and these may serve to rescue a severe phenotype of complete gene inactivation.[44,45] Modification of the *Folh1* gene within the sequence encoding the active site of PSMA/GCPII ensures that no alternative splicing that would enable at least partial restoration of PSMA/GCPII activity can occur. A previous attempt to generate PSMA/GCPII-deficient mice through active site disruption led to embryonic lethality.[24] Here, we show that a small TALEN-mediated deletion within exon 11 of the *Folh1* gene leads to production of viable PSMA/GCPII-deficient mice with no obvious phenotype. In comparison with previous reports characterizing viable PSMA/GCPII-deficient mice,[23,26] residual NAAG hydrolyzing activity in our Folh1$^{-/-}$ mice seems to be negligible. Indeed, while NAAG conversion in saturation was as low as 3% in the brain lysates of our Folh1$^{-/-}$ mice, others have reported that NAAG hydrolyzing activity measured in PSMA/GCPII-deficient mouse brains within the linear range of reaction velocity reached 6% to 18% of the WT values.

Finally, we focused on possible phenotypic differences between Folh1$^{+/+}$ and Folh1$^{-/-}$ mice in the urogenital system rather than the nervous system. We found that PSMA/GCPII-deficient mice aged 69-72 weeks have a higher propensity for bilaterally enlarged seminal vesicles. The dilation of seminal vesicles seems to be solely a result of the accumulation of luminal fluid, as we observed no other cause such as epithelial hyperplasia, cysts, tumors or infections. Interestingly, we

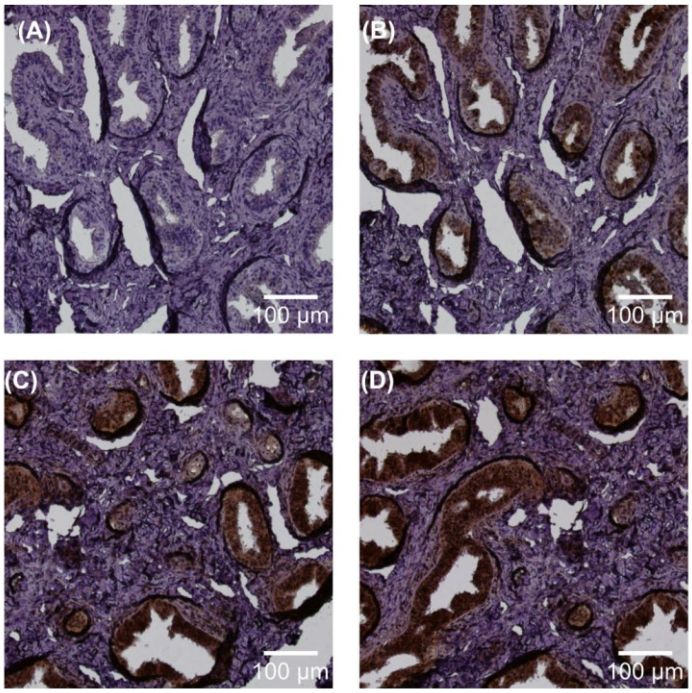

FIGURE 8 Representative immunohistochemical staining of the body of human epididymis. Formalin-fixed paraffin-embedded human epididymis tissue sections were incubated with several anti-PSMA/GCPII antibodies to specifically detect PSMA/GCPII. A, Negative control—immunohistochemistry using only the secondary antibody Histofine Simple Stain™ MAX PO (MULTI) (Nichirei Biosciences Inc.). B, Immunohistochemistry using the antibody GCP-04 (Exbio). C, Immunohistochemistry using the antibody GCP-02.[36] D, Immunohistochemistry using the antibody YPSMA1 (Anogen). [Color figure can be viewed at wileyonlinelibrary.com]

observed this increased propensity for seminal vesicle enlargement to a lesser extent in Folh1$^{+/-}$ mice. It is thus possible that the seminal vesicle dilation is somehow associated with PSMA/GCPII activity, as the amount of PSMA/GCPII in the Folh1$^{+/-}$ mice was roughly half the amount of PSMA/GCPII in Folh1$^{+/+}$ mice, as determined by both Western blot and NAAG-hydrolyzing activity.

Previous studies have reported that enlarged seminal vesicles are one of the signs of aging in C57BL mice.[46,47] In one of these studies, the mice, which had dilation of seminal vesicles caused by accumulation of luminal fluid, were at least 24 months old[46]—much older than the mice investigated in our study. Dilated seminal vesicles have also been reported in aged C57BL mice with a lower age limit (16 months) but in connection with either an infection or the presence of an abdominal tumor,[47] neither of which we observed in our histopathological examination. In addition, several genetically modified mice with a phenotype association to enlarged seminal vesicles can be found in public databases or the literature.[29,48] However, none of the reported genes seems to be connected with PSMA/GCPII.

To investigate the possible source of seminal vesicle enlargement in Folh1$^{-/-}$ mice, we examined the expression profile of PSMA/GCPII in the urogenital system of WT mice using a NAAG-hydrolyzing activity assay. Somewhat surprisingly, low levels of NAAG hydrolyzing activity were detected in the seminal vesicles and most surrounding tissues. In the case of seminal vesicles, we additionally performed Western blot analysis, which showed non-detectable expression of PSMA/GCPII. Indeed, no difference was seen between seminal vesicle lysates of Folh1$^{+/+}$ and Folh1$^{-/-}$ mice suggesting that if PSMA/GCPII is expressed in the seminal vesicles, its level is below the detection limit. In agreement with previous reports,[31,49] almost no NAAG hydrolyzing activity was observed in any of the mouse prostate lobes. In contrast, high levels of NAAG hydrolyzing activity were detected in the mouse spermatic cord and epididymis.

The possibility that PSMA/GCPII is present in seminal vesicles or other urogenital tissues in an amount sufficient for execution of a specific function cannot be excluded. Indeed, the seminal vesicles contain seminal fluid, which represents 60-75% of the seminal vesicle mass.[46] As protein concentration in the seminal fluid can be as high as 86 mg/mL,[50] analysis of seminal vesicle lysates (ie, a mixture of seminal fluid and seminal vesicle cells) could result in dramatic underestimation

of PSMA/GCPII amount in the seminal vesicle cells. Similarly, male urogenital tissues such as the urethra consist of diverse types of cells.[51] If PSMA/GCPII is expressed in only one cell type, the amount of PSMA/GCPII could be physiologically relevant.

Even though we performed the NAAG-hydrolyzing activity assay in reaction conditions highly specific for PSMA/GCPII,[22] other enzymes such as GCPIII potentially could influence the outcome of the analysis. GCPIII is expressed in considerable amounts in the mouse testis and bladder,[52] although no other urogenital system tissues have been examined. To account for the possible involvement of other enzymes including GCPIII, we performed the NAAG-hydrolyzing activity assay in the spermatic cord and epididymis (the tissues with highest levels of NAAG-hydrolyzing activity) of both Folh1$^{+/+}$ and Folh1$^{-/-}$ mice. We concluded that high amounts of PSMA/GCPII within the urogenital system can be only detected in epididymis. Interestingly, the amount of PSMA/GCPII in the epididymis is comparable to the amount in the kidney and 10-fold higher than the amount in the brain.[31] Epididymis is thus one of the most PSMA/GCPII expressing tissue in mice.

Additionally, we found that PSMA/GCPII is expressed throughout all parts of the mouse epididymis, as determined by immunohistochemistry. This agrees with previous findings, in which the researchers saw a strong signal in mouse epididymis after intravenous injection of a low-molecular-weight fluorescent agent targeting PSMA/GCPII.[53,54] To investigate whether our observations may also be applicable to humans, we examined tissue sections of human epididymis. The presence of PSMA/GCPII mRNA in human epididymis has been reported.[55] Using immunohistochemistry with three different antibodies against human PSMA/GCPII, we confirmed that PSMA/GCPII protein is also expressed in the human epididymis.

In humans, ejaculatory duct obstruction is relatively rare but has been shown to be one of the causes of male infertility.[56] It is a matter of speculation whether the absence of PSMA/GCPII in the epididymis is somehow connected with an increased propensity for dilated seminal vesicles. The association between inactivation of the *Folh1* gene and enlargement of seminal vesicles in aged PSMA/GCPII-deficient mice remains enigmatic, and further research is needed.

5 | CONCLUSIONS

We produced PSMA/GCPII-deficient mice by disrupting the PSMA/GCPII active site using TALEN-mediated mutagenesis. We confirmed that PSMA/GCPII protein is not expressed in these mice, and NAAG hydrolyzing activity is almost completely abolished. Young PSMA/GCPII-deficient mice breed normally and do not show any obvious phenotype. Based on investigation of the urogenital system of aged mice, we report that PSMA/GCPII-deficient mice have an increased propensity for enlarged seminal vesicles. The cause of this phenotype remains uncertain, as significant amounts of PSMA/GCPII within the mouse urogenital system were detected only in the epididymis. PSMA/GCPII was also shown to be present in the human epididymis. We thus believe that our findings can set the direction for future work to reveal PSMA/GCPII function in human reproduction.

ACKNOWLEDGEMENTS

The authors would like to acknowledge Jana Starková for preparation of stably transfected cell cultures, Dr. Tomas Olejar for preparation of mouse seminal vesicle sections for histopathology examination and help with interpretation of the data, Adrian Cibula for preparation of human epididymis sections and Dr. Hillary Hoffman for language editing. This work was supported by grant no. GA16-02938S from the Grant Agency of the Czech Republic, InterBioMed project LO1302 and Czech Centre for Phenogenomics project LM2015040 from the Ministry of Education, Youth and Sports of the Czech Republic, and RVO 68378050 from Academy of Sciences of the Czech Republic.

CONFLICT OF INTEREST

The authors declare no conflicts of interest.

ORCID

Jan Konvalinka http://orcid.org/0000-0003-0695-9266

REFERENCES

1. Pinto JT, Suffoletto BP, Berzin TM, et al. Prostate-specific membrane antigen: a novel folate hydrolase in human prostatic carcinoma cells. *Clin Cancer Res*. 1996;2:1445–1451.
2. Luthi-Carter R, Berger UV, Barczak AK, Enna M. Coyle JT. Isolation and expression of a rat brain cDNA encoding glutamate carboxypeptidase II. *Proc Natl Acad Sci USA*. 1998;95:3215–3220.
3. Luthi-Carter R, Barczak AK, Speno H, Coyle JT. Molecular characterization of human brain N-acetylated alpha-linked acidic dipeptidase (NAALADase). *J Pharmacol Exp Ther*. 1998;286:1020–1025.
4. Horoszewicz JS, Kawinski E, Murphy GP. Monoclonal antibodies to a new antigenic marker in epithelial prostatic cells and serum of prostatic cancer patients. *Anticancer Res*. 1987;7:927–935.
5. Bostwick DG, Pacelli A, Blute M, Roche P, Murphy GP. Prostate specific membrane antigen expression in prostatic intraepithelial neoplasia and adenocarcinoma: a study of 184 cases. *Cancer*. 1998; 82:2256–2261.
6. Evans JC, Malhotra M, Cryan JF, O'Driscoll CM. The therapeutic and diagnostic potential of the prostate specific membrane antigen/glutamate carboxypeptidase II (PSMA/GCPII) in cancer and neurological disease. *Br J Pharmacol*. 2016;173:3041–3079.
7. Barinka C, Rojas C, Slusher B, Pomper M. Glutamate carboxypeptidase II in diagnosis and treatment of neurologic disorders and prostate cancer. *Curr Med Chem*. 2012;19:856–870.
8. O'Keefe DS, Su SL, Bacich DJ, et al. Mapping, genomic organization and promoter analysis of the human prostate-specific membrane antigen gene. *Biochim Biophys Acta*. 1998;1443:113–127.
9. Rawlings ND, Barrett AJ. Structure of membrane glutamate carboxypeptidase. *Biochim Biophys Acta*. 1997;1339:247–252.
10. Silver DA, Pellicer I, Fair WR, Heston WDW, CordonCardo C. Prostate-specific membrane antigen expression in normal and malignant human tissues. *Clin Cancer Res*. 1997;3:81–85.

11. Liu H, Moy P, Kim S, et al. Monoclonal antibodies to the extracellular domain of prostate-specific membrane antigen also react with tumor vascular endothelium. *Cancer Res*. 1997;57:3629–3634.
12. Troyer JK, Beckett ML, Wright GL, Jr. Detection and characterization of the prostate-specific membrane antigen (PSMA) in tissue extracts and body fluids. *Int J Cancer*. 1995;62:552–558.
13. Rovenska M, Hlouchova K, Sacha P, et al. Tissue expression and enzymologic characterization of human prostate specific membrane antigen and its rat and pig orthologs. *Prostate*. 2008;68:171–182.
14. Sacha P, Zamecnik J, Barinka C, et al. Expression of glutamate carboxypeptidase II in human brain. *Neuroscience*. 2007;144:1361–1372.
15. Robinson MB, Blakely RD, Coyle JT. Quisqualate selectively inhibits a brain peptidase which cleaves N-acetyl-L-aspartyl-L-glutamate in vitro. *Eur J Pharmacol*. 1986;130:345–347.
16. Robinson MB, Blakely RD, Couto R, Coyle JT. Hydrolysis of the brain dipeptide N-acetyl-L-aspartyl-L-glutamate—identification and characterization of a novel N-acetylated alpha-Linked acidic dipeptidase activity from rat-Brain. *J Biol Chem*. 1987;262:14498–14506.
17. Halsted CH, Ling EH, Luthi-Carter R, Villanueva JA, Gardner JM, Coyle JT. Folylpoly-gamma-glutamate carboxypeptidase from pig jejunum—molecular characterization and relation to glutamate carboxypeptidase II. *J Biol Chem*. 1998;273:20417–20424.
18. Hlouchova K, Navratil V, Tykvart J, Sacha P, Konvalinka J. GCPII variants, paralogs and orthologs. *Curr Med Chem*. 2012;19:1316–1322.
19. Pangalos MN, Neefs JM, Somers M, et al. Isolation and expression of novel human glutamate carboxypeptidases with N-acetylated alpha-linked acidic dipeptidase and dipeptidyl peptidase IV activity. *J Biol Chem*. 1999;274:8470–8483.
20. Bzdega T, Crowe SL, Ramadan ER, et al. The cloning and characterization of a second brain enzyme with NAAG peptidase activity. *J Neurochem*. 2004;89:627–635.
21. Hlouchova K, Barinka C, Konvalinka J, Lubkowski J. Structural insight into the evolutionary and pharmacologic homology of glutamate carboxypeptidases II and III. *FEBS J*. 2009;276:4448–4462.
22. Navratil M, Tykvart J, Schimer J, et al. Comparison of human glutamate carboxypeptidases II and III reveals their divergent substrate specificities. *FEBS J*. 2016;283:2528–2545.
23. Bacich DJ, Ramadan E, O'Keefe DS, et al. Deletion of the glutamate carboxypeptidase II gene in mice reveals a second enzyme activity that hydrolyzes N-acetylaspartylglutamate. *J Neurochem*. 2002;83:20–29.
24. Tsai G, Dunham KS, Drager U, et al. Early embryonic death of glutamate carboxypeptidase II (NAALADase) homozygous mutants. *Synapse*. 2003;50:285–292.
25. Han L, Picker JD, Schaevitz LR, et al. Phenotypic characterization of mice heterozygous for a null mutation of glutamate carboxypeptidase II. *Synapse*. 2009;63:625–635.
26. Gao Y, Xu S, Cui Z, et al. Mice lacking glutamate carboxypeptidase II develop normally, but are less susceptible to traumatic brain injury. *J Neurochem*. 2015;134:340–353.
27. Bacich DJ, Wozniak KM, Lu XCM, et al. Mice lacking glutamate carboxypeptidase II are protected from peripheral neuropathy and ischemic brain injury. *J Neurochem*. 2005;95:314–323.
28. Cao Y, Gao Y, Xu S, et al. Glutamate carboxypeptidase II gene knockout attenuates oxidative stress and cortical apoptosis after traumatic brain injury. *BMC Neurosci*. 2016;17:15.
29. Koscielny G, Yaikhom G, Iyer V, et al. The International Mouse Phenotyping Consortium Web Portal, a unified point of access for knockout mice and related phenotyping data. *Nucleic Acids Res*. 2014;42:D802–D809. Release 7.0.
30. Kasparek P, Krausova M, Haneckova R, et al. Efficient gene targeting of the Rosa26 locus in mouse zygotes using TALE nucleases. *FEBS Lett*. 2014;588:3982–3988.
31. Knedlik T, Vorlova B, Navratil V, et al. Mouse glutamate carboxypeptidase II (GCPII) has a similar enzyme activity and inhibition profile but a different tissue distribution to human GCPII. *FEBS Open Bio*. 2017;7:1362–1378.
32. Tykvart J, Sacha P, Barinka C, et al. Efficient and versatile one-step affinity purification of in vivo biotinylated proteins: expression, characterization and structure analysis of recombinant human glutamate carboxypeptidase II. *Protein Expr Purif*. 2012;82:106–115.
33. Barinka C, Rinnova M, Sacha P, et al. Substrate specificity, inhibition and enzymological analysis of recombinant human glutamate carboxypeptidase II. *J Neurochem*. 2002;80:477–487.
34. Rueden CT, Schindelin J, Hiner MC, et al. ImageJ2: ImageJ for the next generation of scientific image data. *BMC Bioinformatics*. 2017;18:529.
35. Tykvart J, Navratil V, Sedlak F, et al. Comparative analysis of monoclonal antibodies against prostate-specific membrane antigen (PSMA). *Prostate*. 2014;74:1674–1690.
36. Barinka C, Mlcochova P, Sacha P, et al. Amino acids at the N- and C-termini of human glutamate carboxypeptidase II are required for enzymatic activity and proper folding. *Eur J Biochem*. 2004;271:2782–2790.
37. Cermak T, Doyle EL, Christian M, et al. Efficient design and assembly of custom TALEN and other TAL effector-based constructs for DNA targeting. *Nucleic Acids Res*. 2011;39:e82.
38. Miller JC, Tan S, Qiao G, et al. A TALE nuclease architecture for efficient genome editing. *Nat Biotechnol*. 2011;29:143–148.
39. Yoshiki A, Moriwaki K. Mouse phenome research: implications of genetic background. *ILAR J*. 2006;47:94–102.
40. Olson EN, Arnold HH, Rigby PW, Wold BJ. Know your neighbors: three phenotypes in null mutants of the myogenic bHLH gene MRF4. *Cell*. 1996;85:1–4.
41. Pham CT, MacIvor DM, Hug BA, Heusel JW, Ley TJ. Long-range disruption of gene expression by a selectable marker cassette. *Proc Natl Acad Sci USA*. 1996;93:13090–13095.
42. Rais R, Jiang W, Zhai H, et al. FOLH1/GCPII is elevated in IBD patients, and its inhibition ameliorates murine IBD abnormalities. *JCI Insight*. 2016;1:e88634.
43. Caromile LA, Dortche K, Rahman MM, et al. PSMA redirects cell survival signaling from the MAPK to the PI3K-AKT pathways to promote the progression of prostate cancer. *Sci Signal*. 2017;10:eaag3326.
44. Gros-Louis F, Kriz J, Kabashi E, et al. Als2 mRNA splicing variants detected in KO mice rescue severe motor dysfunction phenotype in Als2 knock-down zebrafish. *Hum Mol Genet*. 2008;17:2691–2702.
45. Kraemer N, Issa-Jahns L, Neubert G, et al. Novel alternative splice variants of mouse cdk5rap2. *PLoS ONE*. 2015;10:e0136684.
46. Finch CE, Girgis FG. Enlarged seminal vesicles of senescent C57BL-6J mice. *J Gerontol*. 1974;29:134–138.
47. Pettan-Brewer C, Treuting PM. Practical pathology of aging mice. *Pathobiol Aging Age Relat Dis*. 2011;1, 7202.
48. Donjacour AA, Thomson AA, Cunha GR. Enlargement of the ampullary gland and seminal vesicle, but not the prostate in int-2/Fgf-3 transgenic mice. *Differentiation*. 1998;62:227–237.
49. Bacich DJ, Pinto JT, Tong WP, Heston WD. Cloning, expression, genomic localization, and enzymatic activities of the mouse homolog of prostate-specific membrane antigen/NAALADase/folate hydrolase. *Mamm Genome*. 2001;12:117–123.
50. Dyck MK, Gagne D, Ouellet M, et al. Seminal vesicle production and secretion of growth hormone into seminal fluid. *Nat Biotechnol*. 1999;17:1087–1090.
51. Ruberte Jose CA, Navarro M. *Morphological Mouse Phenotyping: Anatomy, Histology and Imaging*. Madrid: Medica Panamericana; 2017:195–226.
52. Collard F, Vertommen D, Constantinescu S, Buts L, Van Schaftingen E. Molecular identification of beta-citrylglutamate hydrolase as glutamate carboxypeptidase 3. *J Biol Chem*. 2011;286:38220–38230.

53. Neuman BP, Eifler JB, Castanares M, et al. Real-time, near-infrared fluorescence imaging with an optimized dye/light source/camera combination for surgical guidance of prostate cancer. *Clin Cancer Res*. 2015;21:771–780.
54. Kovar JL, Cheung LL, Simpson MA, Olive DM. Pharmacokinetic and biodistribution assessment of a near infrared-labeled PSMA-specific small molecule in tumor-bearing mice. *Prostate Cancer*. 2014;2014:104248.
55. Renneberg H, Friedetzky A, Konrad L, et al. Prostate specific membrane antigen (PSM) is expressed in various human tissues: implication for the use of PSM reverse transcription polymerase chain reaction to detect hematogenous prostate cancer spread. *Urol Res*. 1999;27:23–27.
56. Fisch H, Lambert SM, Goluboff ET. Management of ejaculatory duct obstruction: etiology, diagnosis, and treatment. *World J Urol*. 2006; 24:604–610.

How to cite this article: Vorlová B, Sedlák F, Kašpárek P, et al. A novel PSMA/GCPII-deficient mouse model shows enlarged seminal vesicles upon aging. *The Prostate*. 2018;1–14. https://doi.org/10.1002/pros.23717

Příloha 6

molecular pharmaceutics

Article

Cite This: Mol. Pharmaceutics 2018, 15, 2932−2945

Inhibitor−GCPII Interaction: Selective and Robust System for Targeting Cancer Cells with Structurally Diverse Nanoparticles

Jitka Neburkova,[†,‡,§] Frantisek Sedlak,[†,‡,§,∥] Jirina Zackova Suchanova,[§,∥] Libor Kostka,[⊥] Pavel Sacha,[†] Vladimir Subr,[⊥] Tomas Etrych,[⊥] Petr Simon,[†] Jitka Barinkova,[†] Robin Krystufek,[†] Hana Spanielova,[†,∥] Jitka Forstova,[∥] Jan Konvalinka,[†,#] and Petr Cigler*[,†]

[†]Institute of Organic Chemistry and Biochemistry of the CAS, Flemingovo namesti 2, 166 10 Prague, Czech Republic
[‡]First Faculty of Medicine, Charles University, Katerinska 32, 121 08 Prague, Czech Republic
[∥]Department of Genetics and Microbiology, Faculty of Science, Charles University, Vinicna 5, 128 44 Prague 2, Czech Republic
[⊥]Institute of Macromolecular Chemistry of the CAS, Heyrovskeho namesti 2, 162 06, Prague 6, Czech Republic
[#]Department of Biochemistry, Faculty of Science, Charles University, Hlavova 2030, 128 43 Prague 2, Czech Republic

Supporting Information

ABSTRACT: Glutamate carboxypeptidase II (GCPII) is a membrane protease overexpressed by prostate cancer cells and detected in the neovasculature of most solid tumors. Targeting GCPII with inhibitor-bearing nanoparticles can enable recognition, imaging, and delivery of treatments to cancer cells. Compared to methods based on antibodies and other large biomolecules, inhibitor-mediated targeting benefits from the low molecular weight of the inhibitor molecules, which are typically stable, easy-to-handle, and able to bind the enzyme with very high affinity. Although GCPII is established as a molecular target, comparing previously reported results is difficult due to the different methodological approaches used. In this work, we investigate the robustness and limitations of GCPII targeting with a diverse range of inhibitor-bearing nanoparticles (various structures, sizes, bionanointerfaces, conjugation chemistry, and surface densities of attached inhibitors). Polymer-coated nanodiamonds, virus-like particles based on bacteriophage Qβ and mouse polyomavirus, and polymeric poly(HPMA) nanoparticles with inhibitors attached by different means were synthesized and characterized. We evaluated their ability to bind GCPII and interact with cancer cells using surface plasmon resonance, inhibition assay, flow cytometry, and confocal microscopy. Regardless of the diversity of the investigated nanosystems, they all strongly interact with GCPII (most with low picomolar K_i values) and effectively target GCPII-expressing cells. The robustness of this approach was limited only by the quality of the nanoparticle bionanointerface, which must be properly designed by adding a sufficient density of hydrophilic protective polymers. We conclude that the targeting of cancer cells overexpressing GCPII is a viable approach transferable to a broad diversity of nanosystems.

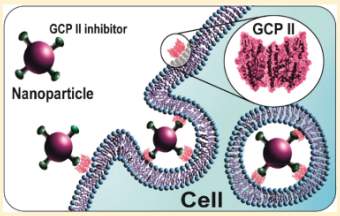

KEYWORDS: *GCPII, PSMA, inhibitor, click chemistry, targeting, cell, nanodiamond, virus-like particle, multivalent binding, polymer, nonspecific interaction*

INTRODUCTION

Targeted delivery of pharmaceuticals into tumor tissues offers promise for precise cancer diagnosis and treatment. Nanoparticle (NP)-based carriers offer several advantages over conventional therapy with cytotoxic drugs. The polyvalency of ligands strengthens binding efficacy, the size of NPs leads to prolonged blood circulation time and enables passive targeting (so-called enhanced permeation effect), and the hollow interior of NPs enables delivery of cargo.[1]

For specific cellular targeting, glutamate carboxypeptidase II (GCPII), also known as prostate-specific membrane antigen (PSMA), is a particularly interesting receptor due to its higher expression in prostate cancer tissue and cancer-associated neovasculature.[2,3] Its abundance correlates with the aggressiveness of the prostate cancer (GCPII is expressed in 80% of cells in malignant lesions[4]) and poor prognosis of the patient. In contrast to surface receptors that are present on all cell types, such as transferrin receptor, GCPII is more tissue-specific. It is primarily expressed in the prostate, central nervous system, small intestine, and kidney; expression in other tissues is much lower.[5] GCPII is a homodimeric transmembrane glycoprotein and metalloprotease with two main natural substrates, the most important of which is *N*-acetyl-L-aspartyl-L-glutamate (NAAG). In the CNS, GCPII cleaves NAAG into the neurotransmitters

Special Issue: Click Chemistry for Medicine and Biology

Received: October 10, 2017
Revised: January 22, 2018
Accepted: February 1, 2018
Published: February 1, 2018

DOI: 10.1021/acs.molpharmaceut.7b00889
Mol. Pharmaceutics 2018, 15, 2932−2945

N-acetyl- L-aspartate and glutamate. In the intestine, where it is also known as folate hydrolase I, GCPII participates in the cleavage of γ-linked glutamates from pteroyl-poly(γ-glutamate), freeing the vitamin folic acid.[6] Although the substrate and physiological function of GCPII in prostate remain unknown, its overexpression in prostate cancer is well-established, and the enzyme has been exploited as a highly specific target for cancer diagnostics and therapies.

Cancer cells overexpressing GCPII have been successfully targeted with NPs bearing antibodies,[7,8] nucleic acid aptamers,[9,10] and specific inhibitors.[11−14] Despite the convenient properties of small molecules, including stability, nonimmunogenicity, and ease of large-scale synthesis, using inhibitors as targeting ligands is not common. NPs bearing inhibitors have been developed for a very small number of targets, including carbonic anhydrase IX[15] and GCPII.[11−14,16−25] This may be due to the fact that enzymes localized on the plasma membrane usually are not cancer- or tissue-specific, and to the lack of known potent inhibitors for these enzymes. Nevertheless, GCPII inhibitors previously have been used with soft polymeric NPs, including in clinical trials,[19] and with inorganic NPs.[16,22,23] Because of the very different methodological approaches and NP structures used in various studies, it is difficult to compare results.

Here, we focus on exploring the structural and chemical diversity of NP systems that can be delivered to their cellular targets using interactions between small inhibitor molecules attached to the NP and GCPII on the surface of the target cell. To do so, we use representatives of different types of NPs: polymer-coated nanodiamonds, virus-like particles based on bacteriophage Qβ and mouse polyomavirus, and polymeric nanoparticles with an inhibitor attached as a targeting ligand. Although targeted nanosystems based on all these NPs have been developed previously, targeting with small molecules is typically a more challenging approach that requires surface optimization. The range of selected particles enables us to investigate nanosystems of different size, flexibility, bionanointerface, and conjugation chemistry. We evaluate targeting efficiency under the same conditions on the same cellular model to identify the potential limitations of these GCPII-inhibitor-targeting systems.

Nanodiamonds (NDs) are relatively polydisperse (in size and shape), nontoxic carbon NPs with unique optical properties, including near-infrared unbleachable fluorescence [derived from nitrogen vacancy (NV) centers] sensitive to magnetic and electric fields.[26] Similar to other inorganic NPs, they aggregate in electrolytes (buffers and media), driven by strong van der Waals forces.[27] NDs can be colloidally stabilized by steric hindrance, either by proteins or by polymers. Although proteins can both stabilize the particles and direct them to the intended target, electroneutral polymers also can reduce nonspecific interactions with proteins and cells, which is crucial for preparation of outstanding NPs for targeting. In a biological environment, interactions of proteins with NPs form a so-called "protein corona" on the NP surface,[28,29] which can be prevented by creating a dense polymeric shell on the NP. Intact, biocompatible, and nonimmunogenic polymers can shield the surface and minimize off-target binding.[30]

NDs without a polymer shell have been targeted to cells using the protein transferrin[31−33] or small protein toxins.[34] While use of a polymer interface can be beneficial for NPs bearing proteins, it is necessary for NPs bearing small molecules, because small molecules do not have a shielding effect on the NPs. Polymer-coated NDs bearing folic acid,[35,36] RGD peptide,[37,38] and anti-HER2 peptide[39] have been targeted to cancer cells with very high efficacy.

Virus-like particles (VLPs) are safe and noninfectious virus derived NPs, usually formed in biological systems into well-defined uniform structures by a self-assembly process from multiple copies of the same capsid protein(s). VLPs are available in various sizes and shapes and display different cell binding properties. VLPs derived from plant viruses and bacteriophages usually do not efficiently bind mammalian cells, whereas VLPs derived from mammalian viruses can bind to the mammalian cell surface, engaging the carbohydrate moieties of glycocalyx.

Mouse polyomavirus (MPyV) is an example of a small (45 nm diameter) dsDNA nonenveloped mouse virus. Historically, VLPs composed of MPyV capsid protein were the first VLPs to be used for gene transfer.[40,41] Because there is no preexisting humoral immunity to MPyV in the human population, MPyV VLPs are suitable for potential clinical use. The MPyV capsid is composed of 72 subunits. Each subunit consists of 5 molecules of the major capsid protein, VP1, which form pentamers. Under experimental conditions, guided *in vitro* disassembly and reassembly can be used for passive cargo loading into the interior of VLPs, as shown for human polyomavirus JC.[42] MPyV uses GD1a, GT1b,[43] and GT1a[44] gangliosides as primary receptors that mediate transport of the virus along an infectious pathway. Moreover, $\alpha_4\beta_1$ integrin has been identified as a secondary receptor.[45] Although viral binding to gangliosides is required for high levels of virus accumulation on the cell surface, the presence of cell-surface glycoproteins also allows for virus attachment and internalization. MPyV VLPs therefore interact with a wide variety of mammalian cells via sialic acid presented on cell surface glycoproteins and glycolipids and enter cells readily. As with NDs, surface modification of VLPs with polymers may be required for selective targeting to the specific receptor and prevention of nonspecific interactions. Recently, we demonstrated that large molecules (the protein transferrin) displayed on the MPyV surface can both retarget the VLP to cancer cells and prevent the interaction with its primary receptors.[46] Targeting with small molecules has not yet been demonstrated for MPyV VLPs.

Bacteriophage Qβ is an example of a small (28 nm diameter) icosahedral virus, VLPs of which have been actively investigated for several nanotechnology applications. Qβ VLPs are highly monodisperse and very stable, and they consist of 180 protein subunits cross-linked by disulfide linkages. Qβ VLPs can package small enzymes to protect and stabilize them.[47] Unlike other types of NPs, Qβ VLPs do not interact with mammalian cells to a great degree, and therefore they do not need to be coated with polymers to decrease nonspecific interactions and efficiently target cells. Qβ VLPs have been modified with transferrin,[48] epidermal growth factor,[49] glycan,[50] and cyclic RGD[51] to target cells, as shown by M. G. Finn and collaborators. Although a polymer coating is not needed *in vitro*, for *in vivo* applications the VLP surface should be covered with polymers to improve pharmacokinetic properties and reduce immunogenicity. Qβ particles have been modified with poly(2-oxazoline)s[52] and oligo(ethylene glycol)-methacrylate[53] to enhance thermal stability and evade immune responses.

Polymeric NPs are among the most widely used NPs for bioapplications, thanks to their variability in composition, which can be adjusted according to the needs of the application.

DOI: 10.1021/acs.molpharmaceut.7b00889
Mol. Pharmaceutics 2018, 15, 2932−2945

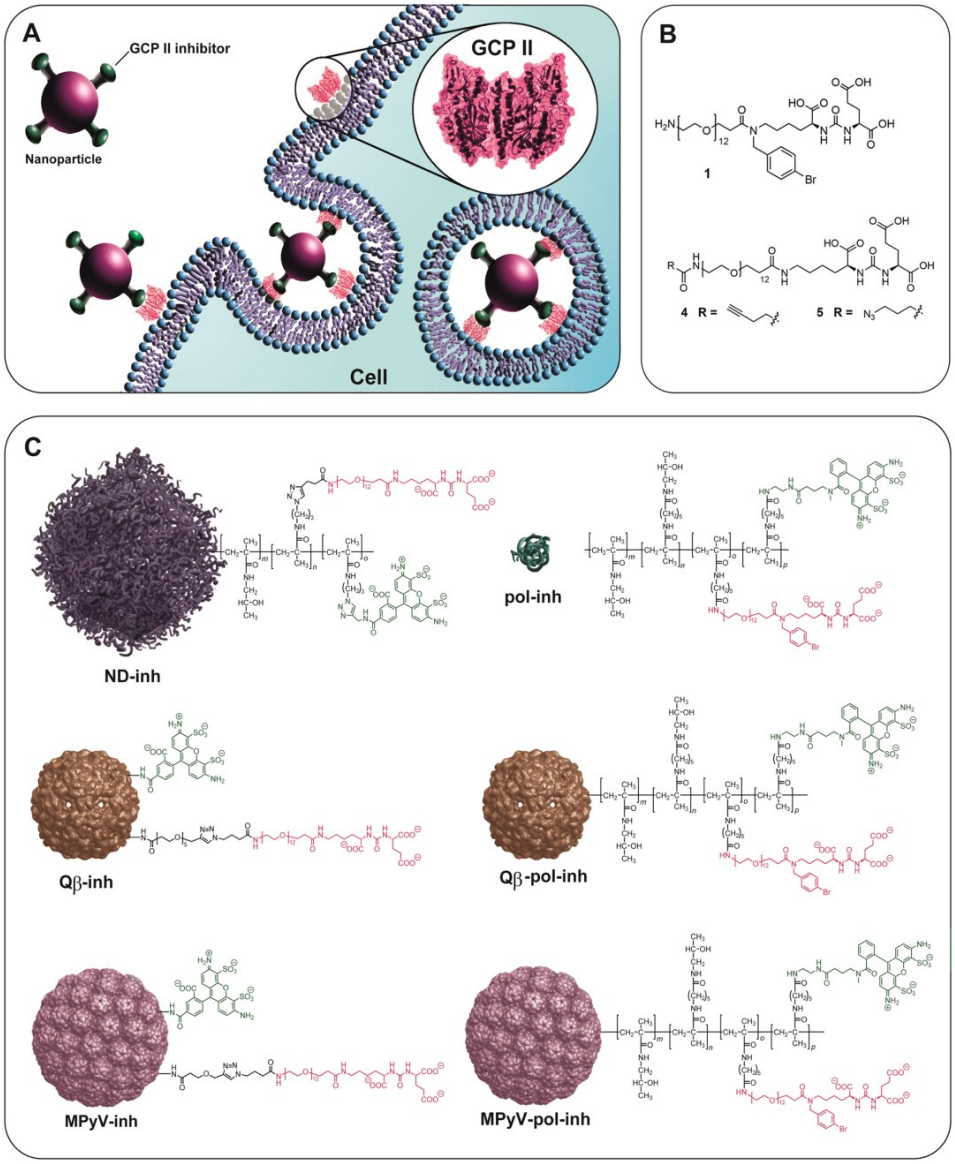

Figure 1. (A) The overall scheme of GCPII targeting using NPs bearing GCPII inhibitors. A NP bearing polyvalent array of GCPII inhibitors binds to GCPII, which is anchored in cell membrane. The nanoparticle is then endocytosed. (B) The structures of the inhibitors **1**, **4**, and **5** used for NP modifications. (C) Schematic illustration of the used NPs and molecular structure of their bionanointerface. Only particles modified with GCPII inhibitors are shown: nanodiamonds (**ND-inh**), small nanoparticles based only on the coating polymer (**pol-inh**), bacteriophage Qβ VLPs (**Qβ-inh**, **Qβ-pol-inh**), and mouse polyomavirus VLPs (**MPyV-inh**, **MPyV-pol-inh**). The corresponding control particles (**ND**, **pol**, **Qβ**, **Qβ-pol**, **MPyV**, and **MPyV-pol**) have always the same structure, but do not contain the GCPII inhibitors (not shown for clarity). For VLPs, the attachment of inhibitor via coating polymer is indicated by the presence of "**pol**" in the abbreviation, while the absence of "**pol**" indicates a direct attachment to surface lysines. See also Table 1 for further details.

DOI: 10.1021/acs.molpharmaceut.7b00889
Mol. Pharmaceutics 2018, 15, 2932−2945

They are not prone to nonspecific interactions with cells, and therefore they are not immediately internalized. On the other hand, polymeric NPs are typically not monodisperse. Polymeric NPs are the only particles assessed in this study that have previously been used with a specific inhibitor to target GCPII. Among the most studied have been block copolymers containing a hydrophobic part, usually poly(lactid) acid, bearing the hydrophobic molecule and a hydrophilic PEG chain exposed to the environment.[12,17,19,20] For nucleic acid delivery, copolymers contained combination of polyethylenimine and PEG.[13,18] Biodegradable, nonimmunogenic, water-soluble, and biocompatible *N*-(2-hydroxypropyl)-methacrylamide (HPMA) copolymer with inhibitor targeting GCPII also has shown potential in bioapplications.[24]

The most widely used conjugation chemistry for modification of NPs with a targeting ligand is amidic coupling, which is the easiest option for molecules that naturally contain carboxyl or amine groups (such as VLPs). For amidic coupling, moieties with activated carboxyl groups with fair stability and selective reactivity to amines are needed. Here, we used the thiazolidine-2-thione group (TT) to fulfill these requirements.[54] An alternative option is use of highly effective bioorthogonal reactions, which do not have significant reactivity toward naturally occurring functional groups. The Huisgen azide–alkyne cycloaddition catalyzed by Cu(I) ions (click reaction) is popular due to its high bioconjugation efficacy without the need for protecting groups, simplicity, and variety of available substrates.[55,56] In this work, we used both amidic coupling and click reaction.

METHODS

Synthesis of GCPII inhibitors and HPMA polymers is described in the Supporting Information.

Preparation of Mouse Polyomavirus VLPs (MPyV, MPyV-inh, MPyV-PEG). MPyV particles consisting of VP1 capsid protein were produced using baculovirus expression system in *Spodoptera frugiperda* (Sf9) cells.[57] Purification of particles in cesium chloride density gradient was followed by concentration through a sucrose cushion as previously described.[57,58]

Labeling of MPyV VLPs with Alexa Fluor 488. Unmodified MPyV VLPs were dialyzed against 0.1 M HEPES, pH 7.9, and the protein concentration was adjusted to 2 mg/mL (20 mg VP1 protein in total). This solution was treated with NHS-Alexa Fluor 488 (ThermoFisher Scientific, final concentration 34 nM, 0.2 equiv per surface lysine; each MPyV VLP contains 720 surface-exposed lysines) at room temperature overnight with gentle shaking (250 rpm, TS-100C, Thermo-Shaker, Biosan). Excess dye was removed by dialysis against 0.1 M HEPES, pH 7.9 (4 °C, overnight with two buffer changes). Two-thirds of the prepared MPyV VLP mixture were used for subsequent preparation of **MPyV-inh** particles. The rest was purified and concentrated by centrifugation through two successive 20% sucrose cushions (35,000 rpm, SW41 Beckman rotor, 3 h) and dissolved in storage buffer (10 mM Tris-HCl, pH 7.4, 150 mM NaCl, 0.01 mM $CaCl_2$), providing the conjugate of MPyV VLPs (4 mg) used as a negative control (**MPyV**).

*Preparation of **MPyV-inh** by Click Reaction.* Alexa Fluor 488-labeled **MPyV** VLPs were first modified with the heterobifunctional linker propargyl-*N*-hydroxysuccinimidyl (NHS) ester (Sigma-Aldrich). To a solution of **MPyV** in 0.1 M HEPES, pH 7.9 (2 mg/mL; total amount 14 mg) was added 4.87 mg of the linker (35-fold molar excess per surface lysine) dissolved in 770 μL of DMSO (10% final concentration of DMSO). The reaction mixture was incubated at room temperature overnight with gentle shaking (250 rpm, TS-100C, Thermo-Shaker, Biosan). Excess reagents were removed by dialysis against 0.1 M HEPES, pH 7.4 (4 °C, overnight, first two buffer changes contained 10% DMSO), providing MPyV VLP–alkyne conjugate.

MPyV VLP–alkyne (5 mg in a final reaction volume of 6 mL), GCPII inhibitor **5** (see Figure 1 and Supporting Information; 213.5 nmol) in 0.1 M HEPES buffer, pH 7.4, containing 10 mM copper sulfate, 100 mM aminoguanidine, 50 mM tris(3-hydroxypropyltriazolylmethyl)amine (THPTA, synthesized according to a previously published procedure[59]), and freshly prepared 100 mM sodium ascorbate were used for click reaction. Copper sulfate and THPTA were mixed in a separate tube in a 1:5 concentration ratio prior to addition to the reaction mixture. The reaction mixture was well-sealed, mixed, and allowed to stand undisturbed at room temperature for 3 h. Excess inhibitor was removed from the resulting **MPyV-inh** conjugates by dialysis (cellulose ester membrane, 300 kDa, Biotech) against 0.1 M HEPES, pH 7.4 (4 °C, overnight), and storage buffer (4 °C, overnight). Finally, the **MPyV-inh** particles were purified and concentrated by centrifugation through two successive 20% sucrose cushions and dissolved in storage buffer.

*Preparation of **MPyV-PEG** Particles.* **MPyV** were dialyzed against 0.1 M HEPES, pH 8.0, with 0.01 mM $CaCl_2$ (4 °C, overnight). Then, the solution of particles (0.95 mg/mL, total amount 0.38 mg) was treated with 0.47 mg of acid-PEG_{13}-NHS ester (Broadpharm, BP-22330, 35-fold excess per surface lysine) at room temperature for 5 h on a rotating mixer. Excess reagents were removed by dialysis against TBS (20 mM Tris-HCl, 150 mM NaCl, pH 7.4) with 0.01 mM $CaCl_2$ (4 °C, overnight).

Characterization of the Particles. The quality of each preparation was examined by electron microscopy and SDS–PAGE. The amounts of VP1 were determined by Qubit protein assay kit (ThermoFisher Scientific). For matrix-assisted laser desorption/ionization mass spectrometry (MALDI) measurements, 15 μL of the sample (25 μg, 1.54 pmol) was mixed with 7.5 μL of 100 mM dithiothreitol (DTT) and 7.5 μL of 10 M urea for 10 min to disassemble the particles. According to MALDI measurements, we found 540 inhibitor molecules per **MPyV-inh** particle.

Preparation of Bacteriophage Qβ Particles (Qβ, Qβ-inh). Qβ particles were prepared according to a previously published procedure.[47] *Escherichia coli* BL21 (DE3) (Invitrogen) cells harboring the plasmid pET28-B (containing capsid protein) were grown in SOC supplemented with kanamycin. Starter cultures were grown overnight at 37 °C, and were used to inoculate larger cultures. Induction was performed with 1 mM IPTG at an OD_{600} of 1.0 in SOB overnight at 25 °C. Cells were harvested by centrifugation in a Beckman Coulter Avanti J-20 XP (rotor JA 17) at 5,400 rcf. The cell lysate was prepared by resuspending the cell pellet with phosphate buffer (0.1 M, pH 7.0) and sonicating at 50 W for 20 min with 5 s bursts and 5 s pause intervals. Cell debris was pelleted by centrifugation (Beckman Coulter Avanti J-20 XP) in a JA 17 rotor for 10 min (27,000 rcf), and 2 M ammonium sulfate was added to the supernatant to precipitate the Qβ VLPs. Pelleted VLPs were resuspended in phosphate buffer. Lipids and membrane proteins were then extracted from particles with 1:1 *n*-

DOI: 10.1021/acs.molpharmaceut.7b00889
Mol. Pharmaceutics 2018, 15, 2932–2945

butanol:chloroform; Qβ VLPs remained in the aqueous layer. Crude Qβ VLPs were further purified by sucrose gradient ultracentrifugation (10−40% w:v). Particles were pelleted out from the sucrose solution by ultracentrifugation in a 70.1 Ti rotor (Beckman) at 70,000 rpm for 2 h.

Labeling of Qβ with Alexa Fluor 488. The unmodified Qβ VLPs (3 mg) were diluted in 0.1 M HEPES, pH 8 (5 mg/mL). This solution was treated with Alexa Fluor 488 5-SDP Ester (ThermoFisher Scientific, final concentration 280 μM, 0.2 equiv per surface lysine; each Qβ VLP contains 720 surface-exposed lysines) at room temperature overnight with gentle shaking (250 rpm, TS-100C, Thermo-Shaker, Biosan). Excess dye was removed by centrifugal filtration (Millipore, Amicon ultra 2 mL, cut off 100 kDa, 6 times) into 0.1 M HEPES, pH 8, providing the conjugate Qβ VLP used as a negative control (**Qβ**). Two-thirds of the prepared Qβ VLP mixture was used for subsequent preparation of Qβ-inh particles (**Qβ-inh**).

*Preparation of **Qβ-inh** by Click Reaction.* First, **Qβ** VLPs were modified with a heterobifunctional linker containing propargyl and NHS ester moieties (alkyne-PEG_5-NHS, Sigma-Aldrich). To a solution of **Qβ** VLPs in 0.1 M HEPES, pH 8 (5 mg/mL; total amount 2 mg), was added 3.94 mg of the linker (17-fold excess per surface lysine) dissolved in 40 μL of DMSO (10% final concentration of DMSO). The reaction mixture was incubated at room temperature overnight with light shaking. Excess reagents were removed by centrifugal filtration (Millipore, Amicon ultra 2 mL, cut off 100 kDa, 8 times) against 0.1 M HEPES, pH 7.4 (first two buffer changes contained 10% DMSO), providing Qβ VLP−alkyne conjugate.

Qβ VLP−alkyne (1.6 mg in a final reaction volume of 160 μL), GCPII inhibitor **5** (see Figure 1 and Supporting Information; 205 nmol) in 0.1 M HEPES buffer, pH 7.4, containing 5.12 mM copper sulfate, 25.6 mM tris(3-hydroxypropyltriazolylmethyl)amine (THPTA), 40 mM aminoguanidine, and freshly prepared 40 mM sodium ascorbate were used for click reaction. Copper sulfate and THPTA were mixed in a separate tube in a 1:5 concentration ratio prior to addition to the reaction mixture. The reaction mixture was well-sealed, mixed, and allowed to stand undisturbed at room temperature for 3 h. The resulting Qβ-inh VLP conjugates were purified from excess reagents by centrifugal filtration (Millipore, Amicon ultra 2 mL, cut off 100 kDa, 8 times) into 0.1 M HEPES, pH 7.4, providing **Qβ-inh** conjugate.

Characterization of the Particles. The quality of each preparation was examined by electron microscopy and SDS−PAGE. The amounts of Qβ VLPs were determined by Qubit protein assay kit (ThermoFisher Scientific). For MALDI measurements, 5 μL of the sample (50 μg, 19.5 pmol) was mixed with 2.5 μL of 100 mM DTT and 2.5 μL of 10 M urea for 10 min to disassemble the particles. According to MALDI measurements, we found 180 inhibitors per **Qβ-inh** particle.

Preparation of Poly(HPMA)-Coated VLPs (MPyV-pol, MPyV-pol-inh, Qβ-pol, and Qβ-pol-inh). Unmodified MPyV VLPs were dialyzed and diluted to a low molarity buffer (0.67 mg/mL, 4 mM HEPES, pH 8, 20 mM NaCl, 4 μM $CaCl_2$). Unmodified Qβ VLPs (1 mg/mL) were dispersed in 25 mM HEPES buffer, pH 8. Three milliliters of MPyV particles (2 mg) was added slowly to a stirred solution of either polymer with inhibitor (pol-inh) or polymer without inhibitor (pol), both with TT reactive groups (3.76 mg/160 μL Milli-Q water, approximately 1 molar equiv to surface lysines on particles). Two milliliters of Qβ particles (2 mg) was added slowly to the stirred solution of pol-inh or pol with TT reactive groups (8.69 mg/mL Milli-Q water, approximately 0.4 equiv of surface lysines on particles). Reaction proceeded for 24 h (room temperature, mixing), and afterward remaining TT reactive groups were quenched by buffered ethanolamine (10 molar equiv to TT reactive groups). The conversion of TT reactive groups was controlled by decrease of their characteristic absorption band at 306 nm. After 12 h, no TT reactive groups were present.

VLP particles were purified by ultracentrifugation in sucrose density gradient (10−40% w:v, SW 28 Beckman rotor, 2 h 30,000 rpm for **MPyV-pol** and **MPyV-pol-inh** and 3 h 40,000 rpm for **Qβ-pol** and **Qβ-pol-inh**). Particles were pelleted out from the sucrose solution by ultracentrifugation at 35,000 rpm (SW 41Ti Beckman rotor) for 3 h.

Preparation of ND and ND-inh. NDs were pretreated and coated with a methacrylate-terminated thin silica layer, according to a previously published procedure.[60] Polymer coating was performed with slight modifications. HPMA (152 mg, 1046 μmol, purchased from Polysciences and freshly purified by FLASH chromatography) and 3-(azidopropyl)-methacrylamide (8 mg, 47.6 μmol, synthesized by methacryloylation of 3-azidopropan-1-amine with methacryloyl chloride[61]) were dissolved in DMSO (480 μL). 2,2′-Azobis(2-methylpropionitrile) (AIBN, 50 mg, 0.305 mmol, recrystallized by thickening an ethanol solution on a rotary evaporator at a maximum temperature of 30 °C) was added to the mixture. The mixture was filtered using a 0.4 μm glass microfiber microfilter. Methacrylate-terminated ND particles (8 mg, 80 μL in DMSO) were added. The reaction proceeded for 3 days under argon at 55 °C. The particles were diluted three times with methanol, centrifuged (21,000 rcf, 30 min), and purified by centrifugation with methanol (25,000 rcf, 30 min, 1 mL, 3 times). Polymer-coated NDs were further modified using azide−alkyne cycloaddition catalyzed by Cu(I) ions with Alexa Fluor 488-alkyne (purchased from Life Technologies) and GCPII inhibitor **4** (see Figure 1 and Supporting Information). NDs were modified with these two ligands in consecutive reactions utilizing the same surface functionalities. Washing procedures were employed after both modification steps. Stock solutions for copper(I)-catalyzed azide−alkyne cycloaddition reactions were prepared in water, except for the Alexa Fluor 488-alkyne, which was prepared in DMSO. The solutions of copper sulfate and THPTA were premixed (in a 1:2 concentration ratio) before they were added to the reaction mixture to yield final concentrations of 0.32 mM and 0.64 mM, respectively. The mixture was filled to the final volume with 50 mM HEPES buffer, pH 7.4. For the reaction of modified NDs with Alexa Fluor 488-alkyne, the reactants were mixed in the following order and final concentrations: colloid of poly-(HPMA)-azide modified NDs (1.2 mg in a final reaction volume of 1536 μL), Alexa Fluor 488-alkyne (10 μM), Cu-catalyst solution (see above), and a freshly prepared solution of sodium ascorbate (5 mM). The reaction mixture was well-sealed, mixed, and left for 3 h with no stirring. Modified NDs were isolated by centrifugation (20,000 rcf, 20 min) and twice washed with 1 mL of water. Half (0.6 mg) of the Alexa Fluor 488 modified NDs was reacted in a click reaction with GCPII inhibitor (320 μM) under the same conditions (in a final volume of 768 μL). Polymer-coated NDs modified with Alexa Fluor 488 (**ND**) and polymer-coated NDs modified with Alexa Fluor 488 and GCPII inhibitor (**ND-inh**) were both treated the same and were washed with water (1 mL, 7 times).

DOI: 10.1021/acs.molpharmaceut.7b00889
Mol. Pharmaceutics 2018, 15, 2932−2945

Surface Plasmon Resonance (SPR) Measurements. All SPR measurements were performed on a four-channel SPR sensor platform (PLASMON IV) developed at the Institute of Photonics and Electronics (IPE) of the Academy of Sciences of the Czech Republic, Prague. Gold SPR chips were loaded into a pure ethanol mixture of alkanethiols containing carboxylic terminal groups [HS-$(CH_2)_{11}$-PEG_4-OH and HS-$(CH_2)_{11}$-PEG_6-O-CH_2-COOH, molar ratio 7:3, Prochimia] with a final concentration of 0.2 mM and incubated for 1 h at 37 °C. The chips were then rinsed with ethanol and deionized water, dried with flow of nitrogen, and mounted to the prism on the SPR sensor. All experiments were performed at 25 °C. The carboxyl groups present on the gold thin sensor were activated by a solution of NHS, 1-ethyl-3-[3-(dimethylamino)propyl]-carbodiimide (EDC) at final concentrations of 12.5 mM and 62.5 mM, respectively, in deionized water for 5 min at a flow rate of 20 μL/min. Excess reagents were removed at a flow rate of 30 μL/min. Next, 10 μg/mL neutravidin in 10 mM sodium acetate buffer, pH 5.0, was loaded for 6 min. Then, a high ionic strength solution (PBS with 0.5 M NaCl) was used to wash out noncovalently bound proteins, followed by 1 M ethanolamine for deactivation of residual activated carboxylic groups. Afterward, the extracellular domain of GCPII modified with biotin (Avi-GCPII, prepared according to Tykvart et al.[62]) was loaded for 10 min. Various NPs (at final concentrations of 5 nM) in TBS were injected (association phase) for several minutes, and then TBS alone was injected (dissociation phase).

Inhibition Assay. The inhibitory effects of all particles and polymers were measured as previously described with minor modifications.[63] Briefly, in each well of a 96-well plate, 250 pg of recombinant GCPII was preincubated for 5 min at 37 °C in 90 μL of reaction buffer (25 mM BisTris propane, 150 mM NaCl, 0.001% (w/w) octaethylene glycol monododecyl ester (Affymetrix), pH 7.4) with a dilution series of inhibitor (particles or polymers). The reaction was started by adding 10 μL of the substrate, 4 μM pteroyldiglutamate. The reaction was stopped after 20 min incubation at 37 °C by adding 10 μL of 25 μM 2-(phoshonomethyl)pentanedioic acid (2-PMPA) and subsequently analyzed with an Agilent 1200 series HPLC using isocratic separation in 2.7% AcCN, 19.5 mM phosphate, pH 6.0, on an Acquity UPLC HSS T3 C18 1.8 μm column (2.1 × 100 mm, Waters) with detection at 281 nm. Obtained data were fitted by logistic equation using GraphPad (GraphPad Software, Inc.), and K_i values were calculated from the log IC_{50} the using Cheng−Prusoff equation.

Flow Cytometry. Cells (U-251$^+$ MG and U-251$^-$ MG; for preparation see Supporting Information) were detached from the dish by trypsinization, resuspended in DMEM (Sigma-Aldrich D5796) supplemented with 4 mM L-glutamine (Gibco) and 10% FBS (Gibco), and counted. An appropriate amount of cells was centrifuged (300 rcf, 5 min, 4 °C) and dissolved in serum free medium without phosphate (SFM-P, DMEM, Sigma-Aldrich D3656). Subsequently, the cells were transferred into a 96-well plate (6×10^4 cells per well) and incubated with NPs (final concentration of 4 nM) for 1 h at 37 °C, 5% CO_2. This incubation was performed in triplicate and with negative controls (SFM-P only). After the treatment, cells were centrifuged (300 rcf, 5 min, 4 °C), resuspended in 200 μL of TBS, and measured with a BD LSRFortessa flow cytometry analyzer (Becton, Dickinson and Company). The data were further analyzed with BD FACSDiva Software, version 6.0. Statistical analysis was performed in R program version 3.3.1. (2016-06-21).

Confocal Microscopy. U-251$^+$ MG and U-251$^-$ MG cells (for preparation see Supporting Information) were grown in 4-chamber Glass Bottom Microwell Dishes (Cellvis, D35C4-20-1.5-N) at approximately 30% confluence, incubated for 1 h at 37 °C, 5% CO_2 with NPs, polymers (12.5 nM, diluted in SFM-P, DMEM, Sigma-Aldrich D5796), or medium only (SFM-P). Subsequently, cells were washed with TBS, fixed with 3.7% formaldehyde for 10 min, washed again in TBS, and counterstained with 500 ng/mL Hoechst 34580 solution (Thermo Scientific). Fluorescence and transmitted light (TL) images were acquired on a Zeiss LSM 780 confocal microscope with ZEN 2011 software. The images were further processed in Fiji software (contrast enhancement of Hoechst channel and TL images).[64]

RESULTS AND DISCUSSION

Design and Preparation of Nanoparticles. To investigate the versatility of cell targeting using GCPII inhibitors, we prepared six different types of particles with various surface modifications, as shown schematically in Figure 1 (for clarity, we present the final investigated particles in **bold**, for example **Qβ-inh**). We attached to the surface of these NPs fluorescent labels (Alexa Fluor 488 or Atto 488; marked green in Figure 1) and GCPII inhibitors (marked red). As a targeting moiety, we used optimized urea-based inhibitors[65,63] **1**, **4**, and **5** that are highly polar and negatively charged, contributing to Coulombic stabilization of the particles in solution. The inhibitors were equipped by linkers terminated with either groups for click chemistry (azide, alkyne) or amino groups for conjugation to activated carboxylic acids. To remove cytotoxic Cu^{2+} ions, which can remain in the sample after click reaction, we used extensive washing procedures diluting the original concentrations of reagents by a factor of minimally 10^7 (see Methods). This decreased the copper concentration far below from cytotoxic limit, which is further suppressed by the use of THPTA ligand.[66] Furthermore, in our previous works utilizing click chemistry on similar nanoparticles,[37,46] we have observed no copper toxicity. Based on these assumptions, we have not involved cytotoxicity tests in this study.

The span of NP structural archetypes studied here includes those currently used in nanomedical applications ranging from imaging and theranostic applications to drug delivery. Polymer-coated NDs are hybrids with solid inorganic cores that retain their original shape and size during all interactions. However, their polymer shell enables flexible adjustment of targeting groups for polyvalent binding. VLPs are usually classified as soft matter nanomaterial; however, they are relatively rigid and do not undergo significant size or shape changes. Nevertheless, attachment of targeting groups to VLPs via flexible linkers can allow for a similarly flexible interaction as in polymer shells on NDs. Finally, our polymeric NPs represent the smallest and most flexible systems used in this study, and are highly susceptible to size and shape changes upon binding to a target.

VLPs from both MPyV and Qβ are formed from proteins containing lysine residues with modifiable amino groups. Both types of VLPs contain approximately 720 surface lysines per particle,[50,67] which we used to modify the particles with dyes and inhibitors either by short linkages or by polymer coating. The first approach involved labeling with Alexa Fluor 488 active ester (providing negative controls and **MPyV** or **Qβ** conjugates) to allow fluorescence visualization. Then, we modified VLPs at the remaining lysines with an excess of a short linker bearing a propargyl group and attached GCPII

DOI: 10.1021/acs.molpharmaceut.7b00889
Mol. Pharmaceutics 2018, 15, 2932−2945

inhibitor−azide conjugates via click chemistry, obtaining **MPyV-inh** and **Qβ-inh** conjugates. Because MPyV VLPs can interact with sialic acid residues, which are ubiquitously distributed and broaden MPyV cell and tissue tropism,[68] we also prepared MPyV VLPs that should avoid these interactions (**MPyV-PEG**). These VLPs were prepared by covering **MPyV** with NHS PEG_{13}-carboxyl.

The second approach for MPyV and Qβ VLP modification involved coating the VLP surface with HPMA copolymer premodified with Atto 488 dye and then with GCPII inhibitors. In addition to dye and inhibitors, the copolymers also contained hydrolytically stable TT reactive groups, which can react with lysine amino groups on the VLP surface, forming amide bonds. The reaction of VLPs with polymer proceeded overnight at pH 8. We then quenched all unreacted TT groups with ethanolamine. This step is very important because unreacted TT groups can cross-link the particles in the pellet after ultracentrifugation. We incubated the VLPs with either copolymer with inhibitor (pol-inh) or copolymer without inhibitor (pol). After purification, we obtained four different types of particles: **MPyV-pol-inh**, **MPyV-pol**, **Qβ-pol-inh**, and **Qβ-pol** (see Figure 1). The same polymer used for modification of particles was reacted in parallel with 1-aminopropan-2-ol and served as two last types of NPs (**pol-inh** and **pol**).

Coating with hydrophilic polymers greatly improves the colloidal stability of NDs in buffers and media used for bioapplications.[30] Here, we modified NDs with a thin silica layer bearing methacrylate moieties, from which polymer chains of *N*-(2-hydroxypropyl)methacrylamide and 3-(azidopropyl)-methacrylamide were grown by radical polymerization. The polymer surface enables efficient modifications, because the azide groups are randomly distributed on flexible chains without substantial steric hindrance from the surface. Using click chemistry, we equipped the NDs with GCPII inhibitor-alkyne. Although NV fluorescent centers in NDs possess excellent optical features for cell imaging,[37,69,70] for the ease of comparison with other particles in this study, we used NDs without NV centers but with attached Alexa Fluor-alkyne dye, providing **ND-inh**.

Characterization of nanoparticles. We characterized the size, morphology, and colloidal stability of all prepared NPs by transmission electron microscopy (TEM) and dynamic light scattering (DLS) (see Supporting Information for methods). TEM confirmed the presence of intact, highly monodispersed VLPs and fairly monodispersed ND particles (Figure 2A, Figure S1). Analysis of the particle size distribution (Figure 2B) revealed diameters of 44.7 ± 1.6 nm for **MPyV-pol-inh**, 27.2 ± 1.6 nm for **Qβ-pol-inh**, and 53.5 ± 12.0 nm for **ND-inh**. Using DLS, we ascertained that the particles do not aggregate (Figure 2C, Figure S2F) at 37 °C. Their hydrodynamic diameters are larger than the diameters obtained from TEM, indicating the presence of hydrated polymer shells in an aqueous environment. DLS data indicated that attachment of the inhibitor through either direct conjugation or a polymer coating does not change colloidal stability of NPs.

Data obtained from SDS−PAGE analysis confirmed that unmodified VLPs can be disassembled into VP1 monomers or dimers (Figure S3). The fluorescent polymers on Qβ VLPs dissociated completely from the coat proteins during sample processing, whereas polymers on MPyV VLPs remained cross-linked with the major capsid protein VP1, forming high molecular weight complexes (Figure S3A,B). In the case of

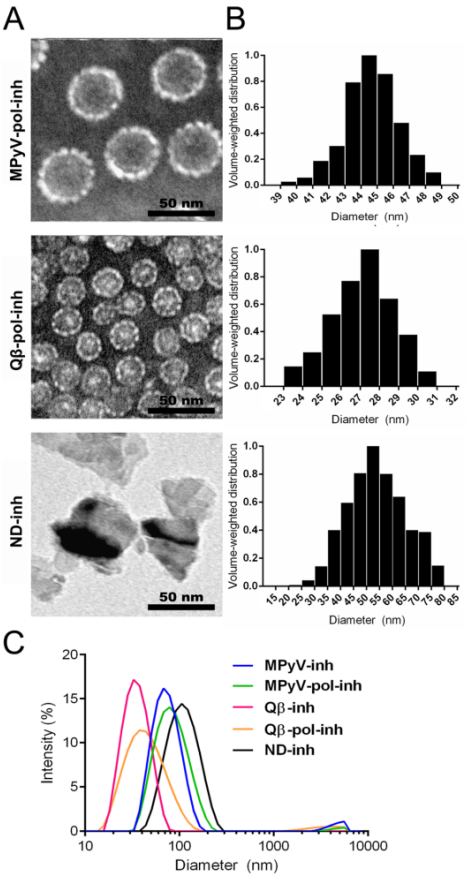

Figure 2. Characterization of NPs. (A) Representative TEM images, negative staining with 2% solution of phosphotungstic acid for **MPyV-pol-inh** and **Qβ-pol-inh**, scale bar = 50 nm. (B) Volume-weighted size distribution of the NPs according to TEM images analysis performed with ImageJ software. (C) Hydrodynamic diameters of NPs with conjugated inhibitors from DLS measurements at 37 °C (concentration 0.25 mg/mL in water).

directly modified VLPs (without polymers), the cross-linking phenomenon was seen in both types of VLPs, but was less pronounced in Qβ VLPs, likely resulting from different structural arrangements of particles. The absence of highly cross-linked complexes in these VLPs suggests that the particles potentially could more easily disassemble in cells to deliver cargo. NDs cannot be stained like proteins (Figure S3A); however, they were clearly detected at the start based on their fluorescent signal (Figure S3B). NDs did not migrate in the gel.

Increased thermal stability of VLPs can be indicative of modification on the particle surface,[52] especially in the case of MPyV, which is structurally less stable than Qβ. We monitored temperature-induced changes in MPyV particle stability by DLS (Figure S2). Nonmodified **MPyV** changed size slightly at

DOI: 10.1021/acs.molpharmaceut.7b00889
Mol. Pharmaceutics 2018, 15, 2932−2945

temperatures over 60 °C (Figure S2A), and our results corresponded well with the observed temperature midpoint of denaturation (T_M = 56 °C) for MPyV particles produced in yeast.[71] Modification with HPMA copolymer resulted in higher thermal stability (up to 80 °C) (Figure S2D,E). Particles with directly conjugated inhibitor (**MPyV-inh**) (Figure S2B) or PEG (negative control, **MPyV-PEG**) (Figure S2C) did not disassemble even after incubation at 90 °C. We assume that the increased stability of the particles is mediated by the high coverage of the MPyV surface with PEG residues, which are present in both samples (the inhibitor linker is composed of PEG). The lower stability of poly(HPMA)-coated MPyV could be caused by incomplete coverage of copolymer on the surface.

Finally, we characterized the efficiency of labeling and inhibitor loading. Due to the nonhomogeneity of dye labeling between the different types of particles, we used the relative fluorescence of particles to normalize the flow cytometry data (Table 1). From quantification of dye on poly(HPMA)-coated VLPs, we estimate that there were approximately 2 HPMA copolymers on each **Qβ-pol-inh** particle and 8 molecules on **Qβ-pol**. Surface coverage of MPyV particles (which have a larger surface area) was higher, with 30 and 35 molecules of HPMA copolymer per **MPyV-pol-inh** and **MPyV-pol** particle, respectively. In general, the number of attached HPMA copolymers was lower than we expected. We hypothesize that this may be due to the high content of TT reactive groups connected to the copolymer backbone with hydrophobic alkyl linkers. Due to the flexibility of the polymer chain, folding and formation of local hydrophobic domains can occur, leading to steric hindrance and lower reactivity of TT moieties.

Table 1. Characterization of Nanoparticle Surface Modifications, Amount of the Fluorophores on the Particles, and Relative Fluorescence Intensities of NPs[a]

particle	polymer	fluorophore	fluorophores/particle	relative fluorescence
ND	HPMA	Alexa Fluor 488	110	7.7
ND-inh	HPMA	Alexa Fluor 488	67	5.3
Qβ		Alexa Fluor 488	72	9.2
Qβ-inh		Alexa Fluor 488	44	3.9
MPyV		Alexa Fluor 488	19	4.4
MPyV-inh		Alexa Fluor 488	63	7.4
MPyV-PEG	PEG	Alexa Fluor 488	30	6.9
Qβ-pol	HPMA	Atto 488	28	12.6
Qβ-pol-inh	HPMA	Atto 488	7	4.7
MPyV-pol	HPMA	Atto 488	114	30.6
MPyV-pol-inh	HPMA	Atto 488	88	23.3
pol	HPMA	Atto 488	3	1.0
pol-inh	HPMA	Atto 488	3	1.4

[a]The fluorescence intensities of the respective NPs were measured at the same molar NP concentration. The obtained values were always normalized to the fluorescence intensity of the NP with the lowest fluorescence intensity, **pol**.

We also used the dye quantification data to determine the number of inhibitor molecules on polymer-coated VLPs (Table 2). Based on known stoichiometry of the dye and inhibitor in the polymer, we obtained 12 and 180 inhibitors for **Qβ-pol-inh** and **MPyV-pol-inh**, respectively. We determined the number of inhibitors on **Qβ-inh** and **MPyV-inh** by MALDI measurement after disassembling Qβ and MPyV VLPs particles to protein subunits by treatment with dithiothreitol and urea. Although the mass spectra of the modified proteins were fairly complex (Figure S4), we were able to quantify the inhibitor loads, obtaining roughly ∼180 inhibitor molecules on **Qβ-inh** and ∼540 on **MPyV-inh** (corresponding to 25 and 75% of modified surface lysines, respectively). There were approximately 1,080 PEG molecules on **MPyV-PEG** (determined by the same approach). MALDI measurement also confirmed that inhibitor and PEG molecules were attached to the protein covalently.

Quantification of inhibitors on ND particles was a more challenging task because they cannot be disassembled to smaller units and measured by MALDI. However, based on an analogous reaction performed under identical conditions with fluorescent dye, we can assume a load of ∼250 inhibitors per ND particle.

Interaction of NPs with GCPII *in Vitro*. To analyze interactions between NPs and GCPII molecules, we performed SPR studies and inhibition assays. SPR measurements enabled us to ascertain the capacity of NPs to bind and recognize GCPII. We immobilized GCPII on SPR chips through a neutravidin−biotin interaction (GCPII+). This connection ensures that the GCPII orientation on the gold sensor is similar to the GCPII position on the plasma membrane. As a negative control, we attached neutravidin alone (GCPII−). SPR detects changes in the refractive index in the immediate vicinity of the surface layer of a sensor chip induced by particle binding to the surface, and because the particles have different refractive indices, we cannot directly compare and quantify their binding to GCPII. However, SPR measurements of all NPs bearing inhibitor verified their selectivity and strong affinity to GCPII+ chips (Figure 3). We also observed a weak interaction between **MPyV** particles and GCPII− chips. This likely reflects off-target binding between VP1 protein and neutravidin, as we observed the same interaction with streptavidin (data not shown). The very low dissociation rate (k_{off}) of the NPs from GCPII indicates an extremely strong interaction between GCPII and the inhibitor attached to the NPs. We surmise that this strength is mediated by cooperative formation of multiple bonds between ligand and layer (i.e., avidity).

Next, we investigated the ability of NPs to inhibit the processing of substrate by GCPII (Table 2). Using an HPLC inhibition assay, which monitors the cleavage of the pteroyldiglutamate substrate to folate and glutamate, we measured K_i values for all NPs decorated with inhibitor as well as for free inhibitors. The small molecule inhibitors showed K_i in low nanomolar range (2−14 nM). Their attachment to nanoparticles resulted in significant increase of inhibition efficacy, reaching subnanomolar (copolymer NP) or low picomolar (other NPs) K_i values. This behavior is most likely associated with high concentration of inhibitors at the NP surface, as documented by multivalent enhancement factors[72] in range units to tens of thousands (Table 2).

In comparison with larger and more bulky targeting ligands (for example cRGD peptide[73] and transferrin,[74,75] associating with their receptors with nanomolar and low nanomolar K_d, respectively), small molecule GCPII inhibitors can be installed on nanoparticle surface conveniently at higher loadings which can result in stronger avidity effects. Correspondingly, GCPII inhibitors reach efficacy similar to small molecule folate.[76]

DOI: 10.1021/acs.molpharmaceut.7b00889
Mol. Pharmaceutics 2018, 15, 2932−2945

Table 2. Inhibition Constants for NPs and Starting Inhibitors (for Structures, see Figure 1) Measured from HPLC Inhibition Assay, Expressed as K_i and IC_{50} with Standard Deviations[a]

	inhibitor type	inhibitors/particle	inhibition: $K_i \pm 1$ SD [pM]	MEF	inhibition: $IC_{50} \pm 1$ SD [pM]
			Nanoparticles		
ND-inh	**4**	250	3.70 ± 0.67	3780	42.1 ± 4.9
pol-inh	**1**	6	323 ± 50	6.63	3660 ± 290
Qβ-pol-inh	**1**	12	3.92 ± 0.83	546	44.6 ± 6.6
Qβ-inh	**5**	180	30.3 ± 4.5	373	344 ± 26
MPyV-pol-inh	**1**	180	2.87 ± 0.60	746	31.9 ± 4.5
MPyV-inh	**5**	540	0.60 ± 0.11	18 800	6.82 ± 1.2
			Inhibitors		
1			2140 ± 290		29 600 ± 4 100
4			14 000 ± 1 700		193 000 ± 26 600
5			11 300 ± 1 200		157 000 ± 19 700

[a]For NPs, the number of inhibitors per particle, inhibitor type, and multivalent enhancement factors (MEF)[72] are shown. MEF = K_i(starting inhibitor)/K_i(nanoparticle).

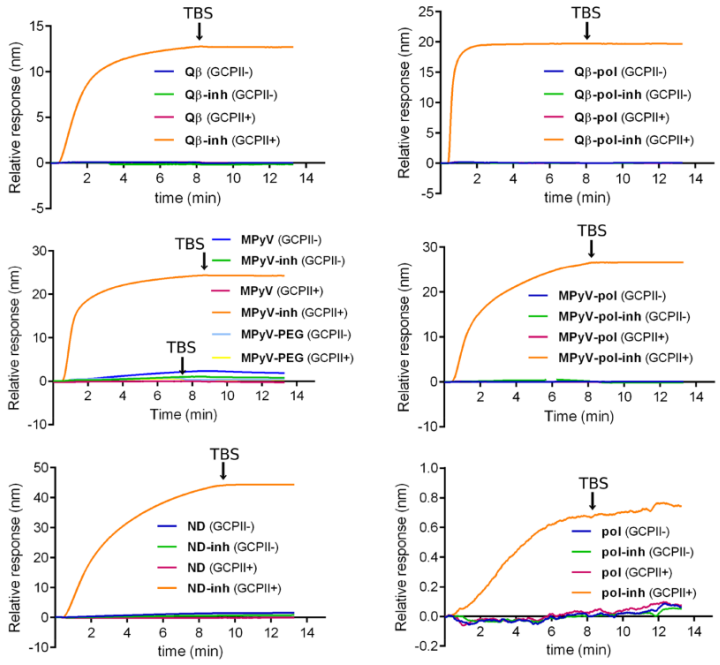

Figure 3. Interaction of NPs with GCPII. Testing of the binding capacity of all NPs to GCPII immobilized on the chip by SPR measurements. GCPII was immobilized on SPR chips through a neutravidin−biotin interaction (GCPII+). As a negative control, we attached neutravidin alone (GCPII−). NPs were injected at final 5 nM concentrations in TBS (association phase) for several minutes, and then TBS alone was injected (dissociation phase).

Cellular Uptake of NPs. Once we had verified interaction between GCPII and our modified NPs with inhibitor, we next focused on monitoring the binding ability and cellular uptake of NPs. We used the human glioblastoma cell line U-251 MG. Depending on the presence of doxycycline in the media (Tet-OffAdvanced System), these cells can overexpress GCPII on their surfaces.[63,77] This enabled us to conduct a comparative study in a very consistent way using only one type of cells. According to the level of GCPII expression, we marked the cells U-251$^+$ MG (with expression) or U-251$^-$ MG (without expression). GCPII is constantly internalized, but the turnover is greatly accelerated after binding of antibody[78,79] or HPMA copolymer with bound inhibitor.[24] The mechanism of action of polymer-induced internalization has not been studied thoroughly; however, it has been shown that antibody-induced endocytosis is clathrin-dependent and mediated by an MXXXL cytoplasmic tail motif.[79]

DOI: 10.1021/acs.molpharmaceut.7b00889
Mol. Pharmaceutics 2018, 15, 2932−2945

We incubated all particles with cells, washed them with buffer, and analyzed the cells using flow cytometry (Figure 4,

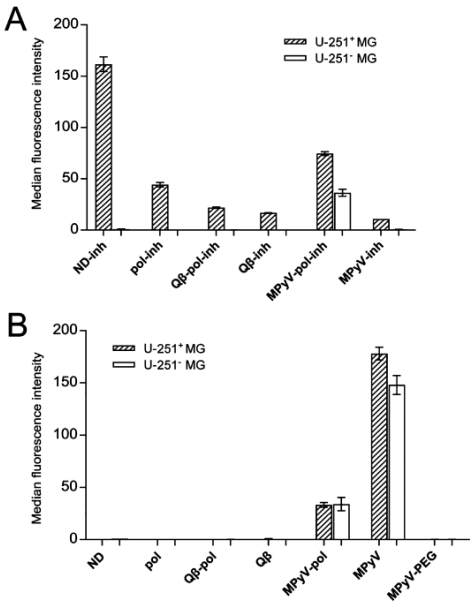

Figure 4. Flow cytometry study of NP association with U-251 MG cells with (U-251$^+$ MG) or without (U-251$^-$ MG) GCPII expression. The graphs show the interaction of NPs with (A) or without (B) inhibitor. Data represent the median of fluorescence intensity (MFI), normalized to autofluorescence of negative cells and adjusted to the relative fluorescence of particles. The standard deviations were calculated from triplicates. There were statistically significant differences between the variants containing inhibitor on U-251$^+$ MG cells and all three negative controls (NP with inhibitor on U-251$^-$ MG cells and NP without inhibitors on either U-251$^+$ MG or U-251$^-$ MG). Obtained p-values were at least $p < 0.001$, one-way ANOVA followed by Tukey's post hoc test.

Figure S5). Because phosphate is a weak competitive inhibitor of GCPII,[80,81] we used phosphate-free buffers and media to avoid potential detachment of particles from the cell surface. Regardless of the size and loading of inhibitor, all particles with inhibitor formed strong interactions with U-251$^+$ MG cells, and relative fluorescence intensities were up to 160 times higher than those observed for U-251$^-$ MG cells (Figure 4A). With the exception of **MPyV-pol-inh**, the nonspecific binding of nanoparticles with inhibitor in the absence of GCPII was negligible. This is consistent with the data obtained from measurement of particles without inhibitor (Figure 4B). Consistent with previously published results, NDs,[37] polymer,[24] and Qβ particles[49] without a targeting ligand (GCPII inhibitor) did not interact with mammalian cells. In contrast, MPyV VLPs had comparably strong interactions with both U-251$^+$ MG and U-251$^-$ MG cells. We assumed that coating MPyV VLPs with polymer in **MPyV-pol** and **MPyV-pol-inh** or PEG_{13} linker (**MPyV-PEG**) would prevent the VP1-specific interaction with cells. Surprisingly, modification with PEG_{13} suppressed the VP1-specific binding of particles to both U-251$^+$ MG and U-251$^-$ MG cells to negligible levels, whereas **MPyV-pol** and **MPyV-pol-inh** VLPs maintained their capacity to interact with both cell variants. The higher load of PEG_{13} molecules (approximately 1,000 molecules) than poly(HPMA) molecules (approximately 30 molecules) per particle and better surface coverage indicate that an optimal load of shielding polymer is necessary to reduce the unwanted interactions of MPyV VLPs with glioblastoma cells. This is especially pronounced in our experimental system, because the U-251 MG cell line, as a representative of brain tissue derived cultures known to abundantly express complex gangliosides,[82] contains high levels of GD1a and GT1b gangliosides,[83] which are major MPyV receptors.[43,44] Interestingly, our results showed that the PEG linker itself or with the attached inhibitor molecule was capable of completely reducing VP1-mediated binding to sialic acid or selectively retargeting particles to GCPII, respectively.

We further analyzed the interaction of NPs with cells using confocal microscopy. We clearly observed a high internalization rate of NPs containing inhibitor in U-251$^+$ MG cells, and no internalization in control experiments (Figure 5A, Figure S6). MPyV VLPs were the only exception; binding of nontargeted non-PEGylated NPs was observed, similar to the flow cytometry results. We observed **MPyV**, **MPyV-pol**, and **MPyV-pol-inh** particles in close association with the plasma membrane (Figure 5B).

■ CONCLUSIONS

In summary, we investigated the robustness of GCPII targeting by a variety of NPs using one cell type model. The glioblastoma cell line U-251 MG provided us the unique possibility to switch on surface expression of GCPII using an external stimulus, instead of using different cell lines (with and without GCPII expression). We therefore were able to compare the targeting in a very consistent and straightforward way. Independent of the NP structure, size, polydispersity, used conjugation chemistry, and loading of targeting inhibitor molecules, we observed that all targeted NPs bound GCPII installed on an SPR chip, inhibited GCPII in solution, and interacted with GCPII on the cell membrane. Inhibition of GCPII was highly effective, reaching low picomolar K_i values for all particles except polymer NPs, which had subnanomolar K_i. We observed an increase in interaction efficacy of the original small molecule inhibitors upon installation on NP surface for 1 to 4 orders of magnitude. This effect is most likely caused by high local concentration of inhibitors which can lead in strong multivalent binding with the target surfaces. However, vast range of the observed enhancement documents specific needs of each nanosystem for recognition and binding.

In general, the specificity of target binding is limited not only by the strength of interaction but also by any other side interactions (either nonspecific or due to an unwanted side specificity). In the case of MPyV VLPs, the interface of which shows a broad tropism and can strongly interact with various receptors, we clearly observed the importance of the surface modification for targeting selectivity. A high load of short PEG chains grafted to surface lysines provided sufficient protection and enabled complete retargeting of MPyV VLPs to GCPII, while a low density of poly(HPMA) did not sufficiently mitigate the side binding. On the other hand, poly(HPMA) grafted from NDs at high density led to excellent and highly selective targeting.

DOI: 10.1021/acs.molpharmaceut.7b00889
Mol. Pharmaceutics 2018, 15, 2932−2945

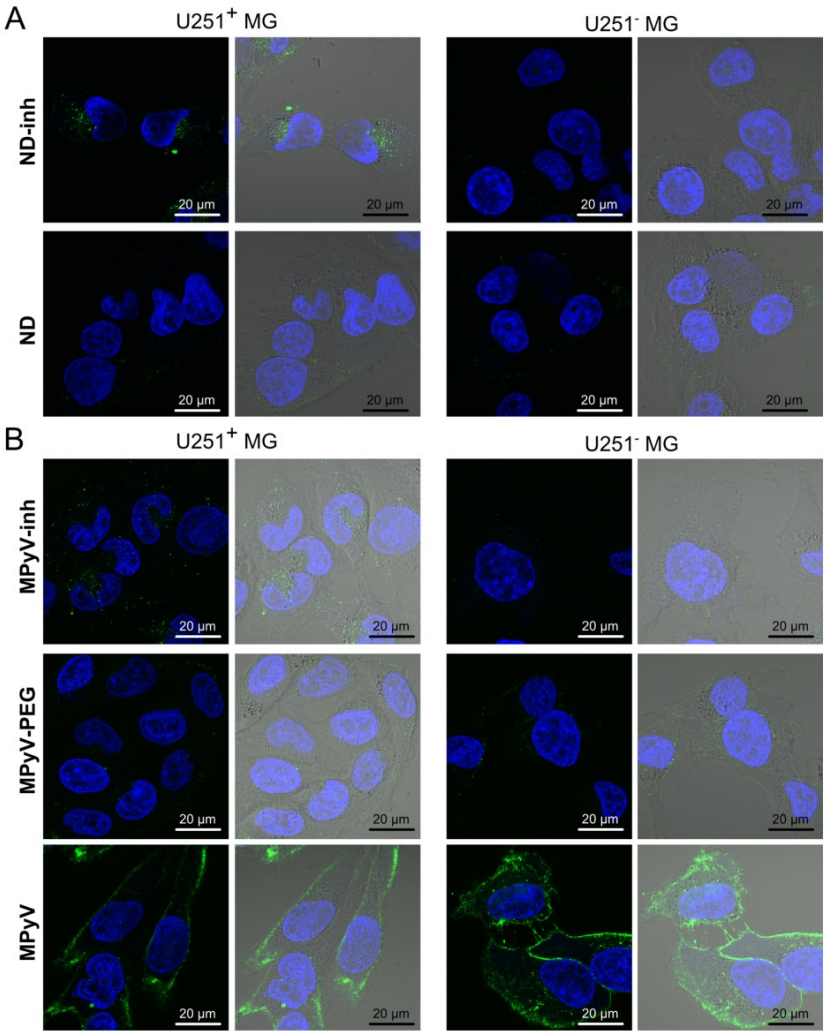

Figure 5. Confocal images of NP uptake by U-251 MG cells with (U-251$^+$ MG) or without (U-251$^-$ MG) GCPII expression incubated with NPs for 1 h. (A) Binding of ND NPs to U-251 MG cells. (B) Binding of MPyV NPs to U-251 MG cells. Confocal sections of representative cells with corresponding signal in green (NPs conjugated with Alexa Fluor 488 or Atto 488) and blue (nuclei with Hoechst staining) channels are shown. Merged images are composed of both channels and bright field image.

Our results indicate that use of small molecule inhibitors with low nanomolar range K_i displayed in polyvalent arrangements on NPs can be highly effective and selective for targeting to cells overexpressing GCPII. The robustness of the approach is limited mostly by the quality of the NP bionanointerface, which can be improved by adding a sufficient density of hydrophilic protective polymers. Based on the comprehensive data set we obtained here and on previously reported work, we believe that targeting of cancer cells overexpressing GCPII is a viable approach transferable to a broad diversity of nanosystems.

■ ASSOCIATED CONTENT

Supporting Information

The Supporting Information is available free of charge on the ACS Publications website at DOI: 10.1021/acs.molpharmaceut.7b00889.

Details of synthesis and characterization (PDF)

DOI: 10.1021/acs.molpharmaceut.7b00889
Mol. Pharmaceutics 2018, 15, 2932−2945

AUTHOR INFORMATION

Corresponding Author

*E-mail: cigler@uochb.cas.cz. Fax: (+)420-220-183-578. Tel: (+)420-220-183-429.

ORCID

Tomas Etrych: 0000-0001-5908-5182

Petr Cigler: 0000-0003-0283-647X

Author Contributions

§J.N., F.S., and J.Z.S. contributed equally.

Notes

The authors declare no competing financial interest.

ACKNOWLEDGMENTS

The authors thank Dr. Jiri Schimer for fruitful discussions and Jana Starkova for her kind help with cell culturing. This work was supported by the Grant Agency of Charles University Project No. 727816 (J.N., P.C.), Grant Agency of the Czech Republic Projects No. 16-16336S (J.N., P.C.) and 16-02938S (L.K., V.S., T.E., F.S., P.S., R.K., J.K.), League Against Cancer Prague (J.Z.S., H.S., J.F.), Project SVV-260426 (J.Z.S), Ministry of Education of the Czech Republic NPU (OP PK) InterBioMed Project LO 1302 (F.S., P.S., R.K., J.K.), and OPPK Project CZ.2.16/3.1.00/24016 (F.S., P.S., R.K., J.K.).

ABREVIATIONS USED

NP, nanoparticle; GCPII, glutamate carboxypeptidase II; PSMA, prostate-specific membrane antigen; NAAG, *N*-acetyl-L-aspartyl-L-glutamate; HPMA, *N*-(2-hydroxypropyl)-methacrylamide; ND, nanodiamond; NV, nitrogen vacancy; VLP, virus-like particle; MPyV, mouse polyomavirus; TT, thiazolidine-2-thione; Sf9, *Spodoptera frugiperda*; NHS, *N*-hydroxysuccinimide; THPTA, tris(3-hydroxypropyltriazolylmethyl)amine; DTT, dithiothreitol; SPR, surface plasmon resonance; TEM, transmission electron microscopy; DLS, dynamic light scattering; MALDI, matrix-assisted laser desorption/ionization mass spectrometry

REFERENCES

(1) Fernandez-Fernandez, A.; Manchanda, R.; McGoron, A. J. Theranostic Applications of Nanomaterials in Cancer: Drug Delivery, Image-Guided Therapy and Multifunctional Platforms. *Appl. Biochem. Biotechnol.* **2011**, *165* (7−8), 1628−1651.

(2) Liu, H.; Moy, P.; Kim, S.; Xia, Y.; Rajasekaran, A.; Navarro, V.; Knudsen, B.; Bander, N. H. Monoclonal Antibodies to the Extracellular Domain of Prostate-Specific Membrane Antigen Also React with Tumor Vascular Endothelium. *Cancer Res.* **1997**, *57* (17), 3629−3634.

(3) Silver, D. A.; Pellicer, I.; Fair, W. R.; Heston, W. D.; Cordon-Cardo, C. Prostate-Specific Membrane Antigen Expression in Normal and Malignant Human Tissues. *Clin. Cancer Res.* **1997**, *3* (1), 81−85.

(4) Bostwick, D. G.; Iczkowski, K. A.; Amin, M. B.; Discigil, G.; Osborne, B. Malignant Lymphoma Involving the Prostate: Report of 62 Cases. *Cancer* **1998**, *83* (4), 732−738.

(5) Maurer, T.; Eiber, M.; Schwaiger, M.; Gschwend, J. E. Current Use of PSMA-PET in Prostate Cancer Management. *Nat. Rev. Urol.* **2016**, *13* (4), 226−235.

(6) Hlouchová, K.; Bařinka, C.; Konvalinka, J. Glutamate Carboxypeptidase II as a Therapeutic Target. In *Proteinases as Drug Targets*; RSC: 2011; pp 62−95.

(7) Mukherjee, A.; Darlington, T.; Baldwin, R.; Holz, C.; Olson, S.; Kulkarni, P.; DeWeese, T. L.; Getzenberg, R. H.; Ivkov, R.; Lupold, S. E. Development and Screening of a Series of Antibody-Conjugated and Silica-Coated Iron Oxide Nanoparticles for Targeting the Prostate-Specific Membrane Antigen. *ChemMedChem* **2014**, *9* (7), 1356−1360.

(8) Nagesh, P. K. B.; Johnson, N. R.; Boya, V. K. N.; Chowdhury, P.; Othman, S. F.; Khalilzad-Sharghi, V.; Hafeez, B. B.; Ganju, A.; Khan, S.; Behrman, S. W.; Zafar, N.; Chauhan, S. C.; Jaggi, M.; Yallapu, M. M. PSMA Targeted Docetaxel-Loaded Superparamagnetic Iron Oxide Nanoparticles for Prostate Cancer. *Colloids Surf., B* **2016**, *144*, 8−20.

(9) Kim, D.; Jeong, Y. Y.; Jon, S. A Drug-Loaded Aptamer−Gold Nanoparticle Bioconjugate for Combined CT Imaging and Therapy of Prostate Cancer. *ACS Nano* **2010**, *4* (7), 3689−3696.

(10) Kolishetti, N.; Dhar, S.; Valencia, P. M.; Lin, L. Q.; Karnik, R.; Lippard, S. J.; Langer, R.; Farokhzad, O. C. Engineering of Self-Assembled Nanoparticle Platform for Precisely Controlled Combination Drug Therapy. *Proc. Natl. Acad. Sci. U. S. A.* **2010**, *107* (42), 17939−17944.

(11) Xu, X.; Wu, J.; Liu, Y.; Saw, P. E.; Tao, W.; Yu, M.; Zope, H.; Si, M.; Victorious, A.; Rasmussen, J.; Ayyash, D.; Farokhzad, O. C.; Shi, J. Multifunctional Envelope-Type siRNA Delivery Nanoparticle Platform for Prostate Cancer Therapy. *ACS Nano* **2017**, *11* (3), 2618−2627.

(12) Sanna, V.; Pintus, G.; Roggio, A. M.; Punzoni, S.; Posadino, A. M.; Arca, A.; Marceddu, S.; Bandiera, P.; Uzzau, S.; Sechi, M. Targeted Biocompatible Nanoparticles for the Delivery of (−)-Epigallocatechin 3-Gallate to Prostate Cancer Cells. *J. Med. Chem.* **2011**, *54* (5), 1321.

(13) Chen, Z.; Penet, M.-F.; Krishnamachary, B.; Banerjee, S. R.; Pomper, M. G.; Bhujwalla, Z. M. PSMA-Specific Theranostic Nanoplex for Combination of TRAIL Gene and 5-FC Prodrug Therapy of Prostate Cancer. *Biomaterials* **2016**, *80*, 57−67.

(14) Banerjee, S. R.; Foss, C. A.; Horhota, A.; Pullambhatla, M.; McDonnell, K.; Zale, S.; Pomper, M. G. 111In- and IRDye800CW-Labeled PLA−PEG Nanoparticle for Imaging Prostate-Specific Membrane Antigen-Expressing Tissues. *Biomacromolecules* **2017**, *18* (1), 201−209.

(15) Janoniene, A.; Liu, Z.; Baranauskiene, L.; Mäkilä, E.; Ma, M.; Salonen, J.; Hirvonen, J.; Zhang, H.; Petrikaite, V.; Santos, H. A. A Versatile Carbonic Anhydrase IX Targeting Ligand-Functionalized Porous Silicon Nanoplatform for Dual Hypoxia Cancer Therapy and Imaging. *ACS Appl. Mater. Interfaces* **2017**, *9* (16), 13976−13987.

(16) Azad, B. B.; Banerjee, S. R.; Pullambhatla, M.; Lacerda, S.; Foss, C. A.; Wang, Y.; Ivkov, R.; Pomper, M. G. Evaluation of a PSMA-Targeted BNF Nanoparticle Construct. *Nanoscale* **2015**, *7* (10), 4432−4442.

(17) Chandran, S. S.; Banerjee, S. R.; Mease, R. C.; Pomper, M. G.; Denmeade, S. R. Characterization of a Targeted Nanoparticle Functionalized with a Urea-Based Inhibitor of Prostate-Specific Membrane Antigen (PSMA). *Cancer Biol. Ther.* **2008**, *7* (6), 974−982.

(18) Chen, Z.; Penet, M.-F.; Nimmagadda, S.; Li, C.; Banerjee, S. R.; Winnard, P. T.; Artemov, D.; Glunde, K.; Pomper, M. G.; Bhujwalla, Z. M. PSMA-Targeted Theranostic Nanoplex for Prostate Cancer Therapy. *ACS Nano* **2012**, *6* (9), 7752−7762.

(19) Hoff, D. D. V.; Mita, M. M.; Ramanathan, R. K.; Weiss, G. J.; Mita, A. C.; LoRusso, P. M.; Burris, H. A.; Hart, L. L.; Low, S. C.; Parsons, D. M.; Zale, S. E.; Summa, J. M.; Youssoufian, H.; Sachdev, J. C. Phase I Study of PSMA-Targeted Docetaxel-Containing Nanoparticle BIND-014 in Patients with Advanced Solid Tumors. *Clin. Cancer Res.* **2016**, *22* (13), 3157−3163.

(20) Hrkach, J.; Hoff, D. V.; Ali, M. M.; Andrianova, E.; Auer, J.; Campbell, T.; Witt, D. D.; Figa, M.; Figueiredo, M.; Horhota, A.; Low, S.; McDonnell, K.; Peeke, E.; Retnarajan, B.; Sabnis, A.; Schnipper, E.; Song, J. J.; Song, Y. H.; Summa, J.; Tompsett, D.; Troiano, G.; Hoven, T. V. G.; Wright, J.; LoRusso, P.; Kantoff, P. W.; Bander, N. H.; Sweeney, C.; Farokhzad, O. C.; Langer, R.; Zale, S. Preclinical Development and Clinical Translation of a PSMA-Targeted Docetaxel Nanoparticle with a Differentiated Pharmacological Profile. *Sci. Transl. Med.* **2012**, *4* (128), 128ra39.

(21) Huang, B.; Otis, J.; Joice, M.; Kotlyar, A.; Thomas, T. P. PSMA-Targeted Stably Linked "Dendrimer-Glutamate Urea-Methotrexate" as a Prostate Cancer Therapeutic. *Biomacromolecules* **2014**, *15* (3), 915−923.

(22) Kasten, B. B.; Liu, T.; Nedrow-Byers, J. R.; Benny, P. D.; Berkman, C. E. Targeting Prostate Cancer Cells with PSMA Inhibitor-Guided Gold Nanoparticles. *Bioorg. Med. Chem. Lett.* **2013**, *23* (2), 565−568.
(23) Moon, S.-H.; Yang, B. Y.; Kim, Y. J.; Hong, M. K.; Lee, Y.-S.; Lee, D. S.; Chung, J.-K.; Jeong, J. M. Development of a Complementary PET/MR Dual-Modal Imaging Probe for Targeting Prostate-Specific Membrane Antigen (PSMA). *Nanomedicine* **2016**, *12* (4), 871−879.
(24) Šácha, P.; Knedlík, T.; Schimer, J.; Tykvart, J.; Parolek, J.; Navrátil, V.; Dvořáková, P.; Sedlák, F.; Ulbrich, K.; Strohalm, J.; Majer, P.; Šubr, V.; Konvalinka, J. iBodies: Modular Synthetic Antibody Mimetics Based on Hydrophilic Polymers Decorated with Functional Moieties. *Angew. Chem., Int. Ed.* **2016**, *55* (7), 2356−2360.
(25) Zhu, C.; Bandekar, A.; Sempkowski, M.; Banerjee, S. R.; Pomper, M. G.; Bruchertseifer, F.; Morgenstern, A.; Sofou, S. Nanoconjugation of PSMA-Targeting Ligands Enhances Perinuclear Localization and Improves Efficacy of Delivered Alpha-Particle Emitters against Tumor Endothelial Analogues. *Mol. Cancer Ther.* **2016**, *15* (1), 106−113.
(26) Rehor, I.; Slegerova, J.; Havlik, J.; Raabova, H.; Hyvl, J.; Muchova, E.; Cigler, P. Nanodiamonds: Behavior in Biological Systems and Emerging Bioapplications. In *Carbon Nanomaterials for Biomedical Applications*; Biomaterials Science and Engineering; Springer: Switzerland, 2016; pp 319−361.
(27) Slegerova, J.; Rehor, I.; Havlik, J.; Raabova, H.; Muchova, E.; Cigler, P. Nanodiamonds as Intracellular Probes for Imaging in Biology and Medicine. In *Intracellular Delivery II*; Prokop, A., Iwasaki, Y., Harada, A., Eds.; Springer Netherlands: Dordrecht, 2014; Vol. 7, pp 363−401.
(28) Monopoli, M. P.; Åberg, C.; Salvati, A.; Dawson, K. A. Biomolecular Coronas Provide the Biological Identity of Nanosized Materials. *Nat. Nanotechnol.* **2012**, *7* (12), 779−786.
(29) Saptarshi, S. R.; Duschl, A.; Lopata, A. L. Interaction of Nanoparticles with Proteins: Relation to Bio-Reactivity of the Nanoparticle. *J. Nanobiotechnol.* **2013**, *11*, 26.
(30) Neburkova, J.; Vavra, J.; Cigler, P. Coating Nanodiamonds with Biocompatible Shells for Applications in Biology and Medicine. *Curr. Opin. Solid State Mater. Sci.* **2017**, *21*, 43−53.
(31) Weng, M.-F.; Chiang, S.-Y.; Wang, N.-S.; Niu, H. Fluorescent Nanodiamonds for Specifically Targeted Bioimaging: Application to the Interaction of Transferrin with Transferrin Receptor. *Diamond Relat. Mater.* **2009**, *18* (2−3), 587−591.
(32) Wang, Z.; Tian, Z.; Dong, Y.; Li, L.; Tian, L.; Li, Y.; Yang, B. Nanodiamond-Conjugated Transferrin as Chemotherapeutic Drug Delivery. *Diamond Relat. Mater.* **2015**, *58*, 84−93.
(33) Li, Y.; Zhou, X. Transferrin-Coupled Fluorescence Nanodiamonds as Targeting Intracellular Transporters: An Investigation of the Uptake Mechanism. *Diamond Relat. Mater.* **2010**, *19* (10), 1163−1167.
(34) Fu, Y.; An, N.; Zheng, S.; Liang, A.; Li, Y. BmK CT-Conjugated Fluorescence Nanodiamond as Potential Glioma-Targeted Imaging and Drug. *Diamond Relat. Mater.* **2012**, *21*, 73−76.
(35) Chan, M. S.; Liu, L. S.; Leung, H. M.; Lo, P. K. Cancer-Cell-Specific Mitochondria-Targeted Drug Delivery by Dual-Ligand-Functionalized Nanodiamonds Circumvent Drug Resistance. *ACS Appl. Mater. Interfaces* **2017**, *9* (13), 11780−11789.
(36) Zhang, B.; Li, Y.; Fang, C.-Y.; Chang, C.-C.; Chen, C.-S.; Chen, Y.-Y.; Chang, H.-C. Receptor-Mediated Cellular Uptake of Folate-Conjugated Fluorescent Nanodiamonds: A Combined Ensemble and Single-Particle Study. *Small* **2009**, *5* (23), 2716−2721.
(37) Slegerova, J.; Hajek, M.; Rehor, I.; Sedlak, F.; Stursa, J.; Hruby, M.; Cigler, P. Designing the Nanobiointerface of Fluorescent Nanodiamonds: Highly Selective Targeting of Glioma Cancer Cells. *Nanoscale* **2015**, *7* (2), 415−420.
(38) Zhao, L.; Xu, Y.-H.; Qin, H.; Abe, S.; Akasaka, T.; Chano, T.; Watari, F.; Kimura, T.; Komatsu, N.; Chen, X. Platinum on Nanodiamond: A Promising Prodrug Conjugated with Stealth Polyglycerol, Targeting Peptide and Acid-Responsive Antitumor Drug. *Adv. Funct. Mater.* **2014**, *24* (34), 5348−5357.
(39) Zhang, T.; Cui, H.; Fang, C.-Y.; Cheng, K.; Yang, X.; Chang, H.-C.; Forrest, M. L. Targeted Nanodiamonds as Phenotype-Specific Photoacoustic Contrast Agents for Breast Cancer. *Nanomedicine* **2015**, *10* (4), 573−587.
(40) Slilaty, S. N.; Aposhian, H. V. Gene Transfer by Polyoma-like Particles Assembled in a Cell-Free System. *Science* **1983**, *220* (4598), 725−727.
(41) Forstová, J.; Krauzewicz, N.; Sandig, V.; Elliott, J.; Palková, Z.; Strauss, M.; Griffin, B. E. Polyoma Virus Pseudocapsids as Efficient Carriers of Heterologous DNA into Mammalian Cells. *Hum. Gene Ther.* **1995**, *6* (3), 297−306.
(42) Ou, W. C.; Wang, M.; Fung, C. Y.; Tsai, R. T.; Chao, P. C.; Hseu, T. H.; Chang, D. The Major Capsid Protein, VP1, of Human JC Virus Expressed in Escherichia Coli Is Able to Self-Assemble into a Capsid-like Particle and Deliver Exogenous DNA into Human Kidney Cells. *J. Gen. Virol.* **1999**, *80* (1), 39−46.
(43) Tsai, B.; Gilbert, J. M.; Stehle, T.; Lencer, W.; Benjamin, T. L.; Rapoport, T. A. Gangliosides Are Receptors for Murine Polyoma Virus and SV40. *EMBO J.* **2003**, *22* (17), 4346−4355.
(44) You, J.; O'Hara, S. D.; Velupillai, P.; Castle, S.; Levery, S.; Garcea, R. L.; Benjamin, T. Ganglioside and Non-Ganglioside Mediated Host Responses to the Mouse Polyomavirus. *PLoS Pathog.* **2015**, *11* (10), e1005175.
(45) Caruso, M. Role of Sialic Acid-Containing Molecules and the 4 1 Integrin Receptor in the Early Steps of Polyomavirus Infection. *J. Gen. Virol.* **2003**, *84* (11), 2927−2936.
(46) Zackova Suchanova, J.; Neburkova, J.; Spanielova, H.; Forstova, J.; Cigler, P. Retargeting Polyomavirus-Like Particles to Cancer Cells by Chemical Modification of Capsid Surface. *Bioconjugate Chem.* **2017**, *28* (2), 307−313.
(47) Fiedler, J. D.; Brown, S. D.; Lau, J. L.; Finn, M. G. RNA-Directed Packaging of Enzymes within Virus-like Particles. *Angew. Chem., Int. Ed.* **2010**, *49* (50), 9648−9651.
(48) Banerjee, D.; Liu, A. P.; Voss, N. R.; Schmid, S. L.; Finn, M. G. Multivalent Display and Receptor-Mediated Endocytosis of Transferrin on Virus-Like Particles. *ChemBioChem* **2010**, *11* (9), 1273−1279.
(49) Pokorski, J. K.; Hovlid, M. L.; Finn, M. G. Cell Targeting with Hybrid Qβ Virus-Like Particles Displaying Epidermal Growth Factor. *ChemBioChem* **2011**, *12* (16), 2441−2447.
(50) Rhee, J.-K.; Baksh, M.; Nycholat, C.; Paulson, J. C.; Kitagishi, H.; Finn, M. G. Glycan-Targeted Virus-like Nanoparticles for Photodynamic Therapy. *Biomacromolecules* **2012**, *13* (8), 2333−2338.
(51) Hovlid, M. L.; Lau, J. L.; Breitenkamp, K.; Higginson, C. J.; Laufer, B.; Manchester, M.; Finn, M. G. Encapsidated Atom-Transfer Radical Polymerization in Qβ Virus-like Nanoparticles. *ACS Nano* **2014**, *8* (8), 8003−8014.
(52) Manzenrieder, F.; Luxenhofer, R.; Retzlaff, M.; Jordan, R.; Finn, M. G. Stabilization of Virus-like Particles with Poly(2-Oxazoline)s. *Angew. Chem., Int. Ed.* **2011**, *50* (11), 2601−2605.
(53) Pokorski, J. K.; Breitenkamp, K.; Liepold, L. O.; Qazi, S.; Finn, M. G. Functional Virus-Based Polymer−Protein Nanoparticles by Atom Transfer Radical Polymerization. *J. Am. Chem. Soc.* **2011**, *133* (24), 9242−9245.
(54) Šubr, V.; Ulbrich, K. Synthesis and Properties of New N-(2-Hydroxypropyl)methacrylamide Copolymers Containing Thiazolidine-2-Thione Reactive Groups. *React. Funct. Polym.* **2006**, *66* (12), 1525−1538.
(55) Lallana, E.; Sousa-Herves, A.; Fernandez-Trillo, F.; Riguera, R.; Fernandez-Megia, E. Click Chemistry for Drug Delivery Nanosystems. *Pharm. Res.* **2012**, *29* (1), 1−34.
(56) Wang, Q.; Chan, T. R.; Hilgraf, R.; Fokin, V. V.; Sharpless, K. B.; Finn, M. G. Bioconjugation by Copper(I)-Catalyzed Azide-Alkyne [3 + 2] Cycloaddition. *J. Am. Chem. Soc.* **2003**, *125* (11), 3192−3193.
(57) Forstova, J.; Krauzewicz, N.; Wallace, S.; Street, A. J.; Dilworth, S. M.; Beard, S.; Griffin, B. E. Cooperation of Structural Proteins

DOI: 10.1021/acs.molpharmaceut.7b00889
Mol. Pharmaceutics 2018, 15, 2932−2945

during Late Events in the Life Cycle of Polyomavirus. *J. Virol.* **1993**, *67* (3), 1405−1413.
(58) Türler, H.; Beard, P. Simian Virus 40 and Polyoma Virus: Growth, Titration, Transformation and Purification of Viral Components. In *Virology: a practical approach*; IRL Press: Oxford, 1985; pp 169−192.
(59) Hong, V.; Presolski, S. I.; Ma, C.; Finn, M. G. Analysis and Optimization of Copper-Catalyzed Azide-Alkyne Cycloaddition for Bioconjugation. *Angew. Chem., Int. Ed.* **2009**, *48* (52), 9879−9883.
(60) Rendler, T.; Neburkova, J.; Zemek, O.; Kotek, J.; Zappe, A.; Chu, Z.; Cigler, P.; Wrachtrup, J. Optical Imaging of Localized Chemical Events Using Programmable Diamond Quantum Nanosensors. *Nat. Commun.* **2017**, *8*, 14701.
(61) Neburkova, J.; Hajek, M.; Rehor, I.; Schimer, J.; Sedlak, F.; Stursa, J.; Hruby, M.; Cigler, P. Targeting Glioma Cancer Cells with Fluorescent Nanodiamonds via Integrin Receptors. In *Methods in Pharmacology and Toxicology*; Humana Press: 2017; DOI: 10.1007/7653_2017_68.
(62) Tykvart, J.; Šácha, P.; Bařinka, C.; Knedlík, T.; Starková, J.; Lubkowski, J.; Konvalinka, J. Efficient and Versatile One-Step Affinity Purification of in Vivo Biotinylated Proteins: Expression, Characterization and Structure Analysis of Recombinant Human Glutamate Carboxypeptidase II. *Protein Expression Purif.* **2012**, *82* (1), 106−115.
(63) Tykvart, J.; Schimer, J.; Bařinková, J.; Pachl, P.; Poštová-Slavětínská, L.; Majer, P.; Konvalinka, J.; Šácha, P. Rational Design of Urea-Based Glutamate Carboxypeptidase II (GCPII) Inhibitors as Versatile Tools for Specific Drug Targeting and Delivery. *Bioorg. Med. Chem.* **2014**, *22* (15), 4099−4108.
(64) Schindelin, J.; Arganda-Carreras, I.; Frise, E.; Kaynig, V.; Longair, M.; Pietzsch, T.; Preibisch, S.; Rueden, C.; Saalfeld, S.; Schmid, B.; Tinevez, J.-Y.; White, D. J.; Hartenstein, V.; Eliceiri, K.; Tomancak, P.; Cardona, A. Fiji: An Open-Source Platform for Biological-Image Analysis. *Nat. Methods* **2012**, *9* (7), 676−682.
(65) Kozikowski, A. P.; Nan, F.; Conti, P.; Zhang, J.; Ramadan, E.; Bzdega, T.; Wroblewska, B.; Neale, J. H.; Pshenichkin, S.; Wroblewski, J. T. Design of Remarkably Simple, yet Potent Urea-Based Inhibitors of Glutamate Carboxypeptidase II (NAALADase). *J. Med. Chem.* **2001**, *44* (3), 298−301.
(66) Hong, V.; Steinmetz, N. F.; Manchester, M.; Finn, M. G. Labeling Live Cells by Copper-Catalyzed Alkyne−Azide Click Chemistry. *Bioconjugate Chem.* **2010**, *21* (10), 1912−1916.
(67) Stehle, T.; Harrison, S. C. Crystal Structures of Murine Polyomavirus in Complex with Straight-Chain and Branched-Chain Sialyloligosaccharide Receptor Fragments. *Structure* **1996**, *4* (2), 183−194.
(68) Krauzewicz, N.; Cox, C.; Soeda, E.; Clark, B.; Rayner, S.; Griffin, B. E. Sustained Ex Vivo and in Vivo Transfer of a Reporter Gene Using Polyoma Virus Pseudocapsids. *Gene Ther.* **2000**, *7* (13), 1094−1102.
(69) Hui, Y. Y.; Hsiao, W. W.-W.; Haziza, S.; Simonneau, M.; Treussart, F.; Chang, H.-C. Single Particle Tracking of Fluorescent Nanodiamonds in Cells and Organisms. *Curr. Opin. Solid State Mater. Sci.* **2017**, *21* (1), 35−42.
(70) Wu, T.-J.; Tzeng, Y.-K.; Chang, W.-W.; Cheng, C.-A.; Kuo, Y.; Chien, C.-H.; Chang, H.-C.; Yu, J. Tracking the Engraftment and Regenerative Capabilities of Transplanted Lung Stem Cells Using Fluorescent Nanodiamonds. *Nat. Nanotechnol.* **2013**, *8* (9), 682−689.
(71) Simon, C.; Klose, T.; Herbst, S.; Han, B. G.; Sinz, A.; Glaeser, R. M.; Stubbs, M. T.; Lilie, H. Disulfide Linkage and Structure of Highly Stable Yeast-Derived Virus-like Particles of Murine Polyomavirus. *J. Biol. Chem.* **2014**, *289* (15), 10411−10418.
(72) Li, M.-H.; Zong, H.; Leroueil, P. R.; Choi, S. K.; Baker, J. R. Ligand Characteristics Important to Avidity Interactions of Multivalent Nanoparticles. *Bioconjugate Chem.* **2017**, *28* (6), 1649−1657.
(73) Lucie, S.; Elisabeth, G.; Stéphanie, F.; Guy, S.; Amandine, H.; Corinne, A.-R.; Didier, B.; Catherine, S.; Alexeï, G.; Pascal, D.; Jean-Luc, C. Clustering and Internalization of Integrin $\alpha v\beta 3$ With a Tetrameric RGD-Synthetic Peptide. *Mol. Ther.* **2009**, *17* (5), 837−843.
(74) Fuchs, H.; Geßner, R. Iodination Significantly Influences the Binding of Human Transferrin to the Transferrin Receptor. *Biochim. Biophys. Acta, Gen. Subj.* **2002**, *1570* (1), 19−26.
(75) Schüler, J.; Frank, J.; Trier, U.; Schäfer-Korting, M.; Saenger, W. Interaction Kinetics of Tetramethylrhodamine Transferrin with Human Transferrin Receptor Studied by Fluorescence Correlation Spectroscopy. *Biochemistry* **1999**, *38* (26), 8402−8408.
(76) Wibowo, A. S.; Singh, M.; Reeder, K. M.; Carter, J. J.; Kovach, A. R.; Meng, W.; Ratnam, M.; Zhang, F.; Dann, C. E. Structures of Human Folate Receptors Reveal Biological Trafficking States and Diversity in Folate and Antifolate Recognition. *Proc. Natl. Acad. Sci. U. S. A.* **2013**, *110* (38), 15180−15188.
(77) Gossen, M.; Bujard, H. Tight Control of Gene Expression in Mammalian Cells by Tetracycline-Responsive Promoters. *Proc. Natl. Acad. Sci. U. S. A.* **1992**, *89* (12), 5547−5551.
(78) Liu, H.; Rajasekaran, A. K.; Moy, P.; Xia, Y.; Kim, S.; Navarro, V.; Rahmati, R.; Bander, N. H. Constitutive and Antibody-Induced Internalization of Prostate-Specific Membrane Antigen. *Cancer Res.* **1998**, *58* (18), 4055−4060.
(79) Rajasekaran, S. A.; Anilkumar, G.; Oshima, E.; Bowie, J. U.; Liu, H.; Heston, W.; Bander, N. H.; Rajasekaran, A. K. A Novel Cytoplasmic Tail MXXXL Motif Mediates the Internalization of Prostate-Specific Membrane Antigen. *Mol. Biol. Cell* **2003**, *14* (12), 4835−4845.
(80) Robinson, M. B.; Blakely, R. D.; Couto, R.; Coyle, J. T. Hydrolysis of the Brain Dipeptide N-Acetyl-L-Aspartyl-L-Glutamate. Identification and Characterization of a Novel N-Acetylated Alpha-Linked Acidic Dipeptidase Activity from Rat Brain. *J. Biol. Chem.* **1987**, *262* (30), 14498−14506.
(81) Barinka, C.; Rinnová, M.; Šácha, P.; Rojas, C.; Majer, P.; Slusher, B. S.; Konvalinka, J. Substrate Specificity, Inhibition and Enzymological Analysis of Recombinant Human Glutamate Carboxypeptidase II. *J. Neurochem.* **2002**, *80* (3), 477−487.
(82) Schnaar, R. L.; Gerardy-Schahn, R.; Hildebrandt, H. Sialic Acids in the Brain: Gangliosides and Polysialic Acid in Nervous System Development, Stability, Disease, and Regeneration. *Physiol. Rev.* **2014**, *94* (2), 461−518.
(83) Yates, A. J.; Markowitz, D. L.; Stephens, R. E.; Pearl, D. K.; Whisler, R. L. Growth Inhibition of Cultured Human Glioma Cells by Beta-Interferon Is Not Dependent on Changes in Ganglioside Composition. *J. Neuropathol. Exp. Neurol.* **1988**, *47* (2), 119−127.

DOI: 10.1021/acs.molpharmaceut.7b00889
Mol. Pharmaceutics 2018, 15, 2932−2945